UTS UNIVERSITY
OF TECHNOLOGY
SYDNEY

Fabrication and machine learning of nanocomposite organic solvent nanofiltration membranes

by Chen Wang

Thesis submitted in fulfilment of the requirements for the degree of

Doctor of Philosophy

under the supervision of Prof HoKyong Shon and Dr Sherub Phuntsho

University of Technology Sydney

Faculty of Engineering and Information Technology

June 2023

CERTIFICATE OF ORIGINAL AUTHORSHIP

I, Chen Wang, declare that this thesis is submitted in fulfilment of the requirements for the award of Doctor of Philosophy, in the Faculty of Engineering and Information Technology at the University of Technology Sydney.

This thesis is wholly my own work unless otherwise referenced or acknowledged. In addition, I certify that all information sources and literature used are indicated in the thesis.

This document has not been submitted for qualifications at any other academic institution.

Production Note:
Signature: Signature removed prior to publication.

Date: 30/06/2023

ACKNOWLEDGEMENTS

The completion of my PhD study required lots of help, guidance, and support from many people: my supervisors, families, colleagues and friends. I would like to express my deepest gratitude to those who have accompanied with me along the fulfilling and meaningful journey.

I really appreciate my principle supervisor Prof. Ho Kyong Shon. He provided me the opportunity to start my PhD study in University of Technology Sydney (UTS). I will gratefully remember his professional mentorship, patient encouragement, and strong support. Without his guidance, I could not achieve the successful outcomes. I would also like to thank my co-supervisor Dr. Sherub Phuntsho for his support and advices during my PhD.

I wish to give my special thanks to my senior colleague Dr. Myoung Jun Park, for his kind support and help for my research study. He guided me to develop my membrane fabrication and modification skills, and also provided me some valuable advices when I faced problems. Moreover, I am grateful to other colleagues Dong Han Seo, Nawshad Akther, Minwei Yao, Jiawei Ren, Hanwei Yu, Federico Volpin, for their help during my PhD study. I also want to thank my good friends Huan Liu, Zehao Zhang, Feng Shan, Qiang Hao, Haoding Xu, Shudi Mao, Wei Huang for making my spare time enjoyable and wonderful.

I would also like to acknowledge the support I received from the external collaborators. I would like to thank Prof. Hideto Matsuyama and Dr. Ralph Rolly Gonzales from Kobe University for helping me with the membrane characterizations and improving the quality of my manuscript. I also appreciate Prof. Enrico Drioli from Institute on Membrane Technology, National Research council in Italy, for revising my manuscript and providing me some valuable comments.

Finally, I would like to thank my parents for their constant encouragement and support during my PhD study. I am especially grateful to my husband, Li Wang, for his accompany during my PhD and support for my research study.

LIST OF PUBLICATIONS

This list includes journal articles or book chapters prepared during my PhD candidate, which are either *part of or **not part of the thesis.

1.**C. Wang[#], M.J. Park[#], D.H. Seo, H.K. Shon, Inkjet printing of graphene oxide and dopamine on nanofiltration membranes for improved anti-fouling properties and chlorine resistance, Separation and Purification Technology 254 (2021) 117604.

2. **M.J. Park[#], C. Wang[#](co-first author), D.H. Seo, R.R. Gonzales, H. Matsuyama, H.K. Shon, Inkjet printed single walled carbon nanotube as an interlayer for high performance thin film composite nanofiltration membrane, Journal of Membrane Science 620 (2021) 118901.

3. *C. Wang, M.J. Park, D.H. Seo, E. Drioli, H. Matsuyama, H.K. Shon, Recent advances in nanomaterial-incorporated nanocomposite membranes for organic solvent nanofiltration, Separation and Purification Technology 268 (2021) 118657.

4. *C. Wang, M.J. Park, D.H. Seo, S. Phuntsho, R.R. Gonzales, H. Matsuyama, E. Drioli, H.K. Shon, Inkjet printed polyelectrolyte multilayer membrane using a polyketone support for organic solvent nanofiltration, Journal of Membrane Science 642 (2021) 119943.

5. *C. Wang, M.J. Park, R.R. Gonzales, S. Phuntsho, H. Matsuyama, E. Drioli, H.K. Shon, Novel organic solvent nanofiltration membrane based on inkjet printing-assisted layer-by-layer assembly, Journal of Membrane Science 655 (2022) 120582.

6. *C. Wang, M.J. Park, H.W. Yu, H. Matsuyama, E. Drioli, H.K. Shon, Recent advances of nanocomposite membranes for layer-by-layer assembly, Journal of Membrane Science 661 (2022) 120926.

7. *C. Wang, L. Wang, A. Soo, N.B. Pathak, H.K. Shon, Machine learning based prediction and optimization of thin film nanocomposite membranes for organic solvent nanofiltration, Separation and purification Technology 304 (2023) 122328.

8. **C. Wang**, M.J. Park, H. Matsuyama, E. Drioli, H.K. Shon, Graphene oxide-based layer-by-layer nanofiltration membrane using inkjet printing for desalination, Desalination 549 (2023) 116357.

9. **M.J. Park, **C. Wang**, R.R. Gonzales, S. Phuntsho, H. Matsuyama, E. Drioli, H.K. Shon, Fabrication of thin film composite membrane for water purification via inkjet printing of aqueous and solvent inks, Desalination 541 (2022) 116027.

10. **H.W. Yu, G. Naidu, C.Y. Zhang, **C. Wang**, A. Razmjou, D.S. Han, T. He, H.K. Shon, Metal-based adsorbents for lithium recovery from aqueous resources, Desalination 539 (2022) 115951.

11. **F. Volpin, U. Badeti, **C. Wang**, J. Jiang, S. Phuntsho, H.K. Shon, Urine Treatment on the International Space Station: Current Practice and Novel Approaches, Membranes 2020, 10, 327.

12. **M.J. Park, G.M. Nisola, D.H. Seo, **C. Wang**, S. Phuntsho, W.J. Chung, H.K. Shon, Chemically crosslinked graphene oxide as a selective layer on electrospun polyvinyl alcohol nanofiber membrane for nanofiltration application, Nanomaterials, 2021, 11, 2867.

13. **D.H. Seo, M. Barclay, M.J. Park, **C. Wang**, K.K. Ostrikov, H.K. Shon, Graphitic Carbon Nanomaterial-Based Membranes for Water Desalination, Chapter 3, The World Scientific Reference of Water Science, pp. 63-88 (2022).

CONFERENCE PRESENTATIONS

1. **C. Wang**, M.J. Park, D.H. Seo, H.K. Shon, Inkjet printing of graphene oxide and dopamine on nanofiltration membranes for improved anti-fouling properties and chlorine resistance, Membrane Society of Australasia Annual Conference, November 23-24, Clayton, Australia, 2020.

2. **C. Wang**, M.J. Park, H.K. Shon, Inkjet printing technology on depositing nanomaterials for thin-film composite membrane fabrication and modification, 5th International Conference on Desalination using Membrane Technology (MEMDES2021), November 14-17, Shanghai, China, 2021.

3. **C. Wang**, M.J. Park, H.K. Shon, Inkjet printed polyelectrolyte multilayer membrane using a polyketone support for organic solvent nanofiltration, International Workshop for Membrane at Kobe university, November 18-19, Kobe, Japan, 2021.

4. **C. Wang**, M.J. Park, H.K. Shon, Inkjet printed polyelectrolyte multilayer membrane using a polyketone support for organic solvent nanofiltration, 13th conference of Aseanian Membrane Society (AMS13), July 4-6, Singapore, 2022.

5. **C. Wang**, M.J. Park, H.K. Shon, Novel organic solvent nanofiltration membrane based on inkjet printing-assisted layer-by-layer assembly, 11th International membrane Science & Technology Conference (IMSTEC2022), December 4-8, Melbourne, Australia, 2022.

TABLE OF CONTENTS

LIST OF TABLES

LIST OF FIGURES

xv

LIST OF ABBREVIATIONS

AC   Acetone

AFM   Atomic force microscopy

ANFs   Aramid nanofibers

ANN   Artificial neural network

AO   Acridine Orange

ATR-FTIR   Attenuated total reflection flourier transformed infrared

BBG   Brilliant blue G

BBR   Brilliant blue R

BN   Boron nitride

BT   Boosted tree

BTAC   1, 2, 4, 5 - benzene tetracarboxylic acyl chloride

BTB   Bromothymol blue

CBD   Cannabidiol

CNT   Carbon nanotube

COFs   Covalent organic frameworks

CSH   Calcium silicate hydrate

CV   Crystal violet

DHF   9,9-dihexylfluorene-2,7-diamine

DI   De-ionized

DMAC   N,N-dimethylacetamide

DMF   Dimethylformamide

DMSO   Dimethyl sulfoxide

DNF   9,9-dinonylfluorene-2,7-diamine

DPF	9,9-dipropylfluorene-2,7-diamine
EA	Ethyl acetate
EB	Evans blue
ECH	(±)-epichlorohydrin
EG	Ethylene glycol
EtOH	Ethanol
EY	Eosin Y
FBN	Functionalized boron nitride
FG	Fast green
FO	Forward osmosis
GA	Glutaraldehyde
GNPs	Gold nanoparticles
GO	Graphene oxide
GQDs	Graphene quantum dots
HEP	Heptane
HEX	Hexane
HF	Hollow fiber
H-PAN	Hydrolysed polyacrylonitrile
HPEI	Hyperbranched polyethyleneimine
HTAL	Hexanoyl triacetic acid lactone
IP	Interfacial polymerization
IPA	Isopropyl alcohol
IPD	Isophthaloyl dichloride
ISA	Integrally skinned asymmetric

ISG	In-situ growth
JGB	Janus Green B
LBL	Layer-by-layer
LS	Langmuir-Schaefer
MB	Methylene blue
MEK	Methyl ethyl ketone
MEOH	Methanol
MF	Microfiltration
ML	Machine learning
MMMs	Mixed matrix membranes
MO	Methyl orange
MOFs	Metal-organic frameworks
MoS_2	Molybdenum disulfide
MPD	m-Phenylenediamine
MR	Methyl red
MWCNT	Multi-walled carbon nanotubes
MWCO	Molecular weight cut-off
NF	Nanofiltration
NMP	N-methypyrrolidone
OS	Orange II sodium salt
OSN	Organic solvent nanofiltration
PA	Polyamide
PAA	Polyacrylic acid
PAN	Polyacrylonitrile

PANI	Polyaniline
PBI	Polybenzimidazole
PCA	Principal component analysis
PD	Partial dependence
PDNPs	Polydopamine nanoparticles
PDAL	Pentyl diacetic lactone
PDDA	Poly(diallyldimethylammonium chloride)
PDMS	Polydimethylsiloxane
PDP	Partial dependence plots
PEG	Poly(ethylene glycol)
PEI	Poly(ethyleneimine)
PEEK	Polyether etherketone
PEMs	Polyelectrolyte multilayers
PET	Polyethylene terephthalate
PI	Polyimid
PIP	Piperzine
PK	Ployketone
PMIA	Poly(m-phenyleneisophthalamide)
POSS	Polyhedral oligomeric silsesquioxane
PP	Polypropylene
PPSU	Polyphenylsulfone
PPy	Polypyrrole
PSF	Polysulfone
PSS	Poly(sodium 4-styrene sulfonate)

PTMSP	Poly(1-(trimethylsilyl)-1-propyne)
PU	Polyurethane
PVDF	Polyvinylidene fluoride
PVP	Poly(vinylpyrrolidone)
PVS	Poly(vinylsulfate)
RB	Rose bengal
RBB	Remazol brilliant blue
RDB	Rhodamine B
RF	Random forest
RMs	Resin microspheres
RMSE	Root mean square error
RO	Reverse osmosis
RO16	Reactive Orange 16
RP	Relative permeability
RS	Relative selectivity
SEM	Scanning electron microscopy
SPEEK	Sulfonated poly(ether ether ketone)
SRNF	Solvent resistant nanofiltration
SVM	Support vector machine
SWCNT	Single walled carbon nanotube
SY	Sunset Yellow
TAPA	Tris (3-aminopropyl) amine
TEM	Transmission electron microscopy
TFC	Thin film composite

TFN	Thin film nanocomposite
TFP	1,3,5-triformylphloroglucinol
THC	Tetrahydrocannabinol
THF	Tetrahydrofuran
TL	Toluene
TMC	Trimesoyl chlorid
TPC	Terephthaloyl chloride
UF	Ultrafiltration
UV	Ultraviolet
WS_2	Tungsten disulfide
XPS	X-ray photoelectron spectroscopy
ZIF-8	Zeolitic imidazolate framework 8

ABSTRACT

Organic solvents are frequently used as reaction agents for organic syntheses in chemical and pharmaceutical industries. Those organic solvents show different degrees of toxicity which could result in health risk upon human exposure. Distillation and evaporation can be used for recovering organic solvents, but both of the processes are expensive and consume large amount of energy. Therefore, a greener process organic solvent nanofiltration (OSN), provides an attractive alternative for the reuse and recovery of organic solvents.

Thin film composite (TFC) membranes are the most commonly used membranes for OSN. For TFC membranes, the active layer is deposited on top of a support layer which are made up of different polymeric materials. Recently, there is an increasing interest in incorporating nanomaterials into TFC OSN membranes to improve the membrane stability and separation performance. This thesis systematically investigated the nanocomposite membrane fabrication and performance prediction for OSN. Inkjet printing technique was used as an effective layer-by-layer (LBL) method for nanocomposite OSN membrane fabrication. Machine learning (ML) based models were utilized for nanocomposite OSN membrane performance prediction.

Specifically, solvent resistant polyketone (PK) polymer was introduced for the first for preparing PK membrane used as the support membrane for OSN membrane fabrication. Polyelectrolytes and single walled carbon nanotube (SWCNT) were used as polycation and polyanion for OSN membrane active layer formation. The effects of membrane fabrication conditions such as bilayer numbers, polyelectrolytes concentrations, nanomaterial concentrations, and cross-linking conditions were investigated in terms of membrane separation performances. In addition, the effects of different cross-linkers: glutaraldehyde (GA), (±)-epichlorohydrin (ECH) and trimesoyl chloride (TMC) on OSN membrane performances were further investigated.

Moreover, ML was used to form prediction models for thin film nanocomposite (TFN) OSN membrane performance evaluation in terms of relative permeability (RP) and relative selectivity (RS). Twenty references including 9252 data points were collected to form four different models: linear, support vector machine (SVM), boosted tree (BT), and artificial neural network (ANN). Among the four models, BT exhibited optimal prediction accuracy in terms of root mean square error (RMSE) and coefficient

of determination (R^2) values for membrane RP (RMSE: 0.295, R^2: 0.918) and RS (RMSE: 0.053, R^2: 0.849) performance prediction.

Overall, this thesis validated and broadened the use of inkjet printing technology and machine learning models as promising methods for nanocomposite OSN membrane fabrication and performance prediction, which may open a new avenue for OSN membrane development.

CHAPTER 1
Introduction

1.1 Research background

Organic solvents are frequently used as reaction agents for organic syntheses in chemical and pharmaceutical industries. Those organic solvents show different degrees of toxicity which could result in health risk upon human exposure (Marchetti, Jimenez Solomon, Szekely, & Livingston, 2014). Distillation and evaporation can be used for recovering organic solvents, but both of the processes are expensive and consume large amount of energy, thus not sustainable in terms of energy consumption (Hermans, Mariën, Van Goethem, & Vankelecom, 2015; Rundquist, Pink, & Livingston, 2012). Therefore, a greener process OSN, provides an attractive alternative for the reuse and recovery of organic solvents due to its economic and environmental benefits (Marchetti et al., 2014; Vandezande, Gevers, & Vankelecom, 2008; A. V. Volkov, Korneeva, & Tereshchenko, 2008). In OSN process, OSN membranes are the most important factor influencing the separation performances. However, most of existing OSN membranes still face many issues, such as organic solvent stability and low solvent permeability, which impede the further development of OSN technology (Ali, Shah, Ihsanullah, & Feng, 2022). Therefore, the fabrication of high performance and chemically stable OSN membranes are essential to accelerate the OSN applications.

Unlike conventional nanofiltration (NF) membranes which separate solutes at nanoscale in aqueous systems, OSN membranes are used in different organic solvent systems, thus these membranes require good physical and chemical stability. TFC membranes are the most commonly used OSN membranes. Polyacrylonitrile (PAN), polypropylene (PP), polysulfone (PSF), and polyimide (PI) are commonly used support membranes for TFC NF membrane preparations (Cheng et al., 2014; S. K. Lim, Goh, Bae, & Wang, 2017; Yang et al., 2021); however, in most conditions, these materials can only be used in separation of mild organic solvents such as ethanol or methanol, or they need further post-treatment (i.e. chemical cross-linking) to increase their stability in other harsh organic solvents. Thus, it is necessary to fabricate excellent solvent resistant support membrane for OSN applications.

LBL assembly is an effective method for fabricating TFC membranes (Ahmad et al., 2022; Ahmad, Goh, Wong, Zulhairun, & Ismail, 2020; C. Wang, Park, Yu, et al., 2022). The LBL assembly typically involves the sequential adsorption of oppositely charged materials via attractive forces such as electrostatic interactions, charge transfer

interaction, covalent bonding, hydrogen bonding, and van der Waals forces. Because of its unique properties, such as versatility, cost-effective strategy, and nanoscale controllability, the LBL method has gained increasing interest in membrane field (Q. Chen et al., 2015; X. Liu et al., 2013). Conventional methods for LBL membrane preparations include dip coating, spray coating and spin coating (Cho, Char, Hong, & Lee, 2001; Kolasinska, Krastev, Gutberlet, & Warszynski, 2009; D. S. Liu et al., 2013), however, these approaches often face certain disadvantages impeding their extensive applications. For example, the dip coating method requires the lengthy preparation steps and consumes large volume of polyelectrolyte solutions which limit its commercial applications (Wood, Chuang, Batten, Lynn, & Hammond, 2006). Spray coating, on the other hand, lacks the control of chemical droplet size, uniformity and velocity. In addition, the waste of numerous polyelectrolyte solutions during the LBL process implies that it is not a green technology (Schlenoff, Dubas, & Farhat, 2000). Spin coating method also produces large amounts of chemical and polymer wastes. Besides, the numerous rinsing steps limit its scalable production (Kiel et al., 2010; Patel, Dobrynin, & Mather, 2007). Considering the limitations of conventional LBL methods, novel LBL methods should be developed.

There are several models applied for OSN performance predictions, such as the solution-diffusion model (J.G. Wijmans, 1995) and the pore-flow model (J. L. Anderson, 1974). However, all these models need to regress some parameters to predict the organic solvent flux and solute rejection at different operating conditions under a fixed chemical system, which limits the development of OSN technique. Therefore, more effective membrane performance prediction models need to be explored for OSN applications.

1.2 Research objectives and scope

Recently, inkjet printing technique has gained increasing interest for various membrane fabrications. The benefits of inkjet printing method include uniform deposition, small amount of materials used, and simple and fast operation steps. This study systematically investigates inkjet printing technique as an alternative LBL assembly method for nanocomposite OSN membrane fabrication. Solvent resistant PK polymer is introduced for the first for preparing PK membrane used as the support membrane to increase OSN membrane solvent stability. In addition, the emergence of ML has become an important data-driven method in chemical and material

engineering field. Considering the advantages of ML, this study utilized ML based models for OSN membrane performance prediction. Specific objectives of this thesis are presented below:

• Fabricate PK support membrane for OSN membrane fabrication to improve the membrane solvent stability.

• Evaluate inkjet printing assisted LBL assembly as an effective method for nanocomposite OSN membrane fabrication.

• Investigate the effects of different cross-linkers on OSN membrane performances.

• Explore and compare different ML models for TFN OSN membrane performance prediction.

1.3 Structure of the study

The structures of the thesis are summarized as below:

Chapter 1 includes the research background, research objectives and scope.

Chapter 2 provides a comprehensive literature review about different kinds of nanocomposite OSN membranes and detailed membrane fabrication processes.

Chapter 3 demonstrates the experimental methods used in this thesis for membrane fabrication, membrane characterizations, and performance evaluation.

Chapter 4 investigates inkjet printing assisted LBL deposition of polyelectrolytes and SWCNT for OSN membrane fabrication.

Chapter 5 further improves the OSN membrane separation performance and evaluates the effect of different cross-linkers for OSN membrane preparation.

Chapter 6 utilizes the ML based models for nanocomposite OSN membrane performance prediction.

Chapter 7 summarizes the conclusions obtained from these studies and provides recommendations for future studies.

CHAPTER 2
Literature review

2.1 Introduction

Organic solvent nanofiltration (OSN), also named as solvent resistant nanofiltration (SRNF) is a relatively new technology that received substantial attention recently. In OSN process, small solvent molecules permeate through the OSN membrane, while the solutes with a molecular weight between 200 and 2000 Da will be rejected (Buonomenna & Bae, 2014; Marchetti et al., 2014; Peshev, Peeva, Peev, Baptista, & Boam, 2011; Vandezande et al., 2008). Compared to the conventional organic solvent separation technologies, OSN process possess several advantages. Firstly, energy consumption is relatively low compared to the distillation and crystallization process requiring high thermal energy (Hermans et al., 2015; Rundquist et al., 2012). Secondly, the operating conditions are significantly milder and no additional additives or chemicals are needed. Lastly, OSN can operate continuously and can also be combined with existing separation techniques to form a hybrid processes (Priske, Lazar, Schnitzer, & Baumgarten, 2016; Vandezande et al., 2008). These advantages offer OSN a great potential to be applied in different types of industries including the food (Teixeira, Santos, & Crespo, 2014; A. V. Volkov et al., 2008), pharmaceutical (Abejón, Garea, & Irabien, 2014; Székely, Bandarra, Heggie, Sellergren, & Ferreira, 2011), fine chemical (Ferreira, Macedo, Cocchini, & Livingston, 2006; Mertens et al., 2007; Valadez-Blanco, Ferreira, Jorge, & Livingston, 2008) and petrochemical industries (Lloyd S White, 2006; Lloyd S White & Wildemuth, 2006). Despite of these clear advantages, there are key challenges which impede the further widespread of OSN for various applications. One of the main challenges is the development of effective and high performing OSN membranes that can be stable in a wide range of organic solvents and at the same time maintaining good membrane performances under harsh operating conditions such as harsh organic solvents, high temperature and elevated pHs (He et al., 2019).

Polymeric membranes are considered to be a favourable candidate for OSN membranes. Compared to ceramic membranes, polymeric membranes have numerous advantages including the large number of available polymers, relatively easy and mild fabrication conditions involved in membrane manufacturing, relatively low cost and the ease of modification and upscaling (Cheng et al., 2014). Despite the numerous advantages of polymeric OSN membranes, unfortunately, most of polymeric materials and membranes face chemical and thermal instability limitations. The interactions

between organic solvents and polymeric membranes can cause the extensive swelling of the membranes and in severe cases, it leads to dissolution of polymers, which contributes to the loss of membrane stability as well as its selectivity. Moreover, the solvent transport mechanism through OSN membranes is complex and complicated than the mechanism for water permeation through NF membranes. Even if the same membrane material is used, different organic solvents may have different interactions with membrane. Besides, the rejection of the same solute in different organic solvents may also be affected by the interaction between the solvents, solutes and the membranes, which complicates the OSN processes (Davood Abadi Farahani, Ma, & Nazemizadeh Ardakani, 2018; S. K. Lim et al., 2017). Thus, preparing the OSN membranes with the high stability in various organic solvents along with the good permeability and selectivity under various organic solvents are the key research gaps that need to be addressed in near future.

Currently, two types of polymeric OSN membranes are used which are integrally skinned asymmetric membranes (ISA) and TFC membranes. For ISA membranes, the skin layer and the porous support layer are made of the same polymeric material. For TFC membranes, the active layer is deposited on top of a support layer which are made up of different polymeric materials (Hermans et al., 2015). Therefore, active layer and support layer of TFC membranes can be modified independently to improve the membrane performance tailored to a targeted molecule or solvent recovery (S. K. Lim et al., 2017). Moreover, varying polymeric materials have significant influence on the performances of OSN membranes. To this date, various polymers are used for preparing OSN membranes, including PAN (Abadikhah et al., 2019), PP (Roy, Ntim, Mitra, & Sirkar, 2011), polyamide (PA) (Maria F Jimenez Solomon, Bhole, & Livingston, 2013; Maria Fernanda Jimenez Solomon, Bhole, & Livingston, 2012), polydimethylsiloxane (PDMS) (Aerts et al., 2006; Gevers, Aldea, Vankelecom, & Jacobs, 2006), PI (Soroko, Lopes, & Livingston, 2011; Soroko, Makowski, Spill, & Livingston, 2011), poly(1-(trimethylsilyl)-1-propyne) (PTMSP) (A. Volkov et al., 2012; Alexey V Volkov et al., 2009), polypyrrole (PPy) (Xianfeng Li, Vandezande, & Vankelecom, 2008), polyurethanes (PU) (Florian, Modesti, & Ulbricht, 2007), polyphenylsulfone (PPSU) (Darvishmanesh, Jansen, et al., 2011; Darvishmanesh, Tasselli, et al., 2011), polybenzimidazole (PBI) (Farahani & Chung, 2019; Xing, Chan, & Chung, 2014), polyaniline (PANI) (Sairam et al., 2010), polyether etherketone

(PEEK) (Hendrix, Koeckelberghs, & Vankelecom, 2014), and PSF (Hołda, De Roeck, Hendrix, & Vankelecom, 2013) et al.

Recently, there is an increasing interest in incorporating nanomaterials into OSN membranes to further improve their separation performances. Various types of nanomaterials such as metal organic frameworks (MOFs) (Yi Li, Li, Soria, Volodine, & Van der Bruggen, 2020), graphene oxide (GO) (S. Wang, Mahalingam, Sutisna, & Nunes, 2019), carbon nanotube (CNT) (Davood Abadi Farahani, Hua, & Chung, 2018), gold (Yanbo Li, Verbiest, & Vankelecom, 2013) and silicon oxide (S. Yuan et al., 2018) have been investigated for the fabrication and modification of OSN membranes. Regarding the various approaches of nanomaterial incorporation for the nanomaterial-based OSN membranes can be classified as follows: (a) embedding nanomaterials into membrane support; (b) incorporation of nanomaterials in the active layer of membranes; (c) surface deposition of nanomaterials on the membrane substrate (nanomaterial coating acting as an active layer); (d) addition of nanomaterials in both active and the support layer; (e) nanomaterials serving as an interlayer between support and the active layer. A schematic overview of above-mentioned strategies for OSN membrane fabrication is shown in **Fig. 2.1**.
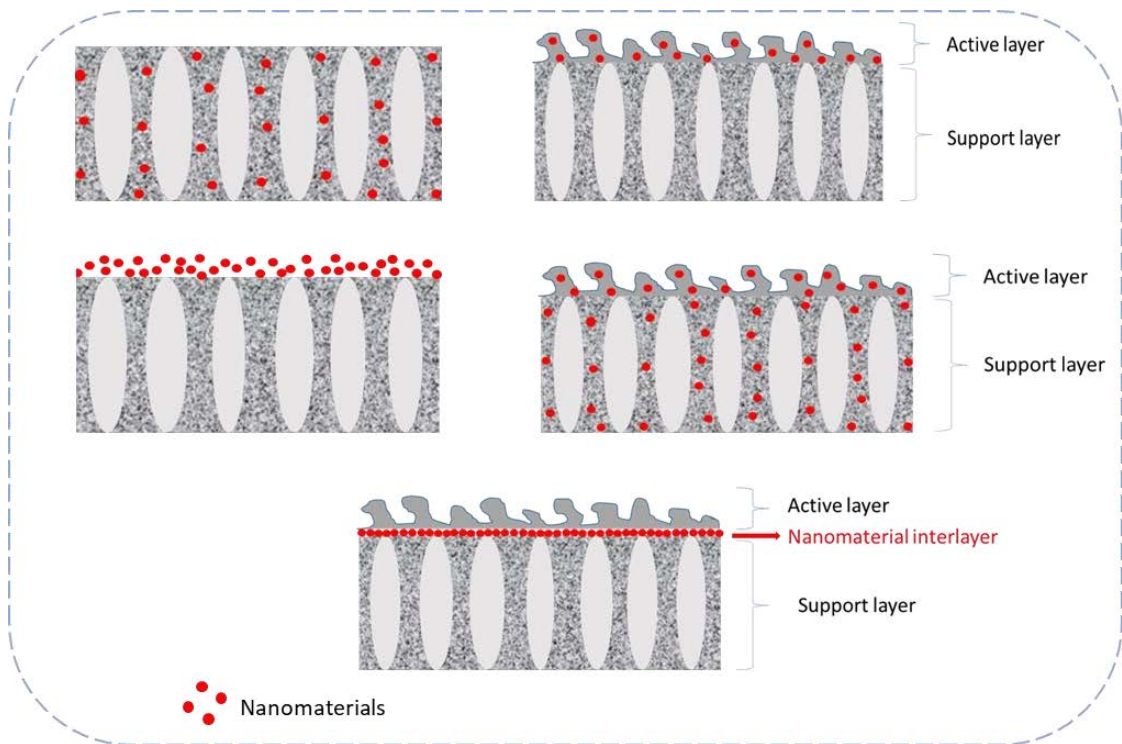
Fig. 2.1. Schematic of nanocomposite membranes produced by different methods: (a) nanomaterial-incorporated in the support layer; (b) incorporation of nanomaterial into

active layer; (c) thin film coating of nanomaterial on the surface of support membrane; (d) embedding nanomaterial into both active layer and the support layer; (e) nanomaterial acting as an interlayer.

In this literature review we aim to provide an overview on the developments of various nanomaterial-based nanocomposite OSN membranes where nanomaterials are incorporated into support layer, active layer, coating on the surface, both active and support layer, and severing as an interlayer. Moreover, this review also discusses the different fabrication methods involved and the improvements in OSN membrane performances when using different types of nanomaterials.

2.2 Nanomaterial-modified substrates

The relative low solvent permeate flux is one of the significant issues impeding the OSN membrane and process implementation in wide range of applications (Buonomenna & Bae, 2014). To address the low solvent permeability problem, various nanomaterials are proposed to be added into polymer matrix for mixed matrix membranes (MMMs) fabrication. The most commonly used method for MMMs preparation is non-solvent induced phase inversion as illustrated in **Fig. 2.2**. Nanomaterials including MOFs, gold nanoparticles, GO, CNTs, SiO_2 and TiO_2 have been used for substrate modifications.
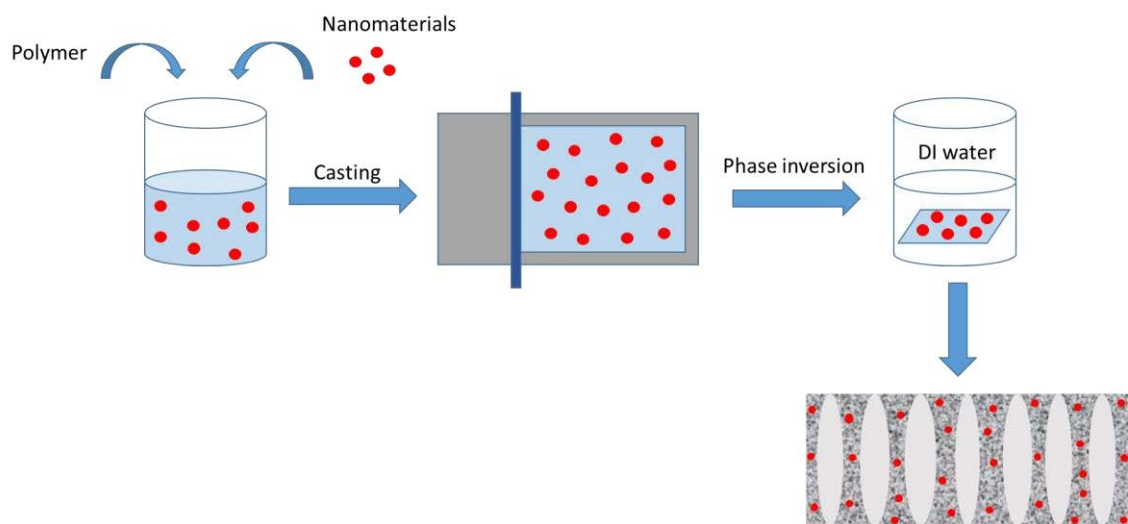
Figure 2.2. Typical steps involved in non-solvent phase inversion for OSN membrane fabrication with nanomaterial-incorporated into substrate.

2.2.1 Metal organic frameworks (MOFs)

MOFs is a type of crystalline material which consists of metal ions incorporated in organic ligands framework. Due to its highly ordered nanoporous structures and large surface area, MOFs could be a suitable candidate for OSN application. Initially, researchers attempted to synthesize the free-standing MOFs membranes, yet, due to the crystalline nature of MOFs, made the free-standing MOFs membrane to be brittle and inflexible, difficult to be incorporated in the membrane module impeding its practical implementation (Meng et al., 2019; Shu et al., 2020). To overcome such limitation, researchers attempted to synthesize the hybrid polymer/MOF membranes which utilize both advantages of polymer (flexibility and mechanical strength) and MOFs (large surface area with high porosity). The most common method used for incorporating MOF nanoparticles into membrane matrix is non-solvent induced phase inversion technique. The prepared membranes present dense surface with an asymmetric morphology.

For example, Karimi et al. (Karimi, Khataee, Safarpour, & Vatanpour, 2020) synthesized zeolitic imidazolate framework 8 (ZIF-8) based membranes, where ZIF-8 nanoparticle sizes of 80 to 100 nm were incorporated into the matrix of polyvinylidene fluoride (PVDF). The ZIF-8 modified PVDF membranes were prepared with ZIF-8 concentrations of 5, 10, 20, 15, 20, and 25 wt%. The MMMs with a ZIF-8 concentration of 25 wt% exhibited rejection of 99.5% and 99.2% for Rose Bengal (RB, 1017 Da) in IPA and ethanol, whereas rejections of RB were 88.4% and 82.7% for pristine PVDF membrane. During the filtration of RB in IPA, only 4.1% flux reduction was observed for MMM with 25 wt% ZIF-8 incorporation, whereas pristine PVDF membrane presented large flux reduction of 16.1%. In the membrane swelling studies, the ZIF-8 modified membranes exhibited lower degree of swelling compared to pristine PVDF membrane in both IPA and ethanol solvents due to reduced pore sizes for large molecule diffusion. For example, in the long term (24 h) filtration of RB in IPA solvent, the pristine PVDF membrane revealed 34% flux reduction, while the ZIF-8 modified membrane only exhibited 9% reduction. However, the structure of ZIF-8 was found to be degraded in polyamide acid solution (an acidic environment) when used for preparing PI based MMMs demonstrating a potential limitation of using ZIF-8 MOFs in MMMs.

Wang et al. (Z. Wang et al., 2019) proposed direct carbonization as a possible approach for transferring the coordinating linkers of ZIF-8 into carbon skeleton. Due to the enhanced porosity and sorption ability, the MMMs exhibited improved permenaces for both water and organic solvent. For example, the composite membrane with 10 wt% carbonized ZIF-8 incorporation showed ethanol permeance of 4.05 L m^{-2} h^{-1} bar^{-1} with congo red rejection of 94.29%. Moreover, all the MMMs were soaked in organic solvents including ethanol, acetone, IPA and N,N-dimethylacetamide (DMAC) for 1 week with negligible weight losses, demonstrating their good stability in organic solvents. Sani et al. (N.A.A. Sani, 2015) investigated the effect of MOFs nanoparticle loadings on the MMMs performance. In this study, MMMs with different loadings of copper-1, 3, 5-benzenetricarboxylate (Cu-BTC) nanoparticles into PPSU membranes were prepared. Results showed that the pure methanol flux of the MMMs with 3 wt% Cu-BTC loading significantly improved > 135 L m^{-2} h^{-1} compared to the pristine PPSU membrane of 102 L m^{-2} h^{-1}. The improvement in solvent flux is caused by the preferential channels for solvent permeation and the interfacial voids created by Cu-BTC providing alternative paths for solvents transportation. In the long-term filtration test (24 h) in methanol containing RO16 dye, the PPSU/Cu-BTC membrane suffered nearly 18.5% and 17.5% decline in permeate flux and dye rejection, respectively, compared to its initial flux and rejection rates. Moreover, this study also revealed that the low concentrations of Cu-BTC incorporation (between 0.5 to 1.0 wt%) in PPSU were observed to exhibit smaller molecular weight cut-off (MWCO) and better separation efficiency than that of pristine PPSU & high concentration Cu-BTC incorporated in PPSU. Such improved performance of low Cu-BTC loading is probably due to the better dispersion and the improved interfacial contact with membranes. This research team also evaluated the influence of varying organic solvents and operating conditions of MMMs on OSN performances (Sani, Lau, Nordin, & Ismail, 2016). The pure methanol flux and the Reactive Orange 16 rejection (RO16, 617.5 Da) were compared before and after pre-treatment with different solvents (methanol, ethanol, IPA, acetonitrile, ethyl acetate, n-hexane and n-heptane) for 48 h. Results showed that the pre-treatment with various solvents could change the hydrophilicity/hydrophobicity of membrane surface resulting in different methanol flux and dye rejection performances. This phenomenon arises mainly due to the reformation of polymeric chains when in contact with organic solvents. They also found that increasing a dye concentration could affect the dye rejection rate without

much variation in methanol flux. In all cases, the PPSU membrane with 0.8 wt% Cu-BTC nanoparticle incorporation presented better separation performance than that of the pristine PPSU membrane. During 180 min filtration of pure methanol, the PPSU-0.8 wt% Cu-BTC membrane only exhibited 8% flux decline, while for the pristine PPSU membrane, observed flux decline was 26%.

Zhu et al. (Zhu et al., 2015) fabricated MMMs via non-solvent induced phase inversion method using poly(m-phenyleneisophthalamide) (PMIA) and MIL-53(Al) as polymer matrix and MOF nanoparticles. Compared to the pristine membrane, the resultant MMMs showed significant higher ethanol permeate flux (improved 289%) and a slightly reduced Brilliant blue G (BBG, 854 Da) rejection (reduced by 4%). The optimum modified membrane (with 0.5 wt% MIL-53(Al)) had a mean pore size of 0.7 nm and could enable passage of mono and divalent salts but rejecting larger organic molecules. They also investigated the influence of organic solvents on the MMMs performance. It was demonstrated that after 10 days of exposure treatment with ethyl acetate or methanol, the modified membrane presented a lower permeate flux but a higher salt rejection.

Gao et al. (Z. F. Gao, Feng, Ma, & Chung, 2019) modified a series of MMMs containing amine-functionalized UiO-66 nanoparticles via vapor-phase crosslinking with tris (3-aminopropyl) amine (TAPA) away from traditional non-solvent induced phase inversion process. After the vapour-phase crosslinking, a thin selective layer was successfully formed on top of a MMMs, which improved the membrane performance in OSN application. Under the optimum condition, the modified membrane showed a 99.2% rejection of RB in IPA and a pure IPA flux which reached up to 11.5 L m^{-2} h^{-1} under 10 bar. Moreover, the vapour-phase cross-linked MMMs presented stable membrane performance under different organic solvents and a long term 14-day rejection test. Such vapour-phase crosslinking method holds great promise in fabricating high performing MMMs based OSN membranes for the separation of organic solvents and solutes in food and pharmaceutical industries.

Campbell et al. (Campbell, Székely, Davies, Braddock, & Livingston, 2014) also introduced an alternative method from the commonly used non-solvent induced phase inversion, which is in-situ growth (ISG) of MOF nanoparticle (HKUST-1) in polymer membrane support layer for hybrid membrane fabrication. The ISG method was also

compared with a mixed matrix membrane synthesized by conventional non-solvent induced phase inversion technique. Results showed that the membranes fabricated by ISG method exhibited uniform distribution of HKUST-1 nanoparticles across the membrane surface and throughout the cross-section, which is different from the MMMs structure with discrete nanoparticles spread across the continuous polymer phase. The OSN performances of membranes produced by both approaches were tested and compared with the pristine polymeric UF membrane. Compared to the pristine UF membrane, the solute rejection was improved when using MMMs synthesized by non-solvent induced phase inversion, while the polystyrene oligomer rejections of the membrane fabricated by ISG method demonstrated further enhancement in rejection compared to the pristine UF membrane as well as MMMs synthesized by the conventional approach. Moreover, the addition of HKUST-1 nanoparticles via ISG method was found to have a positive effect on flux decline compared to the MMMs synthesized via the conventional approach. Furthermore, ISG membranes exhibited a lower decline in acetone flux over time (24 hrs) compared to the MMMs synthesized by the conventional approach. Overall, various approaches and MOFs materials are being implemented to synthesize varying MMMs membranes for OSN applications. In the future, research efforts should be directed toward finding ways to improve the adhesion between polymer and MOF nanoparticles which will lead to further enhancement in membrane performances.

Despite the MOF-based membranes presenting several advantages, there are still challenges to be addressed, such as the uniformity of MOF particle sizes and their dispersion & distribution in the polymer matrix. As nanoparticles tend to form an agglomeration when making these MMMs they act as defect sites in the membranes. One strategy to solve such MOFs nanoparticle agglomeration issues is to modify the MOF particles to improve the arrangement and distribution in the polymer.

For example, Dai et al. (Dai et al., 2019) grew microporous ZIF-8 nanoparticles on the outer surface of the macroporous resin microspheres (RMs) where macroporous RMs acted as a skeleton which prevents the MOFs nanoparticle agglomeration. Then it was mixed with PPSU solution to fabricate high-performance OSN membrane. The obtained PPSU/ZIF-8@RMs membranes demonstrated higher solute rejection compared to PPSU/ZIF-8 and PPSU/RMs membranes, due to the ZIF-8 shells' microporosity and the microsphere structure which reduced the defects between ZIF-

8@RMs and PPSU. The optimal PPSU/ZIF-8@RMs membrane with the filler concentration of 5.0 wt% presented significantly improved Methyl red (MR, 269.3 Da)) rejection of 88.8% compared to the pristine PPSU membrane which exhibited 53% rejection of MR. However, methanol flux was slightly decreased from 35.2 kg m^{-2} h^{-1} of the pristine PPSU membrane to 33.0 kg m^{-2} h^{-1} for the PPSU/ZIF-8@RMs at 1.0 MPa of applied pressure. Under the 12 hrs of OSN performance test, the PPSU/ZIF-8@RMs membrane with 5 wt% nanofiller concentration remained stable in methanol and the MR rejection was maintained at 86.2%.

Yang et al. (H. Yang et al., 2018) synthesized MMMs through the vacuum-assembly method by co-deposition of ZIF-8@GO composites and poly(ethyleneimine) (PEI) solution on a tubular ceramic substrate (see **Fig. 2.3 (a)**). The ZIF-8@GO composites were prepared by in-situ growth of ZIF-8 nanoparticles onto the surface of GO sheets. ZIF-8@GO nanocomposites reveal several advantages as a nanofiller material due to their high surface areas, large pore volumes and most importantly reducing the agglomeration of ZIF-8 nanoparticles in the MMMs. The metal ions contained in ZIF-8 nanoparticles could coordinate and bind with carboxyl groups in GO, leading to the uniform dispersion of ZIF-8 in the GO surfaces. MMMs performance was evaluated in terms of methanol permeate flux and dye molecule rejection. Compared to the ZIF-8/PEI membrane, the methanol permeate flux of the ZIF-8@GO composite membrane was increased with dye rejection of 99.1%. The enhanced performance is due to the uniform dispersion of ZIF-8 particles in PEI substrate, which provides well-defined pathways for organic solvent permeation. During the filtration time of 660 min, the methyl blue rejection of the ZIF-8@GO composite membrane remained above 99% with methanol permeance around 5 L m^{-2} h^{-1} bar^{-1}, indicating its good stability in methanol solvent. In addition, the tubular membrane modules have high packing density, which demonstrates great potential as a module design for industrial-scale OSN processes.

Li et al. (Y. Li et al., 2020) synthesized bound branched PEI on a ZIF-8 surface which lead to uniform distribution of ZIF-8 in the aramid nanofibers (ANFs) (see **Fig. 2.3 (b)**). It is shown that the ZIF-8 was intercalated in the ANFs producing a porous network structure, which increase the porosity of the membrane from 23.3% to 56.9%. Compared to the pristine ANF membrane, the nanocomposite membranes exhibited two times higher permeate flux for both polar solvents (methanol, ethanol, IPA,

acetone, and tetrahydrofuran) and non-polar solvents (hexane and carbon tetrachloride). For the long-term OSN performance test (6 hrs), the nanocomposite membranes showed ethanol and IPA permeances of 2.9 and 1.8 L m^{-2} h^{-1} bar^{-1} respectively, and erythrosine B rejection over 90%. Furthermore, the modified membranes presented good chemical stability with permeances of 28.0 L m^{-2} h^{-1} bar^{-1} for acetone, 4.7 L m^{-2} h^{-1} bar^{-1} for ethanol, and 2.4 L m^{-2} h^{-1} bar^{-1} for hexane. Such highly porous nanocomposite membranes open a new avenue for fabricating high-performance OSN membranes with one-dimensional nanofibers and highly porous MOF nanoparticles.
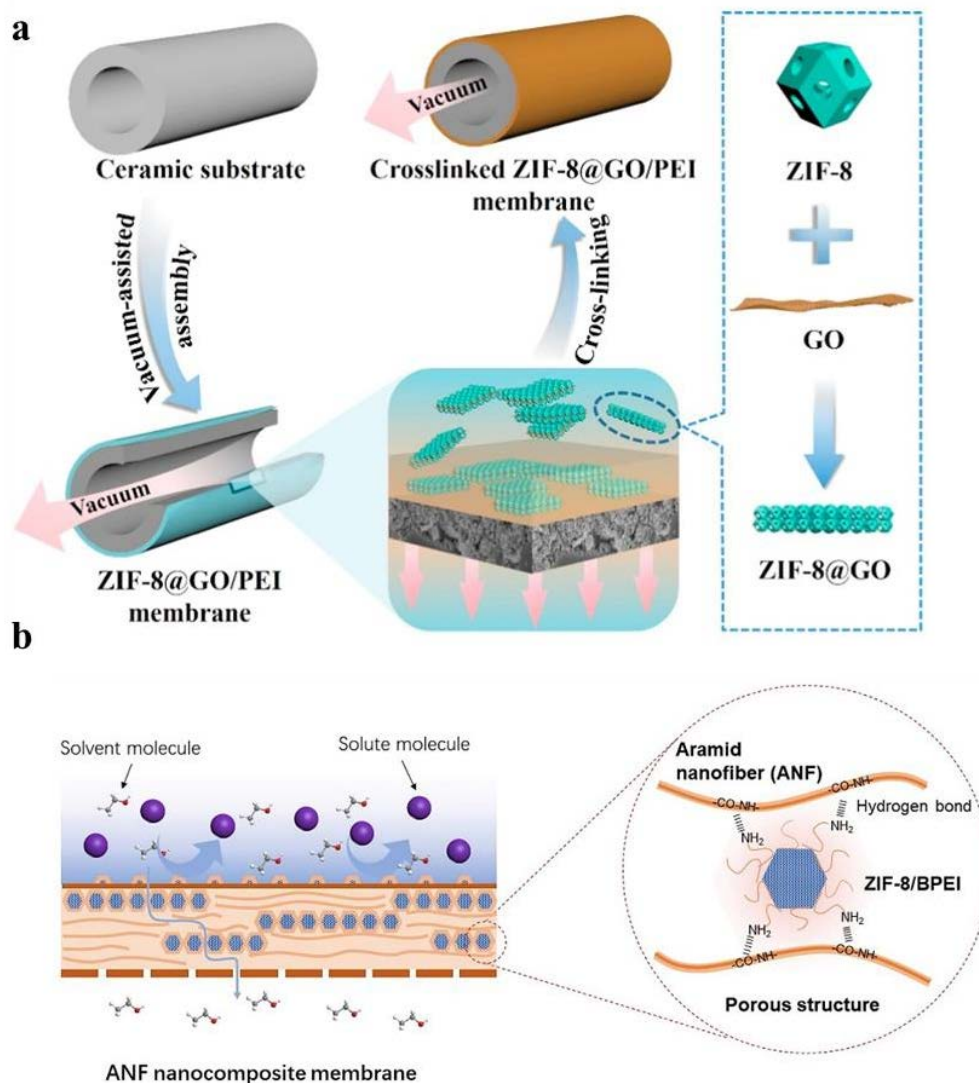
Fig. 2.3. (a) Schematic illustration of fabrication of crosslinked ZIF-8@GO/PEI composite membrane on tubular ceramic substrate via a vacuum-assisted assembly method (adapted from Ref.(H. Yang et al., 2018)). (b) Illustration of the separation

mechanism and molecular permeation in ANF nanocomposite membrane (adapted from Ref.(Y. Li et al., 2020)).

2.2.2 Gold nanoparticles

Gold nanoparticles (GNPs) can effectively generate heat under the irradiation of light, converting the photon energy into thermal energy (photothermal or plasmonic effect). Under light illumination, mobile carriers of the gold nanoparticles are excited and during the relaxation process often energy is released in the form of heat energy, leading to the elevation of temperature surrounding the medium (Esfahani et al., 2019; H. J. Kim et al., 2020). Based on such a mechanism, the nanocomposite membranes containing GNPs can be locally heated by light illumination typically via laser irradiation. The degree of generated heat depends on the number of nanoparticles, the laser light intensity, and the thermal properties of polymers.

For example, Li et al. (Yanbo Li et al., 2013) successfully applied localized membrane heating for hydrophobic membranes by in-situ incorporation of GNPs in PDMS membranes. Transmission electron microscopy (TEM) images proved that the GNPs were uniformly dispersed in the membrane matrix. Under laser irradiation (laser intensity of 0.3 W/cm^2), about 30-60% permeate flux increase was observed for ethanol and a 20% increase for IPA. When the laser intensity was 0.5 W/cm^2, the ethanol permeate flux could improve by up to 200%. The rejections for bromothymol blue and methyl orange (MO) were 98.8% and 99.7% without irradiation, 97.1% and 99.5% with laser irradiation, where no significant reduction in selectivity was observed.

Vanherck et al. (Vanherck, Vankelecom, & Verbiest, 2011) prepared nanocomposite membranes by mixing different amounts of GNPs with PI polymer. The modified membranes were locally heated during the filtration tests by the irradiation of continuous green laser light (visible range). The results show that pure IPA flux could increase by 50% and even up to 168% with different GNPs concentration when considering only the irradiated surface of membranes. Although, localized heating of the membrane had no significant effect on the solute rejection. Overall, localized heating could improve the membrane performances in OSN applications. To further prove the concept, Vanherck and his colleagues fabricated cellulose acetate NF membranes containing different amounts of GNPs(Vanherck, Hermans, Verbiest, &

Vankelecom, 2011). The effect of photothermal heating on the membrane flux and selectivity was evaluated by continuous irradiation of an argon-ion laser using a 514 nm light filter. The work demonstrates that the membrane with GNPs and polymer weight ratio which are less than 2%, the water flux was increased by 15%, and the pure ethanol and IPA fluxes could improve up to 400%. Yet, similar to their previous study the photothermal heating had no significant effect on the rejection of bromothymol blue in ethanol filtration. Another study from this research group compared different synthesis methods to fabricate GNPs containing PI membranes (Vanherck, Verbiest, & Vankelecom, 2011). One method was by in-situ chemical reduction of GNPs, other is by the formation of a composite using preformed poly(vinylpyrrolidone) (PVP) and GNPs. In both synthesis routes, the GNPs were synthesized with an average size of 3 nm on the top surface of the membranes. Yet, there was a significant difference in the GNPs distributions and the membrane behaviours. The preformed PVP/GNPs led to a higher porosity in the membranes, yet the GNPs were easily aggregated. When the GNPs were incorporated via an in-situ chemical reduction process, well-dispersed GNPs with smaller particles were formed in the dense top surface layer, and the larger particles were in the porous substrate. The influence of fabrication methods on the OSN membrane performances was investigated by filtrations of dyes in ethanol and IPA solvents. For membranes fabricated by both approaches, under plasmonic heating of GNPs, higher solvent permeance was achieved without sacrificing the rejection rate of dyes.

2.2.3 Graphene oxide (GO) and carbon nanotubes (CNTs)

GO is a two-dimensional (2D) nanomaterial derived from the chemical exfoliation process of graphite. It consists of carbon atoms arranged in a hexagonal lattice along with different kinds of functional groups being attached (hydroxyl, carbonyl, carboxyl, and epoxide groups) (D. Ji et al., 2019; M. J. Park et al., 2015). GO can be used in membrane fabrication either as a laminate or mixed with polymers (Liang Huang, Li, Zhou, Yuan, & Shi, 2015; S. Lim et al., 2018; M. J. Park et al., 2019; Zinadini, Zinatizadeh, Rahimi, Vatanpour, & Zangeneh, 2014). There are various techniques to prepare GO-based membranes, such as dip-coating, spin-coating, spray-evaporation, drop casting, vacuum filtration, and layer-by-layer assembly (Guan et al., 2017; Lou, Liu, Liu, Shen, & Jin, 2014; Nair, Wu, Jayaram, Grigorieva, & Geim, 2012; Nan, Li, & Cao, 2016; P. Sun et al., 2013). Previously, GO-based membranes are mainly

developed for gas separation and desalination applications (Abraham et al., 2017; H. W. Kim et al., 2013). However, recently, many research efforts are made to include GO in membranes for other molecular separations such as in the field of OSN, and demonstrated a promising result.

For example, Fei et al. (Fei, Cseri, Szekely, & Blanford, 2018) incorporated GO into hydroxylated PBI via blade coating and phase inversion to fabricate mixed matrix composite membranes. Based on the visible-light microscopy data, the GO particles were evenly distributed in the membranes. Compared to the pristine PBI membrane, the composite membrane exhibited 5 times higher permeance in acetone, up to 45.2 ± 1.6 L m^{-2} h^{-1} bar^{-1} without compromising the solute rejections. Moreover, GO-modified membranes exhibited good chemical stability under various organic solvents including acetone, toluene, DMF, THF, methanol, dichloromethane, and acetonitrile, and demonstrated an MWCO of 140 g mol^{-1}. Furthermore, the GO composited membrane achieved a solute rejection (over 93% for Mepenzolate, 420 g mol^{-1}) in both polar and non-polar solvents.

Many researches have demonstrated the benefits of incorporating CNTs into membranes to improve separation performance (Peng, Hu, & Jiang, 2007; Shawky, Chae, Lin, & Wiesner, 2011). CNTs possess unique properties including high flexibility and mechanical strength, the ability to facilitate fast water/solvent transport across the surfaces of CNTs and high surface area with the presence of numerous nanochannels for water/solvent permeation (Rashid & Ralph, 2017; Tasis, Tagmatarchis, Bianco, & Prato, 2006; Vatanpour, Esmaeili, & Farahani, 2014). However, due to the poor and unstable dispersion in water, CNTs need to be functionalized with functional groups such as -OH, -COOH, -COH or -NH$_2$ to improve the dispersion of CNTs in aqueous solvents for membrane fabrications (C. H. Park et al., 2016).

Farahani et al. (Davood Abadi Farahani, Hua, et al., 2018) utilized amine-functionalized multi-walled carbon nanotubes (NH$_2$-MWCNTs) to design MMMs for OSN application. The addition of NH$_2$-MWCNTs into P84 (a commercial polyimide) matrix promoted the membrane porosity and permeability. Compared to the pristine P84 membrane, the prepared MMMs exhibited higher water, ethanol, and IPA permeances. For the MMMs containing 2 mg/g of NH$_2$-MWCNT/P84, the rejection

of Eosin Y (EY, 691.86 Da) was above 98% and the permeance of water, ethanol and IPA was achieved (16.4, 3.3, and 1.4 L m^{-2} h^{-1} bar^{-1}, respectively). Moreover, thermal annealing was introduced to further increase the separation performance of MMMs to smaller solutes. Results showed that after the annealing process at 120°C for 40 min, the OSN membrane showed rejection of 92.1% for tetracycline (MW of 444 g/mol) in IPA solvent. Moreover, annealed MMMs had higher ethanol flux and solute rejections than the control P84 membrane. Furthermore, the 72 hours continuous IPA solvent permeation test revealed that the synthesized MMMs exhibited stable OSN performances. Another study from this research group fabricated MMMs consisting of different concentrations (0.01, 0.03, 0.05, 0.075, and 0.1 wt. %) of carboxyl-functionalized MWCNTs (MWCNTs-COOH) and P84 with 1, 6-hexanediamine acting as a cross-linker for OSN application (Davood Abadi Farahani, Hua, & Chung, 2017). The study reveals that when the MWCNTs-COOH loading was increased from 0.01 to 0.075 wt%, the permeances of water, ethanol, and IPA were increased. However, a higher loading of CNTs reduced the separation performances. Moreover, the synthesized MMMs with 0.05 wt% MWCNTs-COOH, exhibited varying membrane performances under different organic solvents where ethanol permeance of 9.6 L m^{-2} h^{-1} bar^{-1} with RB rejection of 85% was achieved, while IPA permeate flux of 1.8 L m^{-2} h^{-1} bar^{-1} with RB rejection of 99% was achieved. To further enhance the OSN performance of the membrane, thermal annealing with a 3/1 ethylene glycol (EG)/Poly(ethylene glycol) 400 (PEG400) (weight ratio) solution was conducted, the post-annealed MMMs (0.05 wt% MWCNTs-COOH) demonstrated almost 100% rejection for small dye molecule of Safranin O (350.85 Da) in ethanol solvent. Furthermore, they also found that increasing the solute concentration in feed solution resulted in both flux and rejection reduction due to higher osmotic pressure and concentration polarization becoming dominant.

Grosso et al. (Grosso et al., 2014) developed porous asymmetric membranes via non-solvent induced phase separation using the co-polyimide P84 and functionalized MWCNTs (oxidized or aminated). Compared to the pristine P84 membrane (ethanol permeance of 174 L m^{-2} h^{-1} bar^{-1} and Sudan II blue rejection of 17.7%), the MWCNTs modified P84 membranes were found to have higher ethanol permeance (184 L m^{-2} h^{-1} bar^{-1} for MMMs with oxidized MWCNTs and 196 L m^{-2} h^{-1} bar^{-1} for MMMs with aminated MWCNTs) and similar or higher Sudan II blue rejections performances

(17.8% and 20.9%). The MWCNTs reduced the membrane fouling increasing the relative flux with Safranine O compared to the pristine P84 membrane (0.97 and 0.94 for MMMs containing aminated and oxidized MWCNTs, respectively, versus 0.79 obtained with pristine P84 membrane). The lower fouling tendency was more obvious for the P84 membrane containing aminated MWCNTs due to its smoother and more hydrophilic membrane surfaces compared to the P84 membrane containing oxidized MWCNTs. When compared to the membrane performance of commercial NF membranes, functionalized MWCNTs-P84 membranes exhibited competitive membrane performances.

2.2.4 Silica and Titania

In separation membranes, the incorporation of inorganic fillers can make the membranes exhibit better mechanical, thermal, and chemical stability, which is beneficial for its usage in applications involving harsh conditions including high temperatures and aggressive organic solvents (Sforca, Yoshida, & Nunes, 1999). One of such widely studied inorganic filler material is silica. Silica is proven to be a promising inorganic additive for nanocomposite membrane fabrication due to its numerous advantageous features such as chemically inert in nature, high mechanical strength, low cost, large surface area, and containing numerous hydroxyl groups, which will provide membranes with improved chemical stability and hydrophilicity (Jung et al., 2012). Therefore, many research efforts have been directed towards utilizing such advantageous features of inorganic filler material such as silica in the fabrication of high-performing nanocomposite OSN membranes.

For example, Pakizeh et al. (M. Namvar-Mahboub & Pakizeh, 2013) fabricated a nanocomposite TFC membrane using PEI/ amino-functionalized silica as a support layer for OSN application. In order to obtain the stable support layer, different loadings of functionalized silica (0-20 wt%) were used to prepare the nanocomposite OSN membranes. Swelling tests demonstrated that the swelling degrees of the control PEI membrane (2.49 ml/g in MEK and 5.27 ml/g in toluene) was higher than all the other SiO_2-modified PEI membranes. When the silica content was 5 wt%, the support layer achieved the maximum mechanical and chemical stability (swelling degrees of 1.27 ml/g in MEK and 1.79 ml/g in toluene). The OSN performance was then evaluated using a mixture containing dewaxed oil and dewaxing solvents (toluene and methyl ethyl ketone (MEK)). Results showed that the nanocomposite membrane could

achieve the solvent flux of 10.4 L m^{-2} h^{-1} at 15 bar and oil rejection of 94.72% suggesting its great potential in separating dewaxing solvent from dewaxed oil. Moreover, the prepared OSN membrane also demonstrated reasonable performance at a pressure of 20 bar, where no damage in the prepared membrane was observed. Chen et al. (R. Wang, Xu, Sun, Gao, & Lin, 2013) investigated the deposition of poly (diallyldimethy-lammonium, chloride)/sulfonated poly(ether ether ketone) (PDDA/SPEEK) on the silicon composite hydrolyzed polyacrylonitrile (H-PAN) support layer for OSN application. The oppositely charged polyelectrolyte complexes silicon composite OSN membranes exhibited a rejection rate of negatively charged RB (99%) in IPA solvent. In addition, the PEC-based silicon composite membranes were also tested in other polar solvents such as dimethylformamide (DMF) and tetrahydrofuran (THF) and demonstrated good stability with good solvent flux and dye rejection performances. For example, the silicon nanocomposite membrane exhibited THF permeance of 13.9 L m^{-2} h^{-1} bar^{-1} with RB rejection of 98%.

Titania (TiO$_2$) is another well-known inorganic material that exhibits advantageous features for forming a nanocomposite membrane for OSN application including its hydrophilic nature, good chemical and physical stability (S.-H. Liu, Liu, Xu, Wei, & Guo, 2017; Sotto, Boromand, Balta, Kim, & Van der Bruggen, 2011). These features make Titania a highly desirable nanofiller material for OSN membrane fabrication and modification.

Soroko et al. (Soroko & Livingston, 2009) prepared chemically cross-linked organic-inorganic composite membrane by dispersing different concentrations (1, 3, 5, and 10 wt%) of TiO$_2$ nanoparticles with PI using DMF/1,4-dioxane dope solution. When TiO$_2$ nanoparticles loading was increased, the water contact angle decreased and the ethanol permeate flux was increased indicating improved hydrophilicity. Enhanced compaction resistance during the filtration test of DMF proved that TiO$_2$ nanoparticles improved the mechanical stability of the membrane and prevented the collapse of membrane. Moreover, it reduced the flux decline. However, in the DMF filtration test, the impact of TiO$_2$ on improving the solute rejection and the solvent flux was not significant despite the membrane structure changed and became void-free.

P84 and Matrimid are the two most widely used polyimides for asymmetric membrane fabrication which are usually cross-linked via different methods with various cross-

linkers to improve their solvent resistance properties. These cross-linking treatments are often complicated and time-consuming which may hinder industry adoption. To tackle the problems, Li et al. (Yuan Li, Cao, & Li, 2019) utilized poly (4, 4′-oxydiphenylene pyromellitimide) as polymers for hollow fiber (HF) membranes fabrication due to its good mechanical property and stability in both water and organic solvents. Then, they synthesized the nanocomposite HF membrane using TiO_2 with different loadings (1.0, 1.1, and 1.3 wt%) and ethanol solvent. The resultant nanocomposite HF membrane's properties such as porosity, hydrophilicity, and separation performances in aqueous and organic solvent systems were investigated. Results revealed that dope solution with high polyamic acid or ethanol concentration increased the solute rejection but induced a lower solvent permeance. The dope solution with 1.1 wt% TiO_2 incorporation lead to significant improvements in the membrane porosity and hydrophilicity which resulted in optimum membrane performances. This nanocomposite membrane (1.1 wt% TiO_2 incorporation) exhibited DMF permeance of 2.51 L m^{-2} h^{-1} bar^{-1} and rejection of 90.6% and 96.7% for fast green (FG, 808 Da) and RB, respectively. Moreover, long-term separation performances of a 50 hrs OSN experiment in DMF with stable RB rejection demonstrated its good stability in the harsh organic solvent.

2.2.5 Issues and possible solutions

One of the major issues, when synthesizing MMMs or nanomaterial incorporated support layers, is the nanoparticle agglomeration inside the substrate polymer matrix, which will induce the formation of defects that reduced the membrane performances and lead to the wastage of expensive nanomaterials. Modification of the nanoparticles with functional groups (such as amine groups) could be a possible way to tackle such problem (Abadikhah et al., 2018; Zarrabi, Yekavalangi, Vatanpour, Shockravi, & Safarpour, 2016). The modified nanoparticles are expected to have better arrangement and distribution inside the polymer dope solution. Moreover, although the polymers which are chosen for OSN membrane fabrication could be stable in many types of organic solvents, yet, they still face difficulties in aggressive organic solvents, such as dimethyl sulfoxide (DMSO), DMAc, DMF, etc. Thus, various cross-linkers have been used to fabricate membranes with improved chemical stability and selectivity of the membranes. However, the use of cross-linkers is another drawback. Since most of the cross-linker utilize hazardous chemicals and the post-treatments are necessary, which

will increase the overall cost for membrane production. Therefore, to avoid pollution of the environment, exploration of other polymers with good chemical stability in organic solvents should be conducted to reduce the use of cross-linkers or other post treatments which will accelerate the OSN membrane development using the MMMs approach.

2.3 Nanomaterial-modified active layers

Most OSN membranes are ISA membranes produced by non-solvent induced phase inversion. However, the ISA membranes tend to experience limitations such as a tight skin layer leading to relative low solvent permeate flux (Jimenez Solomon, Bhole, & Livingston, 2013; Vandezande et al., 2008). Recently, TFC membranes which consist of two separate layers with an ultrathin active layer (responsible for solvent & solute rejection) on top of a thicker and highly porous support layer (providing a solvent passage & provide mechanical stability) have gained increasing interest for OSN membrane applications due to two different layer's composition and properties could be tuned & controlled during the membrane fabrication process (Szekely, Jimenez-Solomon, Marchetti, Kim, & Livingston, 2014). However, the trade-off between solvent permeability and solute selectivity is still a major issue for polymer-based TFC membranes. Nanomaterial incorporation is one of the approaches to overcome such problems (Yanbo Li, Wee, Martens, & Vankelecom, 2017). Depending on the hydrophilic/hydrophobic properties of the nanomaterials, they can be dispersed into either aqueous or organic solution. The nanocomposite membranes can be prepared through LBL assembly or interfacial polymerization (IP).The basic steps involved in the nanocomposite OSN membrane fabrication are presented in **Fig. 2.4** (LBL method) and **Fig. 2.5** (IP method). Until now, various nanomaterials have been used for the synthesis of nanocomposite OSN membranes including MOFs, graphene quantum dots (GQDs), GO, SiO_2, TiO_2, covalent organic frameworks (COFs) and CNTs, etc.
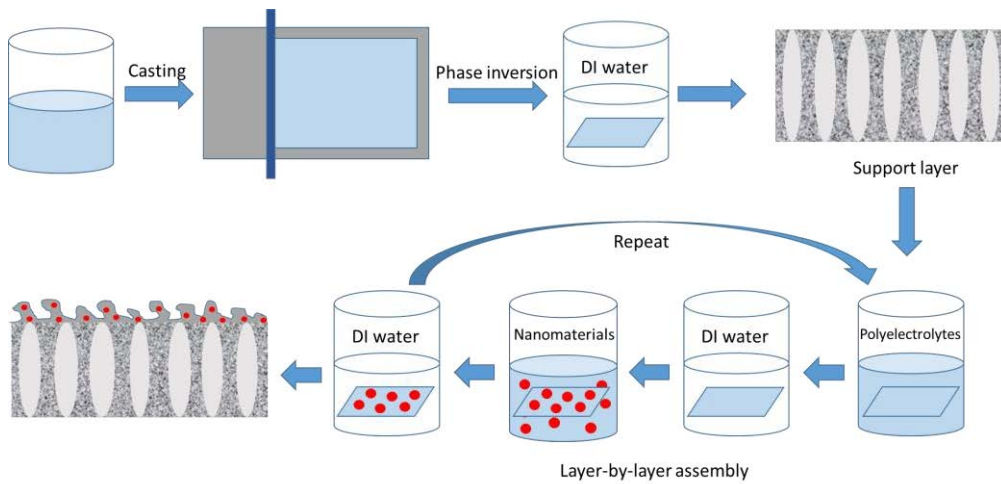
Figure 2.4. Typical steps involved for nanocomposite OSN membrane fabrication via LBL assembly.
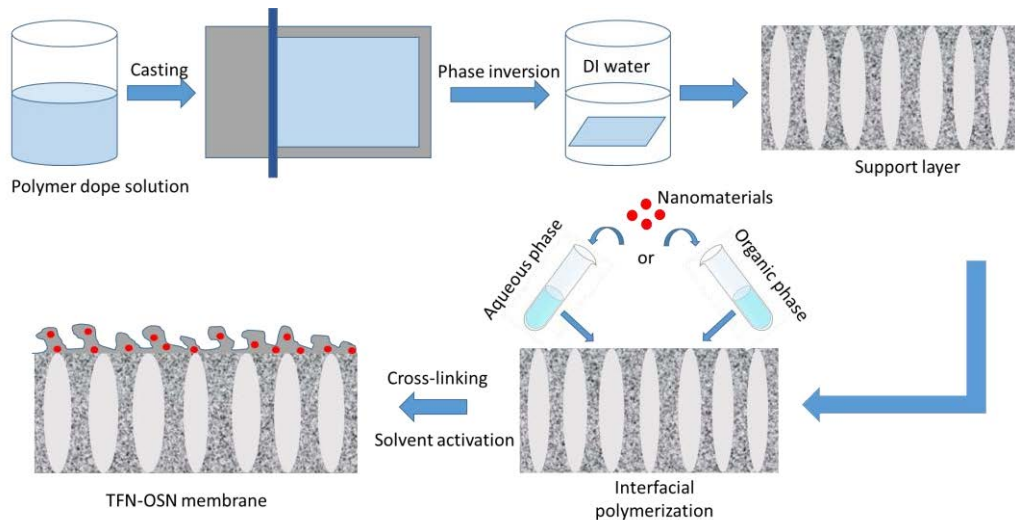
Figure 2.5. Typical steps involved for OSN-TFN membrane fabrication via IP process.

2.3.1 Nanocomposite OSN membrane prepared via LBL assembly

LBL assembly is one of the efficient ways for preparing OSN membranes, which shows the advantages of the adjustable active layer thickness and surface charge (Cheng et al., 2014).

Guo et al. (H. Guo et al., 2016) designed superhydrophilic PEI/polyacrylic acid (PAA)-calcium silicate hydrate CSH nanocomposite NF membranes and then transformed them into superhydrophobic OSN membranes through one-step trimethylperfluorinatedsilane modification (see **Fig. 2.6**). A PAN UF membrane was used as substrate and coated with (PEI/PAA)$_2$ layers by depositing PEI and PAA solutions on the surface for two bicycles. Then the membrane was soaked in 0.5 g/L

PEI-calcium acetate solution, followed by 0.1 g/L PAA-sodium silicate solution each for 20 min. Between each soaking, the membrane was rinsed with DI water to remove the excess chemicals. During this soaking process, CSH nanoparticles were in-suit incorporated into membranes via the reaction of Ca^{2+} and SiO_3^{2-}. This process was repeated until the desired number of multilayers (named as $(PEI/PAA-CSH)_n$). To transform the hydrophilic membrane to a hydrophobic membrane, the $(PEI/PAA-CSH)_2$ membrane was immersed in 0.75 wt% PFTS ethanol solution for 1 h; then it was washed thoroughly and kept in the oven for 2 h at 60°C named as $(PEI/PAA-CSH)_2$-PFTS. Both membranes showed good performances for rejecting dyes in water and ethanol solutions. In addition, the long-term filtration and antifouling tests were conducted by using an aqueous water solution and ethanol solution containing MB, BSA, and HA solutes. Results revealed that both the superhydrophilic and superhydrophobic membranes exhibited high stability and good antifouling property (see **Fig. 2.6 (a)**). In another study from the same research group, they prepared PEM nanocomposite membranes via LBL and counterion exchange methods (Lu, Qin, Wang, An, & Guo, 2021). PDDA/PAA multilayers were LBL deposited on PAN support through electrostatic interaction. During this assembly process, CSH nanoparticles were in-suit grown with the incorporation of precursor in polyelectrolyte solutions. The $[(PDDA/PAA-CSH)_{2.5}]^+Cl^-$ membrane fabrication process is the same as the previous study. Only the difference is the hydrophobic $[(PDDA/PAA-CSH)_{2.5}]^+PFO^-$ membrane prepared via the counterion exchange method by immersing hydrophilic $[(PDDA/PAA-CSH)_{2.5}]^+Cl^-$ membrane in a 0.1 mol/L sodium perfluorooctanoic (PFO^-) solution for a certain time (see **Fig. 2.6 (b)**). Then, the membrane was washed with DI water and dried in an oven for 2 h at 30°C. The obtained $[(PDDA/PAA-CSH)_{2.5}]^+PFO^-$ membrane has a water contact angle of 118° indicating its hydrophobic property. OSN tests revealed that compared to the pristine $[(PDDA/PAA)_{2.5}]^+Cl^-$ membrane, the $[(PDDA/PAA-CSH)_{2.5}]^+Cl^-$ membrane showed higher MB rejection because of the in-suit growth of CSH nanoparticles, which is beneficial for the improvement of membrane compactness. The ethanol permeance of $[(PDDA/PAA-CSH)_{2.5}]^+PFO^-$ membrane was higher than that of $[(PDDA/PAA-CSH)_{2.5}]^+Cl^-$ membrane due to the hydrophobic surface property. In addition, during the 40 h long-term OSN filtration tests (shown in **Fig. 2.6 (c)**), the $[(PDDA/PAA-CSH)_{2.5}]^+PFO^-$ membrane is more stable than $[(PDDA/PAA)_{2.5}]^+PFO^-$ membrane

indicating its anti-swelling performance, which is due to the incorporation of CSH nanoparticles restricting the movement of polymer chains.

Hua et al. (Hua & Chung, 2017) prepared a new class of OSN membranes by deposition of GO nanosheets and polyelectrolytes on a porous PP substrate using the combination of the pressure-assisted filtration method and dip-coating LBL assembly method. The PP membrane was first pre-treated with plasma-inducing PEG grafting, then a prepared GO solution was filtrated on the membrane surface, and the resultant membrane was named TPP/GO. A further modification was conducted by immersing TPP/GO membrane in positively charged polyelectrolytes such as hyperbranched polyethyleneimine (HPEI) and PDDA for 30 min and then negatively charged polyelectrolyte poly(sodium 4-styrene sulfonate) (PSS) for another 30 min, the prepared membrane named as TPP/GO/HPEI/PSS or TPP/GO/PDDA/PSS. Between each immersion, the membrane was rinsed was DI water for 10 sec. In addition, they also prepared an OSN membrane by soaking TPP/GO membrane in a PDA solution for 30 min first and then soaking it in the HPEI solution for another 30 min; this membrane was named TPP/GO/PDA/HPEI. It is found that plasma treatment of PP substrate with PEG polymer is an effective approach to improve the substrate hydrophilicity and enhance its adhesion with GO nanosheets. The TPP/GO/PDA/HPEI membrane with the positive polymer as the outmost layer has high rejections for cationic dyes. For example, it shows a 95% rejection for Alcian blue (MW: 1299 Da) with good ethanol permeance of 14.9 L m^{-2} h^{-1} bar^{-1}. On the other hand, the TPP/GO/HPEI/PSS membrane with a negative PSS as the outmost layer exhibits excellent anionic dye rejections. For example, it presents a 97% rejection for RB with ethanol permeance of 3.1 L m^{-2} h^{-1} bar^{-1}. Overall, this study provides a new strategy for preparing high-performance nanocomposite OSN membranes.

In summary, due to the polymer-based OSN membranes often suffering from swelling issues in harsh organic solvents, effective strategies are conducted to incorporate inorganic nanoparticles to improve the membrane's mechanical and chemical stability. Currently, the CHS, and GO have been investigated to prepare high-performance LBL nanocomposite OSN membranes. However, other nanomaterials such as CNT, MOFs, silica, and TiO_2 are needed to be explored to accelerate the development and open new avenues of OSN.
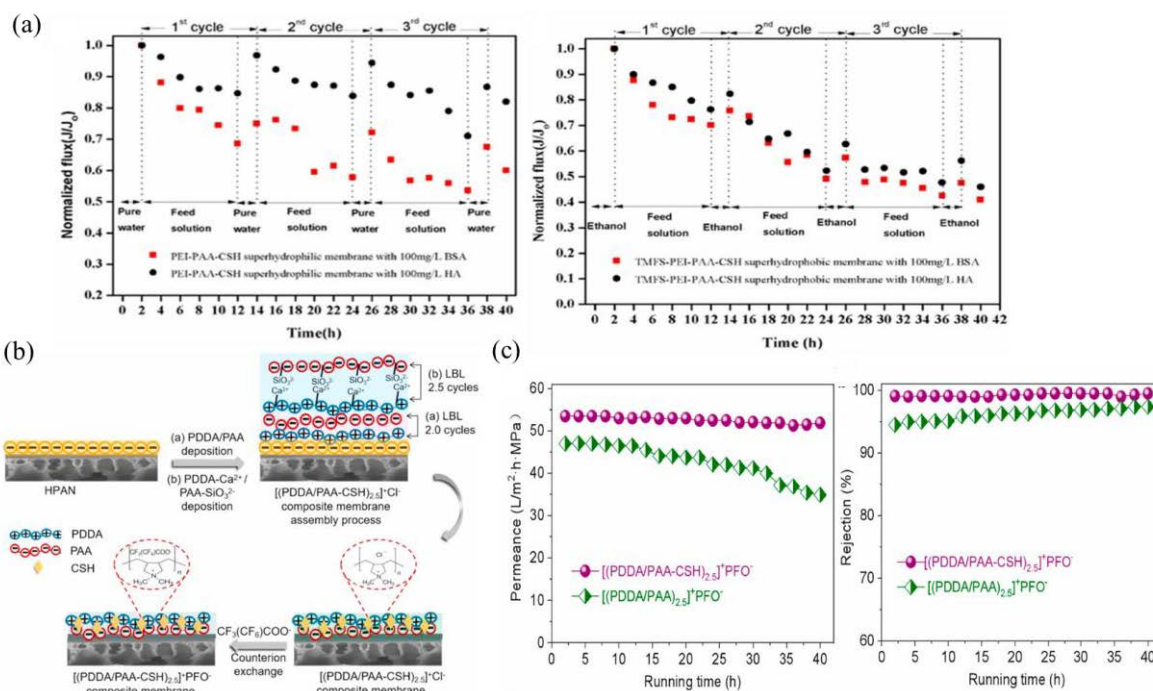
Figure 2.6. (a) Antifouling test of the superhydrophilic (PEI/PAA-CSH)$_2$ and superhydrophobic (PEI/PAA-CSH)$_2$/PFTS membranes under 0.4 Mpa (H. Guo et al., 2016). (b) Schematic diagram of the preparation of hydrophobic [(PDDA/PAA-CSH)$_{2.5}$]$^+$PFO$^-$ composite membrane (Lu et al., 2021). (c) Stability tests of [(PDDA/PAA-CSH)$_{2.5}$]$^+$PFO$^-$ and [(PDDA/PAA)$_{2.5}$]$^+$PFO$^-$ membranes (Lu et al., 2021).

2.3.2 Nanocomposite OSN membrane prepared via IP process

2.3.2.1 Metal organic frameworks

The preparation of defect-free TFN membranes is an effective method for preparing high-performing OSN membranes. IP is a commonly used method for fabricating TFN membrane by the formation of an active layer on top of a porous support layer. Recently, nanomaterials such as MOFs attracted large attention as filler material for TFN membrane synthesis due to their high surface area, uniform and tuneable porosity, scalable synthesis process, and hydrophilicity which are advantageous features for making a high-performing TFN membrane. Therefore, research efforts have been directed to explore and utilize these MOFs based materials in TFN membrane synthesis for OSN applications.

For example, Sorribas et al. (Sorribas, Gorgojo, Tellez, Coronas, & Livingston, 2013) synthesized a range of MOFs-based TFN membranes by incorporating ZIF-8, MIL-

53(Al), NH$_2$-MIL-53(Al) and MIL-101(Cr) (see **Fig. 2.7**) in the PA active layer on top of PI porous supports. Membrane performances were evaluated in OSN on the basis of methanol and THF permeate fluxes and polystyrene oligomers (PS) rejections. In all modified membranes cases, methanol and THF permeate fluxes increased and the PS rejections were higher than 90% (MWCO less than 232 and 295 for methanol and THF, respectively). In addition, it is shown that the improvement of permeate flux was more pronounced in the case of MOFs with larger pore sizes and higher porosity. When incorporated largest pore size MOFs (MIL-101(Cr) (3.4 nm)), there was a significant increase in permeance for methanol from 1.5 to 3.9 L m^{-2} h^{-1} bar^{-1} and THF from 1.7 to 11.1 L m^{-2} h^{-1} bar^{-1}.
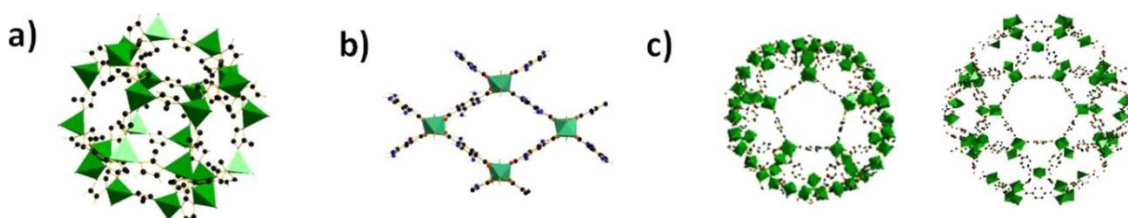
Figure 2.7. (a) Building blocks of ZIF-8; (b) pore system in NH$_2$-MIL-53(Al); (c) building blocks for MIL-101(Cr) (adapted from Ref. (Sorribas et al., 2013))

Carlos et al. (Echaide-Górriz, Sorribas, Téllez, & Coronas, 2016) chose MOFs nanoparticles of MIL-101(Cr), MIL-68(Al) and ZIF-11 with sizes of 70, 103, and 79 nm for TFN membrane fabrication. The nanocomposite membranes were prepared with an ultrathin PA layer (about 100-150 nm) on top of a P84 support. The effects of different solvents (methanol, acetone, and THF) and various solutes (Acridine Orange (AO, MW 265 g mol^{-1}), Sunset Yellow (SY, MW 452 g mol^{-1}), and RB) on TFN membrane performances in OSN has been studied. Results showed that the hydrophilicity of membranes and the interactions of solvent-membrane and solute-membrane are the most important parameters influencing the OSN membrane performances. When ZIF-11 nanoparticles were incorporated into the PA layer, a clear increase in methanol permeate flux was observed compared to other TFN membrane synthesized using two other MOFs. The maximum methanol permeance achieved was 6.2 L m^{-2} h^{-1} bar^{-1} with 90% rejection for SY. Except for the in-situ IP on the substrate, Sarango et al. (Sarango, Paseta, Navarro, Zornoza, & Coronas, 2018) introduced a controlled deposition of MOFs via a dip-coating process in TFN membranes. ZIF-8 and ZIF-67 nanoparticles with sizes of around 70 and 240 nm were coated on top of

P84 support layers. The MOF monolayer on P84 support was beneficial for the IP of the PA layer to produce an effective TFN membrane for OSN. Such an approach for TFN membrane fabrication was simple and effective. During the fabrication process, no excess MOFs particles were lost, which will also reduce the nanomaterial wastage and overall cost of membranes. The resultant TFN membrane exhibited good performance in OSN application with a methanol permeance of 8.7 L m^{-2} h^{-1} bar^{-1} and SY rejection of ~90%.

However, most of the mentioned approaches for the fabrication of ultrathin selective layer for TFN membrane synthesis utilized high concentrations of expensive nanomaterials. Therefore, new methods with simple and efficient nanoparticle incorporation will facilitate the synthesis of novel and cost-effective MOFs based TFN membranes. For example, Xu et al. (Xu, Shen, Chen, & Xu, 2018) developed a rapid and facile method to synthesize the novel β-cyclodextrin-enhanced zeolite imidazole framework-8 (β-CD@ZIF-8) nanoparticles. These nanoparticles were used for the fabrication of TFN membranes via their addition into both the active layer and the PMIA support layer. PMIA is a kind of polymeric material that exhibits advantageous features including its hydrophilic nature and high porosity. Atomic force microscope (AFM) images revealed a much rougher surface in the modified membrane compared to the pristine membrane. The TFN membranes exhibited good solvent resistance in various solvents including methanol, ethanol, IPA, THF, acetone, and ethyl acetate. For the OSN performances, the modified membrane presented pure acetone flux of 62.3 ± 2.3 L m^{-2} h^{-1} and RB rejection of 96.6 ± 1.8 and $94.5 \pm 0.5\%$ in methanol and THF with a dosage of 0.05%(w/v) under 0.6 MPa, respectively. In order to further improve the TFN membrane performance, efforts were made to adjust the PMIA support concentration, optimize the dosage of β-CD@ZIF-8 nanoparticles, and balance between the ratios of aqueous and organic phases. This research demonstrates another potential approach for synthesizing effective TFN-OSN membranes. Navarro et al. (Navarro et al., 2018) introduced an innovative method for depositing a monolayer of MIL-101(Cr) in TFN membranes by transferring a Langmuir-Schaefer (LS) MOF film between the PA layer and the P84 support. Conventional TFN membranes tend to have MOFs agglomeration leading to the formation of unselective defects. Whereas the LS-TFN membranes exhibited defect-free ultrathin MOF film with homogeneous and continuous MIL-101(Cr) coating. Most importantly, this

approach required the smallest amount of MOF particles reported to date (around 3.8 μg cm^{-2}) for the synthesis of MOFs based TFN membranes. Compared to the TFC and TFN membranes synthesized via the conventional IP process, the LS-TFN membranes showed higher methanol permeate flux. Specifically, the LS-TFN membranes exhibited methanol permeances of 10.1 ± 0.5 L m^{-2} h^{-1} bar^{-1} containing SY and 9.5 ± 2.1 L m^{-2} h^{-1} bar^{-1} containing RB with solute rejections over 90%.

During the TFN membrane fabrication, the dispersion of filler materials in organic phase solvent and the compatibility between the fillers and polymers are important parameters that require careful control for the formation of defect-free, effective TFN membrane. For example, Guo et al. (X. Guo et al., 2017) modified the UiO-66-NH$_2$ nanoparticle surface with long alkyl chains to improve the dispersion of MOFs in organic solvents and embedded them in the active layer for TFN membrane fabrication. Due to the improved dispersion of MOFs, the TFN membranes were successfully prepared with an ultrathin PA layer incorporated with MOFs nanoparticles. The TFN membranes exhibited a significant increase in methanol permeate flux without compromising the rejection of tetracycline. The highest methanol permeance of 20 L m^{-2} h^{-1} bar^{-1} and highest rejection for tetracycline ~99% were achieved with 0.15 % (w/v) UiO-66-NH$_2$ nanoparticles loading. Cheng et al. (X. Cheng et al., 2017) studied the incorporation of water-stable UiO-66 MOFs in thin PA NF membranes for TFN membranes preparation. The effects of functionalized ligands (UiO-66-(CH$_3$)$_2$, UiO-66-NH$_2$ and post-synthetic (UiO-66(Ti)) on the membrane pore size, structures and defects were also investigated. The MOFs were well-dispersed within PA layers and did not exhibit obvious defects, which made TFN membranes remain stable in different organic solvents (alcohols, ketones, and ethyl acetate) with the RB rejections over 96%. For the rejection of the same dye, all TFN membranes revealed similar rejection rates. However, the TFN membranes exhibited different rejections for different dyes indicating the dependence on the molecular size of a dye (molecular weight). Due to the varying solute, membrane, and solvent interactions, the TFN membranes demonstrated different RB rejections under different organic solvents.

Another drawback in the preparation of TFN-OSN membranes is that the polymer used for support layers is usually dissolved in highly toxic organic solvents, such as DMAc, DMF and N-methypyrrolidone (NMP). Besides, for the MOF-based TFN membranes, DMF is normally used as an activating solvent during the post-treatment

process. Therefore, to enable a greener synthesis process for MOFs-based TFN membrane fabrication, Paseta et al. (Paseta, Navarro, Coronas, & Téllez, 2019) utilized a less toxic solvent such as DMSO instead of the solvent used for traditional TFC and MOF based TFN membrane fabrication. In this study, the less toxic solvent such as DMSO was able to both dissolve the polymer and to activate the membranes. TFN membranes were successfully synthesized with the incorporation of ZIF-8, ZIF-93, and UiO-66 as nanofillers. When applied in OSN with a feed solution of methanol containing SY, the highest methanol permeance of ~11 L m^{-2} h^{-1} bar^{-1} was obtained using ZIF-93 and UiO-66 as nanofillers. The study shows that the porosity of MOFs, the thickness of the PA layer, and the hydrophilic/hydrophobic properties of the membranes were the main parameters affecting the membrane performances in OSN.

In many MOFs-based TFN membranes studies, TFN membranes are often fabricated with the addition of one kind of MOFs into the membrane active layer. In order to extend the versatility of the membranes, Carlos et al. (Echaide-Gorriz, Navarro, Tellez, & Coronas, 2017) combined two MOFs to prepare a versatile and effective TFN membrane. MIL-101(Cr) and ZIF-11 with different chemical and structural characteristics were embedded in the same membrane simultaneously. Compared to the TFN membrane containing only MIL-101(Cr), the TFN membrane containing only ZIF-11 exhibited higher methanol permeate flux but lower rejection rates for SY and AO. The incorporation of these two MOFs made the TFN membranes with an intermediate performance showing improved rejection rates compared to the TFN membrane embedded with ZIF-11 only and increased methanol permeate flux compared with the TFN membrane incorporated with MIL-101(Cr) only. They also investigated the effect of feed solution temperature on the TFN membrane performances in OSN. Results show that the permeate flux increased with an increase in feed solvent temperature, due to the influence of temperature on the feed solvent viscosity, and less solute and solvents were absorbed on the membrane surface.

To this date, it is challenging to develop nanoporous membranes with the capability of working in dual solvents systems (polar and non-polar solvents). Conventional polymeric membranes could guarantee good membrane performance in one type of solvent while the performance in other types of solvent is not guaranteed. For example, the membranes fabricated by Liang et al. (B. Liang et al., 2018) showed higher permeance of 35 L m^{-2} h^{-1} bar^{-1} for hexane compared to the IPA of 5 L m^{-2} h^{-1} bar^{-1}.

To overcome such a problem, Huang et al. (J. H. Huang et al., 2020) prepared polar-group-enriched conjugated nanoporous membranes (CNMs) for dual solvents treatment. During the fabrication of the active layer, sodium polymethacrylate-grafted UiO-66 nanoparticles were incorporated into the PPy chains. PPy is utilized due to its highly conjugated architecture and abundant –NH- groups, which are reported to have good compatibility and stability in most organic solvents. The highly conjugated structure enables the CNMs with a good affinity towards non-polar solvents, the additional polar groups contribute to the interaction with polar solvents enabling rapid permeance. The TFN membrane exhibited good solvent resistance in ethanol and toluene. TFN membrane performances in OSN showed ultrahigh permeate fluxes in both polar and non-polar solvents. The permeance of ethanol was ~53.9 L m^{-2} h^{-1} bar^{-1}, pentane of ~244.0 L m^{-2} h^{-1} bar^{-1} and hexane was ~172.9 L m^{-2} h^{-1} bar^{-1} with MWCO of 400 Da, which was superior in comparison to state of the art OSN membranes.

2.3.2.2 Graphene quantum dots and graphene oxide

Graphene quantum dots (GQDs) also known as carbon quantum dots (CQDs), graphene oxide quantum dots (GOQDs), or carbon dots (CDs) have gained increasing attention in TFN membrane fabrication. As a kind of zero-dimensional nanomaterials, the sheet size of GQDs are less than 30 nm with a large specific surface area (S. Li, C. Li, et al., 2019a; Tuteja et al., 2016). It has many unique properties including good thermal, chemical and mechanical stability, and good water solubility arising from the presence of numerous oxygen & nitrogen functional groups (Die Ling Zhao & Chung, 2018). Besides, the GQDs could also be synthesised through one-step microwave-assisted pyrolysis of ethylenediamine and citric, utilizing an environmentally friendly precursors and via non-energy intensive, low-temperature processes (Jiang, He, Li, & Cui, 2012). Currently, the CQDs-based OSN membranes are rarely reported. However, the high surface-to-volume ratio and different kinds of functional groups such as -OH, -NH_2, and -CO_2H will provide them a great potential for TFN-OSN membranes fabrication.

Amongst a few notable works, Yuan et al. (Z. Yuan et al., 2018) fabricated a series of TFN membranes by incorporating CQDs in PEI active layer. The resultant membranes combined the advantages of PEI polymer and CQDs nanoparticles. The well cross-linked PEI provided good solvent resistance and solute rejection. The ddition of CQDs increased the solvent transportation in the membrane. It is shown that the TFN

membranes with low carbonated CQDs (highly functionalized) could interact with polar organic solvents, as a result, the permeate flux of IPA was increased to 42.6 L m^{-2} h^{-1} at 10 bar, a 54.3% increase compared to the pristine TFC membrane. However, the permeance of non-polar solvents was suppressed by the low-carbonated CQDs incorporation. In contrast, the TFN membranes with highly carbonated CQDs (low degree of functional groups) accelerated the transport of non-polar solvents while inhibiting the transport of polar solvents. In the 24 h filtration tests in IPA and heptane, the TFN membrane exhibited good stability with stable solvent permeance and retention during the 6 hrs of tests.

Another study by Wu et al. (X. Wu et al., 2019) investigated the effect of moderately carbonized QDs on the TFN membrane performances in OSN application. The moderately carbonized QDs with amphipathic properties combined the properties of hydrophilic (carbonization-free) QDs and hydrophobic (highly carbonized) CQDs, showing affinity towards both polar and nonpolar molecules. With the incorporation of amphipathic CQDs in the active layer, the resultant TFN membranes exhibited permeances of 46.9 and 50.8 L m^{-2} h^{-1} bar^{-1} for acetonitrile and n-hexane, respectively, which are 2 orders of magnitude higher than the conventional TFC membranes. They also evaluated the transfer mechanism models and found that the hydrophilic and hydrophobic QDs showed different molecular transfer mechanisms and the amphipathic CQDs combined the transfer mechanism of the two models. Moreover, the GQD-TFN membrane is rather stable during the continuous operation for 10 days in different solvents (ethanol, acetone, and hexane), with solvent permeance reduction which was less than 23%.

In order to improve the solvent resistance of OSN membranes, Li et al. (S. Li, C. Li, et al., 2019a) fabricated novel PI-based TFN membranes with the incorporation of CQDs (average size of 1.9 nm). The modified TFN membranes without organic solvent activation exhibited a 50% ethanol permeate flux increase compared to the membranes without the CQDs nanoparticles, while no dye rejection decrease was observed. Moreover, after the organic solvent activation (DMF at 80 °C for 30 min), the permeability of ethanol demonstrated an 8-fold increment, from 2.84 to 22.6 L m^{-2} h^{-1} MPa^{-1}, with an increase in the rejection of Rhodamine B (RDB, MW 479.02 g/mol) from 97.8 to 98.6%. Then the longevity test of organic solvent-activated TFN membranes was performed (more than 100 hrs). The TFN membranes exhibited good

solvent resistance with DMF permeance of 18.3 L m^{-2} h^{-1} MPa^{-1} and RB rejection of 99.9%. Moreover, the immersion test of the TFN membranes in both ethanol and DMF were performed for one year at room temperature which showed good solvent stability, indicating that the CQD-based TFN membranes are promising for OSN applications. In another work from this research group, they synthesized amino-functionalized GQDs (aGQDs) and embedded them into the active layer to fabricate novel TFN membranes (S. Li, C. Li, B. Su, et al., 2019). The loadings of aGQDs were 50, 100, 125, 150, 200, and 300 mg L^{-1}, amongst them 125 mg L^{-1} was found to be the optimal loading. Under this aGQDs loading, the aGQDs could be fully utilized without self-aggregation. The synthesized TFN membranes exhibited great improvement in solvent resistance due to the formation of covalent bonding between the active layer and the substrate, but also between the active layer and the aGQDs nanoparticles. With the incorporation of aGQDs, the resultant TFN membrane surface became much smoother. The membrane performances under the optimal condition exhibited the ethanol permeate flux increase by 44% with RDB rejection over 99% compared to pristine TFC membrane. The long-term continuous filtration of 100 mg L^{-1} RB in DMF solution was conducted for more than 768 hrs at room temperature, the TFN membranes presented good chemical/solvent stability with stable rejection for RB above 99% under long-term filtration test in ethanol. Moreover, after being immersed in DMF and NMP at 80°C for 248 h and 232 h, respectively, the aGQDs-based TFN membranes exhibited ethanol permeance of 38 L m^{-2} h^{-1} MPa^{-1} with RDB rejection above 99% and 41 L m^{-2} h-1 MPa^{-1} with RDB rejection over 99%, respectively, indicating its good solvent resistance and high-temperature tolerance, which implies that the aGQDs based TFN membranes have great potential in solvent or valuable solute recovery for chemical and pharmaceutical industries.

Amongst various 2D nanomaterials, GO nanosheets have drawn much interest as a nanofiller material to be embedded in the active layer. There are several advantages to incorporating GO nanosheets into membranes for OSN application. Firstly, the presence of abundant oxygen-containing groups like carboxyl, hydroxyl, and epoxy groups enable good compatibility with various polymers. Secondly, the ultrathin, 2D nature of GO nanosheets enables the formation of ultrathin polymer-GO nanosheets composite layer. Moreover, similar to the GQDs case, GO nanosheets consist of both graphitic planes which can facilitate the non-polar solvent transport as well as edge

planes with numerous functional groups which can facilitate the transport of the polar solvents making them a suitable nanomaterial for OSN application.

To exploit such advantages of GO nanosheets, Shao et al. (Shao, Cheng, Wang, Ma, & Guo, 2014) for the first time, incorporated GO nanosheets into the PPy/PAN-H membrane by adding GO nanosheets into pyrrole ethanol solution before the polymerization. The result demonstrates that the incorporation of GO nanosheets leads to a significant improvement in solvent permeability without lowering RB rejection compared to pristine polymeric PPy/PAN-H membranes. Compared to the PPy/PAN-H membranes, the GO-modified TFN membranes exhibited nearly 945%, 635%, and 302% higher permeate flux for methanol, ethanol, and IPA, respectively. In the long-term OSN filtration, the TFN membranes exhibited constant IPA permeance of 1.21 $L\ m^{-2}\ h^{-1}\ bar^{-1}$ with an RB rejection of 99.0%. Ding et al. (Ding et al., 2015) embedded GO nanosheets into PEI solution followed by IP on the PAN support layer. They used dopamine (DA) to improve the dispersion of GO sheets in PEI solution, as well as DA also enhance the adhesion between the active layer and support layer. The work reveals that horizontally aligned GO nanosheets in the PEI matrix provided unique solvent pathways through the edge planes of GO nanosheets. The GO nanosheet-based TFN membranes presented improved solute rejection and solvent flux. With the 3.0 wt% loading of GO nanosheets, the acetone flux of 15.7 $L\ m^{-2}\ h^{-1}$ at 10 bar and significant improvement in the rejection of PEG (MW 200 $g\ mol^{-1}$) was achieved (66.2% to 96.8%) compared to pristine TFC membranes. Moreover, the GO-modified membranes exhibited good solvent resistance during the long-term operation tests with acetone and ethanol solvents. The flux remained relatively stable around 12.8 and 7.7 $L\ m^{-2}\ h^{-1}$ at 10 bar when tested under these two solvents.

Paseta et al. (Paseta et al., 2020) prepared TFN membranes incorporated with octadecylamine-functionalized rGO nanoparticles. The functionalized rGO presents more hydrophobic nature than the GO, which makes them be well dispersed in the organic solvent phase during the IP reaction. The optimal TFN membrane performance was achieved with an rGO concentration of 0.06 w/v%. The OSN performances showed that compared to the pristine TFC membranes, the ethanol permeances of the TFN membranes increased from 2.8, 3.4, and 3.7 $L\ m^{-2}\ h^{-1}\ bar^{-1}$ to 4.3, 4.6, and 6.0 $L\ m^{-2}\ h^{-1}\ bar^{-1}$ for AO, SY and RB, respectively. The increased ethanol permeate flux is owing to the presence of both polar and non-polar groups in rGO

nanosheets and the creation of a narrow pathway between the nanosheets and the PA active layer. Abadikhah et al. (Abadikhah et al., 2019) synthesized GO-based hybrid nanocomposite membrane decorated with TiO$_2$ nanoparticles (TiO$_2$@rGO) and incorporated them (with loadings of 0.05, 0.2, and 0.4 wt% TiO$_2$@rGO) into the PA layer for TFN-OSN membrane fabrication with antifouling properties (see **Fig. 9**). In order to enhance the compatibility between TiO$_2$@rGO and the PA selective layer, the hybrid nanocomposites (TiO$_2$@rGO) were amino-functionalized before the IP process. The GO nanosheets provide channels for the solvent passage and the TiO$_2$ nanoparticles improve the membrane's hydrophilic characteristics, where the resultant TFN membrane presented good structural stability along with antifouling properties. When the TFN membrane (with 0.2 wt% TiO$_2$@rGO) was soaked in ethanol for 48 hrs, the membrane still exhibited solute rejection capability of >95% for bromothymol blue (BTB) and 97% for RB. The influence of hybrid nanocomposite concentration on the pure solvent permeate flux was evaluated, for example, the *n*-hexane permeances reduced from 1.43 L m^{-2} h^{-1} bar^{-1} to 1.31 and 1.35 L m^{-2} h^{-1} bar^{-1} when the TiO$_2$@rGO concentration increased from 0.05 wt % to 0.2 and 0.4 wt%.
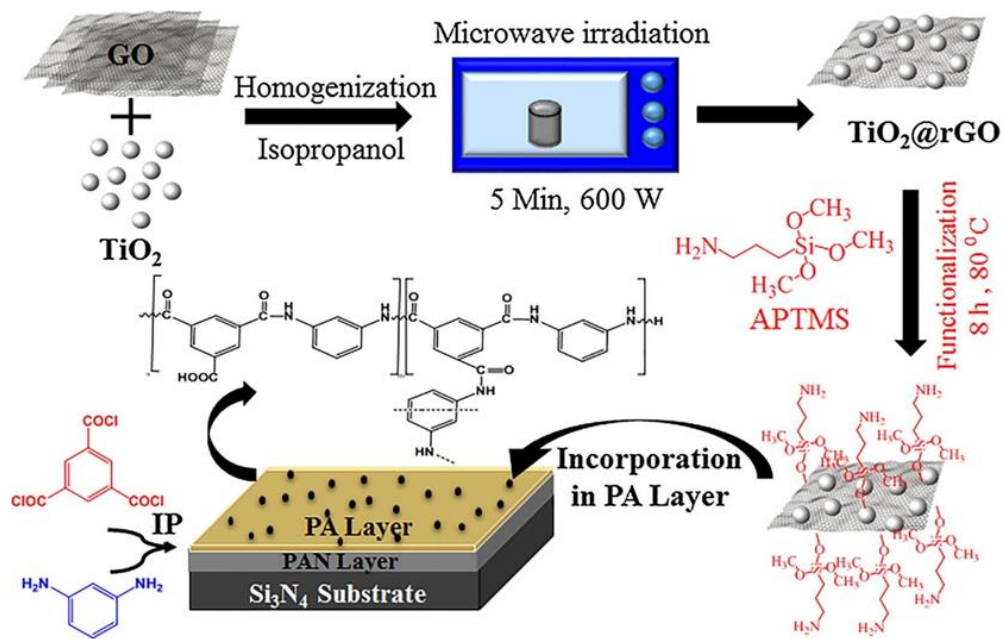
Figure 2.8. Schematic illustration of the fabrication of TiO$_2$@rGO and their incorporation into the PA layer for the TFN membrane fabrication (adapted from Ref. (Abadikhah et al., 2019)).

2.3.2.3 Silica and Titania

As discussed in the previous chapter, silica nanoparticles exhibit several advantageous features including large specific surface area, rich in hydroxyl groups, and ability to accommodate different functional groups making silica to be suitable for high-performance TFN-OSN membrane fabrication. Thus, several studies have been conducted to fabricate effective TFN membranes for OSN applications.

For example, Kebria et al. (Kebria, Jahanshahi, & Rahimpour, 2015) fabricated a series of TFN membranes by adding different loadings of SiO_2 nanoparticles into an aqueous solution phase during the IP process on top of PSf support substrate. SEM images show that the SiO_2 nanoparticles were uniformly dispersed on the surface of the membranes. With the addition of SiO_2 nanoparticles, the TFN membrane's surface became rougher and more hydrophilic. OSN membrane performances were tested using IPA as an organic solvent and crystal violet (CV) as a solute. Compared to membranes without silica nanoparticles, the TFN membranes with 0.03 wt% silica nanoparticle incorporation exhibited a slightly improved solvent flux and a slightly decreased solute rejection. When the SiO_2 loadings were increased from 0.03 wt% to 0.1 wt%, both solvent flux and solute rejection rates were improved with an increasing trend as the loadings of silica nanoparticles were increased, where the membrane performances were improved compared to the membranes without the silica nanoparticles. Liu et al. (Q. Liu, Wu, & Zhang, 2018) also embedded SiO_2 nanoparticles into the active layer via the IP process on the PSf substrate. The TFN membrane performance revealed that the methanol and ethanol permeate fluxes increased dramatically with a slight decline in solute rejection. When the silica nanoparticle loading was 0.025 wt%, optimal membrane performance was achieved, and the permeances for methanol and ethanol were 3.29 and 0.42 L m^{-2} h^{-1} bar^{-1}, respectively with rejections of RB, BTB, CV, and MO over 90%. In the long-term permeation test, the nanocomposite membrane revealed stable permeability and retention in ethanol and methanol solvents. Li et al. (Yifan Li et al., 2016) prepared 3 kinds of functionalized SiO_2 nanoparticles (SiO_2-C_6H_6, SiO_2-SO_3H, and SiO_2-Py) and were incorporated into PEI substrate for TFN-OSN membrane fabrication. The characterization of the TFN membranes revealed that the nanoparticles were uniformly dispersed in the PEI substrate without obvious observable defects. Depending on the incorporation of hydrophobic (SiO_2-C_6H_6) or hydrophilic (SiO_2-

SO$_3$H and SiO$_2$-Py) silica nanoparticles, the resultant TFN membranes presented enhanced solvent permeation for nonpolar or polar solvents, respectively. In particular, the ethanol (polar solvent) permeate flux was elevated from 21.2 to 30.8 L m^{-2} h^{-1} by embedding hydrophilic SiO$_2$ nanoparticles. With the incorporation of hydrophobic SiO$_2$ nanoparticles, the resultant TFN membrane exhibited an increase in permeate flux for n-hexane (non-polar solvents) from 0.1 to 21.7 L m^{-2} h^{-1} due to the presence of silica nanoparticles with different functional groups. Moreover, all the nanocomposite membranes showed good solvent resistance in toluene and heptane.

The TFN membranes tend to experience poor compatibility between the nanoparticles and the polymer substrate and weak interactive force between the active layer and support layer which is detrimental to the membrane's properties. In order to prepare TFN membranes with improved mechanical properties, Chen et al. (Y. Chen, Toth, & He, 2019) introduced N-methyl-Dglucamine assisted dopamine along with SiO$_2$ nanoparticles to increase the binding between the active layer and the support substrate as well as enhanced the compatibility of silica nanoparticles with polymers used in IP process. The TFN membrane with 0.1% wt% SiO$_2$ nanoparticles incorporation exhibited optimal membrane performance with methanol permeances around 2.18 L m^{-2} h^{-1} bar^{-1} along with a rejection of 99.1% for acid red (MW: 509 g mol^{-1}), which was better than the commercial OSN membranes. Moreover, the modified TFN membranes showed good stability under three organic solvents (methanol, ethanol, and IPA) for 15 days of soaking test and two days of organic solvent filtration test. Since dopamine is widely used as a universal binding agent and its high compatibility with many polymers makes it a versatile material for membrane fabrication and modification. This research demonstrates new ways of fabricating mechanically robust, stable TFN membranes using silica nanoparticles with an addition of dopamine.

Zhang et al. (H. Zhang et al., 2014) fabricated a series of TFN membranes with a PEI polymer-SiO$_2$/TiO$_2$ nanoparticle hybrid composite selective layer. Different concentrations (0.2, 0.4, 0.6, and 0.8 wt %) of inorganic precursor tetraethoxysilane and tetra-n-butyltitanate were used to synthesize SiO$_2$ and TiO$_2$ nanoparticles with tuneable structures. The membrane performances in terms of membrane swelling, solvent permeate flux and solute rejection were investigated and compared using n-heptane, toluene, butanone, ethyl acetate, and IPA as solvents, and PEG with different molecular weights as solutes. The synthesized TFN membranes revealed membrane

swelling below 6% in all organic solvents indicating its good solvent resistance properties. Moreover, the increase of SiO_2 nanoparticle loading effectively improved the membrane's solute rejection ability, and the TFN membranes achieved MWCOs of 670, 579, 463, and 394 with addition of 0.2, 0.4, 0.6, and 0.8 wt % TEOS, respectively. In the long-term operation (11 hrs), the stable IPA permeance of 1.46 L m^{-2} h^{-1} bar^{-1} with PEG (1000) rejection of 99.9% was maintained for the TFN membrane with SiO_2, for the TFN membrane with TiO_2, these values were 0.61 L m^{-2} h^{-1} $bar^{-1}$and 99.9%. Cheng et al. (Xiquan Cheng et al., 2017) incorporated different loadings of (0.025, 0.05, 0.075, 0.1, and 0.2 wt%) of P25 (commercial TiO_2 nanoparticles) into PPy active layer via in-situ hydrolysis of $Ti(OC_4H_9)_4$ precursor on top of a PAN support. Different from other TFN-OSN membranes, polypyrrole was selected for active layer formation for IP process. The TiO_2 incorporated PPy mixed membranes showed pure methanol permeance of 46.5 L m^{-2} h^{-1} bar^{-1}, ethanol permeance of 16.2 L m^{-2} h^{-1} bar^{-1}, and THF permeance of 23.1 L m^{-2} h^{-1} bar^{-1}. The dye separation tests demonstrated brilliant blue R (BBR, 792 Da) and RB rejection of 92% and 98%, respectively with IPA permeate flux of 6.5 L m^{-2} h^{-1} bar^{-1}. During the long-term filtration test (48 hrs), the TFN membrane also exhibited stable and ethanol permeance over 8.0 L m^{-2} h^{-1} bar^{-1}, which demonstrates TiO_2 based TFN membrane's great potential in the recovery of organic solvents.

In order to improve the compatibility of TiO_2 nanoparticles with the polymer substrate, amine, and chloride compounds were used for TiO_2 modification. For example, Peyravi et al. (Peyravi, Jahanshahi, Rahimpour, Javadi, & Hajavi, 2014) developed TFN-OSN membranes through in-situ incorporation of functional TiO_2 nanoparticles along with IP for the formation of PA layer on a PI support. 0.05 wt% of aminated and chlorinated TiO_2 were dissolved in the aqueous and organic phases, respectively. Membrane characterizations revealed that TiO_2 nanoparticles were uniformly dispersed throughout the polyamide matrix. In OSN performance tests, the TFN membrane with the chlorinated TiO_2 incorporation demonstrated methanol permeance of 24.8 L m^{-2} h^{-1} bar^{-1} and relative dye rejection of 89.7% and 93% for BTB and CV, respectively. Moreover, the TFN-OSN membranes presented good stability in aggressive DMF solvent due to the chain mobility of TiO_2 nanoparticles.

2.3.2.4 Covalent organic frameworks and carbon nanotubes

Recently, covalent organic frameworks (COFs) nanoparticles have drawn much attention as a nanofiller material for TFN membrane synthesis due to their unique characteristics including, relatively low density and porous structures. In addition, the strong covalent bonds of COFs makes them to be stable in various solvents by assembling of organic building blocks (Diercks & Yaghi, 2017; X. Feng, Ding, & Jiang, 2012). Therefore, COFs can be a promising nanofiller material for the fabrication of stable and good-performance OSN membranes.

To demonstrate the potential of COFs in TFN membrane fabrication, Li et al. (C. Li et al., 2019) developed a series of COF nanoparticles incorporated TFN membranes with enhanced solvent permeance and solute rejection for the OSN process. IP occurred between the m-phenylenediamine (MPD) incorporated with different concentrations COFs (25, 50, 75, 100, and 120 mg L^{-1}) and TMC, followed by chemical crosslinking and solvent activation. The effect of MPD (1.0, 1.5, 2.0, 2.5, 3.0, 3.5 4.0, 4.5, and 5.0 wt%) and TMC (0.10, 0.15, 0.20, 0.25, and 0.30 wt%) concentrations on membrane performances was also evaluated. Under the optimal conditions (MPD 4.0 wt%, TMC 0.20 wt%, 100 mg L^{-1} COFs), the TFN membrane exhibited ethanol permeance of 7.98 L m^{-2} h^{-1} bar^{-1} and RDB rejection of 99.4%. Furthermore, the TFN membrane also presented good solvent resistance after being immersed in DMF solvent at room temperature for more than 100 days and no significant changes in membrane performances were observed after being tested with DMF containing RB for 7 days, which demonstrates its great potential in OSN application.

The preparation of OSN membranes based on the transport of solvents through the CNTs surface is promising for OSN application. Roy et al. (Roy et al., 2011) modified the outer surface of MWCNTs with hydrophilic (-COOH) groups and hydrophobic groups via microwave treatment. During the IP process, the hydrophilic MWCNTs were dispersed in an aqueous solution and the hydrophobic MWCNTs were dispersed in an organic solvent. The CNTs modified TFN membranes with the nanochannels formed between the functionalized MWCNTs and the polymer matrix improved the solvent permeance by an order of magnitude. The optimal TFN membrane performances revealed methanol permeability of 6.28 L m^{-2} h^{-1} bar^{-1} and BBR (826 Da) rejection of 91% with the PEI and isophthaloyl dichloride (IPD) concentration of

0.75 wt% and hydrophobic MWCNTs loading of 0.06 wt%. When loading of 0.06 wt% hydrophilic MWCNTs, the TFN membrane exhibited ethanol permeability of 7.39 L m^{-2} h^{-1} bar^{-1} and BBR rejection of 89%.

2.3.2.5 Issues and possible solutions

During the IP process for TFN membrane synthesis, nanomaterial containing monomer solutions needs to be utilized to form an active layer. Since nanomaterials are relatively expensive compared to pristine polymers, the discharge of nanomaterial-containing solutions is a waste of valuable resources and will also increase the cost of membrane synthesis. Thus, exploring alternative ways for forming active layers is highly attractive and will also make the TFN membranes to be more commercially viable. Moreover, many studies demonstrated that the addition of nanomaterials could relieve the trade-off between membrane permeability and selectivity. However, they are not always been the case as some studies reported that nanomaterial incorporation led to slightly decreased solute rejections regardless of the increased permeate flux. Several other approaches like aqueous additive and solvent activation have been reported to improve solvent flux while maintaining good solute rejections (Maria Fernanda Jimenez Solomon et al., 2012; S. P. Sun, Chung, Lu, & Chan, 2014). Therefore, these approaches could be explored in the near future to fabricate a TFN-OSN membrane with enhanced performance. Furthermore, uncontrolled nanomaterial loadings and size distributions can lead to the generation of defects in the active layer which requires careful control and is a subject for future studies.

2.4 Nanomaterials thin film deposited on substrates serving as an active layer

Nanomaterial thin film membrane is an emerging type of nanomaterial-based membrane that can be used in the OSN process for solvent and solute separation. Different from MMMs-OSN and TFN-OSN membranes with nanomaterials incorporated into polymers, in the case of nanomaterial thin film membrane nanomaterial layer grown or deposited on the substrate surface serves as an active layer. Such kind of membrane with a homogenous selective layer enables minimum solvent transport resistance leading to high solvent permeance. Moreover, since the nanochannels formed by the nanomaterials are the only solvent permeation channels, with precise control of nanomaterial properties and the thickness of the deposited layer,

the fabricated membranes can exhibit optimal separation performance for OSN application (X. Liu, Demir, Wu, & Li, 2015). Therefore, nanomaterial thin film membranes are synthesized using various nanomaterials including MOFs, GO, COFs, etc. via several direct depositions or in-situ growth techniques. For example, most MOF thin film membranes are synthesized via the in-situ growth of MOFs on the support substrate. Another example, for GO thin film membrane synthesis, the pressure-assisted coating process is often utilized as illustrated in **Figure 2.9**. Various nanomaterials-based thin film membrane synthesis and its membrane performance in OSN applications are summarised below.
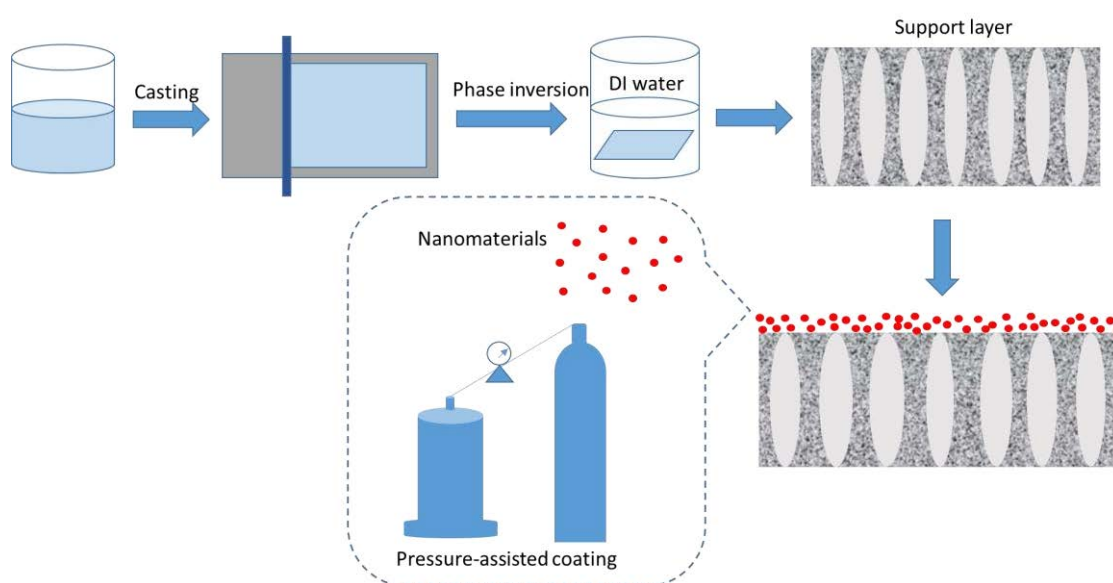
Figure 2.9. Pressure-assisted coating of nanomaterials onto the surface of substrate.

2.4.1 Metal organic frameworks

MOF thin film membranes can fully take advantages of MOFs intrinsic properties and demonstrate good separation performance by controlling the pores size of MOFs (Y. Ma et al., 2019).

Continuous UiO-66-NH$_2$ OSN membrane was fabricated via in-situ solvothermal synthesis on the Matrimid support surface (Ma, Han, Gao, & Chen, 2019). The prepared UiO-66-NH$_2$ thin film membrane exhibited high surface hydrophobicity with moderate methanol permeance of 0.88 L m^{-2} h^{-1} bar^{-1} and RB rejection of 96.33%. In addition, the UiO-66-NH$_2$ thin film membrane demonstrated good chemical stability in various organic solvents including hexane, methanol, and ethanol, implying their great potential in practical applications. Campbell et al. (Campbell et al., 2016)

prepared MOFs and polymer hybrid membranes by in-situ growth of HKUST-1 within the pores of PI membranes. In order to achieve improved membrane performance, chemical modification of the PI substrate was performed. The modified membrane with aryl carboxylic acid moieties enabled the coordination of HKUST-1 directly onto the polymer. Compared to the unmodified membrane, the modified membrane exhibited improved permeability and selectivity. Moreover, the modified membrane was stable during the long-term filtration test (25 hrs) in acetone.

In order to improve the solvent permeate flux through continuous, MOFs-based thin film membranes, the interfacial synthesis method was utilised to produce a thin film of HKUST-1 layer on P84 support surface (James Campbell, 2013). Interfacial synthesis is inspired by the traditional IP method. By using this method, it is expected that the MOF layer form from opposite directions, allowing growth and self-completion in just one single step. Two different fabrication methods were used; in method A, the HKUST-1 layer was grown on the support surface; in method B, the HKUST-1 layer was embedded in the surface pores of the polymer support. The MOF-based membrane fabricated by method B was more flexible compared to the membrane produced by method A. The rejections of solutes by the prepared MOF thin film membranes were not high enough for the OSN processes. Therefore, further work is needed on altering the concentration and the reaction time of HKUST-1 to improve the membrane selectivity. Continuous, ZIF-8-based thin film membranes were successfully fabricated on a porous PES support using an interfacial synthesis approach (Y. Li, Wee, Volodin, Martens, & Vankelecom, 2015). The prepared membranes exhibited good RB rejection in IPA and ethanol. Compared to the solvo-thermal synthesis method, the interfacial synthesis approach is easy for up-scale synthesis, which could be used for the preparation of continuous, large-area, MOF thin film on different membrane supports. Wei et al. (Wei, Gupta, Liu, & Jiang, 2018) introduced a molecular dynamics simulation study of three kinds of continuous ZIF membranes (ZIF-25, ZIF-71, and ZIF-96) for the OSN process. The permeate flux of five different organic solvents (methanol, ethanol, acetone, acetonitrile, and n-hexane) were predicted. Simulation results showed that the ZIF-25 membrane with hydrophobic nature revealed the highest permeate flux for polar organic solvents such as methanol, ethanol, acetone, and acetonitrile, whereas the ZIF-96 membrane presented the highest permeate flux for nonpolar solvents such as n-hexane because of

its hydrophilic property. Based on the MOFs structural and interaction energy analysis, the interaction between the solvent and MOFs is the main factor affecting solvent permeation through the thin film membranes. In addition, the rejection of model solute paracetamol could reach 100% for all the ZIF-based membranes under five different organic solvents.

2.4.2 Graphene oxide

Amongst various nanomaterials for synthesizing thin film membranes, GO is widely used because of its simple preparation process involved, GO forms a stable dispersion in water and exhibits good mechanical and chemical stabilities (Thebo et al., 2018). Moreover, the 2D GO nanosheets can be stacked and form effective nanochannels for fast solvent transport and its tuneable spacing between the nanosheets act as a solute separation layer.

The pressure-assisted filtration is a widely used technique for coating GO nanosheets on the substrate surface. Using this method, GO-based thin film membrane was fabricated by depositing GO nanosheets on a robust hydrophobic PP support (Hua & Chung, 2017). After functionalization with different polyelectrolytes, the composite membrane presented superior OSN performances. When the membrane is modified with HPEI, it exhibited good rejection performance for cationic dyes. For example, it presented ethanol permeance of 14.9 $L\ m^{-2}\ h^{-1}\ bar^{-1}$ with an Alcian blue rejection of 95%. If the GO-based thin film membrane is modified by PSS, it exhibited good separation for anionic dyes. For example, it showed a peremance of 3.1 $L\ m^{-2}\ h^{-1}\ bar^{-1}$ with an RB rejection of 97%. Li et al. (B. Li, Cui, Japip, Thong, & Chung, 2018) prepared an ultrathin GO laminar thin film membrane via pressure-assisted filtration. The GO-based thin film membrane showed pure organic solvent fluxes of 24.89, 7.95, and 12.08 $L\ m^{-2}\ h^{-1}$ at 15 bar for ethanol, IPA, and hexane, respectively. Moreover, its rejection ability for orange II sodium salt (OS), SO, solvent blue 35, RDB, and remazol brilliant blue (RBB) were 56.60%, 86.52%, 4.39%, 66.95%, and 97.11%, respectively. They concluded that Donnan exclusion in the OSN process is less effective than in an aqueous system, whereas the membrane-solute affinity and the size exclusion are the crucial factors affecting the membrane separation performances. In addition, the GO-based thin film membrane exhibited good chemical stability in both polar and nonpolar organic solvents arising from its good chemical stabilities. In the 7-day long-term filtration test of vitamin B 12 in IPA, the GO thin film membrane demonstrated stable

separation performance. Other notable works in GO thin film membrane include the preparation of a thin GO selective layer on the surface of porous PI support via vacuum filtration, followed by the cross-linking which improved the stability of the GO thin film and the GO film with substrates, as a result, stable GO/cross-linked PI composite thin film membrane was prepared (M.-L. Liu et al., 2019). The GO thin film membrane is stable in IPA and DMF and exhibited pure solvent permeances of 11.1, 4.9, and 1.0 L m^{-2} h^{-1} bar^{-1} for water, IPA, and DMF, respectively, with an RB rejection above 94%. Other GO thin film-related membrane studies include a synthesis of rGO composite thin film membrane via vacuum filtration of rGO dispersion through a Nylon microfiltration (MF) membrane (L. Huang et al., 2016). The prepared rGO thin film membrane with a negatively charged surface showed methanol permeance of 75.3 L m^{-2} h^{-1} bar^{-1} with complete rejection of negatively charged Evans blue (EB, 3.4 nm, 960.8 g mol^{-1}) molecules. The methanol permeate flux of rGO membrane was 1.5 times higher than that of the conventional PA-based nanocomposite membrane.

Though the 2D material's lamellar thin film membranes have many benefits in the OSN process, the trade-off between permeability and selectivity is still a major challenge, which mainly arises as each nanomaterial exhibits single spacing channels which provide a single pathway for solvent transportation. Inspired by the unique structure of the aquaporin, GO thin film composite membranes with dual-spacing channels were fabricated to improve the membrane separation performances (S. Wang et al., 2019) (see **Fig. 2.10**). The nanocomposite membrane with the unique structure was obtained by in-situ intercalation and cross-linking of silica nanoparticles into GO nanosheets and then the mixture was filtered through a nylon MF membrane via vacuum filtration method. The nanoparticle with hydrophilic nature widens the solvent transport channel. By altering the nanoparticle-free areas, the GO layers blend and retain the narrow hydrophobic channels for enhancing the solute rejection. Resultant OSN performance demonstrated methanol permeance of 290 L m^{-2} h^{-1} bar^{-1} with 90% rejection for dyes larger than 1.5 nm in size. In long-term filtration experiments, the nanocomposite membrane demonstrated good stability under the different solvents (acetone, methanol, and DMF) with constant permeances after 72 hrs of operation.
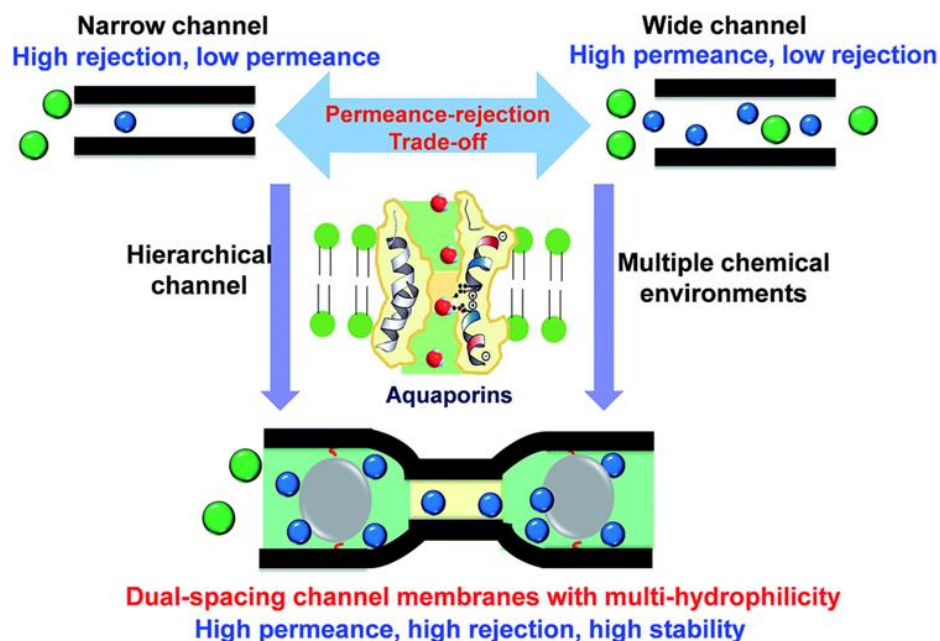
Figure 2.10. The concept of designing alternating dual-spacing channels with tailored chemical microenvironment in 2D material nanocomposite membranes. On the bottom: the green colour implies a hydrophilic domain; the yellow colour indicates the hydrophobic sectors (adapted from Ref. (S. Wang et al., 2019))

Other than the flat sheet configuration of GO-based thin film membranes, researchers also demonstrated the synthesis of nanocomposite hollow fibre membranes by deposition of GO films on the surface of ceramic hollow fibre (Aba, Chong, Wang, Mattevi, & Li, 2015). To obtain the nanocomposite thin film membrane, the hollow fibre was immersed in GO solution with one end sealed and another end connected to a vacuum pump. With the aid of pressure, GO flakes were stacked layer by layer on the surface of the ceramic hollow fibre. They found that at the dry state, the GO films on hollow fibre substrates were not stable due to the drying-related shrinkage effect. However, when keep them in a wet state, the composite hollow fibre membranes remained stable. Compared to most of commercial membranes, the GO thin film hollow fibre membranes exhibited higher permeate fluxes for acetone and methanol with the rejection of molecules larger than 300 Da, demonstrating its great potential in OSN applications.

2.4.3 Covalent organic frameworks

COFs is a promising material for OSN application due to its high organic solvent stability as well as its good thermal stability. In addition, the desirable pore size inside the frameworks provides suitable pathways for solvent molecules permeation without

destroying the COFs' molecular structures. Therefore, COFs were investigated by researchers to exploit its capability in OSN applications.

Shinde et al. (Digambar B. Shinde et al., 2020; D. B. Shinde et al., 2018) utilized Langmuir-Blodgett technique to synthesize three kinds of COF membranes (1,3,5-triformylphloroglucinol (TFP)-9,9-dihexylfluorene-2,7-diamine (DHF) membrane, TFP-9,9-dipropylfluorene-2,7-diamine (DPF) membrane and TFP-9,9-dinonylfluorene-2,7-diamine (DNF) membrane) with similar framework structure but different lengths of alkyl chains. By altering the length of alkyl chains (n-propyl/n-hexyl/n-nonyl), the pore size of COF membranes could be controlled to be 1.72, 1.41, and 1.22 nm, respectively. The pore size of COFs strongly influenced the membrane's solvent permeability and solute separation ability. The permeability of the COF membranes increased in the order of TFP-DPF membrane>TFP-DHF membrane>TFP-DNF membrane, which is consistent with their pore size. Moreover, all the COF membranes exhibited good thermal and chemical stability under various organic solvents (IPA, ethanol, methanol, hexane, heptane, and acetonitrile). This research provides an example of a molecular-level design of COF membranes, which enables precise control of pore sizes for selective solvent/molecule permeation for OSN applications.

2.4.4 Others
Other notable nanomaterial thin film membranes for OSN include the use of other 2D nanomaterials such as boron nitride (BN), molybdenum disulfide (MoS_2), and tungsten disulfide (WS_2).

For example, BN thin film membrane for OSN application was demonstrated by Chen et al.(C. Chen et al., 2018). They developed amino functionalized boron nitride (FBN) based thin film membrane with ultrafast solvent transport performance. Different FBN-based membranes were prepared by changing the FBN thin film membrane thickness of 0.4, 0.7, 1, 1.5, 2, and 8 μm. Due to the thin, laminar structure and stable networks of FBN nanosheets, the FBN-based thin film membranes exhibited good OSN performances. For example, FBN membrane with thickness of 2 μm, exhibited methanol permeance of 560 L m^{-2} h^{-1} bar^{-1} with EB (960Da) rejection of 99%. In addition, the nanocomposite membrane presented good chemical stability in harsh conditions, such as acid, basic and oxidative media for one month arising from good

chemical stability of BN-based materials, indicating its great potential for OSN applications.

Ran et al. (Ran et al., 2020) prepared MoS_2 membranes by vacuum filtration of MoS_2 dispersions on the Nylon membrane surface. The MoS_2 membranes provided good solvent permeance and solute rejections due to its regular transport channel with narrow distribution of channel sizes. Two kinds of MoS_2 membrane were fabricated namely dry MoS_2 (D-MoS_2) and solvated MoS_2 (S-MoS_2). The D-MoS_2 membranes were produced by drying under a vacuum at $40°C$ for 24 hrs before use. For the preparation of S-MoS_2, the resultant membranes were immediately immersed in water maintaining them in a solvated state. Compared to D-MoS_2 membrane, the S-MoS_2 membrane with a thickness of 36 nm exhibited higher permeances of water and acetonitrile, achieving 1881 and 5207 L m^{-2} h^{-1} bar^{-1}, respectively. During the long-term permeation and high-pressure nanofiltration tests, the D-MoS_2 membrane was stable in acetonitrile and IPA, with no obvious permeate flux decline. Both D-MoS_2 and S-MoS_2 membranes presented good solute separation abilities. Near 100% rejections of the solute size above 1.4 nm were demonstrated. Moreover, the MoS_2 membranes also demonstrated high mechanical and chemical stabilities under high pressure and harsh environment such as acid, basic and oxidative solutions. Guo et al. (B. Y. Guo et al., 2019) prepared hydro-MoS_2 membranes on the basis of a hydrothermal method via the introduction of a "supportive" drying process where glycerol acts as the supporting bridge during membrane drying. The hydro-MoS_2 membrane reduced its interlayer spacing from ~ 1.8 to ~ 1.0 nm due to the evaporation of water. Moreover, the hydro-MoS_2 membranes exhibited rejection of ~ 90% to RB (size of ~ 1.45 nm) and IPA permeance of ~ 3 L m^{-2} h^{-1} bar^{-1} over a 7 days filtration test.

Tham et al. (Hui Min Tham, Susilo Japip, & Tai-Shung Chung, 2019) fabricated WS_2 thin film membranes via a pressure-assisted filtration process using WS_2 dispersions onto cross-linked PAN membrane surface. Different WS_2 dispersions were synthesized in different solvents (NMP, ethanol/water, and pure water). The OSN performances of the resultant WS_2 membranes synthesized using different solvents used for the WS_2 dispersions were compared. Amongst the WS_2 membranes prepared using different solvents, the optimal membrane performance was achieved using WS_2 dispersed in NMP dispersions. Under the optimal conditions, the modified WS_2 thin

film membrane exhibited membrane performance with ethanol permeance of 43.35 L m^{-2} h^{-1} bar^{-1} and RBB (626.54 Da) rejection of 86% and a long-term stable rejection of 99% towards EB (960.81 g/mol) in ethanol.

Chen et al. (X. Chen et al., 2018) fabricated an ultrathin nanocomposite membrane by plasma-assisted octamethyl polyhedral oligomeric silsesquioxane (POSS) nanoparticle deposition on a PSf substrate surface. Such ultrathin nanocomposite membrane presented 9.9 times higher ethanol permeances compared to the control PSf membrane. The highest ethanol permeation of 164 $kg \cdot m^{-2} \cdot h^{-1} \cdot bar^{-1}$ was achieved at the nanoparticle concentration of 0.1 wt% and membrane active layer thickness of 50 nm. Moreover, the nanocomposite membrane with hydrophobic but alcohol-philic properties exhibited separation factors of ethanol over water up to 6.5. Siddique et al. (Siddique et al., 2012) synthesized a series of OSN membranes by coating nanosized polymer particles onto a PI support surface. After coating, the polymeric nanoparticles were cross-linked by ultraviolet (UV) light (365 nm wavelength). Two sizes (120 and 300 nm) of polymer nanoparticles with varying concentrations (2.5 and 5 wt%) and the varying number of coatings (1, 2, and 3) were used and investigated for membrane fabrication. The MWCO of modified membranes ranged from 200 to 1000 g mol^{-1} based on the nanoparticle concentration and the thickness of the coating layer which was controlled by the number of coatings. For example, the nanocomposite membrane with 5 wt% polymer particles under 3 times of nanoparticles coating exhibited toluene permeance of 1.8 L m^{-2} h^{-1} bar^{-1} with MWCO around 340 g mol^{-1}.

2.4.5 Issues and possible solutions

Compared to MMMs-OSN and TFN-OSN membranes, nanomaterial-based thin film OSN membranes require higher nanomaterial concentrations to form a selective layer on the substrate surface. Since the nanomaterials are relatively expensive compared to the polymeric materials, the overall cost of such types of membranes will increase, which can be a limitation for their further applications. If a cost-effective nanomaterial synthesis route can be co-developed, then it will generate further practical and industry impact using nanomaterial-based thin film OSN membrane. In addition, the polycrystalline structure of stacked nanomaterials may lead to some inter-crystalline cracks or grain boundary defects, which will deteriorate the OSN membrane performances (X. Li et al., 2017; C. Zhang, Wu, Ma, Wang, & Xu, 2019). Thus, the

fabrication of defect-free nanomaterial layers is necessary for high-performing OSN membranes with good mechanical stability and enhanced membrane performances.

2.5 Nanomaterial incorporated in both active layers and substrates

Except for the above-mentioned approaches for OSN membrane fabrications, recent studies demonstrated other approaches for OSN membrane fabrication. Other approaches include the incorporation of nanomaterial into both selective and support layers, meanwhile maintaining a high resistance to organic solvents. **Fig. 2.11** illustrates the fabrication of the above-mentioned membrane type.
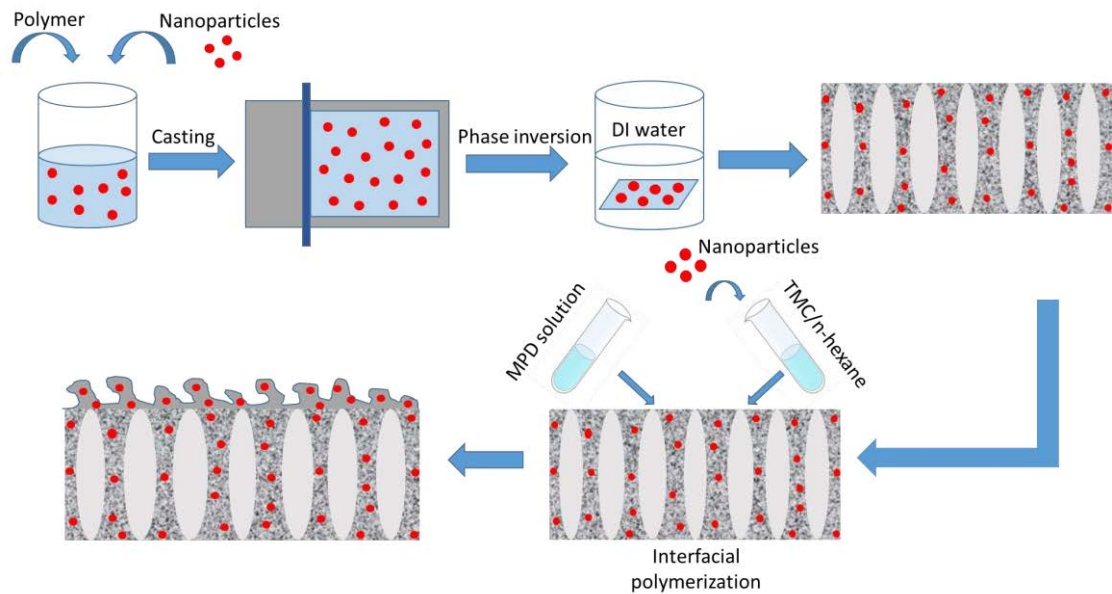
Figure 2.11. Illustration of membrane fabrication process with the nanomaterial-incorporated into both active and support layer for OSN application.

Such a novel type of membrane was demonstrated by incorporating different concentrations (0, 0.02, 0.05, 0.1and 0.2 w/v %) of amino-functionalized UZM-5 (zeolite) and SiO_2 nanoparticles in PA active layer and PEI support layer, respectively (Mahdieh Namvar-Mahboub, Pakizeh, & Davari, 2014). Based on their previous study, the optimal addition of SiO_2 in PEI solution was 5 wt%, under this condition the membrane exhibited optimal physical-chemical stability and membrane performances. AFM results showed that the surface roughness decreased in the range of 0-0.1 wt % UZM-5 loading, while at the 0.2 w/v % UZM-5 loading, an increase of membrane surface roughness was observed. The water contact angle values confirmed this trend with decreased water contact angles in the range of 0-0.1 wt % UZM-5 loading, which confirms its improved membrane hydrophilicity. The OSN performance test showed

that the TFN membrane with optimal UZM-5 concentration (0.02 w/v %) achieved MEK/toluene (mass ratio of 0.81%) permeate flux of 13.85 L m^{-2} h^{-1} and oil rejection of 96.27% at 15 bar.

2.6 Nanomaterial served as interlayers

Most widely used TFC membrane fabrication process involves typical monomer concentrations of ~2 wt% for MPD and 0.15 wt % for TMC, which are used for the IP process. Typical monomer concentrations used in the IP process often lead to a thicker selective layer and rough membrane surface, which is not desirable for effective solvent/solute separation for OSN application as thicker PA layer can lead to slower solvent transport, leading to lower flux membranes (Y. Guo, Li, Su, & Mandal, 2019; S. Li, C. Li, et al., 2019a). Moreover, UF membranes which are often used as support layers for PA layer formation tend to have uneven pore sizes and relatively poor wetting properties, which makes decreasing monomer concentrations for thinner PA layer formation to be unfeasible. During the IP process, the support layer plays a vital role in influencing the structure and properties of the PA selective layer and the final membrane. Therefore, strategies such as the introduction of an interlayer between the PA selective layer and the support layer has been implemented to provide desirable substrate surface condition for the IP process where te interlayer with uniform pores with enhanced wetting properties, leads to uniform distribution and enhanced interaction of aqueous monomer solution with interlayer/support structure and finally forming a controlled, thin and defect-free PA active layer (Z. Wang et al., 2018; Z. Yang et al., 2018; Zhai et al., 2018). Therefore, several nanomaterials have been used as an interlayer material for the fabrication of high-performing TFC membranes for OSN application.

For example, Li et al. (Yanyang Li et al., 2019) modified the PI support surface using cross-linked GO (cGO) nanosheets and successfully optimized the hydrophilicity and the surface roughness of the PI support for IP process. The modified OSN membranes with interlayer required fewer monomer concentrations (0.1 wt% for MPD and 0.005 wt % for TMC) for the formation of an ultra-smooth (average roughness around 2 nm), ultrathin (thickness about 15 nm), hydrophilic and defect-free PA layer. As a result, good membrane performance was demonstrated with ethanol permeance of 41.47 L m^{-2} h^{-1} MPa^{-1} and an RDB (479 Da) rejection of 99.4%. The interlayer-assisted TFC-OSN membrane also exhibited good solvent resistance, after being immersed in DMF

solvent at 80°C for 166 days, the membrane still demonstrated RDB rejection of 98% with ethanol permeance over 45 L m^{-2} h^{-1} MPa^{-1} and RB rejection more than 99% with DMF permeance of 81 L m^{-2} h^{-1} MPa^{-1} after continuous filtration test for 192 hrs.

Liang et al. (Y. Liang et al., 2020) fabricated a novel OSN membrane with a sandwich-like structure where the MPD and TMC form the active layer via the IP process on the GQDs-PEI-modified PI substrate. The thickness of the GQDs-interlayers was reduced to ~25 nm and the surface roughness was ~2 nm. The schematic diagram of the fabrication of GQDs-interlayered OSN membranes is shown in **Fig 2.12**. The GQDs interlayer can be covalently bonded to both the PI substrate and the PA active layer, greatly enhancing the stability of the synthesized OSN membranes. Compared with the pristine interlayer-free TFC membrane, the GQDs-interlayered TFC membrane exhibited an increased ethanol permeance from 33.5 to 40.3 L m^{-2} h^{-1} MPa^{-1} and an increased rejection of RDB from 87.4% to 98.7%. Moreover, the GQDs interlayered TFC membrane also demonstrated outstanding solvent resistance when immersed in pure DMF for 81 days at room temperature and 45 days at 80°C. During the 120 hours of continuous filtration test using RB/DMF solution mixture with a concentration of 100 mg/L at 0.6 MPa, nearly 100% rejection of RB was achieved using the GQDs-interlayered OSN membrane confirming its good solvent stability. This work provides a novel nanomaterial interlayer strategy to develop high-performance nanocomposite membranes for OSN application.
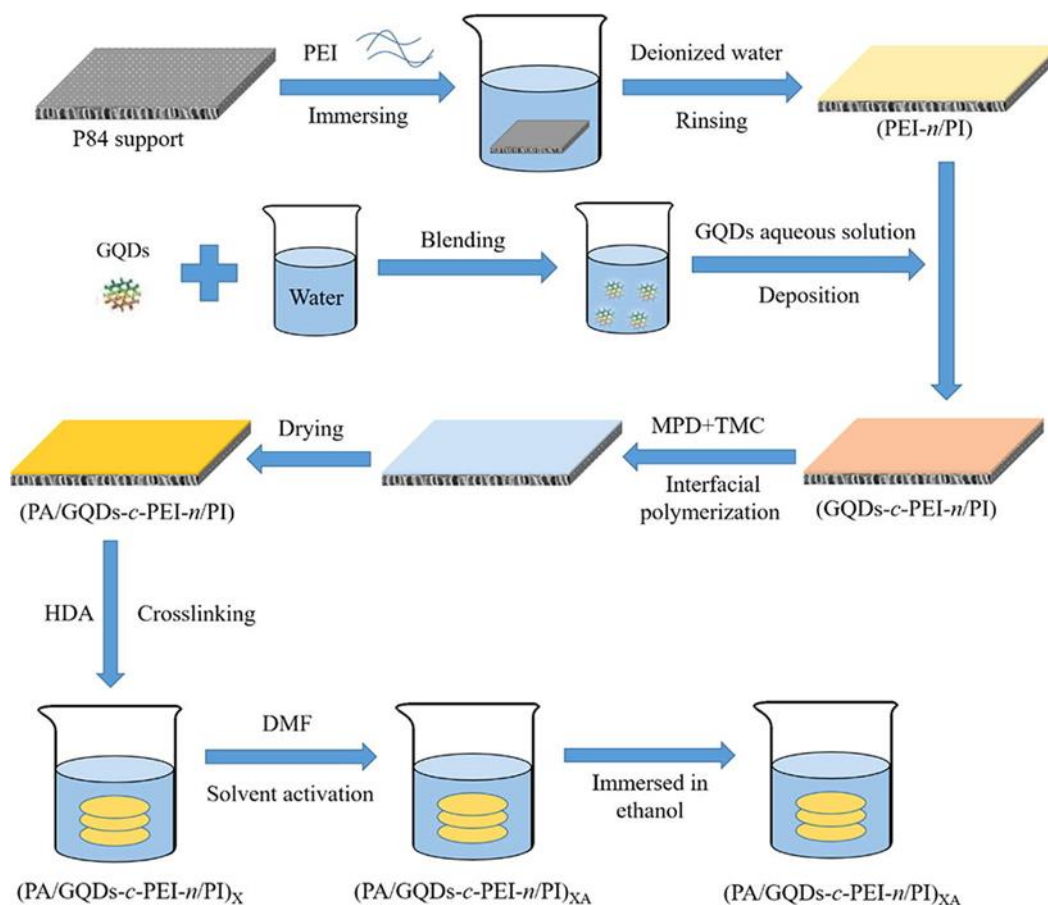
Figure 2.12. Fabrication of GQDs-interlayered OSN membranes (adapted from Ref. (Y. Liang et al., 2020)).

2.7 Conclusions

In this review paper, the nanomaterial-based OSN membranes were summarised and discussed according to different nanofiller materials and different fabrication approaches. Currently, five different configurations of nanomaterial-based OSN membranes have been fabricated and utilized as effective OSN membranes which include, nanomaterial-incorporated into support substrate (MMMs), embedded inside the PA active layers (TFN membranes), thin film coating on the support surface (nanomaterial based thin film membranes), adding into both active layer and support layer and acting as interlayer between the PA layer and the support layer. In addition, the effect of nanomaterial incorporation on the membrane performances for the OSN process was also evaluated. Most of the studies found that with the addition of nanomaterials, the modified membranes exhibited improved OSN performances (increased solvent permeances or improved solute rejections) compared to the pristine membranes. However, in most studies, many nanomaterial-based OSN membranes

still faced the trade-off issue between solvent permeate flux and solute rejection ability, along with limited knowledge of membrane fouling phenomenon during the OSN process under organic solvents, which all require further studies in the near future. Moreover, due to the non-uniform nanoparticle dispersion, the nanomaterial agglomeration is another big issue when fabricating nanomaterial-based OSN membranes which again requires future research efforts. Except for the nanomaterial agglomeration and the dispersion problem, high cost of these nanomaterials is still another drawback impeding their commercial applications. Therefore, effective and efficient synthesis of various nanomaterials requires future exploration and studies for the widespread use of nanomaterial-based OSN membranes in various industries. Furthermore, exploration of other polymers with good mechanical and chemical stabilities in various organic solvents is required in the future to reduce the use of hazardous cross-linkers and maintain reproducible performances in long-term tests. Finally, pilot scale studies using the real solvents separation from industries such as pharmaceutical or petrochemical industries need to be conducted in order to accurately evaluate the benefits and the economic feasibilities of nanomaterial-based OSN membranes in practical applications. These recommendations will certainly promote further understanding and the development of nanomaterial-based OSN membranes for OSN applications and are also desirable for their widespread use in diverse industrial applications involving organic or hazardous solvents.

CHAPTER 3
General experimental methods

3.1 Introduction

This chapter describes the general experimental methods used in this study in terms of membrane fabrication and modification methods, membrane characterizations, and membrane performance evaluations. More specific experimental details can be found in their respective chapters.

3.2 Fabrication and modification techniques

3.2.1 Fabrication of membrane support layer

The support membrane used in this study is PK membrane. The PK membrane fabrication process is depicted in **Fig. 3.1**. The casting solution was prepared by adding PK (12 wt%) and resorcinol (2 wt%) in a mixed salt solution. Detailed preparation procedures can be summarised as: firstly, the mixed salt solution was prepared with lithium chloride, calcium chloride, zinc chloride and water with ratio of 10/10/40/40 (w/w/w/w). Secondly, PK was added into the mixed salt solution with continuous stirring at 80 $^{\circ}$C for at least 2 h then another continuous stirring at 30 $^{\circ}$C for overnight to completely dissolve the PK polymer. Then the resorcinol was added into the PK/mixed salts solution at a temperature to 80 $^{\circ}$C again to obtain a homogenous dope solution. Lastly, the prepared dope solution was stored in a drying oven at 60 $^{\circ}$C for several hours to remove the air bubbles.

The PK membrane was fabricated via non-solvent induced phase separation. Using a casting knife, the dope solution was casted onto non-woven fabric attached on a glass plate with a height of 300 μm. Then the glass plate was immersed into tap water for 10 min. The post treatment was conducted by washing the PK membrane with hydrochloric acid (0.05%), acetone and hexane for 10 min each and then was dried at room temperature.

Figure 3.1. Schematic illustrations of PK support membrane fabrication process.

3.3.2 LBL for membrane active layer formation

Two different polyelectrolyte inks were used for active layer formation. The positively charged polymer ink was prepared with certain concentrations of poly(ethyleneimine) (PEI) solution. The negatively charged ink was prepared with PSS/SWCNT mixed solution or pure SWCNT/GO solutions with certain concentrations. Two commercial HP 63 black cartridges were thoroughly rinsed with de-ionized (DI) water after removing the sponge. Then cartridges were loaded new sponges filled with the prepared inks. A commercial Deskjet 2130 HP printer was used for printing the prepared inks on the membrane surface. The schematic illustration of the process is shown in **Fig. 3.2**. The PK membrane (5 cm × 5 cm) was taped onto an A4-sized polyethylene terephthalate (PET) film and loaded into the HP printer. A computer with printing software was connected to the printer where printing was performed with following settings: paper type of glossy paper with normal quality. The positive ink was firstly printed onto the PK membrane surface with the size of 4.5 cm × 4.5 cm, followed by the printing of negative ink on the same area. Between each printing cycle, the membrane was allowed to dry for 3 min at an ambient temperature. Thus, one bilayer was prepared. The printing process was repeated several times until the desired bilayer numbers were achieved. Subsequently, the cross-linking reactions were performed with different cross-linkers under different cross-linking conditions.
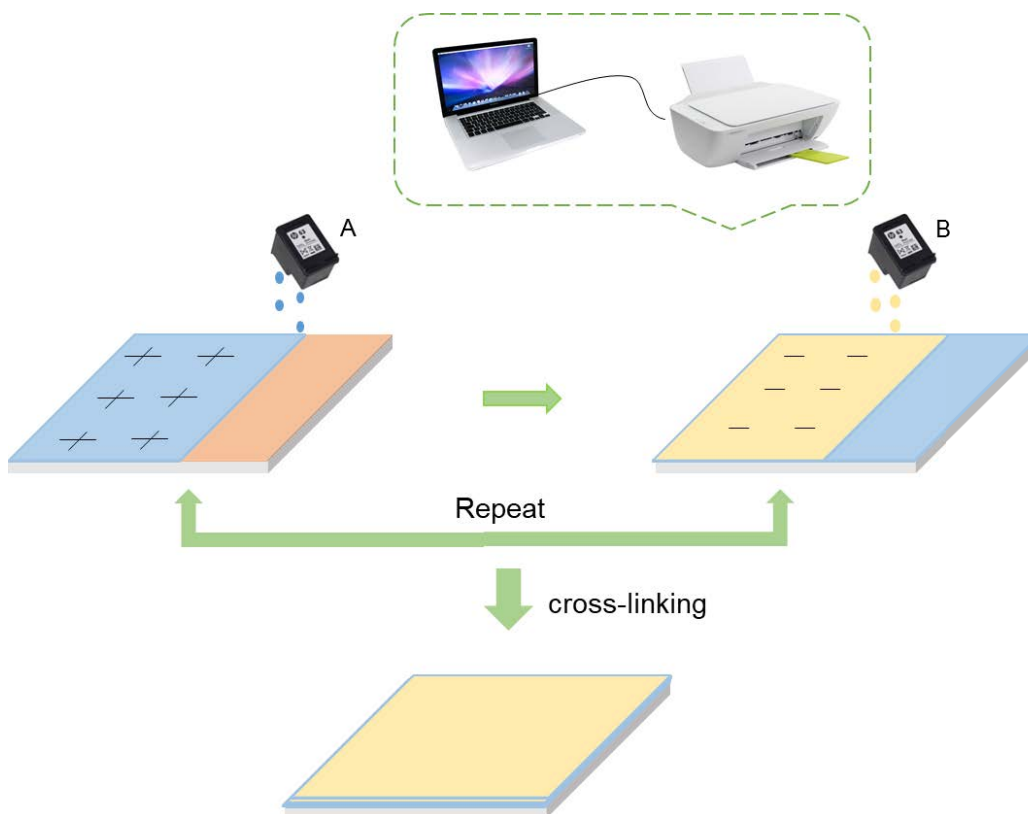
Figure 3.2. Schematic illustrations of the inkjet printing assisted LBL for membrane active layer formation.

3.3 Membrane characterizations

3.3.1 Scanning electron microscope

The membrane surface and cross-section morphologies were characterized by scanning electron microscopy (SEM, Zeiss Supra 55VP, Carl Zeiss AG). For cross-section characterizations, liquid nitrogen was used to fracture membrane samples. All the membrane samples were coated with Au/Pd with a thickness of 5-8 nm using a sputtering coater (EM ACE600, Leica). The SEM images were carried out at a voltage of 5 kV, and each membrane sample was tested in random positions at different image magnifications.

3.3.2 Atomic force microscopy

The membrane surface roughness was characterized by AFM (Park XE7). The scanning area was 5 μm × 5 μm with a pixels of 256. The AFM images for each membrane sample were taken in random positions on membrane surface.

3.3.3 Attenuated total reflectance - Fourier transform infrared spectroscopy

The surface functional groups of membrane samples were evaluated using attenuated total reflection flourier transformed infrared spectroscopy (ATR-FTIR, Affinity-1 Shimadzu). Multiple measurements were conducted in the wavelength range of 1000-3500 cm^{-1} with a signal resolution of 4 cm^{-1} and a minimum of 32 scans.

3.3.4 X-ray photoelectron spectroscopy

The surface chemical composition was analysed using X-ray photoelectron spectroscopy (XPS, JPS-9010 MC, JEOL, Japan) with Al Kα rays. Surface characterizations were carried out by both wide and narrow scans. Surface elemental composition was calculated by Avantage software.

3.3.5 Contact angle

The contact angle values of the membranes were measured by the sessile drop method and analysed by the optical system (Theta Lite 100, Biolin Scientific) equipped with an image analysis software. For the contact angle characterizations, a membrane sample was placed on a platform. Then, droplets were dropped on the membrane sample surface. In the meantime, the images of droplets were captured by a camera. Three measurements in random positions on the membrane surface were recorded to calculate the average contact angle data.

3.4 Membrane OSN performance evaluation

The membrane OSN performances were evaluated with 50 mg/L dyes in different organic solvents. Diagram of the OSN set-up used in this study was shown in **Fig. 3.3**. A commercial CF047 Circular Cell (Sterlitech) with an effect membrane area of 13.85 cm^2 and a PU-2089 Quaternary Gradient HPLC pump (JASCO) were used in OSN process. The applied pressure was maintained at 5 bar. The permeance (J_w) was calculated according to Eq. (1) :

$$J_w = \frac{V}{A\Delta tP} \tag{1}$$

where V is the volume of the permeate (L), A is the effective membrane area (m^2), Δt is the time interval (h), and P (bar) is the operating pressure.

The rejection (R) of dyes was calculated by Eq. (2):

$$R\ (\%) = 100\ \times (1 - \frac{c_p}{c_f}) \tag{2}$$

where C_f and C_p are the dye concentrations in feed and permeate, respectively. Dye concentrations of feed and permeate solutions were measured using a UV–Vis spectrophotometer (Shimadzu).

Figure 3.3. Schematic diagram of the OSN membrane testing device.

CHAPTER 4

Layer-by-layer inkjet printing of polyelectrolytes and single walled carbon nanotube for organic solvent nanofiltration membrane fabrication

4.1 Introduction

Organic solvent nanofiltration (OSN) is an emerging technology used for separating or recovering organic solvents from various kinds of solute/solvent streams utilizing organic solvent resistant membranes. Compared to conventional separation techniques, such as distillation and evaporation, OSN has been considered as a less energy intensive and environmental friendly method (Rundquist et al., 2012; C. Wang et al., 2021). OSN process shows great potential in pharmaceutical, petrochemical and food industry applications (Buonomenna & Bae, 2014; Szekely et al., 2014; Vandezande et al., 2008). In OSN process, OSN membranes are the most important factor influencing the separation performances. However, most of existing OSN membranes still face many issues, such as organic solvent stability and low solvent permeability, which impede the further development of OSN technology. Therefore, the fabrication of high performance and chemically stable OSN membranes are essential to accelerate the OSN applications (Amirilargani, Sadrzadeh, Sudhölter, & de Smet, 2016; Merlet, Pizzoccaro-Zilamy, Nijmeijer, & Winnubst, 2020; Sui, Yuan, Yu, Goh, & Chen, 2020).

In this chapter, we introduced the fabrication of LBL polyelectrolyte multilayer (PEM) membranes for OSN using a commercial inkjet printer, which could deliver precise amounts of polyelectrolyte solutions on the localised regions of the support membrane in rapid manner for the preparation of PEM membranes without intermediate rinsing steps. Compared to traditional LBL membrane assembly methods, numerous rinsing steps were replaced by only one final rinsing step, which significantly reduced the time for LBL membrane fabrication. In this work, organic solvent resistant, PK membrane prepared by M610F PK polymer was used as a substrate for the first time for OSN membrane fabrication. PEI and PSS were used as polycation and polyanion. SWCNT consists of a single graphene cylinder possessing large specific surface area, high flexibility, unique pore structure, and excellent mechanical strength. Moreover, incorporating SWCNT into membranes could help to restrict the polyelectrolyte chains movement and increase the compactness of the membrane, thus improving the membrane physical and chemical stability (S. Li, C. Li, et al., 2019b; Hui Min Tham, Susilo Japip, & Tai-Shung Chung, 2019). PEI solution and PSS/SWCNT mixed solution were alternatively printed on the PK substrate surface to form PEI/PSS-SWCNT multilayers through electrostatic interaction. The effects of number of bilayers, polyelectrolyte concentrations and crosslinking conditions on membrane

OSN performances were evaluated. In addition, membrane stability was tested by immersing them in different organic solvents (ethanol, methanol, IPA, and acetone) and through long term filtration tests. Our findings further elucidate inkjet printing technique as an effective and versatile technique for fabricating PEM OSN membranes, furthermore, we demonstrated for the first time, the use of PK support for OSN application.

4.2 Materials and methods

4.2.1 Materials

PK polymer (M610F) was supplied by Hyosung Corporation (South Korea). Resorcinol, lithium chloride, calcium chloride, zinc chloride, branched PEI (Mw ~ 25000), PSS (Mw ~ 7000), glutaraldehyde (GA) (25 wt% aqueous solution), RB, BBR, Janus Green B (JGB), MO, MB, ethanol, methanol, IPA, and acetone were purchased from Sigma-Aldrich (Australia). Carboxylated SWCNT (SWCNT, Purity: >95 wt%, outer diameter (OD):1–2 nm) powder with a short length (1–3 μm) was purchased from Jiangsu XFNANO Materials Tech CO., Ltd, China. Non-woven TS6005W was bought from Hirose Paper Co., Ltd., Japan. DI water produced from a Milli-Q ultra-pure water system (Millipore) was used in all experiments. All chemicals in this study were used as received.

4.2.2 Preparation of polyketone membrane

The PK membrane fabrication process is depicted in **Fig. 4.1** (a). The casting solution was prepared by adding PK (12 wt%) and resorcinol (2 wt%) in a mixed salt solution. Detailed preparation procedures can be summarised as: firstly, the mixed salt solution was prepared with lithium chloride, calcium chloride, zinc chloride and water with ratio of 10/10/40/40 (w/w/w/w). Secondly, PK was added into the mixed salt solution with continuous stirring at 80 °C for at least 2 h then another continuous stirring at 30 °C for overnight to completely dissolve the PK polymer. Then the resorcinol was added into the PK/mixed salts solution at a temperature to 80 °C again to obtain a homogenous dope solution. Lastly, the prepared dope solution was stored in a drying oven at 60 °C for several hours to remove the air bubbles.

The PK membrane was fabricated via non-solvent induced phase separation. Using a casting knife, the dope solution was casted onto non-woven fabric attached on a glass plate with a height of 300 μm. Then the glass plate was immersed into tap water for

10 min. The post treatment was conducted by washing the PK membrane with hydrochloric acid (0.05%), acetone and hexane for 10 min each and then was dried at room temperature.

4.2.3 Inkjet printing assisted PEM membrane fabrication

The inkjet printed PEM membrane preparation process is presented in **Fig. 4.1** (b). Two different polyelectrolyte inks were used for active layer formation. The positively charged polymer ink was prepared with PEI concentration of 10 g/L. The negatively charged ink was prepared with PSS and SWCNT mixed solution with the concentrations of 2.5 g/L and 0.5 g/L, respectively. Two commercial HP 63 black cartridges were thoroughly rinsed with DI water after removing the sponge. Then loaded new sponges filled with the polyelectrolyte inks. A commercial Deskjet 2130 HP printer was used for printing the prepared inks on the membrane surface. The PK membrane (5 cm × 5 cm) was taped onto an A4-sized PET film and loaded into the HP printer. A computer with printing software was connected to the printer where printing was performed with following settings: paper type of glossy paper with normal quality. The PEI ink (pH 10.8) was firstly printed onto the PK membrane surface with the size of 4.5 cm × 4.5 cm, followed by the printing of PSS/SWCNT ink (pH 7.6) on the same area. Between each printing cycle, the membrane was allowed to dry for 3 min at an ambient temperature. Thus, one bilayer was prepared. The resulting membrane is referred as the $(PEI/PSS-CNT)_n$ with the subscript "n" representing the number of PEI/PSS-CNT bilayers. We fabricated four kinds of membranes with bilayer numbers of 2, 5, 10 and 15, which are named as $(PEI/PSS-CNT)_2$, $(PEI/PSS-CNT)_5$, $(PEI/PSS-CNT)_{10}$, and $(PEI/PSS-CNT)_{15}$, respectively.

Subsequently, the fabricated membranes were washed with DI water for 3 min to remove the unreacted polyelectrolytes. The GA cross-linking solution was prepared with 1: 1 (v/v) DI water and ethanol, 1% (v/v) HCl, and 1 wt% GA. The membrane was finally treated with GA solution for 10 min, then put into dry oven at 90 °C for another 10 min.
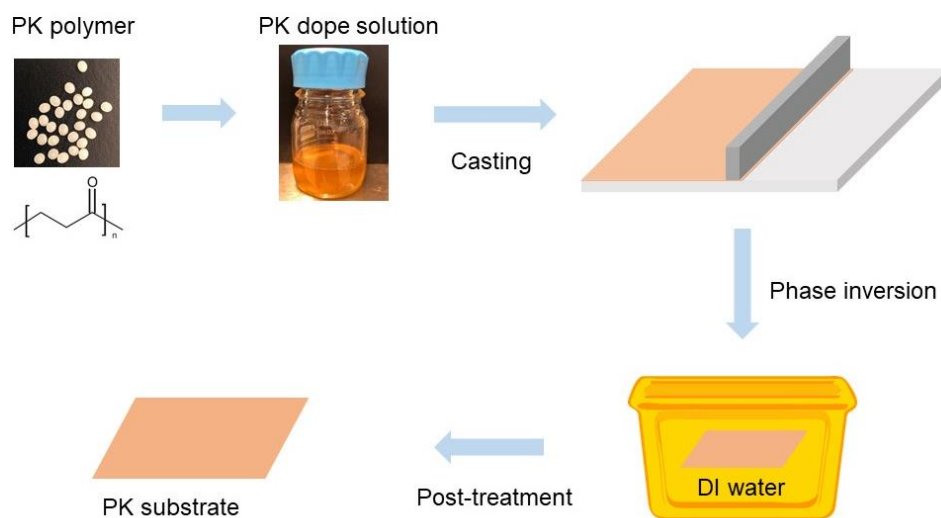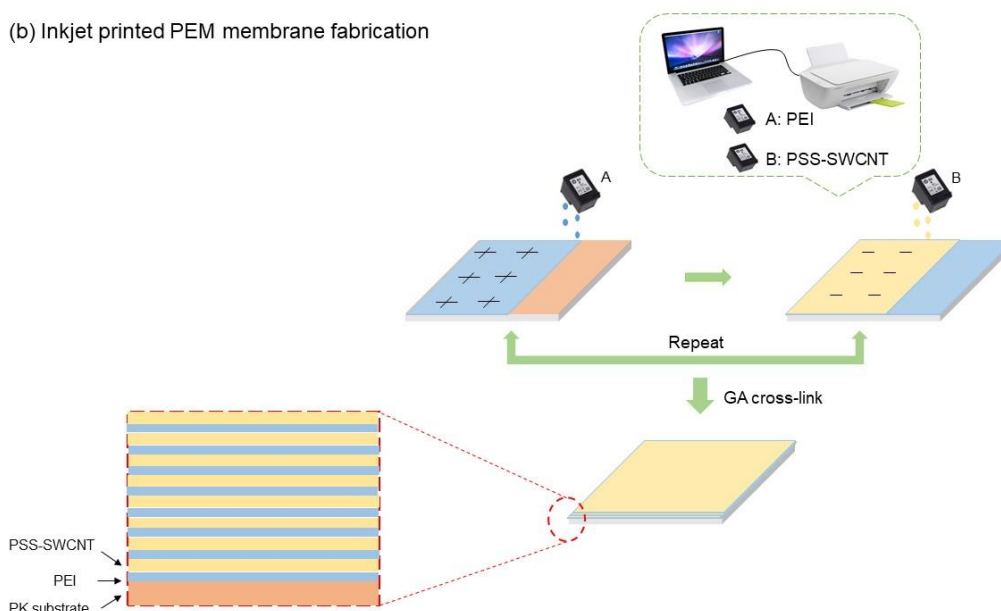
Figure 4.1. Schematic illustrations of (a) the PK membrane fabrication process and (b) the inkjet printing assisted PEM membrane fabrication process.

4.2.4 Membrane characterization

The surface functional groups of PK and PEM membrane were evaluated using ATR-FTIR (Affinity-1 Shimadzu). The surface chemical composition was analysed using X-ray photoelectron spectroscopy (XPS, JPS-9010 MC, JEOL, Japan) with Al Kα rays. The membrane surface morphology and surface roughness were characterized by SEM (Zeiss Supra 55VP, Carl Zeiss AG) and AFM (Park XE7), respectively. For the XPS, ATR-FTIR, SEM and AFM characterizations, each membrane sample was tested for

at least three times in random positions of the membrane surface. The contact angle values of the PK and PEM membranes were measured by the sessile drop method and analysed by the optical system (Theta Lite 100, Biolin Scientific) equipped with an image analysis software. Three measurements in random positions on the membrane surface were recorded to calculate the average contact angle data. The surface zeta potential of PK and PEM membranes were determined by Anton Paar Surpass solid-surface analysis. All measures were conducted using 1 mM KCl solution as background solution at 25 ºC.

4.2.5 Membrane organic solvent nanofiltration performance

The OSN performances of the PEM membranes were evaluated with 50 mg/L dyes in different organic solvents including ethanol, methanol, IPA and acetone. Diagram of the OSN set-up used in this study was shown in **Fig. 4.2**. A commercial CF047 Circular Cell (Sterlitech) with an effect membrane area of 13.85 cm^2 and a PU-2089 Quaternary Gradient HPLC pump (JASCO) were used in OSN process. The applied pressure was maintained at 5 bar. The permeance (J_w) was calculated according to Eq. (1) :

$$J_w = \frac{V}{A\Delta t P}$$

(1)

where V is the volume of the permeate (L), A is the effective membrane area (m^2), Δt is the time interval (h), and P (bar) is the operating pressure.

The rejection (R) of dyes was calculated by Eq. (2):

$$R\ (\%) = 100 \times (1 - \frac{C_p}{C_f})$$

(2)

where C_f and C_p are the dye concentrations in feed and permeate, respectively. Dye concentrations of feed and permeate solutions were measured using a UV–Vis spectrophotometer (Shimadzu).

Figure 4.2. Schematic diagram of the OSN membrane testing device.

4.3 Results and discussion

4. 3.1 Characterizations of PK and inkjet printed PEM membranes

The chemical properties and morphologies of PK and inkjet printed PEM membranes were investigated by FTIR spectroscopy, water contact angle analysis, XPS, SEM and AFM techniques.
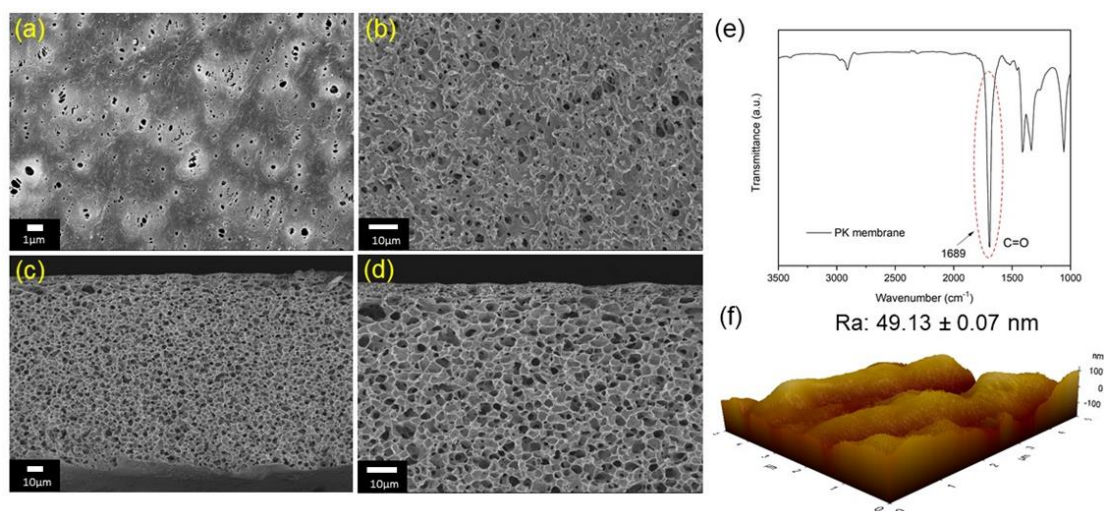
Figure 4.3. Surface properties of PK membranes. (a)-(d) SEM images of (a) top, (b) bottom and (c)-(d) cross section. (e) FTIR spectra. (f) AFM images.

Table 4.1 Basic properties of PK membrane

Properties	Pure water flux	Thickness (μm)

| PK membrane | 425.3 ± 11.3 | 127.5 ± 2.5 |

In **Fig. 4.3** (e), a strong peak at 1689 cm^{-1} revealed which corresponds the carbonyl band (C=O) of typical PK polymer chain containing of CH_2CH_2CO unit. The changes of peak intensity of PEM membranes in **Fig 4.4** (a) appeared at 3395 cm^{-1} mainly attributed to the N–H stretch with characteristic amine group in PEI, and this peak intensity became stronger with increased polyelectrolyte layers. Another characteristic amine group of PEI, namely bending N–H, exhibits broad absorption peak ranging from 1580 ~ 1650 cm^{-1} (Anusha Chandra, E. Bhuvanesh, Priyabrata Mandal, & Sujay Chattopadhyay, 2018), which is overlapping with the absorption peak range of C=O groups in PK substrate. This explains why the bending N–H group peaks from PEI was not clearly observable on the inkjet printed membranes. New peaks at 1126 cm^{-1} and 1173 cm^{-1} which were absent on the pristine PK membrane were observed on the printed membranes. These specific bands referred to stretching of S=O of the –SO$_3$ groups in PSS (Xin Li, Chang Liu, Wenqiang Yin, Tzyy Haur Chong, & Rong Wang, 2019b; Y. Zhao et al., 2016). The carboxyl (C=O) and hydroxyl functional groups (O–H) in SWCNT were not observed on the spectrum of printed membranes because of their absorption rage which are overlapping with ketone (C=O) groups in PK membrane and amine (N–H) groups in PEI. The presence of these specific bands of PEI, PSS and SWCNT clearly prove that the PEI, PSS and SWCNT were successfully printed on the PK substrate surface. In addition, the GA was used as a cross-linker during the PEM membrane fabrication process. As we observed, there was a new peak appearing with increase of bilayers at 1659 cm^{-1}. This should be the imine (–C=N) group resulting from the crosslinking reaction between amine group of PEI and the aldehyde group of GA. It is reported that the FTIR spectrum vibration of imine groups located at 1640 ~ 1690 cm^{-1} (Marin, Simionescu, & Barboiu, 2012).

The contact angle measurements were conducted to evaluate the surface properties of PK and printed PEM membranes (see **Fig. 4.4** (b)). Compared to the contact angle value of the pristine PK membrane (70.32 ± 0.34°), the contact angle of inkjet printed PEM membranes exhibited a decreasing trend as number of bilayers increased, indicating the improvement in hydrophilicity of the membrane. The increase of the hydrophilicity was mainly due to the oxygen functional groups contained in the carbon

nanotubes and the hydrophilic nature of the amine (–NH$_2$) groups in PEI and sulfonate (–SO$_3$) groups in PSS (X. Li et al., 2019b). With increase in number of printing cycles, more PEI/PSS-CNT bilayers were printed on the PK membrane surface leading to higher affinity with water. The contact angle of (PEI/PSS-CNT)$_2$ membrane is 64.93 ± 0.71°, and when the bilayers increased to 5 , 10 and 15, the contact angle values decreased to 62.18 ± 1.6°, 54.68 ± 1.6° and 54.23 ± 0.83°, respectively. It should be noted that the contact angle values of (PEI/PSS-CNT)$_{10}$ and (PEI/PSS-CNT)$_{15}$ membranes were similar. With increasing number of printing cycles, the PK membrane surface was gradually covered with polyelectrolytes and carbon nanotubes. When the number of bilayers reached 10, the PK membrane surface was fully covered. Thus, further increase in the printing cycles did not lead to further increase in membrane's hydrophilicity.
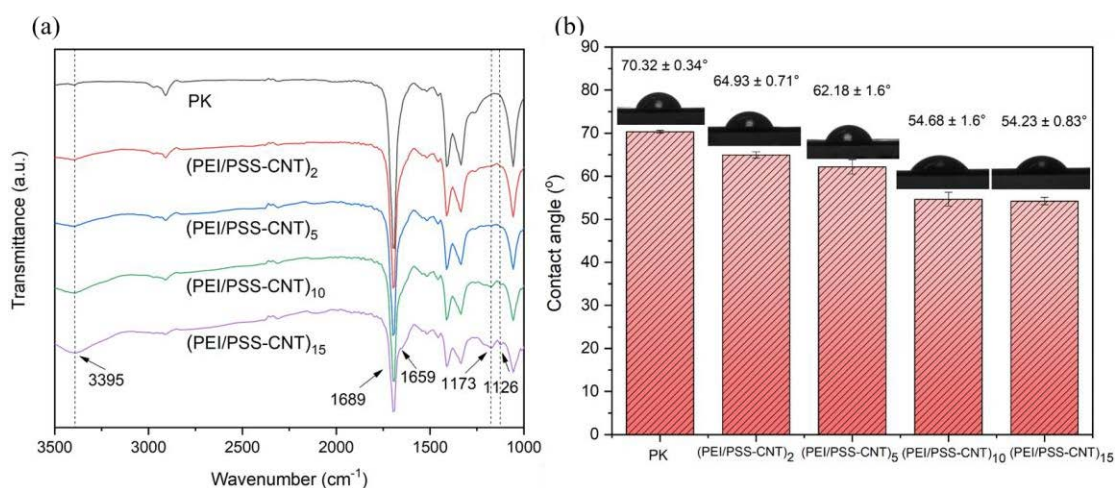
Figure 4.4. (a) FTIR spectra and (b) water contact angle of PK and inkjet printed PEM membranes.

Further analyses of the surface chemical composition of the membranes were conducted using XPS, and the results are shown in **Fig. 4.5** and **Table 4.2**. In order to identify the successful printing of polyelectrolytes on membrane surface, a PK substrate with only PEI printing was prepared and named as PEI. **Fig. 4.5 (a)** shows the wide scan spectra of the membranes, and the spectra indicate the presence of the elements on the membrane surface. Only C and O were found to be presented on the PK support, and the printing of PEI introduced the presence of N on the membrane surface, corresponding to 18.87% of the surface elemental composition. After 10 cycles printing of PEI, PSS and SWCNT, the presence of Na and S were also detected,

proving the successful printing of the mixed PSS and SWCNT ink on the (PEI/PSS-CNT)$_{10}$ membrane. As tabulated in **Table 4.2**, the Na and S content, which were both present from PSS, of the (PEI/PSS-CNT)$_{10}$ membrane were 0.87 and 5.25%, respectively. The N1s narrow scan spectra of the PEI and (PEI/PSS-CNT)$_{10}$ membranes are shown in **Fig. 4.5 (b)**. Only one peak was found to be present in the PEI membrane, corresponding to the amine C—N—H group (399.5-399.7 eV) (Kehrer et al., 2019), which can be found in the structure of the branched PEI used in this study. On the other hand, the subsequent crosslinking with GA resulted in the presence of the imine C=N group (399-399.2 eV) in addition to the amine group, as shown in **Fig. 4.5 (b)** (Mohtasebi, Chowdhury, Hsu, Biesinger, & Kruse, 2016).
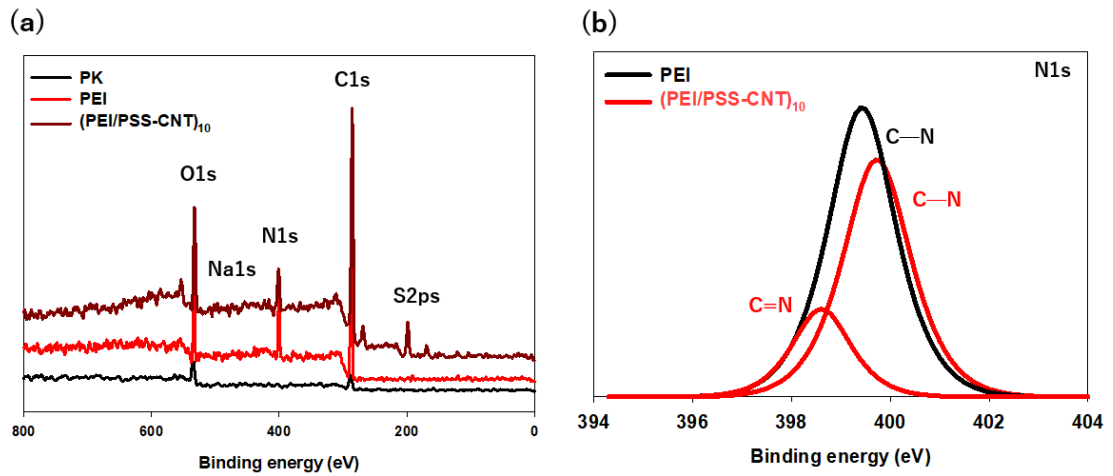
Figure 4.5. XPS (a) wide scan of PK and inkjet printed PEM membranes and (b) narrow N1s scan of the PEM membranes.

Table 4.2 Surface elemental composition of PK and inkjet printed PEM membranes.

Membrane	C (%)	O (%)	N (%)	Na (%)	S (%)
PK	73.34	26.66	-	-	-
PEI	69.46	11.67	18.87	-	-
(PEI/PSS-CNT)$_{10}$	71.83	15.22	6.83	0.87	5.25

The top surface SEM images of PK and inkjet printed PEM membranes are shown in **Fig. 4.3** (a) and **Fig. 4.6** a_1-d_1, respectively. It is clearly seen that the PK membrane surface has highly porous structure with pore size ranging from around 60 nm to 220 nm. Based on the pore size observation, the prepared PK membrane can be classified as a MF membrane. For the inkjet printed PEM membranes, as numbers of printing cycles increased, the porous structures of PK membrane was gradually covered with polyelectrolytes and carbon nanotubes. For the (PEI/PSS-CNT)$_2$ membrane, it apparently observed that there are numbers of surface pores disappeared or reduced pore sizes which might covered by PEI/PSS-CNT layers compared to the PK membrane, but not yet fully covered as some pores present on the membrane surface. The surface of (PEI/PSS-CNT)$_5$ membrane exhibited non-porous structures, with some regions exhibiting uncovered tiny pores. When the number of bilayers increased to 10 and 15, the (PEI/PSS-CNT)$_{10}$ and (PEI/PSS-CNT)$_{15}$ membrane surfaces exhibited full coverage, with no visible pores on the surfaces. These findings were in good agreement with contact angle data and also confirmed the membrane fully coverage when the number of bilayers reached 10. In order to analysis the thickness of the active layers of inkjet printed membranes, cross-section SEM images were performed and shown in **Fig. 4.6** a_2-d_2. With increase in number of bilayers, the active layer became thicker. The thickness of active layer of (PEI/PSS-CNT)$_2$ membrane was 81.4 nm, when the printing bilayers increased to 5, 10 and 15, the thickness of the active layer increased to 142.5 nm, 204.7 nm and 260.0 nm, respectively.

AFM images present the surface roughness of the inkjet printed PEM membranes (**Fig.4.6** a_3-d_3). Compared to the pristine PK membrane (Ra: 49.13 ± 0.07 nm, see **Fig. 4.3** (f)), the surface roughness of printed membranes exhibited minor reduction with increasing numbers of polyelectrolyte bilayers. The surface roughness values of (PEI/PSS-CNT)$_2$, (PEI/PSS-CNT)$_5$, and (PEI/PSS-CNT)$_{10}$ were 45.01 ± 1.06 nm, 44.52 ± 1.51 nm, and 41.54 ± 2.41 nm respectively, which indicated orderly decrement with increasing bilayer numbers. However, 15 bilayers ((PEI/PSS-CNT)$_{15}$) of 42.46 ± 0.84 nm showed insignificant changes in surface roughness comparing with (PEI/PSS-CNT)$_{10}$. Because the open pores which most likely affect to the high roughness of the membrane surface were completely disappeared when the bilayers achieved over 10 as no further decrease in the value of roughness observed. The SEM images of membrane surface also revealed in good agreement with this trend.
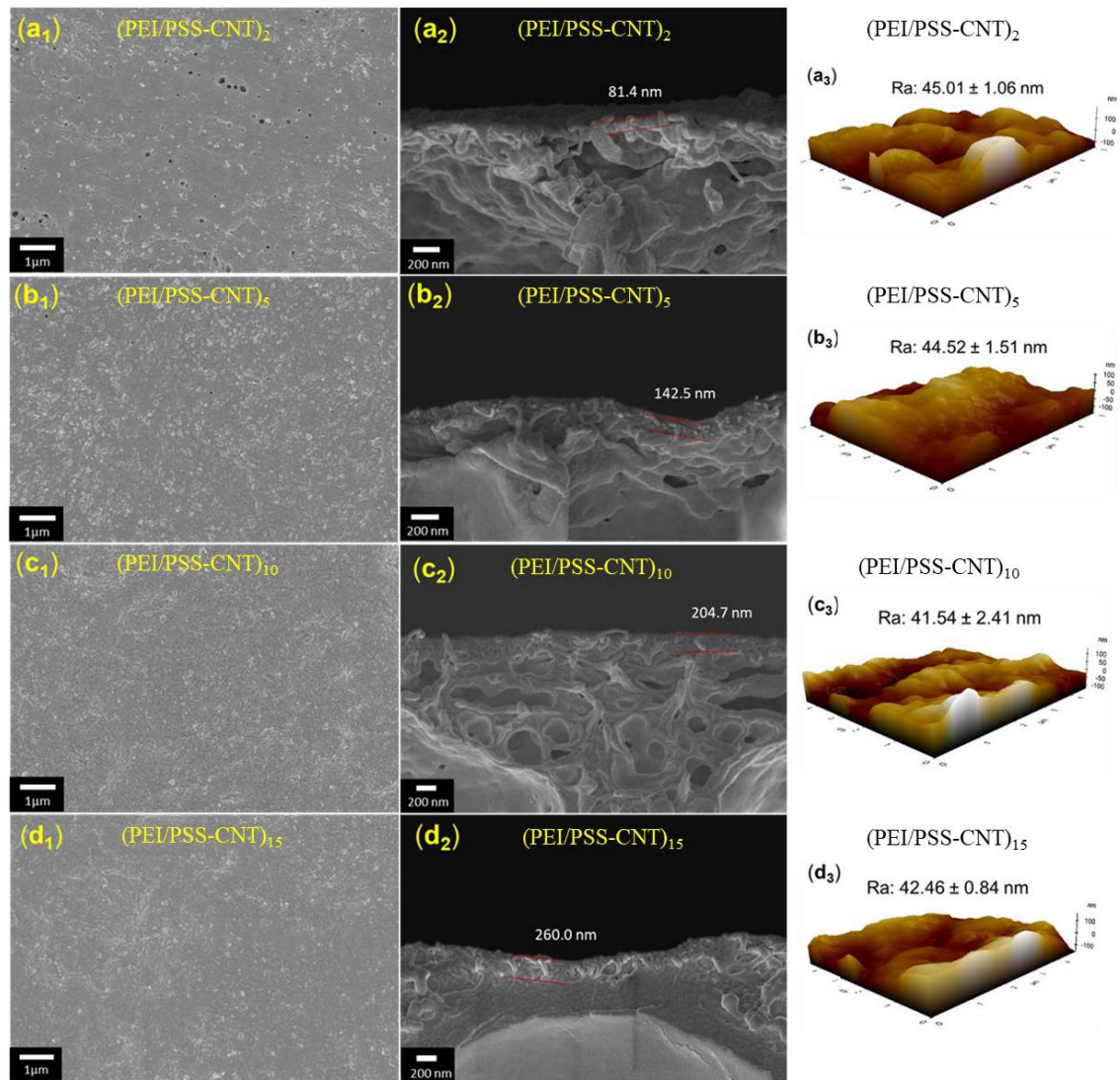
Figure 4.6. (a₁)-(d₁) top surface and (a₂)-(d₂) cross-section SEM images, and (a₃)-(d₃) AFM images of (PEI/PSS-CNT)$_2$ (a₁-a₃), (PEI/PSS-CNT)$_5$ (b₁-b₃), (PEI/PSS-CNT)$_{10}$ (c₁-c₃) and (PEI/PSS-CNT)$_{15}$ (d₁-d₃) membranes.

4.3.2 OSN Performances of the inkjet printed PEM membranes

4.3.2.1 Effect of numbers of bilayers and dye charge

Fig. 4.7 (a) provides the OSN performance of the inkjet printed PEM membranes as a function of different numbers of bilayers. The OSN experiments were conducted using 50 mg/L RB in ethanol as a feed solution at an applied pressure of 5 bar. It is clear that the permeances of the printed membranes decreased with increasing numbers of bilayers. According to the top surface SEM images, the membrane surfaces were gradually covered with polyelectrolytes and carbon nanotube with increasing number of printing cycles. Besides, the thickness of deposited bilayers were also increased

with increased inkjet printing numbers, which are shown in cross-section SEM images in **Fig 4.6**. In detail, the permeance decreased from 16.58 L m^{-2} h^{-1} bar^{-1} for (PEI/PSS-CNT)$_2$ membrane to 5.74 and 2.52 L m^{-2} h^{-1} bar^{-1} for (PEI/PSS-CNT)$_5$ and (PEI/PSS-CNT)$_{10}$ membranes, respectively, and further decreased to 0.92 L m^{-2} h^{-1} bar^{-1} for (PEI/PSS-CNT)$_{15}$ membrane. On the other hand, the RB rejections of the printed membranes showed an incremental trend with increase in number of bilayers, which is due to the excepted reduction in number of uncovered surface pores and decrease in pore sizes. It should be noted that the rejection of the (PEI/PSS-CNT)$_{10}$ and (PEI/PSS-CNT)$_{15}$ membranes were similar. As shown in **Fig. 4.4** (b) and **Fig. 4.6** c$_1$-d$_1$, the (PEI/PSS-CNT)$_{10}$ and (PEI/PSS-CNT)$_{15}$ membranes exhibited similar water contact angle values and top surface morphology with polyelectrolytes and carbon nanotubes fully covering the PK membrane. That is the reason for the similar RB rejections for these two membranes. Yet, (PEI/PSS-CNT)$_{10}$ membrane exhibited higher permeances than the (PEI/PSS-CNT)$_{15}$ membrane due to the thinner active layer thickness, which confirmed by SEM observation as indicated in **Fig. 4.6** c$_2$ and d$_2$. However, there is an marginal improvement of (0.2 %) for RB rejection showed with (PEI/PSS-CNT)$_{15}$ compared to the (PEI/PSS-CNT)$_{10}$ membrane. Therefore, the membrane with bilayer number of 10 was selected for further evaluation of OSN performance as it has higher permeance with reasonable rejection performance at minimal printing.
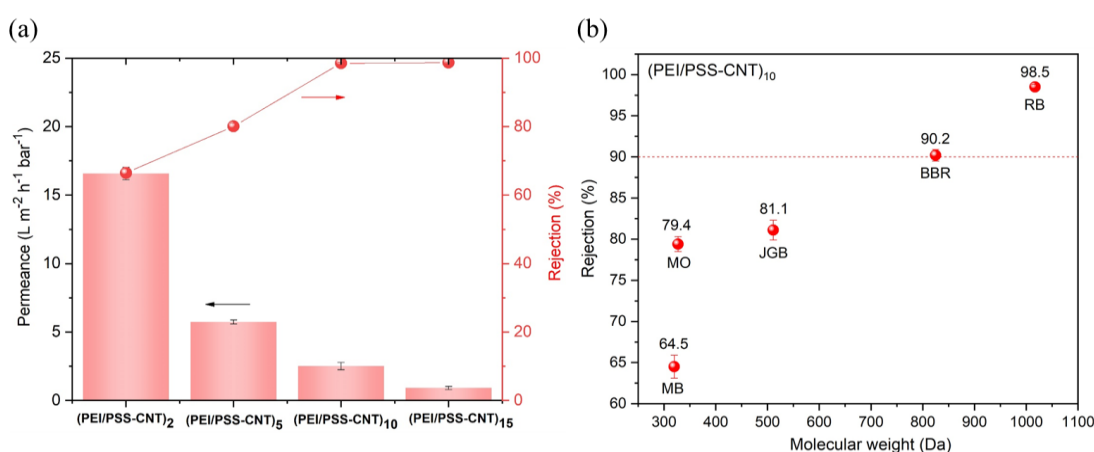
Figure 4.7. (a) OSN performances of inkjet printed PEM membranes with different numbers of bilayers. (b) Rejection performances of (PEI/PSS-CNT)$_{10}$ membrane with different dyes. (OSN operation condition: 5 bar, 50 mg/L dyes in ethanol)

To investigate the effect of SWCNT incorporation in the bilayer and the crosslinking of PEI via GA, two 10 bilayers inkjet printed PEM membranes were prepared without GA cross-linking and without SWCNT incorporation, respectively. As are shown in **Fig. 4.8**, it can clearly see that both two membranes without GA cross-linking and without SWCNT incorporation exhibited poorer RB rejection rate than that of (PEI/PSS-CNT)$_{10}$ membrane. Especially the (PEI/PSS)$_{10}$ membrane without SWCNT incorporation, showed significant drop in RB rejection which only performed of 49.6%. These results indicate that incorporation of SWCNT into the polyelectrolyte multilayers and the use of GA as a cross-linker to react with PEI are both beneficial to improve the compactness and stability of the printed PEM membrane and enhance the rejection performance of dyes (Y. Ji et al., 2010).
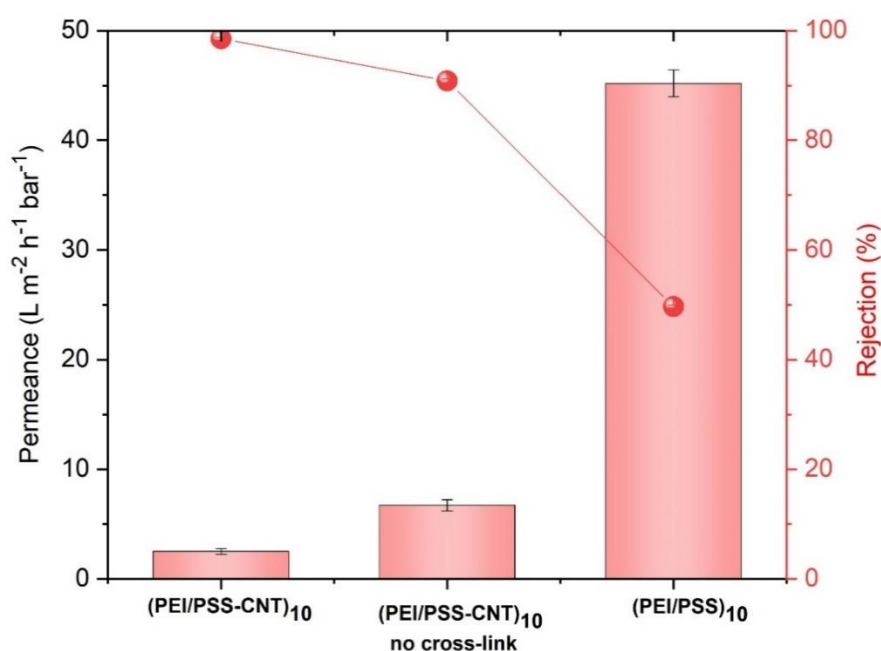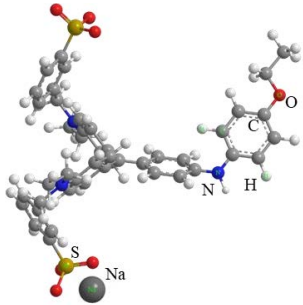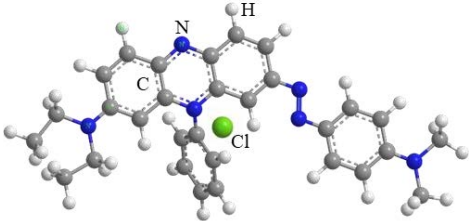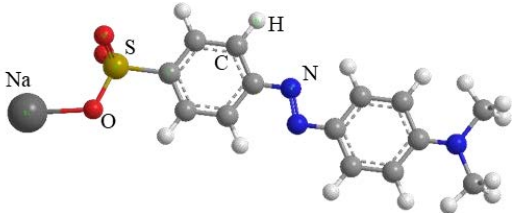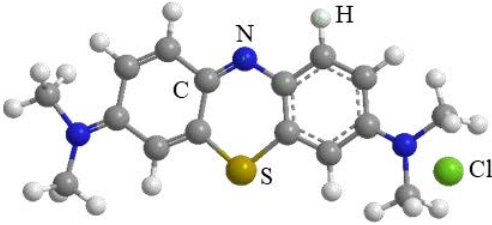
Figure 4.8. Comparison of OSN performances of (PEI/PSS-CNT)$_{10}$ membrane, (PEI/PSS-CNT)$_{10}$ membrane without GA cross-linking and (PEI/PSS)$_{10}$ membrane without CNT incorporation. (OSN operation condition: 5 bar, 50 mg/L RB in ethanol)

In order to evaluate the rejection performance of the printed PEM membranes for different molecular weight dyes, various dyes with molecular weights ranging from 300 to 1017 Da were chosen in this study. The basic properties of these dyes are presented in **Table 4.3**.

Table 4.3 Basic properties of the dyes used for evaluating molecular separation performance of PEM membranes in this study.

Dye	Molecular weight (g/mol)	Charge	Structure
RB	1017	-	
BBR	825	Zwitterion	
JGB	511	+	
MO	327	-	
MB	320	+	

It can be found from **Fig. 4.7** (b) that the dye with high molecular weight, such as RB (1017 Da), could be almost completely separated with a rejection of 98.5%. For the BBR with a molecular weight of 825 Da, the rejection was 90.2%. This indicates the molecular weight cut off (MWCO) of the (PEI/PSS-CNT)$_{10}$ membrane is around 825 Da, which is within the range of OSN membrane MWCO of 200-1000 Da (Marchetti et al., 2014). While for the dyes with low molecular weights, such as JGB (511 Da), MO (327 Da) and MB (300Da), the rejections reduced to 81.1 %, 79.4 % and 64.5%, respectively. It should be noted that the MO and MB had a similar molecular weight, however, the rejection of MO is higher than that of MB. According to previous studies, the rejection performance of a membrane might be the synergetic effect of size exclusion and charge exclusion (Lu et al., 2021). In our case, the zeta potential values (see **Fig. 4.9**) of (PEI/PSS-CNT)$_{10}$ membrane are nearly zero under pH ranging from 6 to 10, indicating the neutral membrane surface. Thus, size exclusion plays a dominant role during the OSN operation in our study. Although the MO and MB have similar molecular, the molecular size of MO (26.14 Å) is larger than that of MB (13.82 Å), which might be an explanation for the different rejection performance of these two dyes.
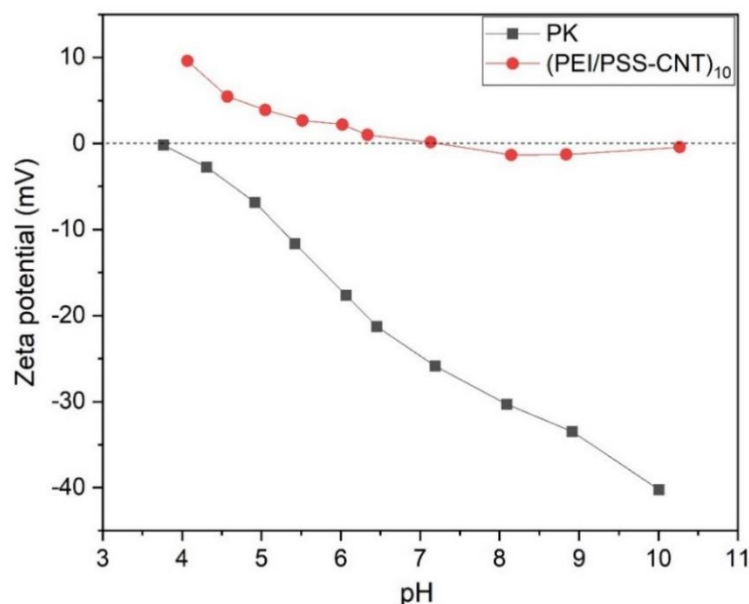
Figure 4.9. Surface zeta potential of PK and (PEI/PSS)$_{10}$ membranes.

4.3.2.2 Effect of polyelectrolyte concentration and cross-linking condition

Previous literatures have shown that the change in the polyelectrolyte concentrations and the cross-linking conditions such as cross-linking time influence the membrane performances including permeability and the selectivity (DuChanois, Epsztein, Trivedi, & Elimelech, 2019; Duong, Zuo, & Chung, 2013; Y. Ji et al., 2010; Korzhova et al., 2020b). Thus, we further investigated the effect of PEI concentrations and the GA cross-linking duration on OSN performances. The number of inkjet printing of 10 cycles and the concentration of PSS/CNT ink were fixed but the concentration of PEI ink was varied to 10, 12.5 and 15 g/L for evaluating OSN performance as shown in **Fig. 4.10** (a). Apparently, the ethanol permeance was decreased with increasing PEI concentration from 10 g/L to 15 g/L, while the MO rejection rate was slightly improved. This trend can be attributed to the higher PEI polyelectrolyte deposition on the membrane surface, which might increase the membrane thickness and generate higher resistance to ethanol permeation (DuChanois et al., 2019; Korzhova et al., 2020b). However, the increase in the MO rejection did show a marked improvement, for example, membrane fabricated with PEI concentration of 10 g/L, the MO rejection was 79.4%, when the PEI concentration was increased to 15 g/L, and the MO rejection was slightly improved to 83.4%. Such minor improvement in MO rejection may arise due to the higher PEI concentration aiding in denser active layer formation. Regarding the observation of low rejection rate of low molecular weight dyes, this could be attributed to chemical structures of polyelectrolytes and the resultant active layer formation. As polyelectrolytes exhibit long molecular chain structures, active layer formed using these long chain of polymers will produce relatively loose structures leading to not high rejection rate of low molecular weight dyes such as MO (S. Zhao & Wang, 2017).

Fig. 4.10 (b) demonstrated the effect of a longer cross-linking duration which resulted in higher cross-linking degree and a denser membrane surface, leading to the decreased permeability and increased MO rejection (Duong et al., 2013; Y. Ji et al., 2010). Similar to the effect of the polyelectrolyte concentration, the increment in MO rejection due to the longer cross linking duration was minor, even when the cross-linking time was increased to 25 min. In summary, increasing the PEI concentration and the GA cross-linking duration both can enhance the membrane performances with increased MO rejections, though the improvement was minor. Considering the

permeability and the selectivity result, the (PEI/PSS-CNT)$_{10}$ membrane fabricated with 10 g/L PEI under cross-linking time of 10 min was the optimal case and such membrane was used in the following studies.
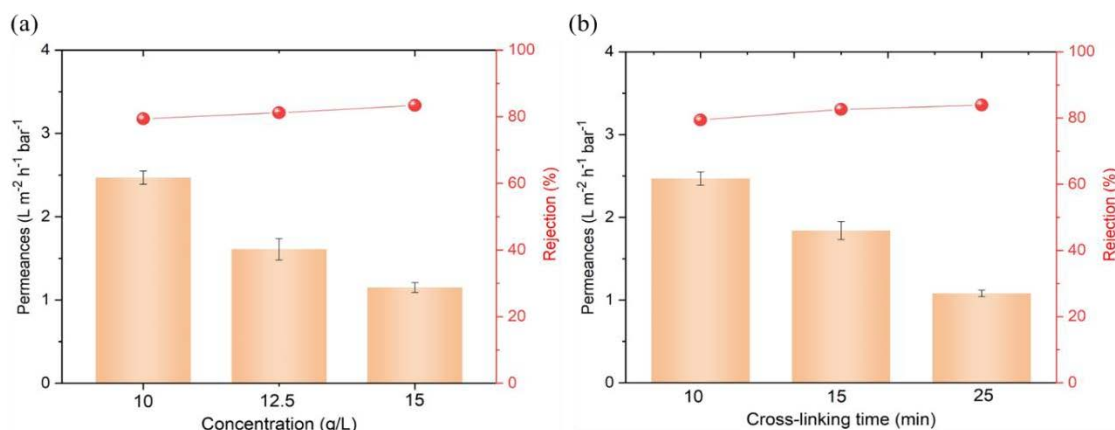
Figure 4.10. Effect of (a) PEI concentration and (b) GA cross-linking duration on the OSN performances. (OSN operation condition: 5 bar, 50 mg/L MO in ethanol)

4.3.3 Stability of the inkjet printed PEM membrane

The stability of the inkjet printed PEM membrane was evaluated by testing them in different kinds of organic solvents. The weight loss and the OSN performance change of the printed PEM membrane were compared before and after soaking in different kinds of organic solvents for two weeks.
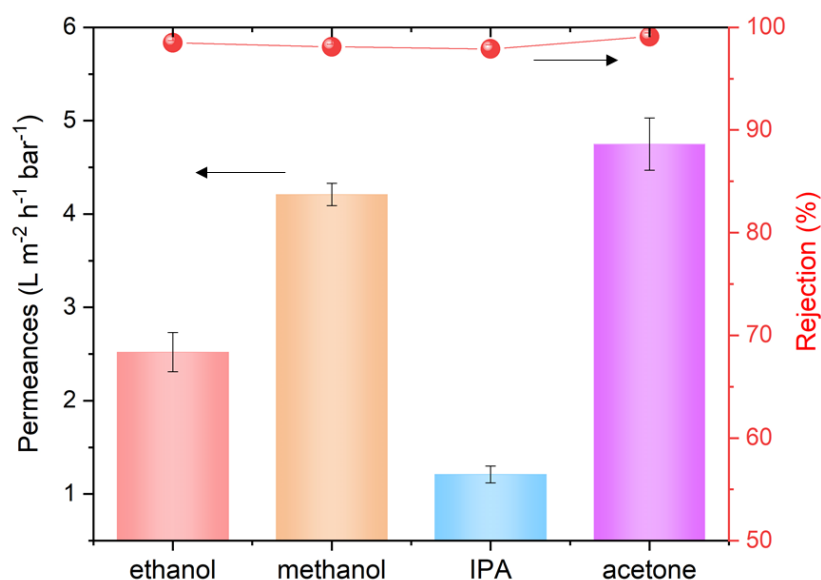
Figure 4.11. OSN performances of (PEI/PSS-CNT)$_{10}$ membrane with different kinds of organic solvents as feed. (OSN operation condition: 5 bar, 50 mg/L RB in different organic solvents)

Fig. 4.11 presents the OSN performances of (PEI/PSS-CNT)$_{10}$ membrane in typical organic solvents including ethanol, methanol, IPA and acetone. The (PEI/PSS-CNT)$_{10}$ membrane exhibited good OSN performances with similar RB rejections (>98%) in four different organic solvents. This result indirectly confirms the chemical and physical stabilities of the PEM membrane fabricated via inkjet printing of PEI/PSS-SWCNT as well as its PEI layer crosslinked by GA cross-linker. The solvent permeability of the membrane in these organic solvents were varying. The permeance values of the PEM membrane in ethanol, methanol, IPA and acetone were 2.52, 4.21, 1.21 and 4.75 L m^{-2} h^{-1} bar^{-1}, respectively, following the order of acetone > methanol >ethanol > IPA. This trend might be due to the combinatorial effects of the interaction between membrane-solvent, membrane-solute and solvent-solute (Y. Chen et al., 2019; Yifan Li et al., 2016; Z. Yuan et al., 2018). The complex reactions are still under exploration and require further studies. In addition, Bhanushali et al. (Bhanushali, Kloos, Kurth, & Bhattacharyya, 2001) verified that the viscosity (μ) and the molar volume (V_m) are the most important physical properties of organic solvents which significantly affect the permeances of solvents. Thus, the V_m/μ value is a key parameter of the solvent permeability. **Table 4.4** summarises the basic properties of these organic solvents which include the viscosity, molecular weight, density, molar volume, and V_m/μ parameter. It can be found that the order of the V_m/μ parameter is in accordance with order of permeability of these organic solvents. Acetone has the highest V_m/μ value of 231.50 and the IPA has the lowest V_m/μ value of 32.26. This result helps to explain the differences in permeance of our PEM membranes under these organic solvents.

Table 4.4 Properties of different organic solvents used in this study.

Solvents	Viscosity (cP), 20°C	Molecular weight (g mol^{-1})	Density (g cm^{-3})	Molar volume (cm^3 mol^{-1})	V_m/μ
ethanol	1.20	46.07	0.789	58.39	48.66
methanol	0.59	32.04	0.792	40.45	68.56
IPA	2.37	60.10	0.786	76.46	32.26
acetone	0.32	58.08	0.784	74.08	231.5

(Viscosity is referred as µ. Molar volume is referred as V_m. Molar volume is calculated by molecular weight divided by density.)

PK polymer is proven to exhibit good mechanical properties and chemical resistance. It has a high melting point of 260 ºC and good behaviour over a broad temperature range (Nakagawa et al., 2020). The ketone (C=O) groups provide strong intramolecular and intermolecular interactions, making it resistant to most organic solvents, such as hexane, acetone, DMF, NMP, and DMAC (Gupta, Schulte, Flood, & Spruiell, 2001; Xianfeng Li et al., 2010). The organic solvents resistance properties of the prepared PK membrane were tested by soaking 1 cm × 5 cm PK membrane samples in four different solvents (ethanol, methanol, IPA and acetone) for two weeks. The weight of the PK samples and the percentages of weight loss after soaking PK membranes in different organic solvents were measured and shown in **Table 4.5**. It is clear that all the PK membrane samples exhibited negligible weight loss after soaking in ethanol, methanol, IPA and acetone for two weeks. Such finding confirms that the prepared PK membrane exhibit good solvent stability.

Table 4.5 Percentages of weight loss after soaking PK membranes in different organic solvents for two weeks.

PK membrane	Organic solvent	Weight before (mg)	Weight after (mg)	Weight loss (%)
1	ethanol	15.1/15.2	15.1/15.0	0.00%/1.32%
2	methanol	15.0/15.1	14.9/14.9	0.67%/1.32%
3	IPA	15.5/15.3	15.4/15.1	0.65%/1.31%
4	acetone	15.8/15.9	15.8/15.9	0.00%/0.00%

Then, the stability of (PEI/PSS-CNT)$_{10}$ membrane was evaluated by soaking the membrane under different organic solvents for two weeks at room temperature. The weight loss and the changes in OSN performances were compared before and after soaking the PEM membranes in different organic solvents. The results are presented in **Table 4.6** and **Fig. 4.12**.

Table 4.6 Percentages of weight loss after soaking (PEI/PSS-CNT)$_{10}$ membranes in different organic solvents for two weeks.

(PEI/PSS-CNT)$_{10}$ membrane	Organic solvent	Weight before (mg)	Weight after (mg)	Weight loss (%)
1	ethanol	47.6/46.0	47.2/45.9	0.8%/0.2%
2	methanol	44.8/41.9	44.5/41.7	0.7%/0.5%
3	IPA	46.1/50.4	46.0/50.4	0.2%/0.0%
4	acetone	51.1/51.2	50.8/50.9	0.6%/0.6%

In **Table 4.6**, it is clear that all the (PEI/PSS-CNT)$_{10}$ samples exhibited negligible weight loss after soaking them in ethanol, methanol, IPA and acetone for two weeks. All the membrane weight loss percentages were less than 0.8%. In addition, as shown in **Fig. 4.12**, after soaking the membrane in four different organic solvents for two weeks, the OSN performances of the membranes showed negligible change. These results indicate that the inkjet printed PEI/PSS-CNT layer had good physical and chemical stability in varying organic solvents such as ethanol, methanol, IPA and acetone.
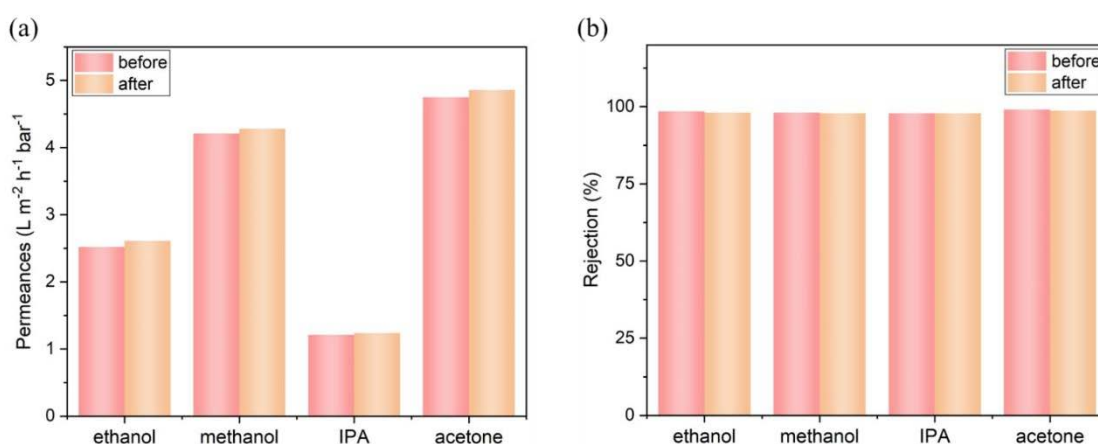
Figure 4.12. The OSN performance changes after soaking the (PEI/PSS-CNT)$_{10}$ membranes in different organic solvents for two weeks. (a) Permeability; (b) RB rejection (OSN operation condition: 5 bar, 50 mg/L RB in organic solvents)

In order to further investigate the stability of the inkjet printed (PEI/PSS-CNT)$_{10}$ membrane in different organic solvents, 12 hours continuous OSN tests were conducted and the results are presented in **Fig. 4.13**. It can be found that the permeances of the (PEI/PSS-CNT)$_{10}$ membranes showed a slight decrement during the continuous operation of 12 hours. But the decrease in permeances were minor with only 5.2%, 4.3%, 8.3% and 4.2% reduction for ethanol, methanol, IPA and acetone, respectively. In the continuous filtration process, the concentration polarization and the dye deposition on the membrane might lead to the membrane fouling so the slight reduction of solvents permeance appeared for all tests. Overall, the stable RB rejection and permeance performances during the 12 hours of filtration in different solvents further confirm the physical and chemical resistances of the inkjet printed PEM membrane.
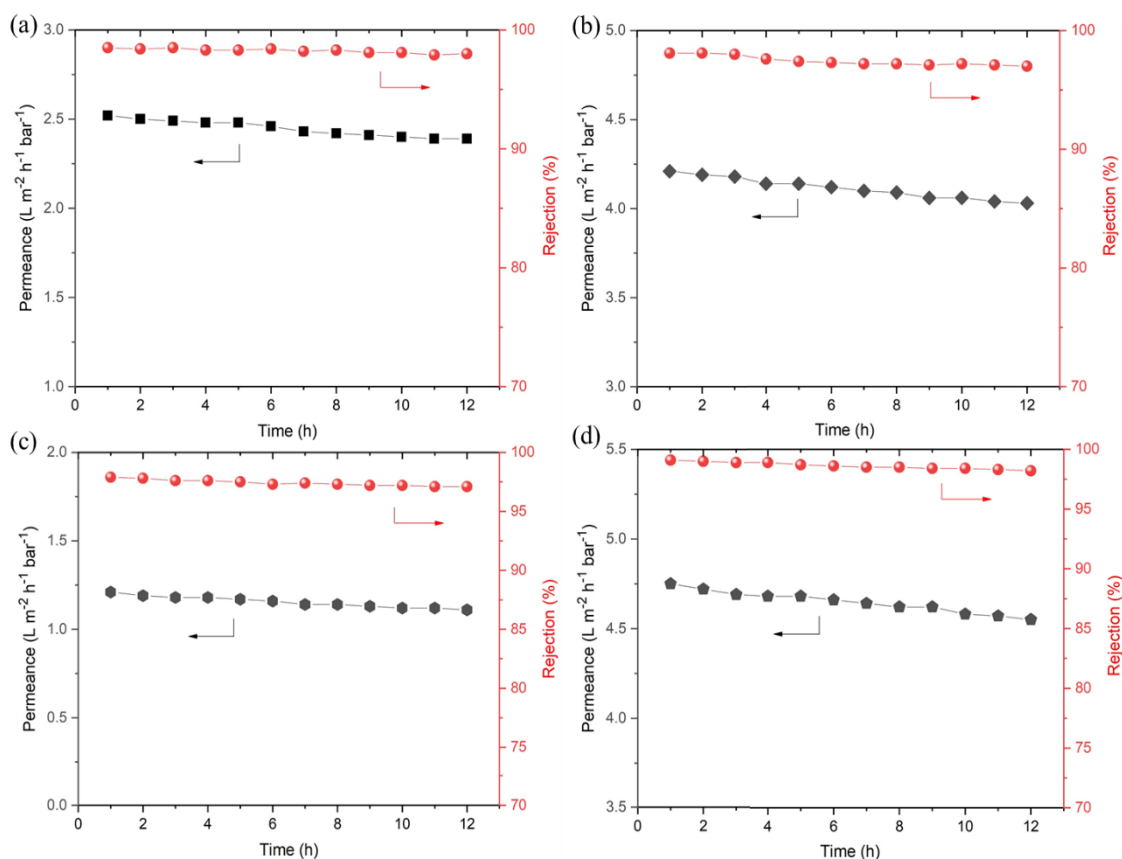
Figure 4.13. The stability of (PEI/PSS-CNT)$_{10}$ membranes in different organic solvents. (a) ethanol; (b) methanol; (c) IPA and (d) acetone. (OSN operation condition: 5 bar, 12 hours operation and 50 mg/L RB in organic solvents)

Table 4.7 shows the comparison of OSN performances between inkjet printed (PEI/PSS-CNT)$_{10}$ membranes and PEM membranes fabricated from previous studies. The (PEI/PSS-CNT)$_{10}$ membrane shows relatively high permeances with the good RB or MO rejections compared to most of PEM membranes.

Table 4.7 A comparison of OSN performances between inkjet printed (PEI/PSS-CNT)$_{10}$ membranes and PEM membranes fabricated from previous studies.

Membrane	Solute	Solvent	Permeances (L m^2 h bar^{-1})	Rejection (%)	Ref.
(PDDA/SPEEK)$_{20}$	MO	IPA	4.5	68	(Xianfeng Li, Steven De Feyter, Dongju Chen, Steliana Aldea, & Vankelecom, 2008)
	RB		0.5	99	
(PDDA/SPEEK)$_5$	RB	IPA	~ 0.3	~ 98	(Xianfeng Li et al., 2010)
	MO		~ 0.8	~78	
(PDDA/ poly(vinylsulfate) (PVS))$_5$	RB	IPA	1.57	> 99	(Ahmadiannamini, Li, Goyens, Meesschaert, et al., 2012)
(PAA pH 4/PDDA pH 7)$_5$	RB	IPA	0.03	97.0 ± 2.1	(Ahmadiannamini, Li, Goyens, Joseph, et al., 2012)
(PDDA/PVS)$_3$	RB	IPA	~ 0.25	~ 99	(Joseph, Ahmadiannamini, Jishna, Volodin, & Vankelecom, 2015)
(PAH pH7.5/PAA pH 3.5)$_5$	RB	IPA	0.05 ± 0.09	99 ± 1	(Ilyas et al., 2016)
PEI2K-GA	MO	ethanol	1.4 ± 0.3	89.6 ± 1.6	(Y. Huang, Sun, Wu, & Feng, 2018)
[(PDDA/PAA-CSH)$_{2.5}$]$^+$PFO$^-$	MB	ethanol	~ 6.0	~ 68	(Lu et al., 2021)
(PEI/PSS-CNT)$_{10}$	RB	ethanol	2.52	98.5	This work
		IPA	1.21	97.9	
(PEI/PSS-CNT)$_{10}$	MO	ethanol	2.47	79.4	

4.4 Conclusions

In this chapter, the porous PK membrane as substrate was fabricated via typical non-solvent induced method and inkjet printing technique was applied as an alternative method for LBL PEM membrane fabrication. The PEM layer was successfully synthesized via inkjet printing of polyanion and polyanion with SWCNT which indicated superior OSN performance with chemical and physical stabilities in various organic solvents. Effects of number of bilayers, polyelectrolyte concentration, and cross-linking condition on the OSN membrane performances were evaluated. The optimal (PEI/PSS-CNT)$_{10}$ membrane exhibited ethanol, methanol, IPA and acetone permeances of 2.52, 4.21, 1.21 and 4.75 L m^{-2} h^{-1} bar^{-1}, respectively, along with the good dye rejection rates (RB> 98%, MO ~79.4%).   By increasing the PEI concentration and GA cross-linking reaction time, the rejection performance of MO was increased but insignificant. In addition, the membrane weights and performances had negligible changes before and after soaking the inkjet printed PEM membranes in various organic solvents. Furthermore, the long term OSN performance test revealed no obvious degradation in membrane performances for continuous 12 hours tests, which confirm the stability of fabricated PEM membrane. Compared to conventional LBL assembly, we demonstrate the advantages of using inkjet printing techniques for PEM membrane fabrication which includes the minimum chemical consumption, significant reduction in membrane fabrication time and the formation of thinner active layers. Our work may further advance the development of LBL PEM membrane for OSN application as well as utilization of inkjet printing technique in OSN membrane fabrication.

CHAPTER 5

Inkjet printing assisted layer-by-layer for organic solvent nanofiltration membrane fabrication: effect of different cross-linkers

5.1 Introduction

Current polymeric OSN membranes can be fabricated to ISA membranes or TFC membranes (Hermans et al., 2015). Compared to the ISA membranes comprising of a single material with a porous substructure and active layer formed simultaneously, TFC membranes with active and support layers are made from different materials showing advantages of optimizing them independently to meet required application purposes (C. Wang et al., 2021). Among different methods in synthesizing TFC membranes, LBL deposition of polyelectrolytes is a versatile approach to fabricate the active layer of OSN membranes (Joseph, Ahmadiannamini, Hoogenboom, & Vankelecom, 2014). The key advantage of the LBL electrostatic self-assembly method is that the thickness of the active layer is easily controlled by adjusting the number of deposited layers. In addition, differently targeted OSN membranes can be prepared by carefully selecting polyelectrolytes types and manipulating synthesis conditions, such as pH, ionic strength and cross-linking degree (Xin Li, Liu, & Van der Bruggen, 2020; Xin Li, Chang Liu, Wenqiang Yin, Tzyy Haur Chong, & Rong Wang, 2019a).

In last chapter, we utilized the inkjet printing method for PEM OSN membrane preparation using the solvent resistant PK membrane as a substrate. PEI was used as the positive ink, and PSS/SWCNT mixed ink was used as the negative ink. The prepared PEM membrane showed good OSN performance along with excellent solvent stability. In this chapter, we further optimized the membrane fabrication process by using PEI and pure SWCNT as positive and negative inks, respectively. Moreover, three different cross-linking agents: GA, ECH and TMC were used for post modification. PEI and SWCNT inks were alternatively deposited on the PK membrane surface to create PEI/SWCNT multilayers via electrostatic interaction. The effects of PEI and SWCNT concentrations, bilayer numbers, different cross-linkers, and cross-linking conditions were evaluated in terms of membrane OSN performances. The stability of the LBL OSN membrane was evaluated by soaking the LBL-OSN membranes in ethanol, methanol, DMF, IPA, and acetone for three weeks. It should be noted that most studies of the OSN only focus on using different approaches to improve OSN membrane performance without pointing out what particular applications these membranes can be applied for. Therefore, in the last section of this study, we proposed possible applications for the inkjet-printed PEI/SWCNT

multilayer membranes, which could provide further information on the applications of OSN membranes.

5.2 Experimental section

5.2.1 Materials

PK polymer (M610F) was provided by Hyosung Company (South Korea). LiCl, CaCl$_2$, ZnCl$_2$, and resorcinol purchased from Sigma-Aldrich (Australia) were used for dope solution preparation. Branched PEI (Mw ~ 25000) from Sigma Aldrich (Australia) and carboxylated SWCNT (> 95 wt% purity) from XFNANO Materials Technology (China) served as positive and negative inks for inkjet printing, respectively. GA (25 wt%), TMC (98% purity), and (±)-epichlorohydrin (ECH) (> 99% purity) supplied by Sigma-Aldrich (Australia) were used as cross-linkers to react with PEI for surface modification. Different dyes of RB (Mw: 1017 Da) and MO (Mw: 327 Da), and organic solvents, including acetone, methanol, DMF, ethanol and IPA (Sigma-Aldrich, Australia) were used for performance evaluations. The properties of organic solvents used in this study are shown in **Table 5.1**. Non-woven (TS6005W) fabric support supplied by Hirose Paper (Japan) was used for PK membrane fabrication. All chemicals in this study were used as received without further purification.

Table 5.1 Properties of different organic solvents used in this study.

Solvents	Viscosity (cP), 20°C	Molecular weight (g mol^{-1})	Density (g cm^{-3})	Molar volume (cm^3 mol^{-1})	Vm /μ
ethanol	1.20	46.07	0.789	58.39	48.66
methanol	0.59	32.04	0.792	40.45	68.56
DMF	0.92	73.09	0.944	77.43	84.16
IPA	2.37	60.10	0.786	76.46	32.26
acetone	0.32	58.08	0.784	74.08	231.5

5.2.2 LBL OSN membrane fabrication

The PK substrate was prepared following the same procedure in the last chapter. The LBL OSN membrane preparation process is shown in **Fig. 5.1**. The positive ink was

prepared with PEI concentration of 5.0, 7.5 and 10.0 g/L dissolving in DI water. The negative water-based ink was 0.5 and 1.0 g/L SWCNT. The positive ink was firstly printed on a PK membrane surface, then the negative ink was printed on the same area. The effective printing area is 4.5 cm × 4.5 cm. The fabricated membrane is named as the (PEI/SWCNT)$_n$, where the "n" represents the PEI/SWCNT bilayer numbers.

Subsequently, the prepared LBL-OSN membrane was modified by three kinds of cross-linkers (GA, ECH and TMC). The GA cross-linking solution was prepared by adding certain amount of GA and 1% (v/v) HCl into DI water and ethanol mixed solution (1:1) (M. J. Park, Gonzales, Abdel-Wahab, Phuntsho, & Shon, 2018). The LBL-OSN membrane was cross-linked with the GA solution for 10 min, then oven-cured at 90°C for 10 min. The ECH of 6 wt% aqueous solution was used to cross-link the membrane for a certain time, followed by the oven-cured at 65°C for 10 min. The TMC (0.1 wt% in n-hexane) solution was used to treat the membrane for a certain time, and then oven-cured at 80°C for 5 min. The cross-linking conditions mention above are referred from the previous studies (Fang, Shi, & Wang, 2013; C. Feng, Xu, Li, Tang, & Gao, 2014; Lin, Fang, Du, Yao, & Zhu, 2019; C. Wang, Park, Seo, et al., 2022). For easy identification, (PEI/SWCNT)n-GA, (PEI/SWCNT)n-ECH, and (PEI/SWCNT)n-TMC were used to refer the inkjet-printed LBL membranes cross-linked by GA, ECH, and TMC, respectively.
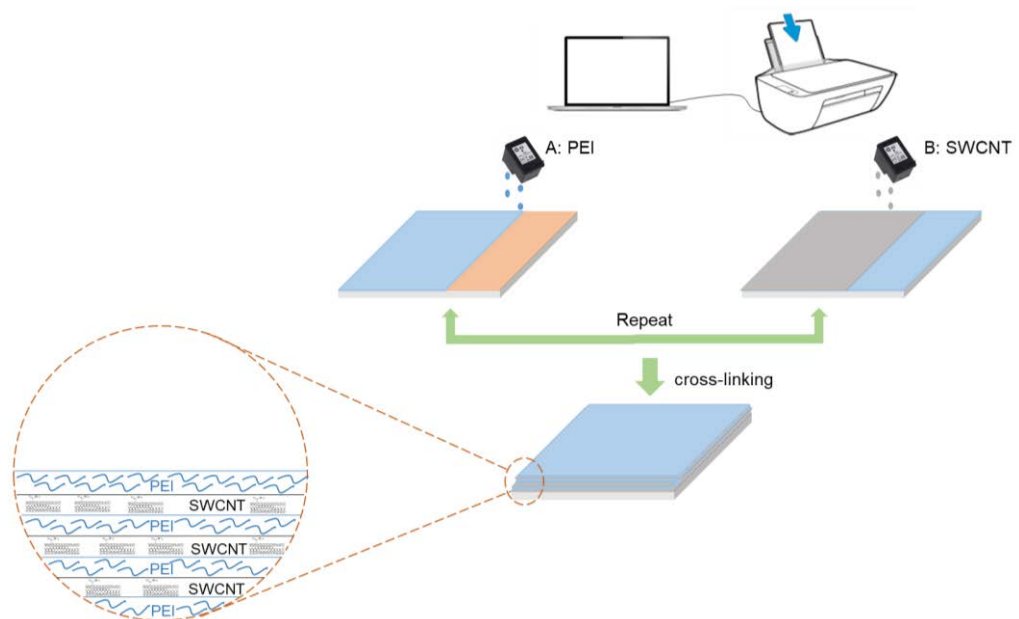
Figure 5.1. Schematic diagrams of the LBL-OSN membrane preparation process.

5.2.3 Membrane characterization

FTIR (IRAffinity-1 Shimadzu) was used to evaluate the surface functional groups of the fabricated membranes. XPS (JPS-9010 MC, Japan) with Al Kα rays was applied to analyse the surface chemical composition. Water contact angle was measured by the Theta Lite 100 system (Biolin Scientific). SEM (Zeiss Supra 55VP) was used to characterize the membrane structures. AFM (Park XE7) analysis was performed to characterize the membrane surface roughness. All the characterizations were repeated three times for each sample.

5.2.4 OSN performance evaluation

The OSN performances of the inkjet printed LBL membranes were investigated by an OSN set-up (see **Fig. 5.2**). A commercial circular cell (CF047, Sterlitech) was used to hold the membrane and a HPLC pump (PU-2089, JASCO) was used to supply pressure. The feed solutions with a concentration of 50 mg/L were prepared by dissolving dyes in organic solvents. The permeance (J_w) was calculated according to Eq. (1):

$$J_w = \frac{V}{A\Delta tP}$$

(1)

where V (L) is the permeate volume, A (m^2) is the membrane area, Δt (h) is the filtration time, and P (bar) is the filtration pressure.

The dye rejection (R) performance was calculated according to Eq. (2):

$$R\ (\%) = 100\ \times (1 - \frac{C_p}{C_f})$$

(2)

where C_p and C_f refer to dye concentrations in permeate and feed, respectively.
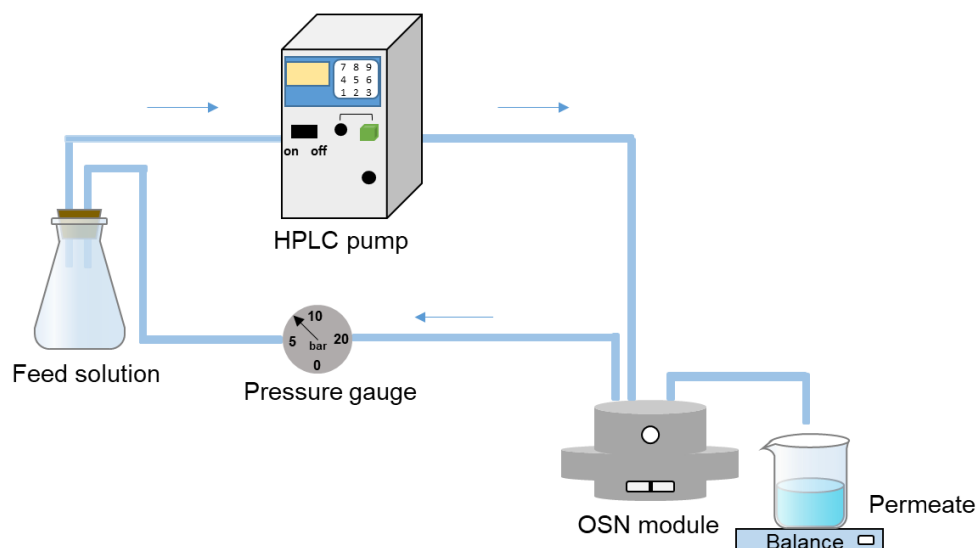
Figure 5.2. Schematic illustration of the OSN set-up.

5.3 Results and discussions

5.3.1 The effects of ink concentrations and printing cycles on membrane performances

Firstly, the effects of PEI and SWCNT concentrations on the inkjet-printed LBL-OSN membrane performances were evaluated by testing the following concentrations: 5.0, 7.5 and 10.0 g/L PEI and 0.5 and 1.0 g/L SWCNT. The printing cycle was fixed at 10, which was confirmed by our previous study to ensure sufficient materials deposition to form a defect-free selective layer on the PK membrane (C. Wang, Park, Seo, et al., 2022). The OSN tests were performed with feed solution of 50 mg/L RB in ethanol under 5 bar. The OSN performances of different LBL membranes are shown in **Table 5.2**. Apparently, when the SWCNT concentration was 0.5 g/L, the ethanol permeance decreased from 6.80 to 3.68 L m^{-2} h^{-1} bar^{-1} with the increase of PEI concentration from 5.0 to 10.0 g/L. The RB rejection slightly increased from 97.6% to 98.6%. This trend can be attributed to the increased LBL thickness by deposition of a larger amount of PEI ink on the PK membrane surface, which might result in higher resistance to ethanol permeation with higher RB rejection (Korzhova et al., 2020a; S. Zhao & Wang, 2017). These trends were also found when the SWCNT concentration of 1 g/L was used. When the PEI concentration increased from 5.0 to 7.5 and 10.0 g/L, the ethanol permeances decreased from 3.61 to 2.16 and 1.24 L m^{-2} h^{-1} bar^{-1}, respectively, with RB rejection increased from 98.0% to 98.3% and 99.3%, respectively. Similarly, when the PEI concentrations were 5.0 and 10.0 g/L, increasing SWCNT concentration from

0.5 to 1.0 g/L led to the enhanced RB rejections with decreased ethanol permeances. With the increase in SWCNT concentration, a larger amount of SWCNT deposited on the membrane surface which would tighten the membrane surface and increase the membrane thickness leading to the improvement of the membrane rejection performance and reduction of membrane permeability. Due to the pharmaceutical regulations, organic solvents used for APIs production are required to be highly purified. To improve the recyclability of organic solvents, the membrane rejection performance is preferred to be high enough (above 99%) (Geens, De Witte, & Van der Bruggen, 2007). Thus, the PEI concentration of 10.0 g/L and SWCNT concentration of 1.0 g/L were chosen for further performance studies.

Table 5.2 The performances of different OSN membranes fabricated under various PEI and SWCNT concentrations.

Membrane	PEI concentration (g/L)	SWCNT concentration (g/L)	Cross-linker	Permeability (L m^{-2} h^{-1} bar^{-1})	RB rejection (%)
1	5.0	0.5	GA	6.80 ± 0.44	97.6 ± 0.3%
2	10.0	0.5	GA	3.68 ± 0.36	98.6 ± 0.3%
3	5.0	1.0	GA	3.61 ± 0.16	98.0 ± 0.3%
4	7.5	1.0	GA	2.16 ±0 .21	98.3 ± 0.2%
5	10.0	1.0	GA	1.24 ± 0.12	99.3 ± 0.2%

It was however noticed that the permeability of the LBL-OSN membrane printed using 10.0 g/L PEI and 1.0 g/L SWCNT was relatively lower compared to other membranes fabricated under different concentrations. In order to optimize the membrane permeability, LBL membranes with different printing cycles were further investigated to find the optimal printing cycle under this concentration condition.

Before testing the membrane performances, the surface morphologies and properties of the LBL-OSN membranes prepared with different printing cycles were investigated and summarised in **Fig. 5.3** and **Fig. 5.4**. In **Fig. 5.3 (a)**, all the membranes showed an absorption peak (1689 cm^{-1}) indicating the C=O of ketone groups contained in the PK polymer (C. Liu, Saeki, Cheng, Luo, & Matsuyama, 2019). The changes of peak

intensity at 3395 cm^{-1} of printed LBL membranes were mainly attributed to the N–H stretch of amine groups containing in PEI (Anusha Chandra, E Bhuvanesh, Priyabrata Mandal, & Sujay Chattopadhyay, 2018; Q. Li, Chen, Liu, & Kentish, 2018). In addition, another absorption peak (1580 ~ 1650 cm^{-1}) of the amine group of PEI (Korzhova et al., 2020b) should be exhibited by the membranes. However, this absorption range overlaps with the absorption range of ketone groups from the PK membrane. That is the reason why the N–H peaks of PEI polymer cannot be distinguished on the LBL OSN membranes. Similarly, the C=O and O–H groups of SWCNT were overlapped with C=O groups of PK polymer and N–H groups of PEI polymer which were not distinguished on the absorption ranges of the LBL OSN membranes either. In addition, the series of LBL membranes with different printing cycles were prepared using GA as a cross-linker. The crosslinking reaction between the aldehyde group of GA and N–H group of PEI will create imine (–C=N) group, a new peak at 1659 cm^{-1} emerging with the increased bilayers, which confirmed the cross-linking reaction between PEI and GA and the formation of imine group (Kalmoush, El-Sakhawy, Kamel, Salama, & Hesemann, 2020).

The membrane surface hydrophilicity properties were evaluated by the water contact angle measurements (see **Fig. 5.3 (b)**). The pristine PK membrane had a contact angle value of 70.32 ± 0.34°, which indicated that the PK membrane surface is slightly hydrophilic. The contact angle values of the LBL OSN membranes decreased when increased the bilayer numbers, indicating the increase in membrane hydrophilicity. The –NH$_2$ groups in PEI polymer and the oxygen functional groups in SWCNT lead to the improved hydrophilicity (Tian, Wang, Goh, Liao, & Fane, 2015). At higher bilayer numbers, larger amount of PEI and SWCNT were deposited on the membrane surface with stronger affinity with water. Specifically, the water contact angle values of (PEI/SWCNT)$_5$-GA, (PEI/SWCNT)$_8$-GA and (PEI/SWCNT)$_{10}$-GA membrane were 67.46 ± 1.01°, 64.38 ± 0.62° and 62.21 ± 1.02°, respectively.

XPS analysis was conducted to further confirm the surface chemical composition of the printed membranes. Results are shown in **Fig. 5.3 (c) and (d)** and **Table 5.3**. It should be noted that the PEI membrane was prepared only by printing of PEI polymer on PK membrane surface to confirm the successful printing of PEI. The wide scan element spectra of the LBL OSN membranes is shown in **Fig. 5.3 (c)**. It is clear that only C and O can be found on the PK membrane surface, and the deposition of PEI

polymer lead to the appearance of N element on the PEI membrane surface. **Fig. 5.3 (d)** presents the narrow scan spectra of N1s of the (PEI/SWCNT)$_8$-GA and PEI membranes. For the PEI membrane, only one peak was found, because of the C–N groups containing in the PEI polymer. However, for the (PEI/SWCNT)$_8$-GA membrane, aside from the amine group, the crosslinking reaction between PEI and GA lead to the appearance of the C=N groups (S. Zhao & Wang, 2017). The detailed reaction scheme can be found in **Fig. 5.6** in section 3.2.
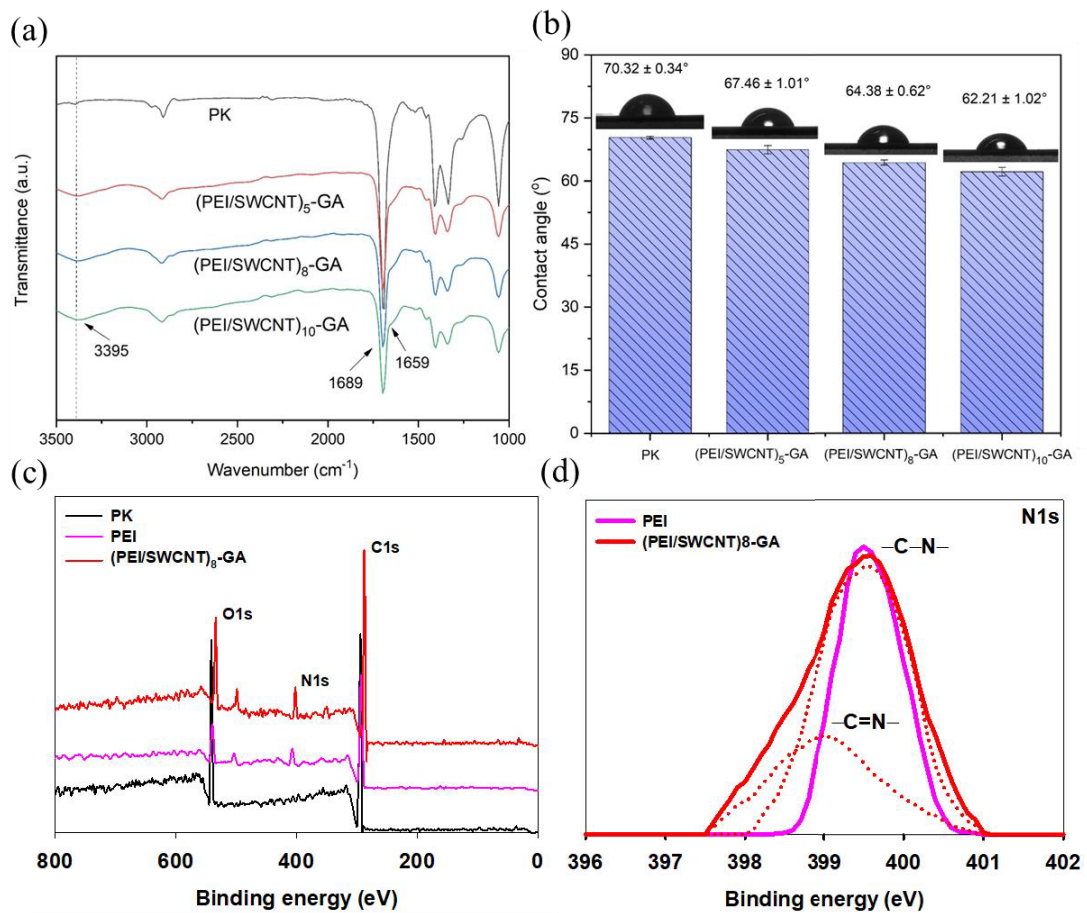
Figure 5.3. Membrane characterizations (a) FTIR, (b) contact angle, (c) XPS wide scan, and (d) XPS N1s narrow scan (The dotted lines show the deconvoluted peaks).

Table 5.3 Surface elemental composition of PK and inkjet printed membranes.

Membrane	C (%)	O (%)	N (%)
PK	80.71	19.29	-
PEI	85.16	8.27	6.57

(PEI/SWCNT)$_8$-GA	87.52	7.37	5.11

Fig. 5.4 exhibites the SEM characterizations of PK and LBL OSN membranes. For the surface analysis in **Fig. 5.4 (a$_1$) to (d$_1$)**, the PK membrane has a porous surface structure (pore size: 60~220 nm). However, the LBL OSN membranes exhibited dense surface with no visible pores. For the cross-section SEM images in **Fig. 6.4 a$_2$-d$_2$**, with the increased bilayer numbers, the thickness of the active layer increased. In specific, the active layer thickness of (PEI/SWCNT)$_5$-GA, (PEI/SWCNT)$_8$-GA and (PEI/SWCNT)$_{10}$-GA membrane were 55.9 ± 1.5, 87.1 ± 1.7 and 109.5 ± 4.9 nm, respectively.
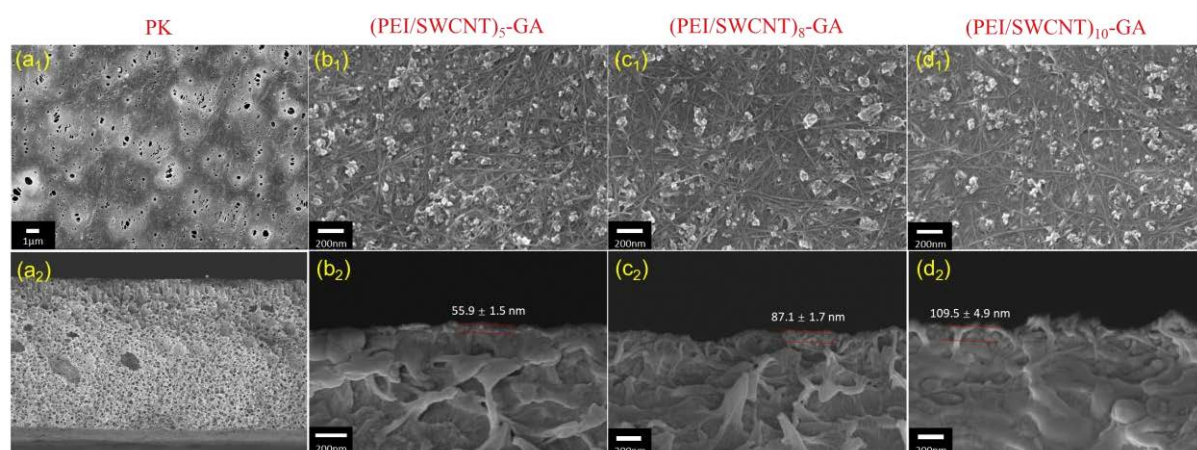
Figure 5.4. SEM images of PK, (PEI/SWCNT)$_5$-GA, (PEI/SWCNT)$_8$-GA and (PEI/SWCNT)$_{10}$-GA membranes, top surface ((a$_1$)-(d$_1$)) and cross-section ((a$_2$)-(d$_2$)).

The results of the effect of different numbers of bilayers on the OSN performance were shown in **Fig. 5.5**. It is clearly seen that the permeance of the LBL OSN membranes decreased with the increased bilayer numbers. At higher printing cycles, the layer thickness increases due to increased depositions of PEI and SWCNT on the membrane surface (as indicated by cross-section SEM images in **Fig. 5.4**) and this generates higher resistance to ethanol permeation thereby decreasing ethanol permeability. Specifically, the ethanol permeability decreased from 5.68 L m^{-2} h^{-1} bar^{-1} of (PEI/SWCNT)$_5$-GA membrane to 2.17 and 1.24 L m^{-2} h^{-1} bar^{-1} for (PEI/SWCNT)$_8$-GA and (PEI/SWCNT)$_{10}$-GA membranes, respectively. The RB rejections of the LBL OSN membranes presented an upward trend with the increased bilayer numbers because of the denser membrane surface structures. The RB rejections of

(PEI/SWCNT)$_5$-GA, (PEI/SWCNT)$_8$-GA and (PEI/SWCNT)$_{10}$-GA were 96.4%, 99.2% and 99.3%, respectively. Although the rejections of the (PEI/SWCNT)$_8$-GA and (PEI/SWCNT)$_{10}$-GA membranes were similar, the permeance of (PEI/SWCNT)$_8$-GA (2.17 L m^{-2} h^{-1} bar^{-1}) was higher than that of (PEI/SWCNT)$_{10}$-GA (1.24 L m^{-2} h^{-1} bar^{-1}). Therefore, the bilayer number of 8 was selected as optimum cycles for further preparation of printed LBL membranes as it has shown higher permeability with good rejection performance.
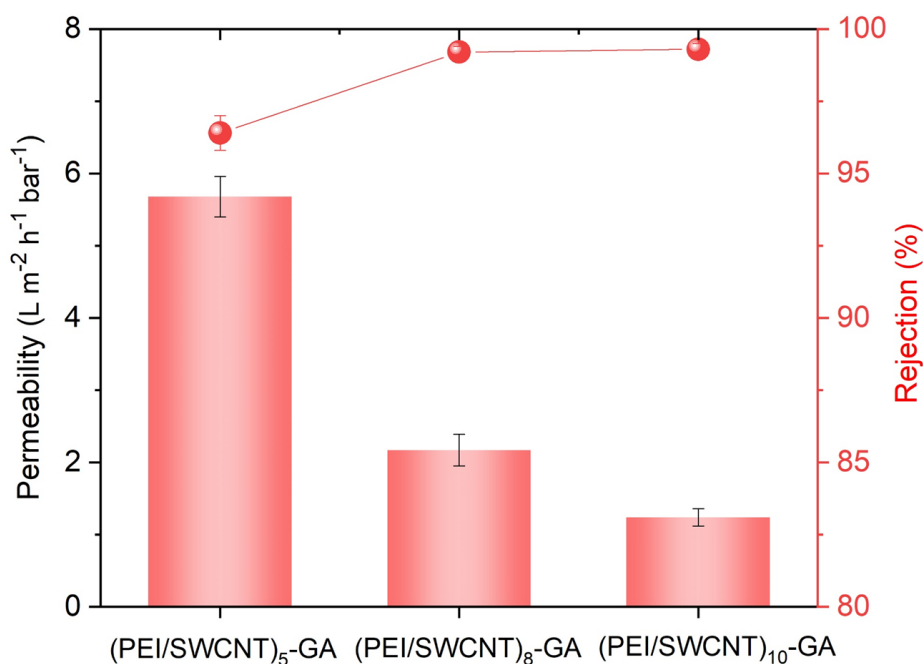
Figure 5.5. The effect of different bilayer numbers on the OSN performance. (OSN test condition: 50 mg/L RB in ethanol, 5 bar)

5.3.2 The effect of cross-linking conditions on membrane performances

Aside from GA, there are also other cross-linkers, such as ECH and TMC, which can be used to cross-link the amine groups of PEI during the post-treatment of the inkjet-printed LBL membranes (J. Gao, Sun, Zhu, & Chung, 2016). As far as we know, it is the first time to conduct and compare the effect of the modification of different cross-linking agents for the preparation of LBL membranes for OSN, which can provide options for optimal cross-linkers for OSN membrane modification. The molecular structures of GA, ECH and TMC along with their reactions with PEI were displayed in **Fig. 5.6.** The crosslinking reactions between the aldehyde groups of GA and N–H groups of PEI can form imine (–C=N) groups (Q. Li et al., 2018). The hydrogen atoms of the amine groups can react with the epoxy groups of ECH via nucleophilic addition

reaction (Kotte, Hwang, Han, & Diallo, 2015). The reaction of acyl chloride in TMC and amine group in PEI can form an amide group (D. Wu, Huang, Yu, Lawless, & Feng, 2014).
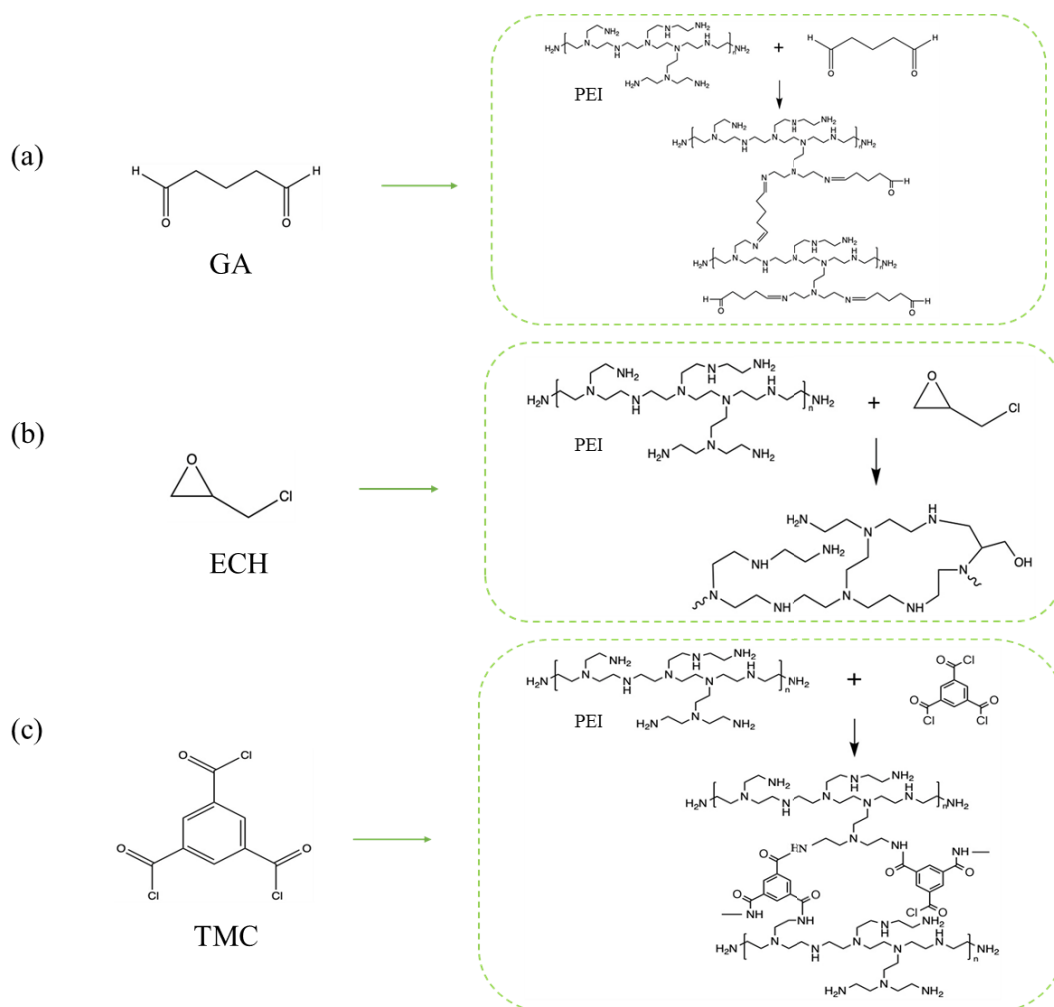
Figure 5.6. The chemical structures and reactions between PEI and (a) GA, (b) ECH and (c) TMC.

Firstly, three different inkjet-printed LBL membranes namely (PEI/SWCNT)$_8$-GA, (PEI/SWCNT)$_8$-ECH and (PEI/SWCNT)$_8$-TMC were characterized by SEM and AFM (see **Fig. 5.7**). From the top surface SEM images of (PEI/SWCNT)$_8$-GA (**Fig. 5.7** (a$_1$)) and (PEI/SWCNT)$_8$-ECH (**Fig. 5.7** (b$_1$)) membranes, the polymer particles and the long chain structures of SWCNT nanomaterial could be clearly seen. However, for (PEI/SWCNT)$_8$-TMC (**Fig. 5.7** (c$_1$)) membrane, it appears like a dense layer covering on the membrane surface leading to the low visibility of PEI particles and SWCNT structures. The cross-section images (**Fig. 5.7** (a$_2$)-(c$_2$)) confirmed the above findings. Compared to the (PEI/SWCNT)$_8$-GA (87.1 ± 1.7 nm) and (PEI/SWCNT)$_8$-

ECH (79.5 ± 0.2 nm) membranes, the (PEI/SWCNT)$_8$-TMC membrane exhibited higher active layer thickness of 151.6 ± 1.6 nm. Also, the surface roughness (**Fig. 5.7** (a$_3$)-(c$_3$)**)** of (PEI/SWCNT)$_8$-TMC membrane (34.23 ± 1.76 nm) was lower than those of (PEI/SWCNT)$_8$-GA (42.29 ± 1.89 nm) and (PEI/SWCNT)$_8$-ECH (38.23 ± 2.19 nm) membranes, which was mainly due to the thick layer coated on the membrane surface providing the smoother surface structures.
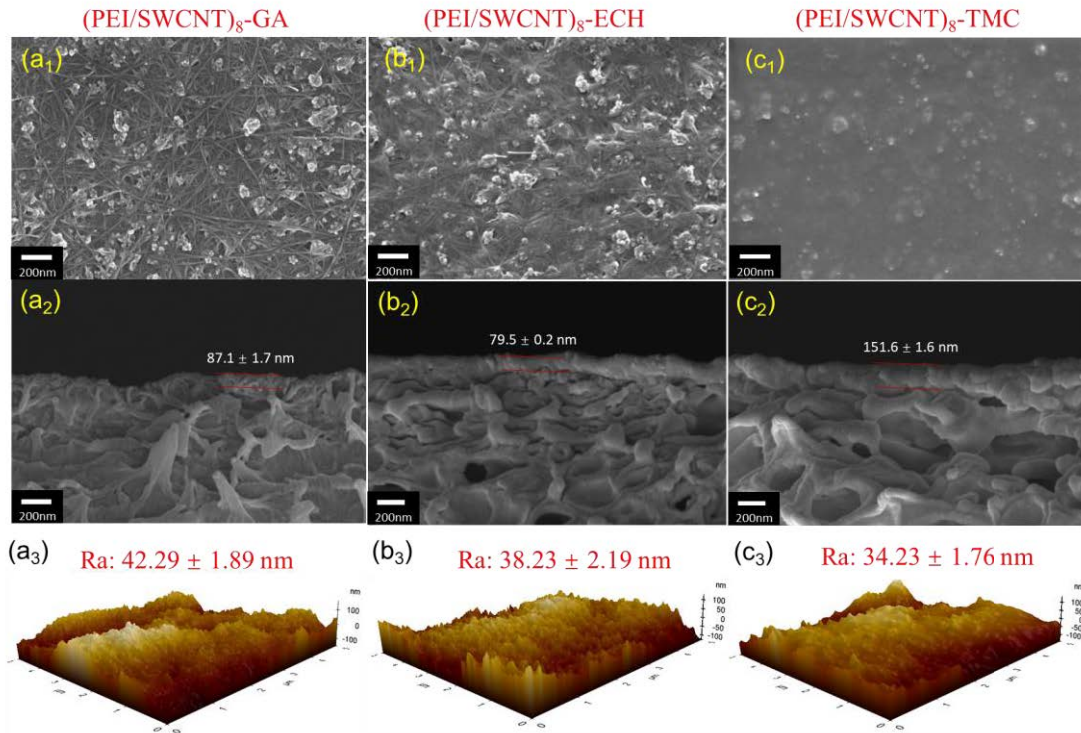
Figure 5.7. (a$_1$)-(c$_1$) top surface SEM images, (a$_2$)-(c$_2$) cross-section SEM images, and (a$_3$)-(c$_3$) AMF images of (PEI/SWCNT)$_8$-GA (a$_1$-a$_3$), (PEI/SWCNT)$_8$-ECH (b$_1$-b$_3$) and (PEI/SWCNT)$_8$-TMC (c$_1$-c$_3$) membranes.

The influence of GA, ECH and TMC modifications on the OSN performances of the inkjet-printed LBL membranes is shown in **Fig. 5.8**. Among the three printed LBL-OSN membranes, (PEI/SWCNT)$_8$-ECH membrane exhibited the highest permeance with a value of 6.81 L m^{-2} h^{-1} bar^{-1}, followed by (PEI/SWCNT)$_8$-GA with a permeance of 2.17 L m^{-2} h^{-1} bar^{-1}. The difference in ethanol permeance might be attributed to the membrane surface hydrophilicity. As shown in **Fig. 5.9**, the contact angle of (PEI/SWCNT)$_8$-ECH membrane is $40.39 \pm 1.25°$, which was significantly lower than that of (PEI/SWCNT)$_8$-GA membrane ($64.38 \pm 0.62°$). The difference in membrane surface hydrophilicity results from the different cross-linking reactions between PEI

and cross-linkers of GA and ECH (C. Feng et al., 2014). When GA used as the cross-linker, the primary amino groups of PEI can react with the aldehyde group of GA to form an imine (–C=N) group (see **Fig. 5.6** (a)). The –C=N group is not as hydrophilic as amino and hydroxyl groups leading to the less hydrophilic membrane surface. For ECH, during the cross-linking reaction with PEI, hydroxyl groups are produced (see **Fig. 5.6** (b)) resulting in a more hydrophilic membrane surface. The (PEI/SWCNT)$_8$-TMC membrane showed the lowest permeance of 0.95 L m^{-2} h^{-1} bar^{-1}, attributed to the much thicker active layer (**Fig. 5.7** (c$_2$)). Despite the active layer thickness, the (PEI/SWCNT)$_8$-GA and (PEI/SWCNT)$_8$-ECH membranes exhibited higher RB rejections compared to the (PEI/SWCNT)$_8$-TMC membrane. Similar findings can also be found in another study (J. Gao et al., 2016). These results indicated that the printed LBL membrane cross-linked by TMC could not improve its rejection performance. Compared to the membrane modified by ECH, membrane modified by GA showed higher rejection performance indicating its more effective cross-linking reactions, as well as the least surface pore size (J. Gao et al., 2016).
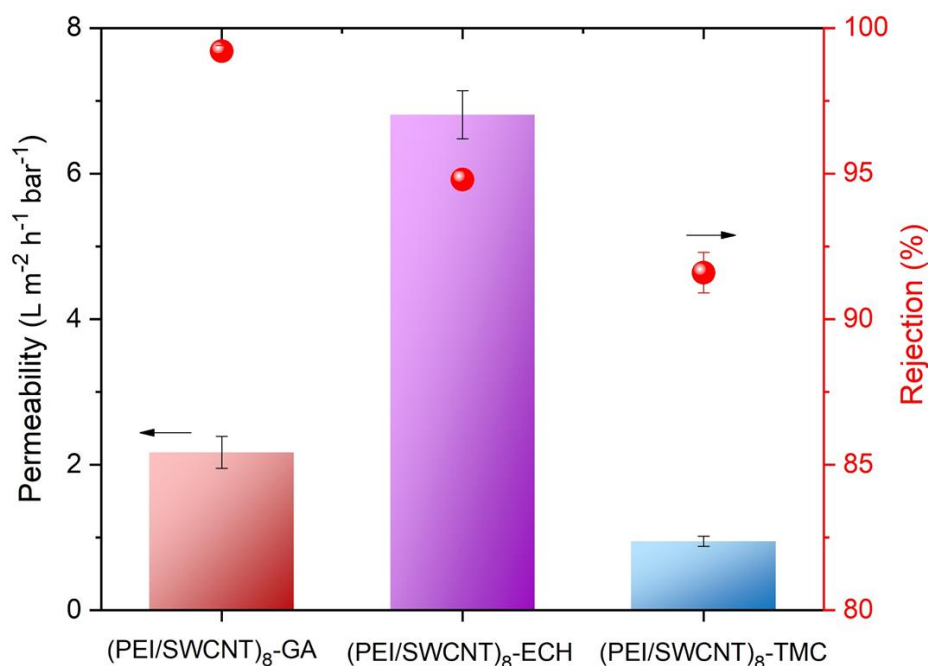
Figure 5.8. The effect of different cross-linkers on the OSN performance. (OSN test condition: 50 mg/L RB in ethanol, 5 bar)
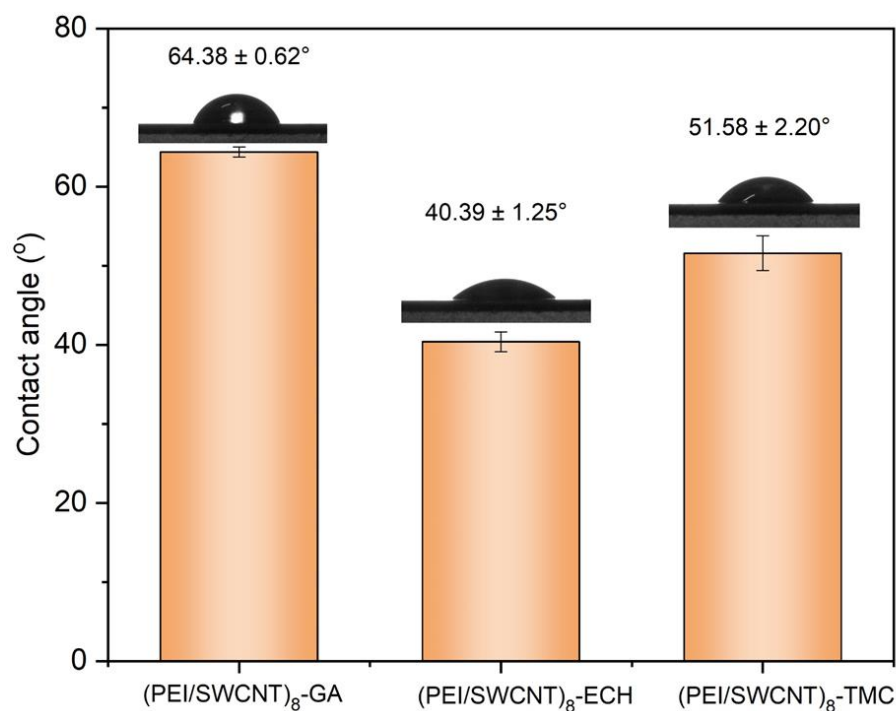
Figure 5.9. Water contact angle of inkjet printed LBL-OSN membranes fabricated with different cross-linkers.

Considering the relatively low RB rejection performance of (PEI/SWCNT)$_8$-ECH and (PEI/SWCNT)$_8$-TMC membranes, we further investigated whether the rejection performance can be improved by changing the cross-linking conditions, i.e., cross-linking time. For ECH cross-linker, 6 wt% ECH in aqueous solution was used to cross-link the membrane for 10, 20 and 30 min, respectively, followed by oven-cured at 65°C for 10 min. For TMC cross-linker, 0.1 wt% TMC in n-hexane solution was used to treat the membrane for 30 s, 1 min and 2 min, respectively, then oven-cured at 80°C for 5 min. OSN performances of LBL membranes fabricated under different cross-linking time are displayed in **Fig. 5.10**. In **Fig. 5.10** (a), it can be seen that the increment in RB rejection was not significantly pronounced (from 94.8% to 96.7%) with the increase of ECH cross-linking time. However, the permeance dramatically decreased from 6.81 to 2.63 L m^{-2} h^{-1} bar^{-1} when the cross-linking time increased from 10 to 30 min. A similar trend was also found with the TMC-modified LBL-OSN membranes in **Fig. 5.10** (b). Increasing the cross-linking time from 30 s to 2 min resulted in RB rejection increasing from 91.6 to 92.4%, while the permeance decreased from 0.95 to 0.38 L m^{-2} h^{-1} bar^{-1}. In summary, increasing cross-linking time of ECH

and TMC could enhance the RB rejection performances, but the improvement was not too significant considering the drastic drop in membrane permeability.
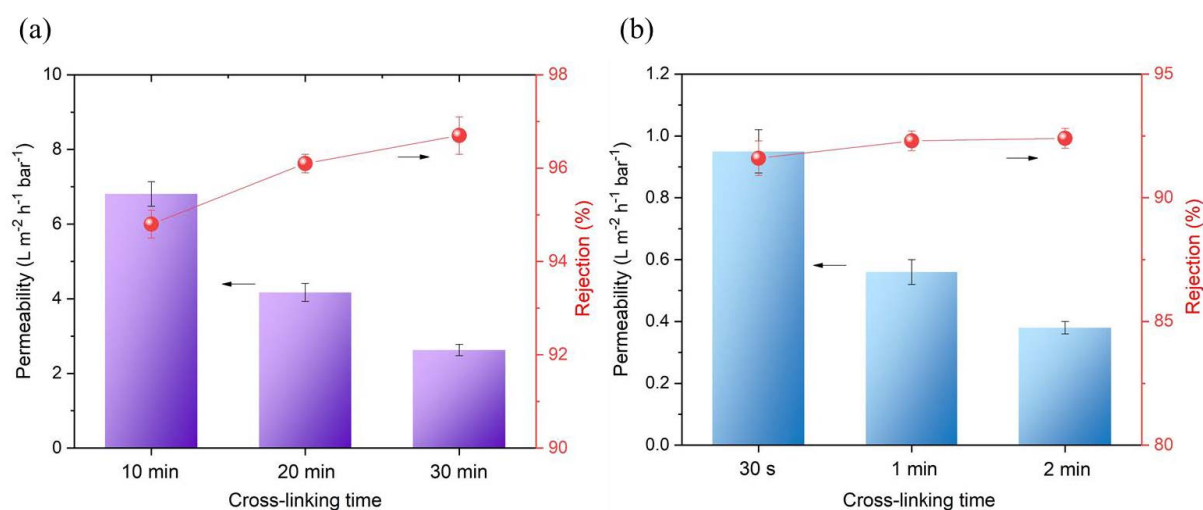
Figure 5.10. OSN performance with different cross-linking time (a) ECH as cross-linker and (b) TMC as cross-linker. (OSN test condition: 50 mg/L RB in ethanol, 5 bar)

From the results described above, changing cross-linking time was found to be not efficient to improve the membrane rejection. Thus, in this section, we further evaluate membrane performances with different GA concentrations. The GA cross-linking solution was prepared by adding 1.0 wt%, 1.5 wt%, 2.0 wt% and 2.5 wt% of GA, respectively, along with 1% (v/v) HCl in DI water and ethanol mixed solution (1:1). The LBL-OSN membrane was cross-linked with the above mentioned GA solutions for 10 min, then oven-cured at 90°C for 10 min. **Fig. 5.11** shows the OSN performances of the inkjet-printed LBL membranes fabricated with different GA concentrations. The MO rejection of the printed LBL membranes exhibited an increasing trend with the increase of GA concentrations, which is mainly due to the higher degree of cross- linking between PEI polymer and GA (Y. Ji et al., 2010; S. Zhao & Wang, 2017). Cross-linking with 1, 1.5, 2, and 2.5 wt% GA resulted in the respective MO rejection values of 76.5, 82.4, 89.4, and 89.2 %. On the other hand, the permeance decreased dramatically from 2.17 L m^{-2} h^{-1} bar^{-1} to 1.21, 0.56 and 0.24 L m^{-2} h^{-1} bar^{-1} with the GA concentrations of 1, 1.5, 2, and 2.5 wt%, respectively. It should be noted that the rejection performance of the printed LBL membrane prepared with GA concentration of 2 wt% and 2.5 wt% were similar, but the permeance of 2 wt% was higher. This indicates that the optimal GA concentration for the MO rejection

was 2 wt% since further increase in GA concentration did not lead to enhanced MO rejection.

In summary, cross-linking agent concentration has a greater effect on the membrane performance compared to cross-linking time (J. Gao et al., 2016). Among the three cross-linkers tested in this study, GA is observed to be the best cross-linking agent for printed LBL membrane modification. In addition, GA solution was prepared in a DI water-ethanol mixed solution, and ECH solution was prepared in DI water, which are much greener than the TMC solution prepared in n-hexane solvent. Because of the poor performances and the principles to develop greener membranes (Szekely et al., 2014), TMC cross-linking agent is not recommended for the LBL-OSN membrane modification.
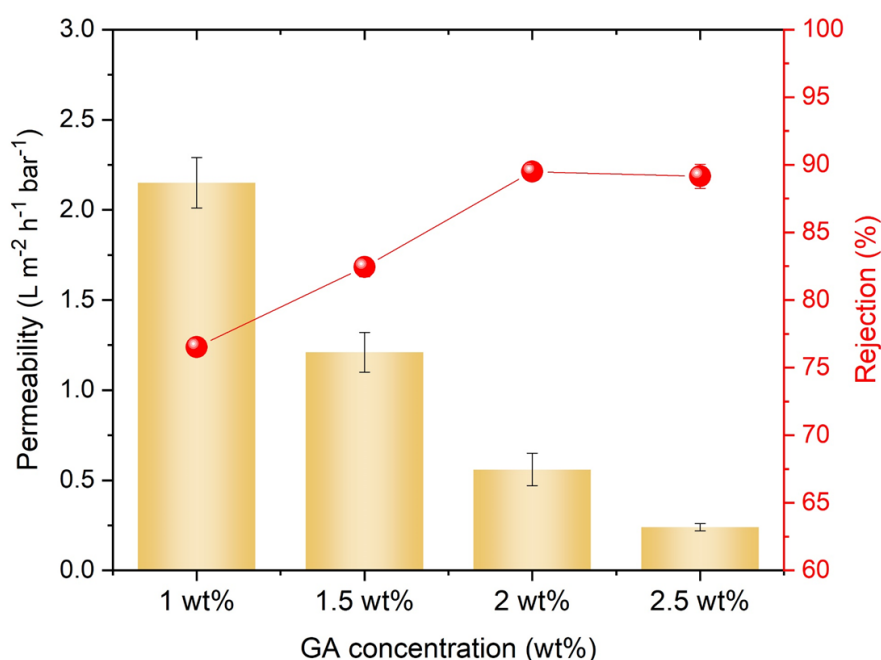
Figure 5.11. Effect of GA concentration on the OSN performances. (GA cross-linking time: 10 min, OSN test condition: 50 mg/L MO in ethanol, 5 bar)

5.3.3 Stability performance of the LBL OSN membrane

PK membrane has been proven to have high mechanical strength and excellent organic solvent resistance property. It shows good resistance to most organic solvents and even harsher solvents, such as DMF, NMP, DMAC, and hexane (C. Liu et al., 2020). In order to evaluate the organic solvent resistance of the inkjet-printed LBL membrane, membrane samples (size 1 cm × 5 cm) were soaked in acetone, IPA, DMF, methanol

and ethanol for three weeks. The results of the weight loss and OSN performances were shown in **Table 5.4** and **Fig. 5.12**.

In **Table 5.4**, negligible weight loss (less than 0.7%) was observed after immersing in the above mentioned five organic solvents for three weeks. Moreover, in **Fig. 5.12**, after immersing the (PEI/SWCNT)$_8$-GA membrane in acetone, IPA, DMF, methanol and ethanol for three weeks, the OSN performances revealed an insignificant change. The results confirm that the LBL-OSN membranes have good stability in various organic solvents.
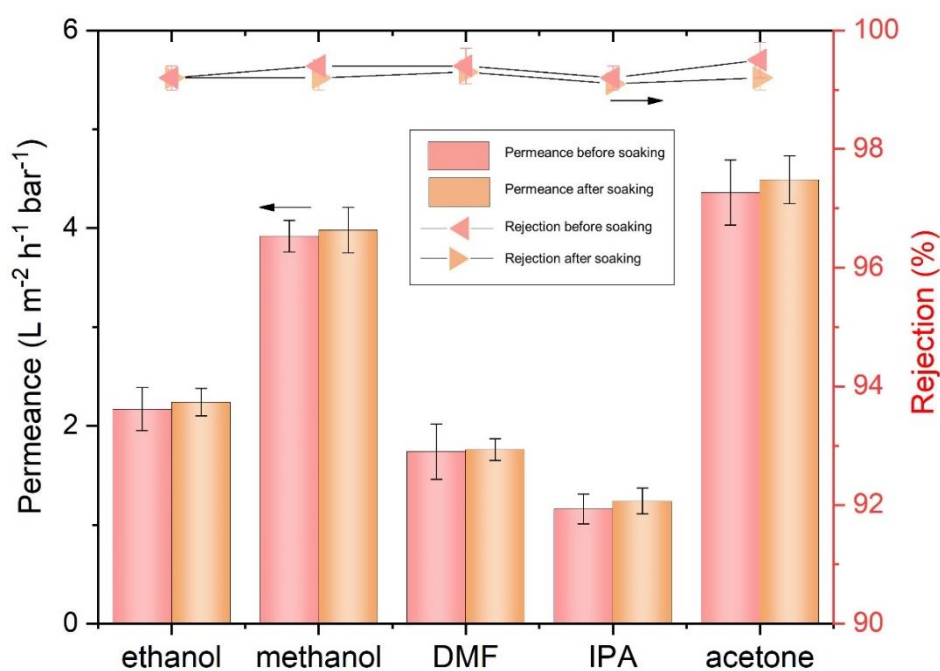
Figure 5.12. Membrane stability test by soaking (PEI/SWCNT)$_8$-GA membrane in various organic solvents for three weeks. (OSN test condition: 50 mg/L RB, 5 bar)

Table 5.4. (PEI/SWCNT)$_8$-GA membrane weight loss after immersing in various organic solvents for three weeks.

(PEI/SWCNT)$_8$-GA membrane	Organic solvent	Weight before (mg)	Weight after (mg)	Weight loss (%)
1	ethanol	53.0/48.3	52.8/48.0	0.4%/0.6%
2	methanol	51.7/49.5	51.7/49.2	0.0%/0.6%
3	DMF	53.0/53.0	52.8/52.9	0.3%/0.2%

| 4 | IPA | 52.9/49.2 | 52.7/48.9 | 0.4%/0.6% |
| 5 | acetone | 52.9/53.1 | 52.5/52.7 | 0.7%/0.7% |

5.3.4 Applications of the inkjet-printed LBL OSN membranes

As we mentioned in the introduction, most previous studies only focused on using different approaches to improve OSN membrane performances. But few studies discussed the specific applications for their fabricated OSN membranes. Solvent recovery by OSN has been proved to have a great potential in many solvent-intensive industries, such as the pharmaceutical industry, which will provide various benefits in terms of environment, economy, and safety. In pharmaceutical industry, general specification for solvent purity is around 99%. For our inkjet-printed LBL membrane, the (PEI/SWCNT)$_8$-GA membrane (PEI 10.0 g/L, SWCNT 1.0 g/L, and GA 1 wt%) provided the RB (Mw: 1017 Da) rejection over 99% with acetone, IPA, DMF, methanol and ethanol permeability of 4.36, 1.16, 1.74, 3.92 and 2.17 L m^{-2} h^{-1} bar^{-1}, respectively. A number of pharmaceutical compounds such as Fidaxomicin (MW: 1058 Da), Candicidin (MW: 1109 Da) and Temsirolimus (MW: 1030 Da) have similar molecular weight as RB, as shown in **Fig. 5.13** (a). Take Candicidin for example, as an antibiotic, it exhibits high antifungal activity against a variety of fungi, particularly Candida albcans. Crude Candicidin are normally cultivated for several days at appropriate temperature. Since the crude Candicidin, in some cases, may be essentially free from the foreign impurities (Selman A. Waksman & Lechevalier, 1961). The printed (PEI/SWCNT)$_8$-GA membrane can be used for the organic solvent recovery or separation from the Candicidin/solvent mixed solutions during the synthesis process.

The OSN membrane can also be applied in the hemp industry. In Australia, the hemp industry, especially the production of medical cannabis, is legal. Cannabis products, like tetrahydrocannabinol (THC) and cannabidiol (CBD) (see **Fig. 5.13** (b)), have a molecular weight of 314.5. These compounds have been thoroughly investigated from chemical, medicinal and biological perspectives, and have also been applied in clinical trials. The process of the biosynthesis of cannabis products will produce several by-products including pentyl diacetic lactone (PDAL) (MW: 182 Da), hexanoyl triacetic acid lactone (HTAL) (224 Da), and olivetol (MW: 180 Da) (Bloemendal, van Hest, & Rutjes, 2020; Tahir, Shahbazi, Rondeau-Gagne, & Trant, 2021). Our inkjet-printed

(PEI/SWCNT)$_8$ membrane prepared with PEI 10.0 g/L, SWCNT 1.0 g/L, and GA 2 wt% exhibited nearly 90% MO (Mw: 326 Da) rejection, which can be suitably applied for the THC or CBD solute separation during the formation process. Since the by-products have a lower molecular weight, they will pass through the membrane to the permeate side leaving the higher molecular weight THC and CBD in the feed solution. Finally, based on the discussions, our future works will include test applications of OSN membrane performances using these real products.

(a)

Fidaxomicin	Candicidin	Temsirolimus
$C_{52}H_{74}Cl_2O_{18}$ (1058)	$C_{59}H_{84}N_2O_{18}$ (1109)	$C_{56}H_{87}NO_{16}$ (1030)
Fidaxomicin is a macrolide antibiotic used to treat diarrhea associated with *Clostridium difficile* infection.	Candicidin is an antibiotic obtained from *Streptomyces griseus* and active against some fungi of the genus *Candida*.	Temsirolimus is a antineoplastic agent used in the treatment of renal cell carcinoma (RCC) that works by inhibiting mTOR.

(b)

Cannabidiol (CBD)	Tetrahydrocannabinol (THC)
$C_{21}H_{30}O_2$ (314.5)	$C_{21}H_{30}O_2$ (314.5)

Both CBD and THC products play roles in pain, immune function, stress, and sleep.

Figure 5.13. (a) Three drugs with similar molecular weight of RB; (b) Two cannabis products with similar molecular weight of MO.

5.4 Conclusions

In this chapter, novel LBL-OSN membranes were fabricated by alternative printing of PEI and SWCNT inks on PK support membranes using the inkjet printing technology, followed by post cross-linking treatment with GA, ECH, and TMC. The effects of PEI and SWCNT concentrations, bilayer numbers, and cross-linking conditions were evaluated in terms of OSN membrane performances. PEI concentration of 10.0 g/L and SWCNT concentration of 1.0 g/L with eight cycles of printing bilayers were

chosen as optimal conditions for preparing LBL membranes. Among the three cross-linking agents, GA was found to be the best option for printed LBL membrane modification with the best OSN performances. In addition, compared to the cross-linking time, cross-linking agent concentration was found to have a greater effect on the membrane modification in terms of rejection performances. Moreover, the inkjet-printed LBL membranes showed negligible changes in membrane weights and performances after immersing in five organic solvents for three weeks. Finally, the benefits of the inkjet printing method for LBL membrane formation were discussed and the possible applications of our printed LBL membranes in the pharmaceutical and hemp industries were proposed. This work could further develop inkjet printing method for OSN membrane preparations and applications.

CHAPTER 6

Machine learning based prediction of thin film nanocomposite membranes for organic solvent nanofiltration

6.1 Introduction

In OSN process, OSN membranes are the key parameters influencing the separation performances. In chapter 4 and 5, we introduced the inkjet printing assisted LBL method for fabricating high performance nanocomposite OSN membranes. In this chapter, we further investigated using ML based models for nanocomposite OSN performance prediction. Currently, the impact of OSN technique is rather limited. The main reason is complex OSN process which includes the interactions between the membrane materials, the solutes and the organic solvent (Merlet et al., 2020). These complex interactions complicate the formation of an effective model to predict the separation performances of OSN membranes.

There are several models applied for OSN performance predictions, such as the solution-diffusion model (J.G. Wijmans, 1995) and the pore-flow model (J. L. Anderson, 1974). However, these models need to regress some parameters to predict the organic solvent flux and solute rejection at different operating conditions under a fixed chemical system, which limits the development of OSN technique. Recently, the emergence of machine learning (ML) has become an important data-driven method in chemical and material engineering field (Butler, Davies, Cartwright, Isayev, & Walsh, 2018; Venkatasubramanian, 2018). There are a variety of studies in membrane field utilizing ML method for membrane performance predictions including the reverse osmosis (RO) (Jeong, Chung, & Tong, 2021; Lee & Kim, 2020; Yeo, Xie, Wang, & Zhang, 2020), NF (Jeong et al., 2021; Lee & Kim, 2020), forward osmosis (FO) (K, Mungray, Agarwal, Ali, & Chandra Garg, 2021), ultrafiltration (UF) (Fetanat et al., 2021), gas separation (Yuan et al., 2021), exchange membrane fuel cell (H. Chen et al., 2021; Ding et al., 2021), membrane bioreactor (Kamali, Appels, Yu, Aminabhavi, & Dewil, 2021; Viet & Jang, 2021). The ML was first used as predictive models for OSN solvent flux prediction was introduced by Goebel et al. in 2019 (Goebel & Skiborowski, 2020). In their study, the developed models could predict the permeances of different organic solvents with a mean percentage error below 9%, which exhibited superior results in terms of accuracy and parameter precision compared to the previous models. In addition, the developed model can also be successfully applied to predict the membrane solvent flux in organic solvent mixtures. This group then developed another ML based predictive models for solute rejection prediction in OSN process (Goebel, Glaser, & Skiborowski, 2020). The rejection

performances for various solutes were recorded using PuraMem S600 membranes under six different organic solvents systems. At the meantime, model candidates were evaluated in terms of accuracy and parameter precision. Moreover, the solution rejection performances in mixed organic solvent systems were investigated by analysing previous permeation data using PuraMem 280 membranes. The developed models for solute rejection predictions in both pure and mixed organic solvents systems exhibit good accuracy and decent parameter precision with deviations between measured and predicted values less than 10% for most experimental data. Hu et al. (Hu et al., 2021) established three different ML algorithms including ANN, random forest (RF), and SVM for commercial OSN membrane performance predictions. Predictive models for both permeance and rejection predictions were evaluated with more than 18 parameters. In order to elucidate the important parameters affecting membrane performances, principal component analysis (PCA) was conducted. Results showed that the factors affecting both permeance and rejection are similar. The trained ML models could predict OSN membrane performances with 98% accuracy for permeance and 91% accuracy for rejection.

In this study, we conducted a summary of previous research work on nanocomposite OSN membranes with the nanomaterial incorporated into the PA layers and established different models (ANN, BT, SVM and linear) for membrane performance prediction. It should be noted that because the nanocomposite membranes in this study were fabricated with the nanomaterial incorporated into PA layer during IP process, the prepared nanocomposite membranes are TFN-OSN membranes. The operating principles of ANN function on the use of multiple nodes designated as inputs, hidden layers and outputs; mimicking the human brain to reach conclusions. The advantages of using ANN allow broad ranges of data to be categorized (Dumitru & Maria, 2013). BT displays a high degree of bias which are constructed layer by layer to predict results. It can convert weak learning algorithms into stronger learners; however, this requires sets of data that can be processed with a higher degree of accuracy than that of guessed predictions (Schapire, 2003). SVM uses an optimal separating 2D or 3D hyperplane between two classes of data that need binary or multiclass categorization. Multiple SVMs are trained using the bag and bootstrap method which is then aggregated onto this plane (Cervantes, Garcia-Lamont, Rodríguez-Mazahua, & Lopez, 2020). The optimal hyperplane is then identified by processing prepared data, followed by its use

to predict results. Finally, linear prediction models use regression modelling to produce a forecast based on the averages of linear data points along the graph.

The accuracy of these models in terms of permeance and rejection performances were compared and discussed. Parameter contribution analysis was conducted to evaluate the important parameters influencing membrane RP and RS performances. Moreover, in order to evaluate the degree of effects of different parameters on prediction, partial dependence plots (PDP) were conducted to provide the optimal conditions for nanocomposite OSN membrane fabrication.

6.2 Methodologies

6.2.1 Data Collection

The experimental data were collected from 20 articles about the performances of nanocomposite OSN membranes with the nanomaterial incorporated into PA layers, a total of 9252 data points. The 20 articles were searched through Google Scholar with keywords such as thin film nanocomposite organic solvent nanofiltration membranes, nanocomposite membranes for organic solvent nanofiltration, and nanocomposite membranes for solvent resistance nanofiltration. Data were obtained from the tables and figures. Some figures which are hard to obtain data directly, the online Plot Digitizer 2.6.8 as an effective tool to figure out their values. Two commonly used parameters organic solvent permeability and solute selectivity were chosen to characterize membrane performances. It should be noted that the two parameters (relative permeability (RP) and relative selectivity (RS)) for evaluating membrane performances are the extent of the changes with the incorporation of nanomaterials into membranes. The original values of the membrane permeability and selectivity are not directly comparable due to the different performances of control membranes without nanomaterials incorporation. Thus, RP and RS are used as outputs for the model formation. Both RP and RS are calculated based on the ratios of the respective values to control values.

Other key parameters effecting membrane performances have been selected and summarised in **Table 6.1** based on our previous experience. The parameters of the conditions for membrane fabrication include membrane substrate type, amine monomer type and chloride monomer type with varying concentrations for the active layer formation. The parameters of the nanomaterial properties include nanomaterial

type, size and loading. Water contact angle and surface roughness are used to describe membrane surface properties. The parameters of the OSN operation condition are classified into solvent and solute conditions. Solvent conditions include: solvent type, molecular weight, viscosity, density, and molar volume. Solute conditions include: solute type, concentration, molecular weight, and charge properties.

Table 6.1 Parameters affecting the performances of TFN-OSN membranes for model formations.

Category		Parameters
Membrane fabrication conditions		Substrate type
		Amine monomer
		Amine monomer concentration
		Chloride monomer
		Chloride monomer concentration
Membrane properties		Water contact angle
		Surface roughness
Nanomaterial properties		Nanomaterial type
		Nanomaterial size
		Nanomaterial loading
OSN test conditions	Solvent	Solvent type
		Molecular weight
		Viscosity
		Density
		Molar volume
	Solute	Solute type
		Molecular weight
		Concentration
		Charge property

6.2.2 Machine learning-based models for data analysis

6.2.2.1 Missing data and categorical data

Handling missing values is important for building accurate and reliable ML models. Missing data is the unreported features in the literature. In this work, in order to compare more machine learning algorithms, firstly, we have to deal with the missing

input data. The missing values are commonly imputed by the mean or median values. Based on the previous studies (Sinharay, Stern, & Russell, 2001; Van Buuren, 2018), we used the mean value to impute the dataset for the ML methods which cannot handle the missing data, such as linear, SVM, and ANN models. The missing value was kept in their raw format for boosted tree model, which can process their raw format of missing values. For the categorical variables, we used dummy encoding for these variables (Potdar, Pardawala, & Pai, 2017). We created one dummy variable for each level of each categorical variable. An illustration of the model formation process is shown in **Fig. 6.1**. The collected data was randomly split between training and testing datasets. 80% of the dataset was used for training and 20% for testing. We used cross-validation to evaluate model performance and tune the hyperparameters. All the experiments were conducted in MATLAB 2021b and all the results were the mean of five repeated experiments with different random seeds.
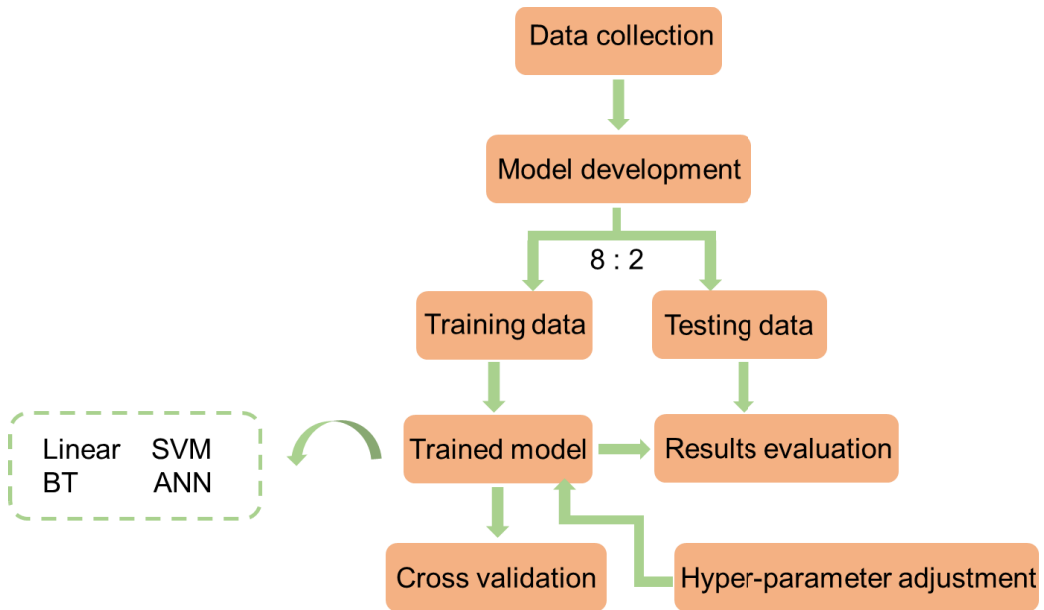
Figure 6.1. An illustration of the model formation process.

6.2.2.2 Development of linear model

For a given training data $\{(x^1, y^1), ..., (x^l, y^l)\} \in \chi \times \mathbb{R}$ of known sample values of x and corresponding values of y, where χ denotes the space of the input features, a linear model (see **Fig. 2 (a)**) for the membrane performance prediction can be described as:

$$f(x) = a_0 + a_1 * x_1 + \cdots + a_n * x_n, \quad (1)$$

where a_0 is the bias of the model, $a_i = [a_1, \ldots, a_n]$ represents the coefficients of the model and $x_i = [x_1, x_2, \ldots, x_n]$ stands for the features of each sample affecting the performance of the membrane, such as loading, nanoparticle size, solvent type, and etc. The linear model can be reformed in matrix form as $y_a = XA$, where y_a represents the performance of the given membrane and in this case, as either RP or RS.

The most commonly used method for determining the model coefficient in the linear regression is the least square method. The least square method requires the explicit inversion of a matrix, which needs substantial computations. In this study, we use QR decomposition (Gander, 1980) to solve the model coefficients. The QR decomposition is a decomposition of the matrix into an orthogonal matrix and a triangular matrix. It is normally used to solve linear least square problems.

Once the model coefficients a_i is obtained, the predicted value of the membrane performance can be calculated by the linear model based on equation (1). It is worth noting that, in practice, most models contain nonlinearity and our linear assumption is arbitrary. Although the accuracy of linear regression may not be high, we can still use it as a baseline to compare with other methods.

6.2.2.3 Development of Support Vector Machine

SVM is a machine learning algorithm (see **Fig. 6.2 (b)**) which is suitable for both classification and regression problems. In this study, the multivariable SVM regression method is employed to predict membrane performance. The main role is that the algorithm takes a training dataset and transforms it into a high-dimensional Hilbert space using a non-linear mapping function (Suthaharan, 2016). Linear regression is then performed in this feature space by constructing a linear model as given below:

$$f(x) = \sum_{i=1}^{n} a_i \phi(x_i) + b \qquad (2)$$

where a_i is the trainable model coefficient, $\phi()$ is the mapping function, and b' is the bias term. Our goal is to find a function $f(x)$ that has the most ε deviation from the actually obtained targets y_i for all training data, and at the same time is as flat as possible. In other words, errors are tolerated as long as the value is less than ε, but will not accept any deviation larger than this. Flatness in equation (2) means the

requirement of a small a_i. One way to ensure this is to minimize the norm, i.e. $||a||^2 = \sum a^2$. We can consider this issue as a convex optimization problem:

$$\text{minimize } \frac{1}{2}||a||^2$$

$$\text{subject to } \left| y_i - \sum_{i=1}^{n} a_i \phi(x_i) - b \right| \leq \varepsilon$$

In order to solve this problem efficiently, minimizing the regularized objective function using a Limited-memory Broyden-Fletcher-Goldfarb-Shanno solver with ridge regularization is conducted.

6.2.2.4 Development of Boosted Trees

BT (see **Fig. 6.2 (c)**) iteratively combine the weak learner, which is slightly better than random method, into a strong learner (Freund, Schapire, & Abe, 1999). The goal of boosted tree is to find an approximation, $\hat{f}(x)$, of the function $f^*(x)$, which maps instances x to their output values. The model can be described as:

$$f_m(x) = f_{m-1}(x) + a_m \phi_m(x),$$

where a_m is the weight of the m_{th} functions $\phi_m(x)$, which are the models of the decision trees. The initial function $f_0(x)$ is constructed by minimizing the loss function:

$$f_0(x) = arg \min_{\alpha} \sum_{i=1}^{l} L(y_i, \alpha).$$

The rest of the model are expected to minimize

$$\left(a_m, \phi_m(x)\right) = arg \min_{a,\phi} \Sigma_i^l L(y_i, f_{m-1}(x_i) + a\phi(x_i)).$$

In this method, instead of directly solving the optimization problem, each ϕ_m can be considered as a greedy step in the gradient descent procedure. In this case, each h_m is trained on a new dataset $D = \{x_i, r_{mi}\}_{i=1}^{N}$ at the mth iteration. The pseudo-residuals r_{mi} are obtained by:

$$r_{mi} = \left[\frac{\partial L\left(y_i, f(x)\right)}{\partial f(x)} \right]_{f(x)=f_{m-1}(x)}$$

The value of a_m is subsequently computed by solving a line search optimization problem.

6.2.2.5 Development of Artificial Neural Network

ANN model is proposed and developed on the basis of modern neuroscience, which reflects the structure and function of the human brain. A common neural network is a hierarchical structure as shown in **Fig. 6.2 (d)**. Each layer of neurons is fully interconnected with the lower layer neurons. There is no same-layer connection between neurons and do not form a cycle. Such a neural network structure is usually called a "multi-layer feedforward neural network". The input layer neuron receives external input, the hidden layer and output layer neurons process the signal, and the final result is displayed by the output layer neurons.

In this study, a three-layer feedforward neural network is presented to predict the membrane performance, consisting of input, hidden, and output layers. The number of neurons in input and output layers are based on the numbers of input factors and responses. We conduct extensive ablation study to choose the size of the hidden layers. Then, train the network with different parameters and choose the network with the smallest mean square error. Consequently, we choose hidden layer size as hidden1 (100, 73) and hidden2 (1,100). ReLU activation function is applied between the hidden layers.
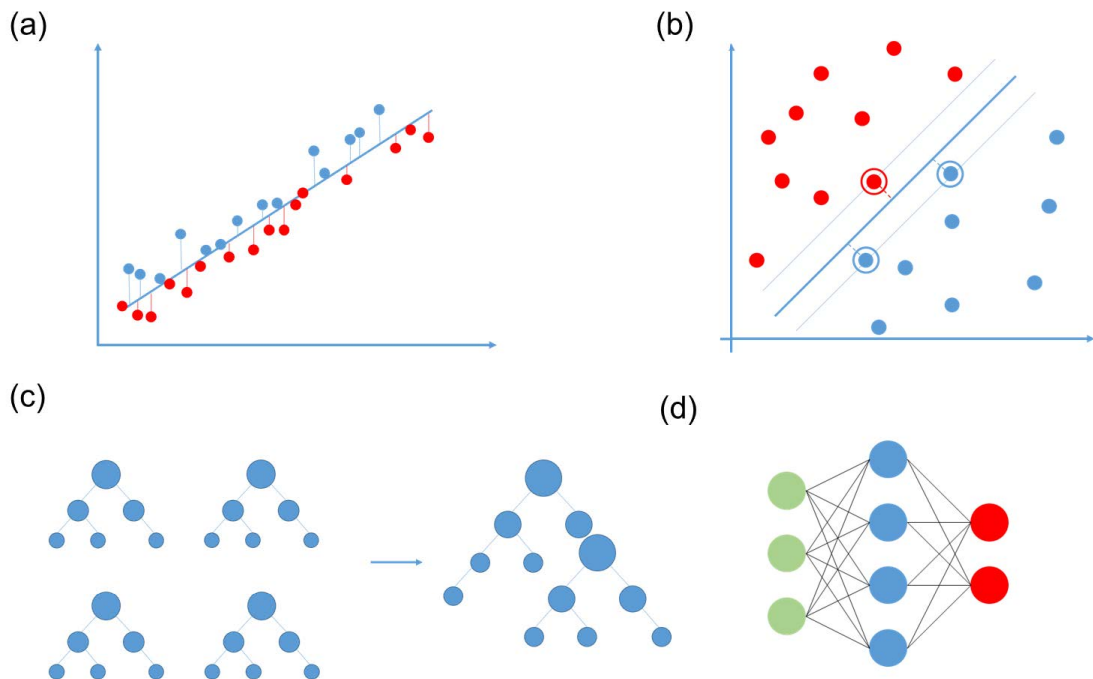
Figure 6.2. Architecture of (a) linear model, (b) SVM model, (c) BT model, and (d) ANN model.

6.2.3 Univariate feature importance analysis

We examine the importance of each predictor individually using an F-test. The hypothesis of the F-test is that the response values grouped by predictor variable values are drawn from populations with the same mean. The alternative hypothesis that the population means are not all the same. A small p-value of the test statistic indicates that the corresponding predictor is important. We use -$\log_{10}$ (p) as importance indicator. Thus, an important feature has higher score value.

6.2.4 Model Interpretation Method

The PDP were constructed to interpret the model results. PDP show the marginal effect of each feature against the RP and RS performance. Different from feature importance analysis which exhibit variables with the different impacts on response, the partial dependence plots illustrate how features can affect model predictions.

Consider partial dependence on a subset x^s of the whole predictor variable set $x_i = [x_1, x_2, \ldots, x_n]$. A subset x^s includes one variable: $x^s = \{x_{s1}\}$. Let X^c be the complementary set of x^s in x. A predicted response $\hat{f}(x)$ depends on all variables in x:

$$\hat{f}(x) = \hat{f}(x^s, x^c)$$

The partial dependence of the predicted responses on a subset x^s is defined by the expectation of predicted responses with respect to the complementary set x^c:

$$\hat{f}^s(x^s) = E_c[f(x^s, x^c)] = \int \hat{f}(x^s, x^c) p_c(x^c) dx^c$$

where $p_c(x^c)$ is the marginal probability of x^c.

Assuming that each observation is equally likely, and the dependence between XS and XC and the interactions of XS and XC in responses are not strong, we can estimate the partial dependence by using the observed predictor data as follows:

$$\hat{f}^s(x^s) \approx \frac{1}{l} \sum_{i=1}^{l} \hat{f}(x^s, x_i^c)$$

where l is the number of observations and x_i is the ith observation.

6.3. Results and Discussion

6.3.1 Data description and linear relationship between variables

The collected database includes 119 different kinds of membranes based on different support membrane types, nanoparticle types, loading, amine monomer and chloride monomer concentrations. The support membranes include PAN, PI, PSF, and PMIA. Commonly used nanoparticles for TFN-OSN membrane fabrication are GO graphene Gs. Other nanomaterials include silicon dioxide (SiO_2), Ti_3C_2Tx (the most explored MXenes), SNW-1, and polydopamine nanoparticles (PDNPs). The nanoparticle loadings range from 0 to 30 wt%. But most of loadings range from 0 to 1 wt%. Extremely high loading rate is observed for GQD nanoparticles. The amine monomers/polymers include PEI, MPD, piperzine (PIP), and PDMS, with concentrations ranging from 1 to 20 wt%. But most of concentrations range from 1 to 2 wt%. Extremely high concentration is observed for PDMS monomer. The chloride monomers are TMC, terephthaloyl chloride (TPC) and 1, 2, 4, 5 - benzene tetracarboxylic acyl chloride (BTAC), with concentrations ranging from 0.1 to 2 wt%.

There are 11 different kinds of solutes in this study, including AO, MO, CV, SY, RDB, BTB, Methyl blue (MB), RB, PEG, oligomer and tetracycline with molecular weight ranging from 200 to 2000 Da. The solute concentrations range from 6.54 to 500 mg/L. The solute concentration can influence membrane performance because of the osmotic pressure and concentration polarization effects (Luo & Wan, 2011). 10 different types of organic solvents are summarised in this study, including ethanol (EtOH), ethyl acetate (EA), heptane (HEP), acetone (AC), IPA, toluene (TL), methanol (MEOH), methyl ethyl ketone (MEK), hexane (HEX), and THF. The most frequently used organic solvent is IPA, followed by MEOH, EtOH, HEP, AC, TL, THF, EA, MEK and HEX.

Optimally, porous nanoparticles can provide fast pathways for solvents going through the channels, thus, the TFN-OSN membranes with the incorporation of nanoparticles into active layers should have enhanced membrane permeability with the RP values higher than 1 (Zarrabi et al., 2016). Higher RP means greater permeability. In the meantime, the TFN-OSN membranes are desired to have the improved rejection performance with the RS values higher than 1 (Lai et al., 2016). Higher RS means

greater selectivity. **Fig. 6.3 (a)** and **(c)** illustrate the RP and RS performances as a function of nanoparticle loadings. It can be seen that the incorporation of nanoparticles can increase RP by up to 9 times, mostly around 1 to 2 times. For the RS, TFN-OSN membranes exhibit improved performances by up to 1.7 times, mostly around 1 to 1.2 times. In addition, no clear trend is observed between membrane OSN performances and nanoparticle loading parameter. It is mainly due to the effect other parameters needed to be considered such as the amine and chloride concentrations and the complex OSN process. **Fig. 6.3 (b)** and **(d)** presented the RP and RS performances as a function of nanoparticle size. At the larger nanoparticle size (>100 nm), larger variances are observed for both RP and RS. Because the larger nanoparticle size may cause intensive interruption inside the polyamide network and lead to more porous structures of the active layer, leading to an increase in the membrane permeability and decreased selectivity. In order to systemically analysis the effect of each parameter on the membrane performances (RP and RS), in the next section, all the parameters are used as independent inputs for different ML model formations. RP and RS performances as a function of other parameters such as amine concentration, chloride concentration, solvent properties, and solute properties can be found in **Fig. 6.4** and **Fig. 6.5**.
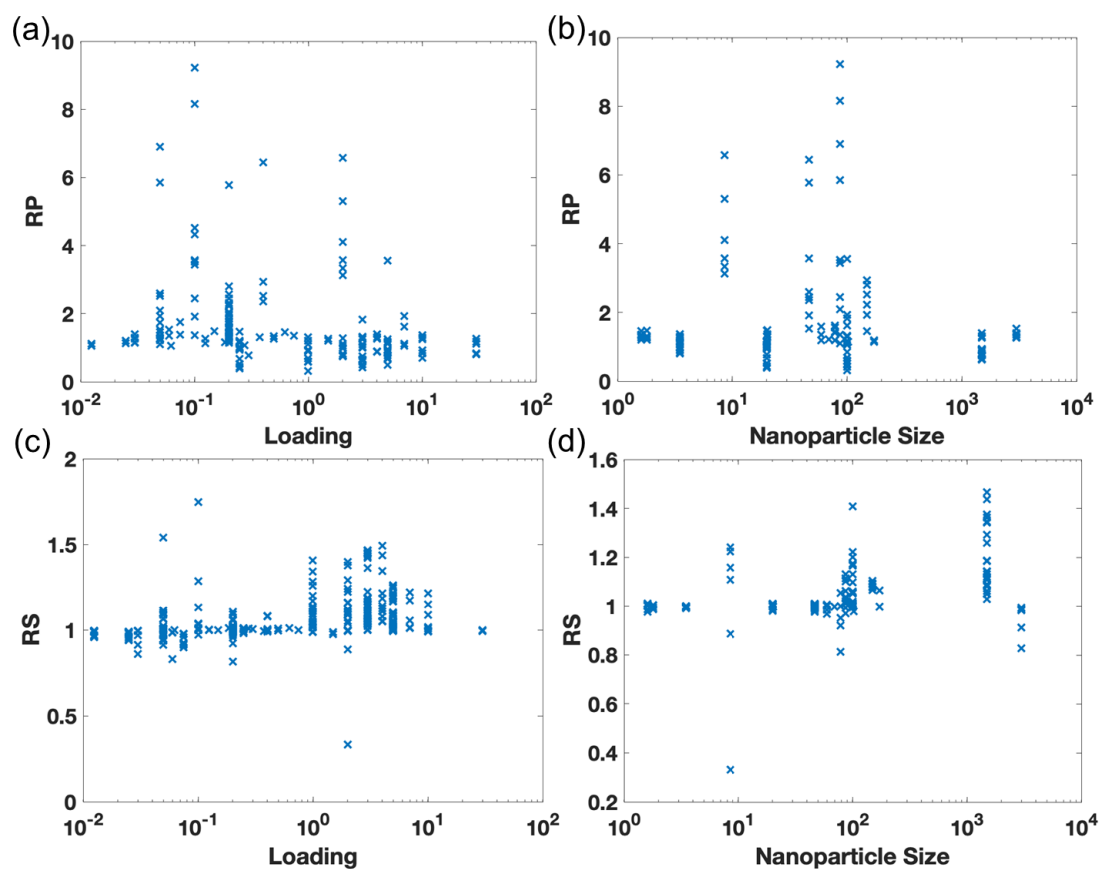
Figure 6.3. RP performance as a function of (a) nanoparticle loading and (b) nanoparticle size, RS performance as a function of (c) nanoparticle loading and (d) nanoparticle size.
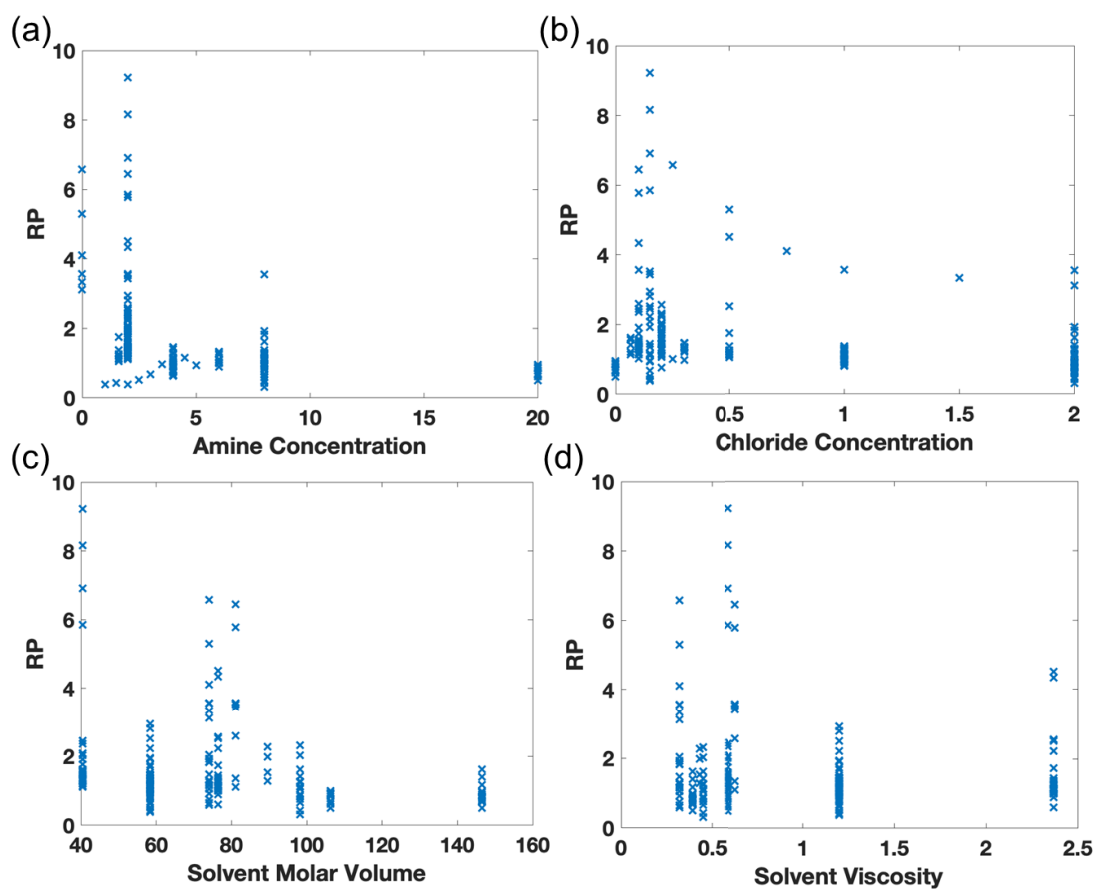
Figure 6.4. RP performance as a function of (a) amine concentration, (b) chloride concentration, (c) solvent molar volume, and (d) solvent viscosity.
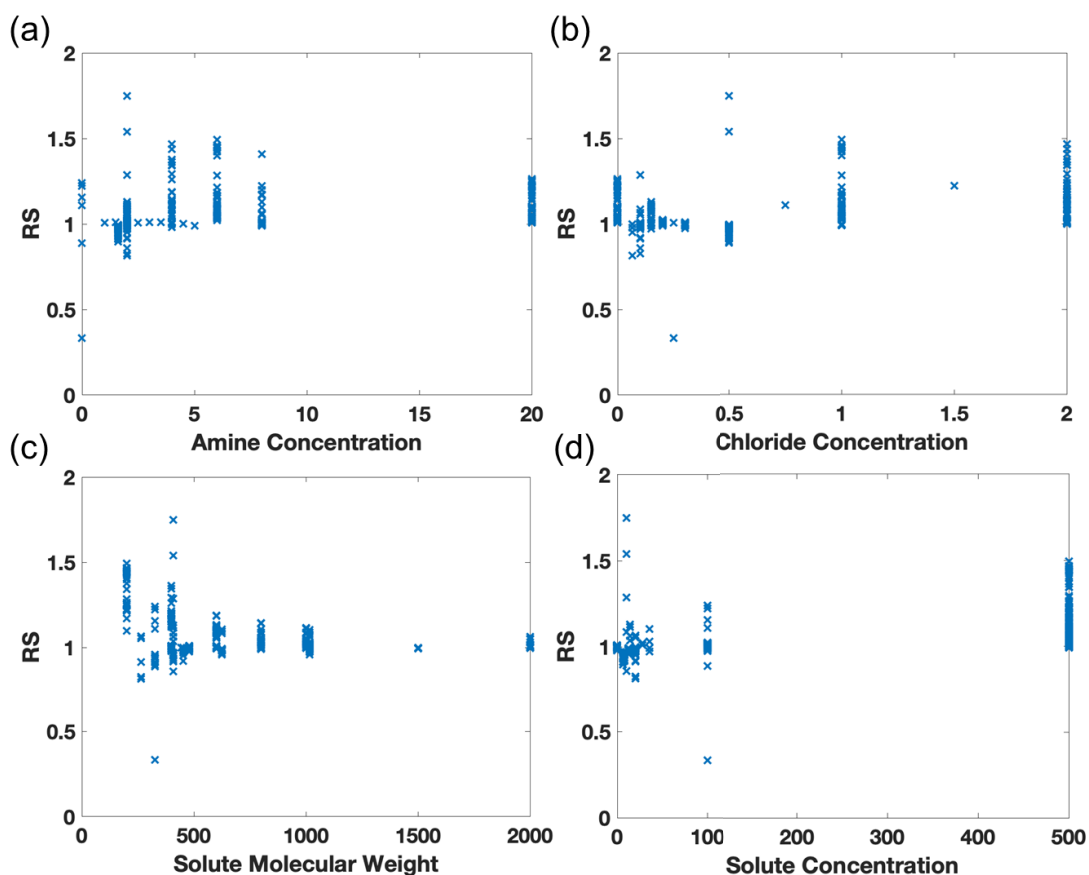
Figure 6.5. RS performance as a function of (a) amine concentration, (b) chloride concentration, (c) solute molecular weight, and (d) solute concentration.

6.3.2 Comparison and evaluation of different ML models

Four different kinds of ML models including linear model, SVM model, BT model and ANN model, were trained separately to predict the TFN-OSN performances in terms of RP and RS. The inputs used for training the models were substrate type, nanoparticle type, nanoparticle size, nanoparticle loading, amine monomer type, amine concentration, chloride monomer type, chloride concentration, water contact angle, surface roughness, organic solvent type, solvent properties (molecular weight, viscosity, density and molar volume), solute type, solute concentration, solute charge and solute molecular weight. The predicted outputs (RP and RS) of the training dataset based on linear, SVM, BT, and ANN methods can be found in **Fig. 6.6** and **Fig. 6.7**, respectively. The predicted outputs (RP and RS) of the test dataset using above four methods can be found in **Fig. 6.8** and **Fig. 6.9**, respectively.
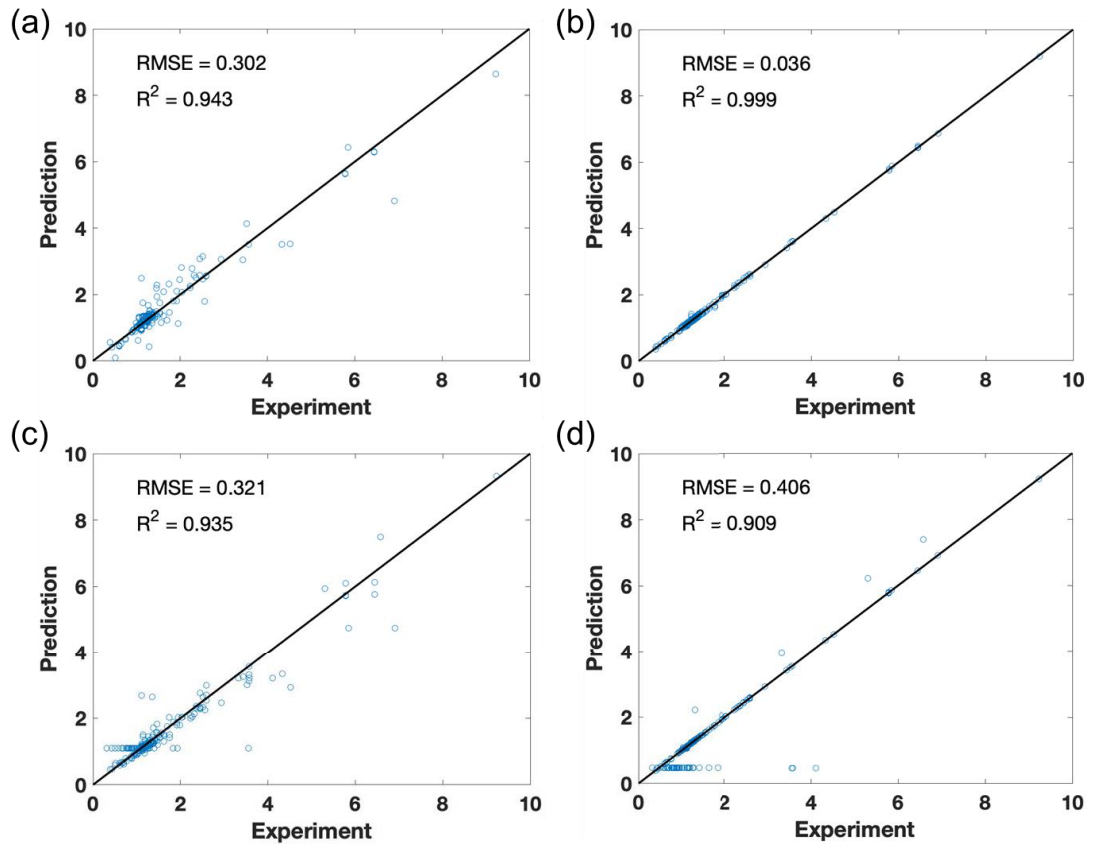
Figure 6.6. Prediction models of training dataset for RP, (a) linear model, (b) SVM model, (c) BT model, and (d) ANN model.
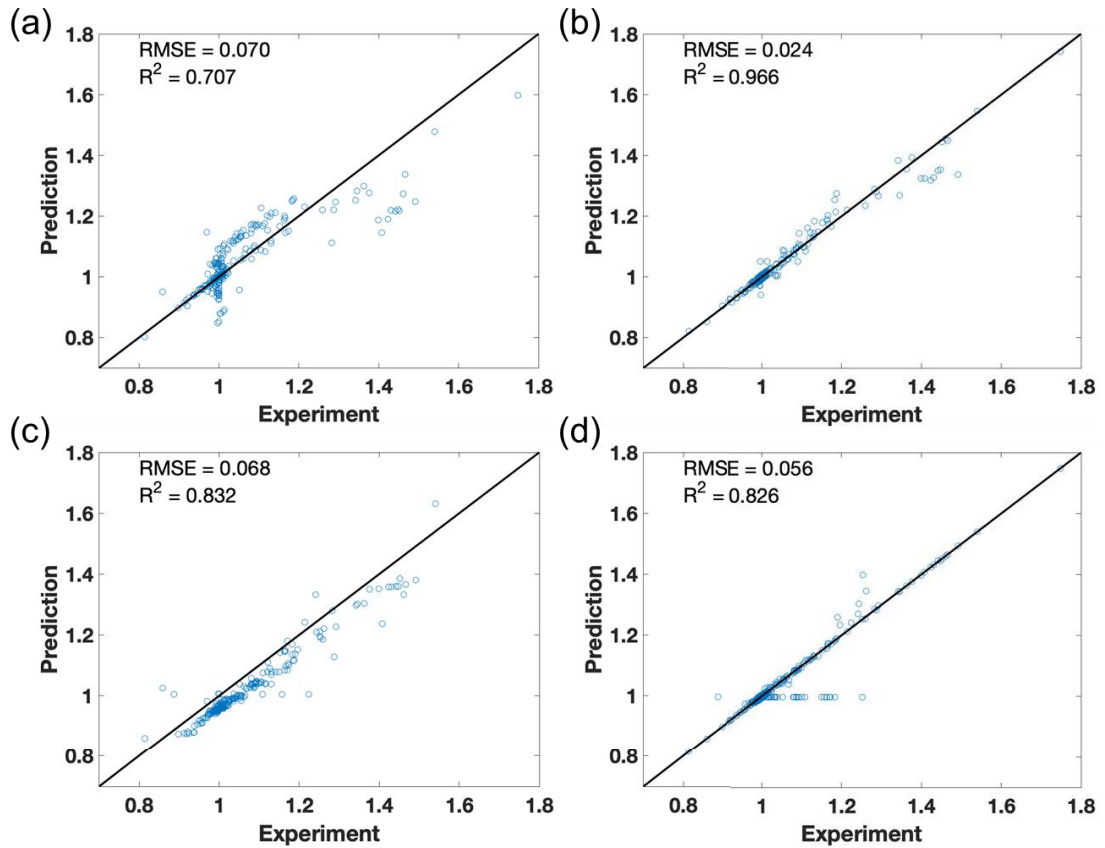
Figure 6.7. Prediction models of training dataset for RS, (a) linear model, (b) SVM model, (c) BT model, and (d) ANN model.

The prediction accuracy of a model is normally evaluated by both RMSE and coefficient of determination (R^2). As shown in **Fig. 6.8**, for RP performance prediction, the linear model showed the RMSE and R^2 values of 0.492 and 0.783, respectively. The RMSE and R^2 values of SVM models were 0.451 and 0.835, respectively. For BT model, the RMSE and R^2 were 0.295 and 0.918, respectively. The ANN model exhibited RMSE and R^2 values of 0.493 and 0.802, respectively. It can be seen that among the four different models, the BT model revealed the best prediction accuracy with the highest R^2 and the lowest RMSE values. The high R^2 (0.918) of the BT model indicated consistent prediction of RP performance of the TFN-OSN membranes. The linear model exhibited the worst prediction results since the relationship between the inputs and outputs is not linear. ANN is commonly used because of its good prediction potential. However, good prediction performance is based on large amounts of datasets (Jawad, Hawari, & Javaid Zaidi, 2021). In this work, because of the limited studies about TFN-OSN membranes, the amount of the collected data is not sufficient. Thus, the prediction accuracy of ANN model in this study is not desirable. For BT and SVM

methods, model formations are not highly dependent on the amount of collected data, and explains why BT and SVM models exhibited higher prediction accuracy than the ANN model (Han & Chung, 2016). Therefore, both BT and SVM models are preferable for small amounts of data prediction. Compared to SVM, the BT method showed better prediction performance because most models in practice contains nonlinearity. However, the decision boundary of SVM is normally a surface or a hyperplane on high dimensions. Thus, the SVM is suitable for handling the problems that are close to linearly separable condition (Heikamp & Bajorath, 2014). For the BT method, as a decision tree, it contains more than two trees. In addition, it is a non-linear mapping of the predicted performances and input features. That are the reasons why the BT method has better performance than SVM (De'ath, 2007).

The prediction accuracy results for RS predictions were shown in **Fig. 6.9**. It is clear that BT model is still the best prediction model among these four ML models. In detail, the linear model showed the RMSE and R^2 values of 0.078 and 0.489, respectively. The RMSE and R^2 values of SVM models were 0.075 and 0.711, respectively. For BT model, the RMSE and R^2 were 0.053 and 0.849, respectively. The ANN model exhibited RMSE and R^2 values of 0.052 and 0.789, respectively. It should be noted that R^2 values for all the models for RS predictions are not as high as 90%. This is mainly due to the limited available data for TFN-OSN membrane performance, the complex OSN process, and different experimental uncertainties and conditions. However, it is still a reasonable prediction compared to other studies (K et al., 2021; Yeo et al., 2020).
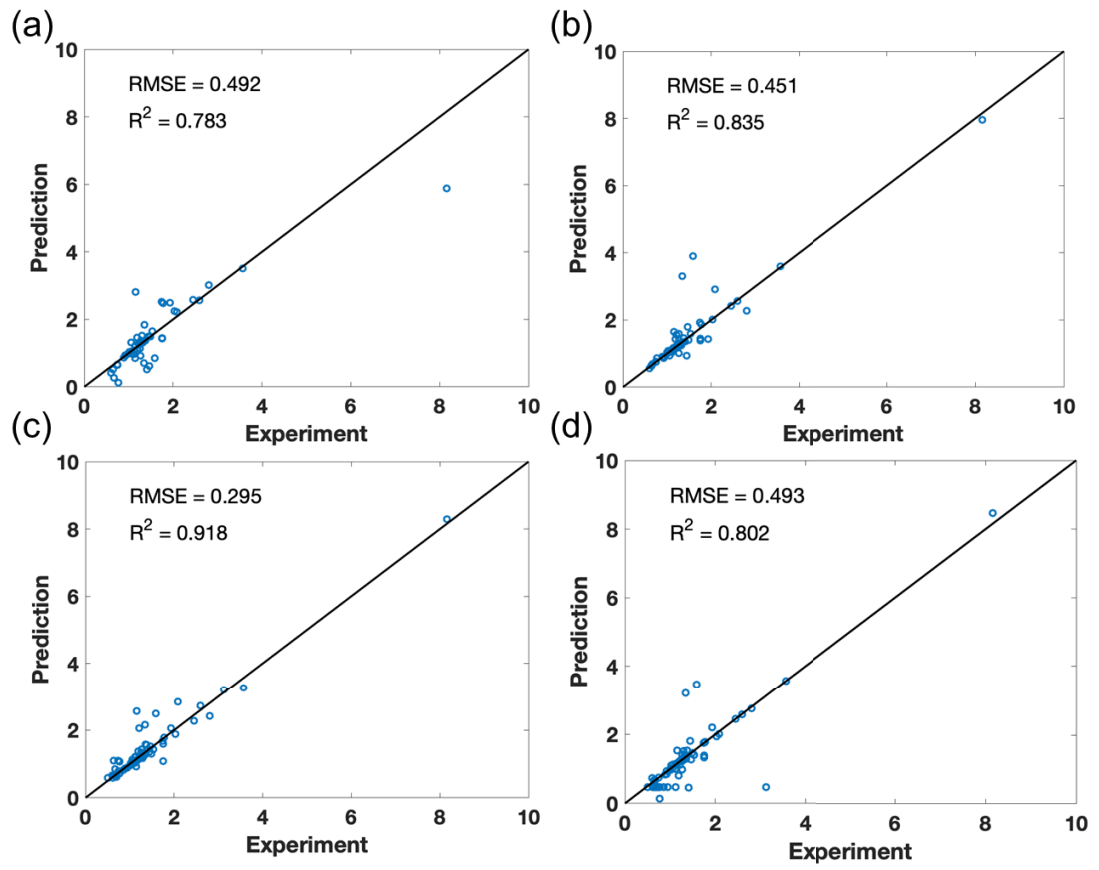
Figure 6.8. Prediction models for RP, (a) linear model, (b) SVM model, (c) BT model, and (d) ANN model.
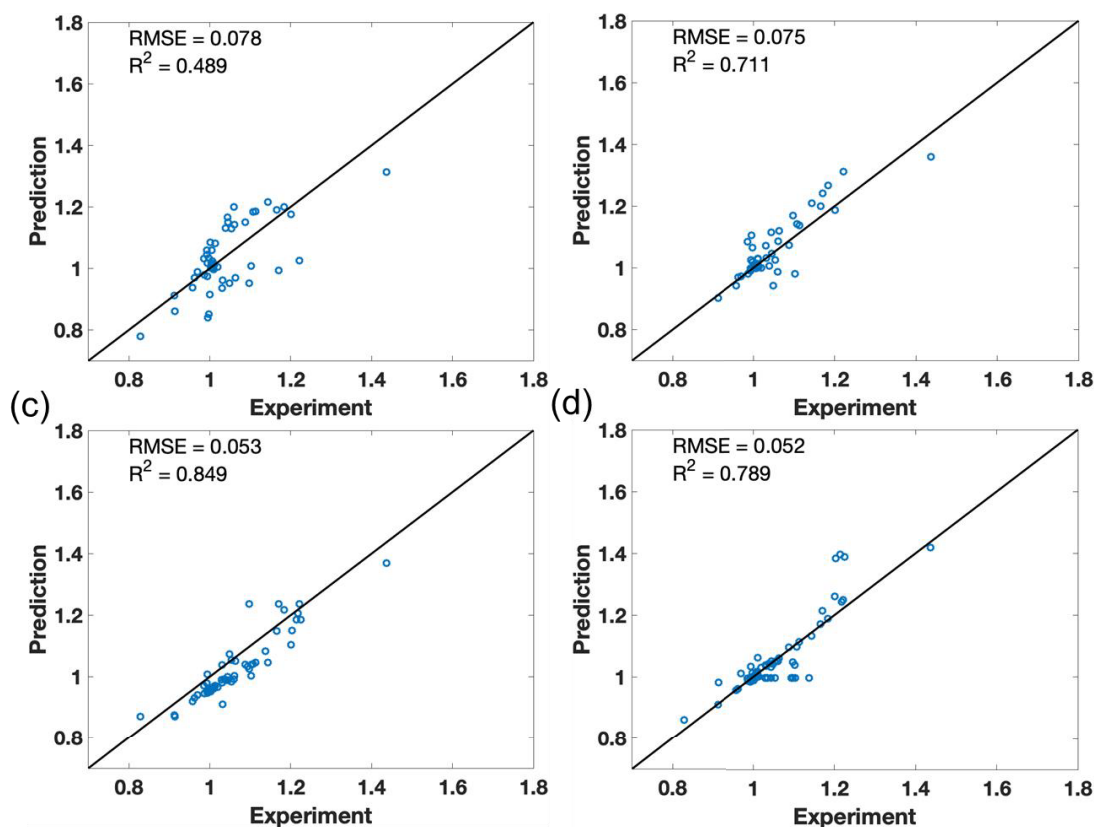
Figure 6.9. Prediction models for RS, (a) linear model, (b) SVM model, (c) BT model, and (d) ANN model.

6.3.3 Parameter Contribution Analysis

In order to have a clear view about the effect of each parameter on the membrane performances (RP and RS), the contributions of each parameter on the RP and RS performances are illustrated in **Fig.6.10**.
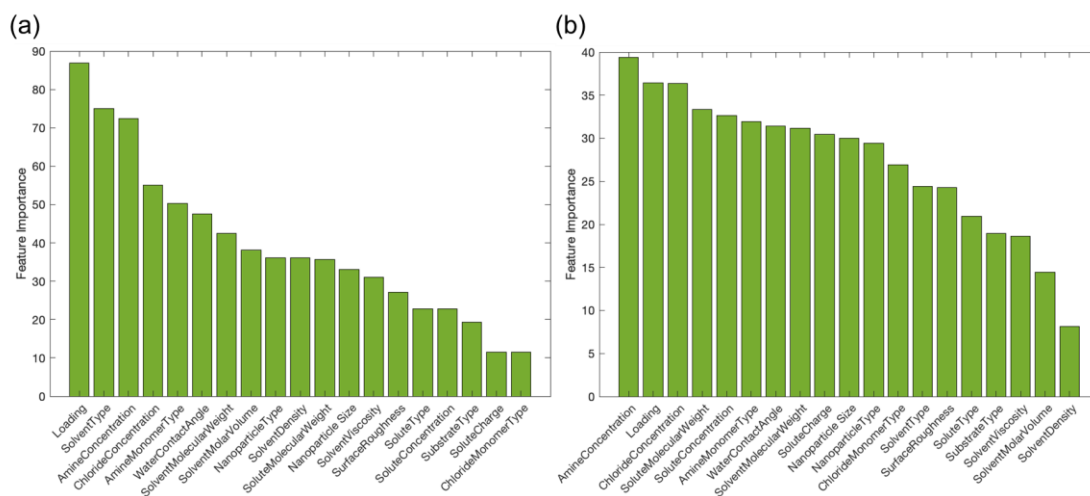
Figure 6.10. Parameter importance contributions for (a) RP and (b) RS.

It can be seen from **Fig. 6.10** that the nanoparticle loading is a key parameter for both RP and RS for TFN-OSN membranes. Therefore, the choice of the proper nanomaterial and nanomaterial loading can control the membrane performances and breakdown the trade-off between membrane permeability and selectivity. The amine and chloride concentrations also have a great influence on both the membrane RP and RS performances. It means that the IP process is important for TFN-OSN membrane fabrications because of the formation of the active layer via the IP process which will determine the membrane final performances (Seah et al., 2020). The IP process is normally a very sensitive process and the reaction between amine monomer and chloride monomer is very fast (R. Zhang, Yu, Shi, Zhu, & Van der Bruggen, 2019). Therefore, for TFN-OSN membrane preparation, the control of the amine and chloride monomer concentrations during the IP process need to be carefully considered.

In addition, as shown in **Fig. 6.10 (a)**, water contact angle also plays an important role for membrane RP performance, whereby a higher water contact angle means greater hydrophobicity. On the contrary, lower water contact angle implies a more hydrophilic membrane surface. In OSN process, the feed solvent properties also need to be considered when prepare a membrane with hydrophilic or hydrophobic surface properties. There are polar and non-polar solvents. For example, EtOH, MEOH, AC and IPA are polar solvents. HEP, HEX and TL are non-polar solvents. It is reported that the hydrophobic OSN membranes exhibited significantly higher permeability for non-polar solvents (Buonomenna & Bae, 2014; H. Guo et al., 2016). Moreover, solvent viscosity (μ) and solvent molar volume (V_m) can also affect the permeances of solvents. Some studies reported that the V_m/μ value is an important parameter influencing the solvent permeability. They concluded that the higher V_m/μ value may be the reason leading to the better the permeance (Bhanushali et al., 2001; C. Wang, Park, Seo, et al., 2022). Different organic solvents typically have different viscosities and molar volumes leading to different V_m/μ values. The summary of the solvent's properties including viscosity, molar volume, V_m/μ values is shown in **Table 6.2**. For membrane RS performance, as shown in **Fig. 6.10 (b)**, the solute molecular weight also plays an important role. Normally, the membrane shows higher rejection for solutes with larger molecular weights. On the contrary, the rejection will decrease for the solute with a smaller molecular weight (C. Wang, Park, Seo, et al., 2022).

Other factors such as the support membrane type, nanomaterial type, and membrane surface roughness et al. play relatively minor roles on the RP and RS performances of the TFN-OSN membranes. For example, for support membrane type, the membrane separation performances are mainly determined by active layer properties. Thus, compared with the active layer, the support layer shows less significant influence (J. Wang et al., 2017). Compared to the nanoparticle loading which is critically important for IP process for the active layer formation, the nanomaterials with various types can be used with the optimization of the TFN membrane preparation to achieve the optimal membrane performances. As for the membrane surface roughness, the lower roughness is proved to have better anti-fouling properties. However, in our collected references, all the solute concentrations are less than 500 mg/L which will not have a significant effect on membrane fouling.

Table 6.2. Properties of various solvents listed in this manuscript.

Solvents	Viscosity (cP) 20ºC	Surface tension (mN m^{-1})	Molecular weight (g mol^{-1})	Density (g cm^{-3})	Polarity
MEOH	0.59	22.50	32.04	0.792	polar
EtOH	1.20	22.39	46.07	0.789	polar
AC	0.32	25.20	58.08	0.784	polar
IPA	2.37	23.00	60.10	0.786	polar
HEX	0.31	18.43	86.18	0.655	non-polar
HEP	0.39	20.21	100.2	0.684	non-polar
TL	0.59	28.52	92.14	0.867	non-polar
THF	0.63	26.40	72.11	0.889	polar
MEK	0.43	24.60	72.11	0.805	polar
EA	0.45	23.75	88.10	0.897	polar

6.3.4 Partial Dependence Analysis

In order to further investigate the effect of different parameters on the membrane performance prediction, partial dependence (PD) analysis was conducted using the optimal BT model. The partial dependence can average values of all data to evaluate the impact trends of one or two parameters on the membrane RP and RS performances. The results are shown in **Fig. 6.11** and **Fig. 6.12**.
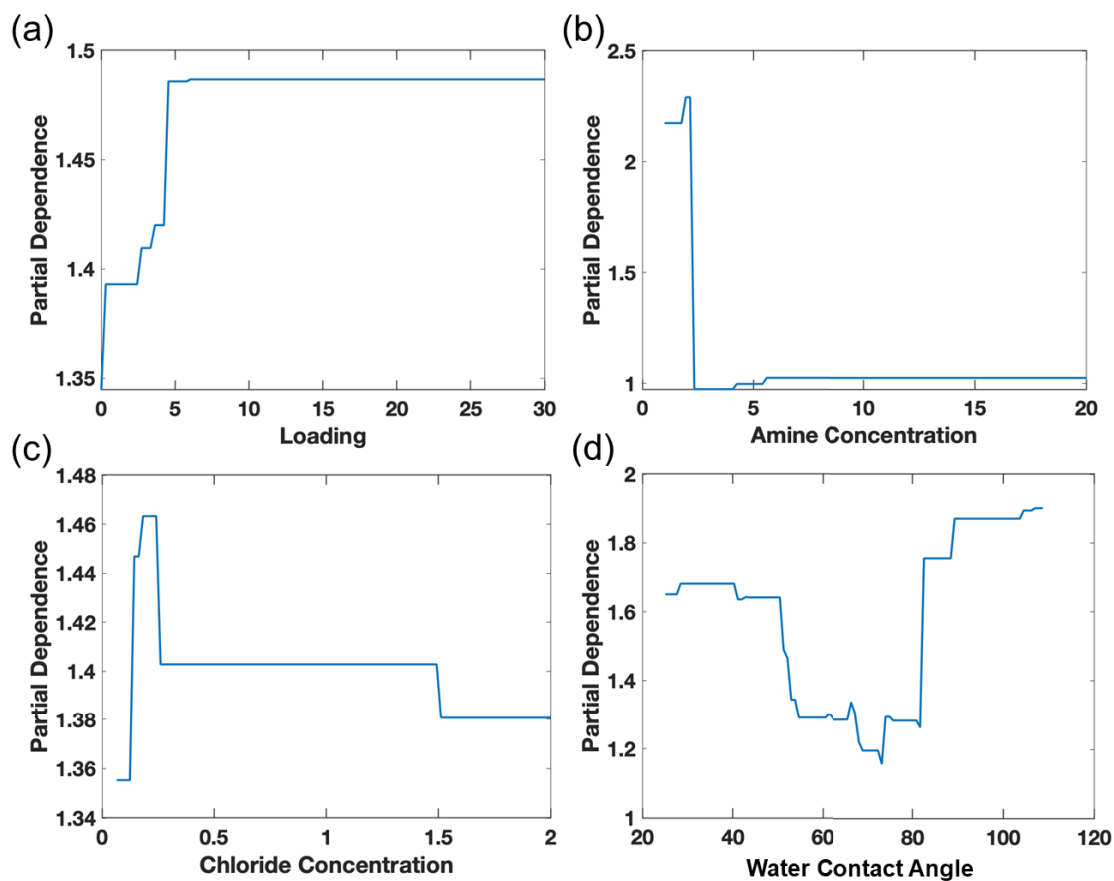
Figure 6.11. Partial dependence plots for (a) loading, (b) amine concentration, (c) chloride concentration, and (d) water contact angle on the RP performance.
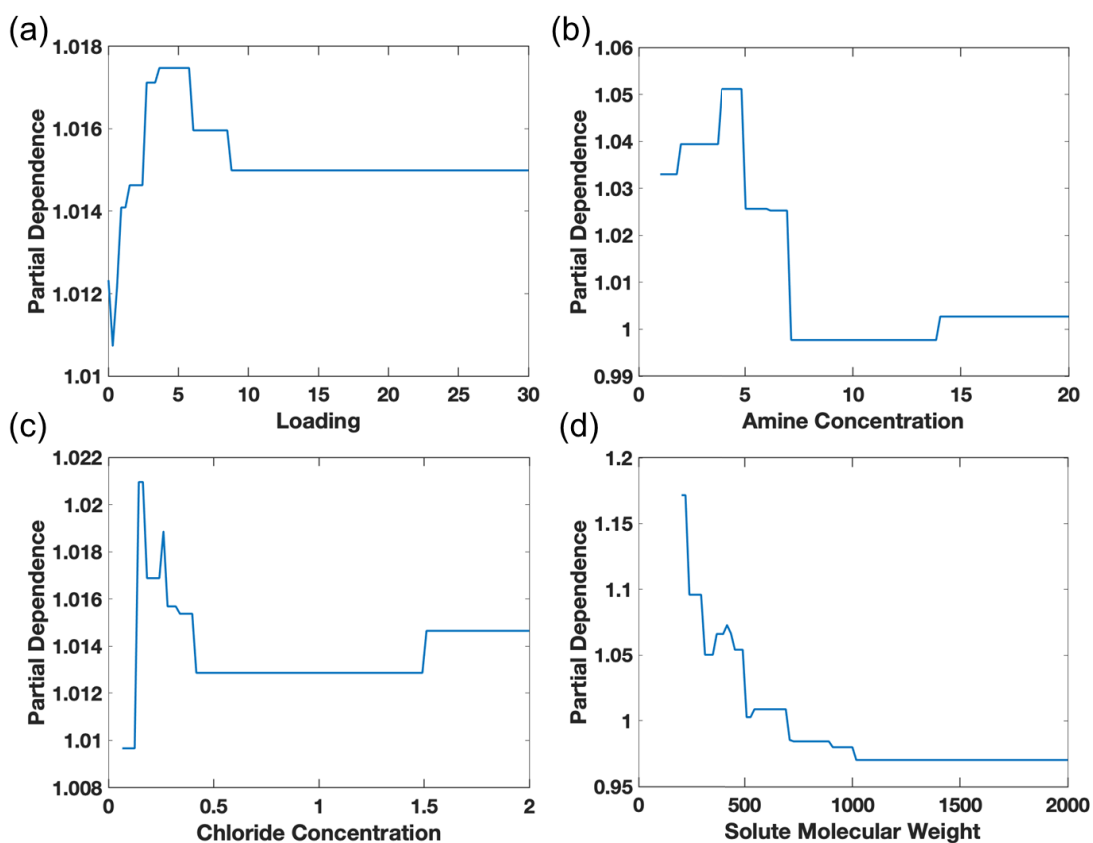
Figure 6.12. Partial dependence plots for (a) loading, (b) amine concentration, (c) chloride concentration, and (d) solute molecular weight on the RS performance.

Fig. 6.11 (a) and **Fig. 6.12 (a)** illustrated nanoparticle loading PD plots on RP and RS performances with the loading data distribution. It is clearly shown that when the nanoparticle loading is less than 5 wt%, increasing the nanoparticle loading can raise both RP and RS performances of OSN membranes. It implies that careful control of nanoparticle loading can achieve good permeability while preserving good selectivity performance. The incorporation of nanoparticles into active layer during IP process can create voids between polymers and nanoparticles, thus, improving the porosity of the polymer system leading to the improved solvents permeation (Lau et al., 2015). In addition, the porous structures of nanoparticles can also provide faster pathways for solvents to travel through. When the nanoparticle loading was higher than 5 wt%, the membrane RP performance remains stable, while membrane RS performance decreases. It is mainly due to the tendency of nanoparticle agglomeration at high nanoparticle concentration, which will weak the positive effects of nanoparticle incorporation resulting in stable or decreased membrane performances (D. L. Zhao et al., 2020).

Fig. 6.11 (b) and **Fig. 6.12 (b)** showed the PD plots with amine concentration distribution on RP and RS, respectively. For RP in **Fig. 6.11 (b)**, the optimal amine concentration is below around 2 wt%. When the amine concentration is higher than 2 wt%, the RP performance decreases. For RS in **Fig. 6.12 (b)**, the optimal amine concentration is below around 5 wt%. The RS performance decreases if the amine concentration is higher than 5 wt%. **Fig. 6.11 (c)** and **Fig. 6.12 (c)** showed the PD plots with chloride concentration distribution on RP and PS, respectively. For RP in **Fig. 6.11 (c)**, the optimal chloride concentration is ranging from 0.15 wt% to 0. 2 wt%. When the chloride concentration is higher than this range, the RS performance decreases. For RS in **Fig. 6.12 (c)**, the optimal chloride concentration is below around 0.15 wt%. The RS performance decreases if the chloride concentration is higher than 0.15 wt%. In short, the amine monomer with a concentration of around 2 wt% and the chloride monomer with a concentration of around 0.15 wt%, would deliver the most optimal conditions to enhance both the permeability and selectivity of TFN-OSN membranes.

Fig. 6.11 (d) illustrated the PD plots with the water contact angle distribution. As we illustrated before, the effect of the water contact angle should be classified by different feed solvent types. For lower contact angle with a hydrophilic surface property, membranes show higher permeability for polar solvents. For higher contact angle with a hydrophobic surface property, membranes exhibit higher permeability for non-polar solvents (H. Guo et al., 2016). In **Fig. 6.11 (d)**, the partial dependence of the water contact angle maintains relatively stable at the range of around 25° to around 50°, and decreases from 50° to 70°. Then, the partial dependence of water contact angle increases from around 70° to 90° and finally stabilised between 90° to 110°. This means that membranes with super-hydrophilic or super-hydrophobic surface property exhibits better RP performance based on different feed solvent types. **Fig. 6.12 (d)** illustrated the PD plots with the solute molecular weight distribution. It can be seen that with the increase of the solute molecular weight, the effect of the partial dependence on RS decreases. In these cases, the RS is a relative value which is compared to the baseline control TFC-OSN membrane without nanoparticle incorporation. Typically, the membrane shows greater rejection to solute with higher molecular weight (Amirilargani et al., 2016). For example, most of the TFC-OSN membranes can exhibit much higher rejection performances for the solute with

molecular weights greater than 1000 Da. Thus, for the TFN-OSN membranes with nanoparticle incorporation, the increase of rejection performances for the solute with molecular weight higher than 1000 Da are not obvious leading to the lower RS values. On the contrary, because of the low rejection performances of the control TFC-OSN membranes for solute with lower molecular weight, the increase of the rejection performance is more obvious with increased RS values.

6.4. Conclusion

In this work, we have collected 9252 data points from 20 references about TFN-OSN membranes and utilized machine learning to form four different models: linear, SVM, BT and ANN for predicting membrane permeability and selectivity. Among four established models, BT models exhibited optimal prediction accuracy in terms of RMSE and R^2 values for membrane RP and RS performance prediction, followed by SNM, ANN and linear models. 19 parameters namely: substrate type, nanomaterial type, nanomaterial size, nanomaterial loading, amine monomer, amine monomer concentration, chloride monomer, chloride monomer concentration, solvent type, molecular weight, viscosity, density, molar volume, solute type, molecular weight, concentration, and charge property were inputs that were collected - variables which could influence membrane RP and RS performance - were tested across four predictive models in this parametric contribution analysis. Results showed that for TFN-OSN membrane RP performance, nanoparticle loading, amine concentration, chloride concentration, water contact angle, solvent viscosity, and molar volume are the main parameters influencing RP performance. For TFN-OSN membrane RS performance, nanoparticle loading, amine concentration, chloride concentration, and solute molecular weight play important roles in this ML-driven, membrane performance prediction study.

BT model was then further used for partial dependence analysis to investigate parameters independently to find out what conditions improved for TFN-OSN membrane performance. When the nanoparticle loading is less than 5 wt%, increasing the nanoparticle loading can raise both RP and RS performances of OSN membranes. When the nanoparticle loading was higher than 5 wt%, the membrane RP performance remains stable, while the membrane RS performance declines. The amine monomer with a concentration of around 2 wt% and the chloride monomer with a concentration of around 0.15 wt% are the most optimal conditions to enhance both the permeability

and selectivity of TFN-OSN membranes. The water contact angle values of 25o to around 50o and between 90o to 110o showed higher RP values, indicating membranes with super-hydrophilic or super-hydrophobic surface properties exhibit higher RP performances based on different feed solvent types. Overall, our work paves new ways for both TFN-OSN membrane performance prediction and opportunities for designing and developing high-performance membranes.

CHAPTER 7

Conclusions and Recommendations

7.1 Conclusions

OSN has been considered as an effective and green process for organic solvent purification and separation. However, there are still some challenges faced by OSN membranes, such as poor solvent stability and relatively low organic solvent permeance. Therefore, this research has focused on developing high performance nanocomposite membranes with enhanced separation performances and membrane stability for OSN applications. Organic solvent resistant PK membrane was prepared and used as substrate to improve OSN membrane stability. Novel inkjet printing technique was introduced as an alternative method for preparing LBL OSN membrane with thin active layer and good separation performance. Finally, ML based models were developed and compared for TFN-OSN membrane performance prediction, which could provide some valuable information for OSN membrane further development. Conclusions for each chapters are summarized below and recommendations are provided for future studies.

Chapter 4 investigated the inkjet printing technique as an efficient way to fabricate LBL-PEM for OSN application. PEI and PSS were used as polycation and polyanion, respectively. SWCNT was incorporated into membranes to enhance the membrane physical and chemical stability. The PK membrane served as a substrate for OSN because of its organic solvent resistance property in nature. The effects of numbers of bilayer, polyelectrolyte concentration, and the cross-linking condition on the membrane OSN performances were evaluated. The best OSN performance was achieved with 10 bilayers of polyelectrolytes printing, noted as $(PEI/PSS-CNT)_{10}$. The $(PEI/PSS-CNT)_{10}$ membrane exhibited ethanol, methanol, IPA and acetone permeances of 2.52, 4.21, 1.21 and 4.75 L m^{-2} h^{-1} bar^{-1}, respectively, along with good dye rejection rate (RB rejection > 98%). Moreover, the inkjet printed OSN membrane was found to be stable after soaking in different organic solvents for two weeks. The membrane weights and the performances exhibited negligible changes. The 12 hours continuous filtration tests also confirmed the membrane stability property. Our work broadened the use of inkjet printing technology for LBL membrane fabrication and validated the technology as a promising method for producing multilayer OSN membranes, which may open a new avenue for OSN membrane preparations.

Chapter 5 further improved the OSN membrane separation performance and evaluated the effect of different cross-linkers for OSN membrane preparation. PEI and SWCNT

were used as polycation and polyanion, respectively, and printed on a PK membrane surface, followed by post-treatment using three different cross-linking agents: GA, ECH and TMC. The effects of PEI and SWCNT concentrations, bilayer numbers, and cross-linking conditions in the formation of the selective layers were evaluated in terms of membrane OSN performances. PEI concentration of 10.0 g/L and SWCNT concentration of 1.0 g/L with eight cycles of printing bilayers were chosen as optimal conditions. GA cross-linking was found to give the best membrane performance, and thus GA was considered as the best cross-linking agent for inkjet-printed LBL membrane modification among the three kinds of cross-linkers. The (PEI/SWCNT)$_8$-GA exhibited RB rejection over 99% with high organic solvent permeances. Compared to the cross-linking time, cross-linking agent concentration was found to have a greater effect on the membrane modification in terms of rejection performance. Moreover, the inkjet-printed LBL membrane showed negligible changes in membrane weight and OSN performance after immersion in different organic solvents over a period of three weeks, indicating its high mechanical and chemical stability. Finally, the possible applications of our printed LBL membranes in the pharmaceutical and hemp industries were evaluated.

In Chapter 6, ML was used to form prediction models for TFN OSN membrane performance evaluation in terms of RP and RS. Twenty references including 9252 data points were collected to form four different models: linear, SVM, BT, and ANN. Among the four models, BT exhibited optimal prediction accuracy in terms of RMSE and coefficient of determination (R^2) values for membrane RP (RMSE: 0.295, R^2: 0.918) and RS (RMSE: 0.053, R^2: 0.849) performance prediction. Parameter contribution analysis indicated that nanoparticle loading, amine concentration, chloride concentration, water contact angle, solvent viscosity, and molar volume are the main parameters influencing RP performance. For RS performance, nanoparticle loading, amine concentration, chloride concentration, and solute molecular weight play important roles. Partial dependence analysis indicated that the optimal conditions for TFN-OSN membrane fabrication are nanoparticle loading less than 5 wt%, the amine concentration around 2 wt%, and the chloride concentration around 0.15 wt%. In addition, membrane with super-hydrophilic or super-hydrophobic surface property exhibited higher RP performance based on different feed solvent types. Overall, this

work introduced new ways both for TFN OSN membrane performance prediction and for higher performance membrane design and development.

7.2 Recommendations

Solvent resistant PK support was successfully fabricated and provided the OSN membrane with good solvent stability. The inkjet printing assisted LBL assembly was used as an alternative method for nanocomposite OSN membrane fabrication. The inkjet printed LBL-OSN membranes showed good separation performances and solvent stability. ML based models were developed for TFN OSN membrane performance prediction and also provided valuable information for OSN membrane further development. Based on the results obtained from these studies, the following recommendations are provided for future scientific research and membrane commercialization.

• As mentioned in Chapter 6, most previous studies only focused on using different approaches to improve OSN membrane performances. But few studies discussed the specific applications for their fabricated OSN membranes. In our study, we discussed the possible applications of our printed LBL membranes in the pharmaceutical and hemp industries. But further experiments should be carried out to test the membrane separation performances of real solute products from pharmaceutical and hemp industries to accelerate the commercialization of OSN.

• In our research, SWCNT were used as nanomaterials for OSN membrane fabrication and to improve membrane separation performance and solvent stability. Except for SWCNT, other functional nanomaterials can be further explored for nanocomposite OSN membrane fabrication.

• The ML based models in this study were used for TFN-OSN membrane performance prediction. Some optimal membrane fabrication conditions were proposed. Thus, further studies can be conducted based on these optimal conditions for high performance TFN OSN membrane fabrication.

REFERENCES

Aba, N. F. D., Chong, J. Y., Wang, B., Mattevi, C., & Li, K. (2015). Graphene oxide membranes on ceramic hollow fibers – Microstructural stability and nanofiltration performance. *Journal of Membrane Science, 484*, 87-94.

Abadikhah, H., Kalali, E. N., Behzadi, S., Khan, S. A., Xu, X., & Agathopoulos, S. (2018). Amino functionalized silica nanoparticles incorporated thin film nanocomposite membrane with suppressed aggregation and high desalination performance. *Ploymer, 154*, 200-209.

Abadikhah, H., Kalali, E. N., Behzadi, S., Khan, S. A., Xu, X., Shabestari, M. E., & Agathopoulos, S. (2019). High flux thin film nanocomposite membrane incorporated with functionalized TiO2@reduced graphene oxide nanohybrids for organic solvent nanofiltration. *Chemical Engineering Science, 204*, 99-109.

Abejón, R., Garea, A., & Irabien, A. (2014). Analysis and optimization of continuous organic solvent nanofiltration by membrane cascade for pharmaceutical separation. *AIChE Journal, 60*(3), 931-948.

Abraham, J., Vasu, K. S., Williams, C. D., Gopinadhan, K., Su, Y., Cherian, C. T., Grigorieva, I. V. (2017). Tunable sieving of ions using graphene oxide membranes. *Nature Nanotechnology, 12*(6), 546.

Aerts, S., Vanhulsel, A., Buekenhoudt, A., Weyten, H., Kuypers, S., Chen, H., Jacobs, P. (2006). Plasma-treated PDMS-membranes in solvent resistant nanofiltration: Characterization and study of transport mechanism. *Journal of Membrane Science, 275*(1-2), 212-219.

Ahmad, N. A., Goh, P. S., Wong, K. C., Mamah, S. C., Ismail, A. F., & Zulhairun, A. K. (2022). Accelerated spraying-assisted layer by layer assembly of polyethyleneimine/titania nanosheet on thin film composite membrane for reverse osmosis desalination. *Desalination, 529*, 115645.

Ahmad, N. A., Goh, P. S., Wong, K. C., Zulhairun, A. K., & Ismail, A. F. (2020). Enhancing desalination performance of thin film composite membrane through layer by layer assembly of oppositely charged titania nanosheet. *Desalination, 476*, 114167.

Ahmadiannamini, P., Li, X., Goyens, W., Joseph, N., Meesschaert, B., & Vankelecom, I. F. J. (2012). Multilayered polyelectrolyte complex based solvent resistant nanofiltration membranes prepared from weak polyacids. *Journal of Membrane Science, 394-395*, 98-106.

Ahmadiannamini, P., Li, X., Goyens, W., Meesschaert, B., Vanderlinden, W., De Feyter, S., & Vankelecom, I. F. J. (2012). Influence of polyanion type and cationic counter ion on the SRNF performance of polyelectrolyte membranes. *Journal of Membrane Science, 403-404*, 216-226. doi:10.1016/j.memsci.2012.02.052

Ali, S., Shah, I. A., Ihsanullah, I., & Feng, X. (2022). Nanocomposite membranes for organic solvent nanofiltration: Recent advances, challenges, and prospects. *Chemosphere*, 136329.

Amirilargani, M., Sadrzadeh, M., Sudhölter, E. J. R., & de Smet, L. C. P. M. (2016). Surface modification methods of organic solvent nanofiltration membranes. *Chemical Engineering Journal, 289*, 562-582.

Bhanushali, D., Kloos, S., Kurth, C., & Bhattacharyya, D. (2001). Performance of solvent-resistant membranes for non-aqueous systems: solvent permeation results and modeling. *Journal of Membrane Science, 189*(1), 1-21.

Bloemendal, V., van Hest, J. C. M., & Rutjes, F. (2020). Synthetic pathways to tetrahydrocannabinol (THC): an overview. *Org Biomol Chem, 18*(17), 3203-3215.

Buonomenna, M. G., & Bae, J. (2014). Organic Solvent Nanofiltration in Pharmaceutical Industry. *Separation & Purification Reviews, 44*(2), 157-182.

Butler, K. T., Davies, D. W., Cartwright, H., Isayev, O., & Walsh, A. (2018). Machine learning for molecular and materials science. *Nature, 559*(7715), 547-555.

Campbell, J., Burgal, J. D. S., Szekely, G., Davies, R. P., Braddock, D. C., & Livingston, A. (2016). Hybrid polymer/MOF membranes for Organic Solvent Nanofiltration (OSN): Chemical modification and the quest for perfection. *Journal of Membrane Science, 503*, 166-176.

Campbell, J., Székely, G., Davies, R. P., Braddock, D. C., & Livingston, A. G. (2014). Fabrication of hybrid polymer/metal organic framework membranes: mixed matrix membranes versus in situ growth. *J. Mater. Chem. A, 2*(24), 9260-9271.

Cervantes, J., Garcia-Lamont, F., Rodríguez-Mazahua, L., & Lopez, A. (2020). A comprehensive survey on support vector machine classification: Applications, challenges and trends. *Neurocomputing, 408*, 189-215.

Chandra, A., Bhuvanesh, E., Mandal, P., & Chattopadhyay, S. (2018). Surface modification of anion exchange membrane using layer-by-layer polyelectrolytes deposition facilitating monovalent organic acid transport. *Colloids Surfaces A: Physicochemical Engineering Aspects, 558*, 579-590.

Chandra, A., Bhuvanesh, E., Mandal, P., & Chattopadhyay, S. (2018). Surface modification of anion exchange membrane using layer-by-layer polyelectrolytes deposition facilitating monovalent organic acid transport. *Colloids and Surfaces A: Physicochemical and Engineering Aspects, 558*, 579-590.

Chen, C., Wang, J., Liu, D., Yang, C., Liu, Y., Ruoff, R. S., & Lei, W. (2018). Functionalized boron nitride membranes with ultrafast solvent transport performance for molecular separation. *Nat Commun, 9*(1), 1902. doi:10.1038/s41467-018-04294-6

Chen, H., Shan, W., Liao, H., He, Y., Zhang, T., Pei, P., Chen, J. (2021). Online voltage consistency prediction of proton exchange membrane fuel cells using a machine learning method. *International Journal of Hydrogen Energy, 46*(69), 34399-34412.

Chen, Q., Yu, P., Huang, W., Yu, S., Liu, M., & Gao, C. (2015). High-flux composite hollow fiber nanofiltration membranes fabricated through layer-by-layer

deposition of oppositely charged crosslinked polyelectrolytes for dye removal. *Journal of Membrane Science, 492*, 312-321.

Chen, X., Porto, C. L., Chen, Z., Merenda, A., Allioux, F. M., d'Agostino, R., Dumee, L. F. (2018). Single step synthesis of Janus nano-composite membranes by atmospheric aerosol plasma polymerization for solvents separation. *Sci Total Environ, 645*, 22-33.

Chen, Y., Toth, M., & He, C. (2019). Facile and fast fabrication of high structure-stable thin film nanocomposite membrane for potential application in solvent resistance nanofiltration. *Applied Surface Science, 496*.

Cheng, X., Ding, S., Guo, J., Zhang, C., Guo, Z., & Shao, L. (2017). In-situ interfacial formation of TiO 2 /polypyrrole selective layer for improving the separation efficiency towards molecular separation. *Journal of Membrane Science, 536*, 19-27.

Cheng, X., Jiang, X., Zhang, Y., Lau, C. H., Xie, Z., Ng, D., Shao, L. (2017). Building Additional Passageways in Polyamide Membranes with Hydrostable Metal Organic Frameworks To Recycle and Remove Organic Solutes from Various Solvents. *ACS Appl Mater Interfaces, 9*(44), 38877-38886.

Cheng, X. Q., Zhang, Y. L., Wang, Z. X., Guo, Z. H., Bai, Y. P., & Shao, L. (2014). Recent Advances in Polymeric Solvent-Resistant Nanofiltration Membranes. *Advances in Polymer Technology, 33*(S1), n/a-n/a.

Cho, J., Char, K., Hong, J. D., & Lee, K. B. (2001). Fabrication of highly ordered multilayer films using a spin self-assembly method. *Advanced Materials, 13*(14), 1076-1078.

Dai, J., Li, S., Liu, J., He, J., Li, J., Wang, L., & Lei, J. (2019). Fabrication and characterization of a defect-free mixed matrix membrane by facile mixing PPSU with ZIF-8 core–shell microspheres for solvent-resistant nanofiltration. *Journal of Membrane Science, 589*.

Darvishmanesh, S., Jansen, J. C., Tasselli, F., Tocci, E., Luis, P., Degrève, J., Van der Bruggen, B. (2011). Novel polyphenylsulfone membrane for potential use in solvent nanofiltration. *Journal of Membrane Science, 379*(1-2), 60-68.

Darvishmanesh, S., Tasselli, F., Jansen, J. C., Tocci, E., Bazzarelli, F., Bernardo, P., Van der Bruggen, B. (2011). Preparation of solvent stable polyphenylsulfone hollow fiber nanofiltration membranes. *Journal of Membrane Science, 384*(1-2), 89-96.

Davood Abadi Farahani, M. H., Hua, D., & Chung, T.-S. (2018). Cross-linked mixed matrix membranes (MMMs) consisting of amine-functionalized multi-walled carbon nanotubes and P84 polyimide for organic solvent nanofiltration (OSN) with enhanced flux. *Journal of Membrane Science, 548*, 319-331.

Davood Abadi Farahani, M. H., Hua, D., & Chung, T.-S. (2017). Cross-linked mixed matrix membranes consisting of carboxyl-functionalized multi-walled carbon nanotubes and P84 polyimide for organic solvent nanofiltration (OSN). *Separation and Purification Technology, 186*, 243-254.

Davood Abadi Farahani, M. H., Ma, D., & Nazemizadeh Ardakani, P. (2018). Nanocomposite membranes for organic solvent nanofiltration. *Separation & Purification Reviews*, 1-30.

De'ath, G. (2007). Boosted tree for ecological modeling and prediction. *Ecology, 88*(1), 243-251.

Diercks, C. S., & Yaghi, O. M. J. S. (2017). The atom, the molecule, and the covalent organic framework. *355*(6328).

Ding, R., Ding, Y., Zhang, H., Wang, R., Xu, Z., Liu, Y., Liu, J. (2021). Applying machine learning to boost the development of high-performance membrane electrode assembly for proton exchange membrane fuel cells. *Journal of Materials Chemistry A, 9*(11), 6841-6850.

Ding, R., Zhang, H., Li, Y., Wang, J., Shi, B., Mao, H., Liu, J. (2015). Graphene oxide-embedded nanocomposite membrane for solvent resistant nanofiltration with enhanced rejection ability. *Chemical Engineering Science, 138*, 227-238.

DuChanois, R. M., Epsztein, R., Trivedi, J. A., & Elimelech, M. (2019). Controlling pore structure of polyelectrolyte multilayer nanofiltration membranes by tuning polyelectrolyte-salt interactions. *Journal of Membrane Science, 581*, 413-420.

Dumitru, C., & Maria, V. (2013). Advantages and Disadvantages of Using Neural Networks for Predictions. *Ovidius University Annals, Series Economic Sciences, 13*(1).

Duong, P. H. H., Zuo, J., & Chung, T.-S. (2013). Highly crosslinked layer-by-layer polyelectrolyte FO membranes: Understanding effects of salt concentration and deposition time on FO performance. *Journal of Membrane Science, 427*, 411-421.

Echaide-Gorriz, C., Navarro, M., Tellez, C., & Coronas, J. (2017). Simultaneous use of MOFs MIL-101(Cr) and ZIF-11 in thin film nanocomposite membranes for organic solvent nanofiltration. *Dalton Trans, 46*(19), 6244-6252.

Echaide-Górriz, C., Sorribas, S., Téllez, C., & Coronas, J. (2016). MOF nanoparticles of MIL-68(Al), MIL-101(Cr) and ZIF-11 for thin film nanocomposite organic solvent nanofiltration membranes. *RSC Advances, 6*(93), 90417-90426.

Esfahani, M. R., Koutahzadeh, N., Esfahani, A. R., Firouzjaei, M. D., Anderson, B., & Peck, L. (2019). A novel gold nanocomposite membrane with enhanced permeation, rejection and self-cleaning ability. *Journal of Membrane Science, 573*, 309-319.

Fang, W., Shi, L., & Wang, R. (2013). Interfacially polymerized composite nanofiltration hollow fiber membranes for low-pressure water softening. *Journal of Membrane Science, 430*, 129-139.

Farahani, M. H. D. A., & Chung, T.-S. (2019). A novel crosslinking technique towards the fabrication of high-flux polybenzimidazole (PBI) membranes for organic solvent nanofiltration (OSN). *Separation and Purification Technology, 209*, 182-192.

Fei, F., Cseri, L., Szekely, G., & Blanford, C. F. (2018). Robust Covalently Cross-linked Polybenzimidazole/Graphene Oxide Membranes for High-Flux Organic Solvent Nanofiltration. *ACS Appl Mater Interfaces, 10*(18), 16140-16147.

Feng, C., Xu, J., Li, M., Tang, Y., & Gao, C. (2014). Studies on a novel nanofiltration membrane prepared by cross-linking of polyethyleneimine on polyacrylonitrile substrate. *Journal of Membrane Science, 451*, 103-110.

Feng, X., Ding, X., & Jiang, D. J. C. S. R. (2012). Covalent organic frameworks. *41*(18), 6010-6022.

Ferreira, F. C., Macedo, H., Cocchini, U., & Livingston, A. G. (2006). Development of a liquid-phase process for recycling resolving agents within diastereomeric resolutions. *Org. Process Res. Dev., 10*(4), 784-793.

Fetanat, M., Keshtiara, M., Low, Z.-X., Keyikoglu, R., Khataee, A., Orooji, Y., Razmjou, A. (2021). Machine Learning for Advanced Design of Nanocomposite Ultrafiltration Membranes. *Industrial & Engineering Chemistry Research, 60*(14), 5236-5250.

Florian, E., Modesti, M., & Ulbricht, M. (2007). Preparation and characterization of novel solvent-resistant nanofiltration composite membranes based on crosslinked polyurethanes. *Ind. Eng. Chem. Res., 46*(14), 4891-4899.

Freund, Y., Schapire, R., & Abe, N. (1999). A short introduction to boosting. *Journal-Japanese Society For Artificial Intelligence, 14*(771-780), 1612.

Gander, W. (1980). Algorithms for the QR decomposition. *Res. Rep, 80*(02), 1251-1268.

Gao, J., Sun, S.-P., Zhu, W.-P., & Chung, T.-S. (2016). Green modification of outer selective P84 nanofiltration (NF) hollow fiber membranes for cadmium removal. *Journal of Membrane Science, 499*, 361-369.

Gao, Z. F., Feng, Y., Ma, D., & Chung, T.-S. (2019). Vapor-phase crosslinked mixed matrix membranes with UiO-66-NH2 for organic solvent nanofiltration. *Journal of Membrane Science, 574*, 124-135.

Geens, J., De Witte, B., & Van der Bruggen, B. (2007). Removal of API's (Active Pharmaceutical Ingredients) from Organic Solvents by Nanofiltration. *Separation Science and Technology, 42*(11), 2435-2449.

Gevers, L. E., Aldea, S., Vankelecom, I. F., & Jacobs, P. A. (2006). Optimisation of a lab-scale method for preparation of composite membranes with a filled dense top-layer. *Journal of Membrane Science, 281*(1-2), 741-746.

Goebel, R., Glaser, T., & Skiborowski, M. (2020). Machine-based learning of predictive models in organic solvent nanofiltration: Solute rejection in pure and mixed solvents. *Separation and Purification Technology, 248*.

Goebel, R., & Skiborowski, M. (2020). Machine-based learning of predictive models in organic solvent nanofiltration: Pure and mixed solvent flux. *Separation and Purification Technology, 237*.

Grosso, V., Vuono, D., Bahattab, M. A., Di Profio, G., Curcio, E., Al-Jilil, S. A., Fontananova, E. (2014). Polymeric and mixed matrix polyimide membranes. *Separation and Purification Technology, 132*, 684-696.

Guan, K., Shen, J., Liu, G., Zhao, J., Zhou, H., & Jin, W. (2017). Spray-evaporation assembled graphene oxide membranes for selective hydrogen transport. *Separation and Purification Technology, 174*, 126-135.

Guo, B. Y., Jiang, S. D., Tang, M. J., Li, K., Sun, S., Chen, P. Y., & Zhang, S. (2019). MoS2 Membranes for Organic Solvent Nanofiltration: Stability and Structural Control. *J Phys Chem Lett, 10*(16), 4609-4617.

Guo, H., Ma, Y., Qin, Z., Gu, Z., Cui, S., & Zhang, G. (2016). One-Step Transformation from Hierarchical-Structured Superhydrophilic NF Membrane into Superhydrophobic OSN Membrane with Improved Antifouling Effect. *ACS Appl Mater Interfaces, 8*(35), 23379-23388.

Guo, X., Liu, D., Han, T., Huang, H., Yang, Q., & Zhong, C. (2017). Preparation of thin film nanocomposite membranes with surface modified MOF for high flux organic solvent nanofiltration. *AIChE Journal, 63*(4), 1303-1312.

Guo, Y., Li, S., Su, B., & Mandal, B. (2019). Fluorine incorporation for enhancing solvent resistance of organic solvent nanofiltration membrane. *Chemical Engineering Journal, 369*, 498-510.

Gupta, P., Schulte, J., Flood, J., & Spruiell, J. (2001). Development of high-strength fibers from aliphatic polyketones by melt spinning and drawing. *Journal of applied polymer science, 82*(7), 1794-1815.

Han, I.-S., & Chung, C.-B. (2016). Performance prediction and analysis of a PEM fuel cell operating on pure oxygen using data-driven models: A comparison of artificial neural network and support vector machine. *International Journal of Hydrogen Energy, 41*(24), 10202-10211.

He, X., Sin, H., Liang, B., Ghazi, Z. A., Khattak, A. M., Khan, N. A., Tang, Z. (2019). Controlling the Selectivity of Conjugated Microporous Polymer Membrane for Efficient Organic Solvent Nanofiltration. *Advanced Functional Materials, 29*(32).

Heikamp, K., & Bajorath, J. (2014). Support vector machines for drug discovery. *Expert Opin Drug Discov, 9*(1), 93-104.

Hendrix, K., Koeckelberghs, G., & Vankelecom, I. F. (2014). Study of phase inversion parameters for PEEK-based nanofiltration membranes. *Journal of Membrane Science, 452*, 241-252.

Hermans, S., Mariën, H., Van Goethem, C., & Vankelecom, I. F. J. (2015). Recent developments in thin film (nano)composite membranes for solvent resistant nanofiltration. *Current Opinion in Chemical Engineering, 8*, 45-54.

Hołda, A. K., De Roeck, M., Hendrix, K., & Vankelecom, I. F. (2013). The influence of polymer purity and molecular weight on the synthesis of integrally skinned polysulfone membranes. *Journal of Membrane Science, 446*, 113-120.

Hu, J., Kim, C., Halasz, P., Kim, J. F., Kim, J., & Szekely, G. (2021). Artificial intelligence for performance prediction of organic solvent nanofiltration membranes. *Journal of Membrane Science, 619*.

Hua, D., & Chung, T.-S. (2017). Polyelectrolyte functionalized lamellar graphene oxide membranes on polypropylene support for organic solvent nanofiltration. *Carbon, 122*, 604-613.

Huang, J. H., Cheng, X. Q., Zhang, Y., Wang, K., Liang, H., Wang, P., Shao, L. (2020). Polyelectrolyte Grafted MOFs Enable Conjugated Membranes for Molecular Separations in Dual Solvent Systems. *Cell Reports Physical Science, 1*(4).

Huang, L., Chen, J., Gao, T., Zhang, M., Li, Y., Dai, L., Shi, G. (2016). Reduced Graphene Oxide Membranes for Ultrafast Organic Solvent Nanofiltration. *Adv Mater, 28*(39), 8669-8674.

Huang, L., Li, Y., Zhou, Q., Yuan, W., & Shi, G. (2015). Graphene oxide membranes with tunable semipermeability in organic solvents. *Advanced Materials, 27*(25), 3797-3802.

Huang, Y., Sun, J., Wu, D., & Feng, X. (2018). Layer-by-layer self-assembled chitosan/PAA nanofiltration membranes. *Separation and Purification Technology, 207*, 142-150.

Ilyas, S., Joseph, N., Szymczyk, A., Volodin, A., Nijmeijer, K., de Vos, W. M., & Vankelecom, I. F. J. (2016). Weak polyelectrolyte multilayers as tunable membranes for solvent resistant nanofiltration. *Journal of Membrane Science, 514*, 322-331.

J. L. Anderson, J. A. Q. (1974). Restricted transport in small pores. *Biophysical Journal, 14*, 130-150.

J.G. Wijmans, R. W. B. (1995). The solution-diffusion model: a review *Journal of Membrane Science, 107*, 1-21.

James Campbell, R. P. D., Chris Braddock, A.G. Livingston. (2013). Improving the Permeance of Hybrid Polymer/Metal organic framework (MOF) membranes for organic solvent nanofiltration- Development of MOF thin films via interficial synthesis. *Journal of Materials Chemistry A, 00*.

Jawad, J., Hawari, A. H., & Javaid Zaidi, S. (2021). Artificial neural network modeling of wastewater treatment and desalination using membrane processes: A review. *Chemical Engineering Journal, 419*.

Jeong, N., Chung, T. H., & Tong, T. (2021). Predicting Micropollutant Removal by Reverse Osmosis and Nanofiltration Membranes: Is Machine Learning Viable? *Environ Sci Technol, 55*(16), 11348-11359.

Ji, D., Xiao, C., An, S., Zhao, J., Hao, J., & Chen, K. (2019). Preparation of high-flux PSF/GO loose nanofiltration hollow fiber membranes with dense-loose structure for treating textile wastewater. *Chemical Engineering Journal, 363*, 33-42.

Ji, Y., An, Q., Zhao, Q., Chen, H., Qian, J., & Gao, C. (2010). Fabrication and performance of a new type of charged nanofiltration membrane based on polyelectrolyte complex. *Journal of Membrane Science, 357*(1-2), 80-89.

Jiang, J., He, Y., Li, S., & Cui, H. (2012). Amino acids as the source for producing carbon nanodots: microwave assisted one-step synthesis, intrinsic photoluminescence property and intense chemiluminescence enhancement. *Chemical communications, 48*(77), 9634-9636.

Jimenez Solomon, M. F., Bhole, Y., & Livingston, A. G. (2013). High flux hydrophobic membranes for organic solvent nanofiltration (OSN)—Interfacial polymerization, surface modification and solvent activation. *Journal of Membrane Science, 434*, 193-203.

Joseph, N., Ahmadiannamini, P., Hoogenboom, R., & Vankelecom, I. F. (2014). Layer-by-layer preparation of polyelectrolyte multilayer membranes for separation. *Polymer Chemistry, 5*(6), 1817-1831.

Joseph, N., Ahmadiannamini, P., Jishna, P. S., Volodin, A., & Vankelecom, I. F. J. (2015). 'Up-scaling' potential for polyelectrolyte multilayer membranes. *Journal of Membrane Science, 492*, 271-280.

Jung, I.-K., Gurav, J. L., Ha, T.-J., Choi, S. G., Baek, S., & Park, H.-H. (2012). The properties of silica aerogels hybridized with SiO2 nanoparticles by ambient pressure drying. *Ceramics International, 38*, S105-S108.

K, A., Mungray, A., Agarwal, S., Ali, J., & Chandra Garg, M. (2021). Performance optimisation of forward-osmosis membrane system using machine learning for the treatment of textile industry wastewater. *Journal of Cleaner Production, 289*.

Kalmoush, A., El-Sakhawy, M., Kamel, S., Salama, A., & Hesemann, P. (2020). A green method for preparation of amino acids functionalized 2, 3-dialdehyde cellulose. *Egyptian Journal of Chemistry, 63*(9), 8-9.

Kamali, M., Appels, L., Yu, X., Aminabhavi, T. M., & Dewil, R. (2021). Artificial intelligence as a sustainable tool in wastewater treatment using membrane bioreactors. *Chemical Engineering Journal, 417*.

Karimi, A., Khataee, A., Safarpour, M., & Vatanpour, V. (2020). Development of mixed matrix ZIF-8/polyvinylidene fluoride membrane with improved performance in solvent resistant nanofiltration. *Separation and Purification Technology, 237*.

Kebria, M. R. S., Jahanshahi, M., & Rahimpour, A. (2015). SiO$_2$ modified polyethyleneimine-based nanofiltration membranes for dye removal from aqueous and organic solutions. *Desalination, 367*, 255-264.

Kehrer, M., Duchoslav, J., Hinterreiter, A., Cobet, M., Mehic, A., Stehrer, T., & Stifter, D. (2019). XPS investigation on the reactivity of surface imine groups with TFAA. *Plasma Processes and Polymers, 16*(4), 1800160.

Kiel, M., Mitzscherling, S., Leitenberger, W., Santer, S., Tiersch, B., Sievers, T., Bargheer, M. (2010). Structural Characterization of a Spin-Assisted Colloid−Polyelectrolyte Assembly: Stratified Multilayer Thin Films. *Langmuir, 26*(23), 18499-18502.

Kim, H. J., Lee, J. S., Park, J. M., Lee, S. J., Hong, S. J., Park, J. S., & Park, K.-H. (2020). Fabrication of Nanocomposite Complexed with Gold Nanoparticles on

Polyaniline and Application to Their Nerve Regeneration. *ACS Appl. Mater. Interfaces*.

Kim, H. W., Yoon, H. W., Yoon, S.-M., Yoo, B. M., Ahn, B. K., Cho, Y. H., Kwon, S. (2013). Selective gas transport through few-layered graphene and graphene oxide membranes. *Science, 342*(6154), 91-95.

Kolasinska, M., Krastev, R., Gutberlet, T., & Warszynski, P. (2009). Layer-by-layer deposition of polyelectrolytes. Dipping versus spraying. *Langmuir, 25*(2), 1224-1232.

Korzhova, E., Déon, S., Koubaa, Z., Fievet, P., Lopatin, D., & Baranov, O. (2020a). Modification of commercial UF membranes by electrospray deposition of polymers for tailoring physicochemical properties and enhancing filtration performances. *Journal of Membrane Science, 598*, 117805.

Korzhova, E., Déon, S., Koubaa, Z., Fievet, P., Lopatin, D., & Baranov, O. (2020b). Modification of commercial UF membranes by electrospray deposition of polymers for tailoring physicochemical properties and enhancing filtration performances. *Journal of Membrane Science, 598*.

Kotte, M. R., Hwang, T., Han, J.-I., & Diallo, M. S. (2015). A one-pot method for the preparation of mixed matrix polyvinylidene fluoride membranes with in situ synthesized and PEGylated polyethyleneimine particles. *Journal of Membrane Science, 474*, 277-287.

Lai, G. S., Lau, W. J., Goh, P. S., Ismail, A. F., Yusof, N., & Tan, Y. H. (2016). Graphene oxide incorporated thin film nanocomposite nanofiltration membrane for enhanced salt removal performance. *Desalination, 387*, 14-24.

Lau, W. J., Gray, S., Matsuura, T., Emadzadeh, D., Chen, J. P., & Ismail, A. F. (2015). A review on polyamide thin film nanocomposite (TFN) membranes: History, applications, challenges and approaches. *Water Res, 80*, 306-324.

Lee, S., & Kim, J. (2020). Prediction of Nanofiltration and Reverse-Osmosis-Membrane Rejection of Organic Compounds Using Random Forest Model. *Journal of Environmental Engineering, 146*(11).

Li, B., Cui, Y., Japip, S., Thong, Z., & Chung, T.-S. (2018). Graphene oxide (GO) laminar membranes for concentrating pharmaceuticals and food additives in organic solvents. *Carbon, 130*, 503-514.

Li, C., Li, S., Tian, L., Zhang, J., Su, B., & Hu, M. Z. (2019). Covalent organic frameworks (COFs)-incorporated thin film nanocomposite (TFN) membranes for high-flux organic solvent nanofiltration (OSN). *Journal of Membrane Science, 572*, 520-531.

Li, Q., Chen, G. Q., Liu, L., & Kentish, S. E. (2018). Spray assisted layer-by-layer assembled one-bilayer polyelectrolyte reverse osmosis membranes. *Journal of Membrane Science, 564*, 501-507.

Li, S., Li, C., Song, X., Su, B., Mandal, B., Prasad, B., Gao, C. (2019a). Graphene quantum dots-doped thin film nanocomposite polyimide membranes with enhanced solvent resistance for solvent-resistant nanofiltration. *ACS Appl. Mater. Interfaces, 11*(6), 6527-6540.

Li, S., Li, C., Song, X., Su, B., Mandal, B., Prasad, B., Gao, C. (2019b). Graphene quantum dots-doped thin film nanocomposite polyimide membranes with enhanced solvent resistance for solvent-resistant nanofiltration. *ACS applied materials interfaces, 11*(6), 6527-6540.

Li, S., Li, C., Su, B., Hu, M. Z., Gao, X., & Gao, C. (2019). Amino-functionalized graphene quantum dots (aGQDs)-embedded thin film nanocomposites for solvent resistant nanofiltration (SRNF) membranes based on covalence interactions. *Journal of Membrane Science, 588*.

Li, X., Goyens, W., Ahmadiannamini, P., Vanderlinden, W., De Feyter, S., & Vankelecom, I. (2010). Morphology and performance of solvent-resistant nanofiltration membranes based on multilayered polyelectrolytes: Study of preparation conditions. *Journal of Membrane Science, 358*(1-2), 150-157.

Li, X., Liu, C., & Van der Bruggen, B. (2020). Polyelectrolytes self-assembly: versatile membrane fabrication strategy. *Journal of Materials Chemistry A, 8*(40), 20870-20896.

Li, X., Liu, C., Yin, W., Chong, T. H., & Wang, R. (2019a). Design and development of layer-by-layer based low-pressure antifouling nanofiltration membrane used for water reclamation. *Journal of Membrane Science, 584*, 309-323.

Li, X., Liu, C., Yin, W., Chong, T. H., & Wang, R. (2019b). Design and development of layer-by-layer based low-pressure antifouling nanofiltration membrane used for water reclamation. *Journal of Membrane Science, 584*, 309-323.

Li, X., Liu, Y., Wang, J., Gascon, J., Li, J., & Van der Bruggen, B. (2017). Metal–organic frameworks based membranes for liquid separation. *Chemical Society Reviews, 46*(23), 7124-7144.

Li, X., Vandezande, P., & Vankelecom, I. F. (2008). Polypyrrole modified solvent resistant nanofiltration membranes. *Journal of Membrane Science, 320*(1-2), 143-150.

Li, Y., Cao, B., & Li, P. (2019). Effects of dope compositions on morphologies and separation performances of PMDA-ODA polyimide hollow fiber membranes in aqueous and organic solvent systems. *Applied Surface Science, 473*, 1038-1048.

Li, Y., Li, C., Li, S., Su, B., Han, L., & Mandal, B. (2019). Graphene oxide (GO)-interlayered thin-film nanocomposite (TFN) membranes with high solvent resistance for organic solvent nanofiltration (OSN). *Journal of Materials Chemistry A, 7*(21), 13315-13330.

Li, Y., Li, J., Soria, R. B., Volodine, A., & Van der Bruggen, B. (2020). Aramid nanofiber and modified ZIF-8 constructed porous nanocomposite membrane for organic solvent nanofiltration. *Journal of Membrane Science, 603*.

Li, Y., Mao, H., Zhang, H., Yang, G., Ding, R., & Wang, J. (2016). Tuning the microstructure and permeation property of thin film nanocomposite membrane by functionalized inorganic nanospheres for solvent resistant nanofiltration. *Separation and Purification Technology, 165*, 60-70.

Li, Y., Verbiest, T., & Vankelecom, I. (2013). Improving the flux of PDMS membranes via localized heating through incorporation of gold nanoparticles. *Journal of Membrane Science, 428*, 63-69.

Li, Y., Wee, L. H., Martens, J. A., & Vankelecom, I. F. (2017). Interfacial synthesis of ZIF-8 membranes with improved nanofiltration performance. *Journal of Membrane Science, 523*, 561-566.

Li, Y., Wee, L. H., Volodin, A., Martens, J. A., & Vankelecom, I. F. (2015). Polymer supported ZIF-8 membranes prepared via an interfacial synthesis method. *Chem Commun (Camb), 51*(5), 918-920.

Liang, B., Wang, H., Shi, X., Shen, B., He, X., Ghazi, Z. A., Li, L. (2018). Microporous membranes comprising conjugated polymers with rigid backbones enable ultrafast organic-solvent nanofiltration. *Nature Chemistry, 10*(9), 961-967.

Liang, Y., Li, C., Li, S., Su, B., Hu, M. Z., Gao, X., & Gao, C. (2020). Graphene quantum dots (GQDs)-polyethyleneimine as interlayer for the fabrication of high performance organic solvent nanofiltration (OSN) membranes. *Chemical Engineering Journal, 380*.

Lim, S., Park, M. J., Phuntsho, S., Mai-Prochnow, A., Murphy, A. B., Seo, D., & Shon, H. (2018). Dual-layered nanocomposite membrane incorporating graphene oxide and halloysite nanotube for high osmotic power density and fouling resistance. *Journal of Membrane Science, 564*, 382-393.

Lim, S. K., Goh, K., Bae, T.-H., & Wang, R. (2017). Polymer-based membranes for solvent-resistant nanofiltration: A review. *Chinese Journal of Chemical Engineering, 25*(11), 1653-1675.

Lin, C.-E., Fang, L.-F., Du, S.-Y., Yao, Z.-K., & Zhu, B.-K. (2019). A novel positively charged nanofiltration membrane formed via simultaneous cross-linking/quaternization of poly(m-phenylene isophthalamide)/polyethyleneimine blend membrane. *Separation and Purification Technology, 212*, 101-109.

Liu, C., Saeki, D., Cheng, L., Luo, J., & Matsuyama, H. (2019). Polyketone-based membrane support improves the organic solvent resistance of laccase catalysis. *J Colloid Interface Sci, 544*, 230-240.

Liu, C., Takagi, R., Shintani, T., Cheng, L., Tung, K. L., & Matsuyama, H. (2020). Organic Liquid Mixture Separation Using an Aliphatic Polyketone-Supported Polyamide Organic Solvent Reverse Osmosis (OSRO) Membrane. *ACS Appl Mater Interfaces, 12*(6), 7586-7594.

Liu, D. S., Ashcraft, J. N., Mannarino, M. M., Silberstein, M. N., Argun, A. A., Rutledge, G. C., . . . Hammond, P. T. (2013). Spray Layer-by-Layer Electrospun Composite Proton Exchange Membranes. *Advanced Functional Materials, 23*(24), 3087-3095.

Liu, M. L., Wang, J., Guo, J. L., Lu, T. D., Cao, X. L., & Sun, S.-P. (2019). Graphene oxide/cross-linked polyimide (GO/CLPI) composite membranes for organic solvent nanofiltration. *Chemical Engineering Research and Design, 146*, 182-189.

Liu, Q., Wu, X., & Zhang, K. (2018). Polysulfone/Polyamide-SiO(2) Composite Membrane with High Permeance for Organic Solvent Nanofiltration. *Membranes (Basel), 8*(4).

Liu, S.-H., Liu, M., Xu, Z.-L., Wei, Y.-M., & Guo, X. (2017). A novel PES-TiO2 hollow fiber hybrid membrane prepared via sol-gel process assisted reverse thermally induced phase separation (RTIPS) method. *Journal of Membrane Science, 528*, 303-315.

Liu, X., Demir, N. K., Wu, Z., & Li, K. (2015). Highly water-stable zirconium metal–organic framework UiO-66 membranes supported on alumina hollow fibers for desalination. *J. Am. Chem. Soc., 137*(22), 6999-7002.

Liu, X., Qi, S., Li, Y., Yang, L., Cao, B., & Tang, C. Y. (2013). Synthesis and characterization of novel antibacterial silver nanocomposite nanofiltration and forward osmosis membranes based on layer-by-layer assembly. *Water research, 47*(9), 3081-3092.

Lou, Y., Liu, G., Liu, S., Shen, J., & Jin, W. (2014). A facile way to prepare ceramic-supported graphene oxide composite membrane via silane-graft modification. *Applied Surface Science, 307*, 631-637.

Lu, Y., Qin, Z., Wang, N., An, Q.-F., & Guo, H. (2021). Counterion exchanged hydrophobic polyelectrolyte multilayer membrane for organic solvent nanofiltration. *Journal of Membrane Science, 620*.

Luo, J., & Wan, Y. (2011). Effect of highly concentrated salt on retention of organic solutes by nanofiltration polymeric membranes. *Journal of Membrane Science, 372*(1-2), 145-153.

Ma, D., Han, G., Gao, Z. F., & Chen, S. B. (2019). Continuous UiO-66-Type Metal-Organic Framework Thin Film on Polymeric Support for Organic Solvent Nanofiltration. *ACS Appl Mater Interfaces, 11*(48), 45290-45300.

Ma, Y., Dong, Z., You, M., Zhang, Y., Feng, X., Ma, X., & Meng, J. (2019). Formation of a thin and continuous MOF membrane with 2-D MOF nanosheets as seeds via layer-by-layer growth. *Chemical communications, 55*(68), 10146-10149.

Marchetti, P., Jimenez Solomon, M. F., Szekely, G., & Livingston, A. G. (2014). Molecular separation with organic solvent nanofiltration: a critical review. *Chem Rev, 114*(21), 10735-10806.

Marin, L., Simionescu, B., & Barboiu, M. (2012). Imino-chitosan biodynamers. *Chemical Communications, 48*(70), 8778-8780.

Meng, Y., Shu, L., Liu, L., Wu, Y., Xie, L.-H., Zhao, M.-J., & Li, J.-R. (2019). A high-flux mixed matrix nanofiltration membrane with highly water-dispersible MOF crystallites as filler. *Journal of Membrane Science, 591*, 117360.

Merlet, R. B., Pizzoccaro-Zilamy, M.-A., Nijmeijer, A., & Winnubst, L. (2020). Hybrid ceramic membranes for organic solvent nanofiltration: State-of-the-art and challenges. *Journal of Membrane Science, 599*.

Mertens, P. G., Cuypers, F., Vandezande, P., Ye, X., Verpoort, F., Vankelecom, I. F., & De Vos, D. E. (2007). Ag0 and Co0 nanocolloids as recyclable quasihomogeneous metal catalysts for the hydrogenation of α, β-unsaturated

aldehydes to allylic alcohol fragrances. *Applied Catalysis A: General, 325*(1), 130-139.

Mohtasebi, A., Chowdhury, T., Hsu, L. H. H., Biesinger, M. C., & Kruse, P. (2016). Interfacial Charge Transfer between Phenyl-Capped Aniline Tetramer Films and Iron Oxide Surfaces. *The Journal of Physical Chemistry C, 120*(51), 29248-29263.

N.A.A. Sani, W. J. L., A.F. Ismail. (2015). Polyphenylsulfone-based solvent resistant nanofiltration (SRNF) membrane incorporated with copper-1,3,5-benzenetricarboxylate (Cu-BTC) nanoparticles for methanol separation. *RSC Advances, 5*(17), 13000-13010.

Nair, R., Wu, H., Jayaram, P., Grigorieva, I., & Geim, A. (2012). Unimpeded permeation of water through helium-leak–tight graphene-based membranes. *Science, 335*(6067), 442-444.

Nakagawa, K., Uchida, K., Wu, J. L. C., Shintani, T., Yoshioka, T., Sasaki, Y., Matsuyama, H. (2020). Fabrication of porous polyketone forward osmosis membranes modified with aromatic compounds: Improved pressure resistance and low structural parameter. *Separation and Purification Technology, 251*.

Namvar-Mahboub, M., & Pakizeh, M. (2013). Development of a novel thin film composite membrane by interfacial polymerization on polyetherimide/modified SiO2 support for organic solvent nanofiltration. *Separation and Purification Technology, 119*, 35-45.

Namvar-Mahboub, M., Pakizeh, M., & Davari, S. (2014). Preparation and characterization of UZM-5/polyamide thin film nanocomposite membrane for dewaxing solvent recovery. *Journal of Membrane Science, 459*, 22-32.

Nan, Q., Li, P., & Cao, B. (2016). Fabrication of positively charged nanofiltration membrane via the layer-by-layer assembly of graphene oxide and polyethylenimine for desalination. *Applied Surface Science, 387*, 521-528.

Navarro, M., Benito, J., Paseta, L., Gascon, I., Coronas, J., & Tellez, C. (2018). Thin-Film Nanocomposite Membrane with the Minimum Amount of MOF by the Langmuir-Schaefer Technique for Nanofiltration. *ACS Appl Mater Interfaces, 10*(1), 1278-1287.

Park, C. H., Tocci, E., Fontananova, E., Bahattab, M. A., Aljlil, S. A., & Drioli, E. (2016). Mixed matrix membranes containing functionalized multiwalled carbon nanotubes: Mesoscale simulation and experimental approach for optimizing dispersion. *Journal of Membrane Science, 514*, 195-209.

Park, M. J., Gonzales, R. R., Abdel-Wahab, A., Phuntsho, S., & Shon, H. K. (2018). Hydrophilic polyvinyl alcohol coating on hydrophobic electrospun nanofiber membrane for high performance thin film composite forward osmosis membrane. *Desalination, 426*, 50-59.

Park, M. J., Lim, S., Gonzales, R. R., Phuntsho, S., Han, D. S., Abdel-Wahab, A., Shon, H. K. (2019). Thin-film composite hollow fiber membranes incorporated with graphene oxide in polyethersulfone support layers for enhanced osmotic power density. *Desalination, 464*, 63-75.

Park, M. J., Phuntsho, S., He, T., Nisola, G. M., Tijing, L. D., Li, X.-M., Shon, H. K. (2015). Graphene oxide incorporated polysulfone substrate for the fabrication of flat-sheet thin-film composite forward osmosis membranes. *Journal of Membrane Science, 493*, 496-507.

Paseta, L., Luque-Alled, J. M., Malankowska, M., Navarro, M., Gorgojo, P., Coronas, J., & Téllez, C. (2020). Functionalized graphene-based polyamide thin film nanocomposite membranes for organic solvent nanofiltration. *Separation and Purification Technology, 247*.

Paseta, L., Navarro, M., Coronas, J., & Téllez, C. (2019). Greener processes in the preparation of thin film nanocomposite membranes with diverse metal-organic frameworks for organic solvent nanofiltration. *Journal of Industrial and Engineering Chemistry, 77*, 344-354.

Patel, P. A., Dobrynin, A. V., & Mather, P. T. (2007). Combined effect of spin speed and ionic strength on polyelectrolyte spin assembly. *Langmuir, 23*(25), 12589-12597.

Peng, F., Hu, C., & Jiang, Z. (2007). Novel ploy (vinyl alcohol)/carbon nanotube hybrid membranes for pervaporation separation of benzene/cyclohexane mixtures. *Journal of Membrane Science, 297*(1-2), 236-242.

Peshev, D., Peeva, L. G., Peev, G., Baptista, I. I. R., & Boam, A. T. (2011). Application of organic solvent nanofiltration for concentration of antioxidant extracts of rosemary (Rosmarinus officiallis L.). *Chemical Engineering Research and Design, 89*(3), 318-327.

Peyravi, M., Jahanshahi, M., Rahimpour, A., Javadi, A., & Hajavi, S. (2014). Novel thin film nanocomposite membranes incorporated with functionalized TiO2 nanoparticles for organic solvent nanofiltration. *Chemical Engineering Journal, 241*, 155-166.

Potdar, K., Pardawala, T. S., & Pai, C. D. (2017). A comparative study of categorical variable encoding techniques for neural network classifiers. *International journal of computer applications, 175*(4), 7-9.

Priske, M., Lazar, M., Schnitzer, C., & Baumgarten, G. (2016). Recent Applications of Organic Solvent Nanofiltration. *Chemie Ingenieur Technik, 88*(1-2), 39-49.

Ran, J., Zhang, P., Chu, C., Cui, P., Ai, X., Pan, T., Xu, T. (2020). Ultrathin lamellar MoS2 membranes for organic solvent nanofiltration. *Journal of Membrane Science, 602*.

Rashid, M., & Ralph, S. F. (2017). Carbon nanotube membranes: synthesis, properties, and future filtration applications. *Nanomaterials, 7*(5), 99.

Roy, S., Ntim, S. A., Mitra, S., & Sirkar, K. K. (2011). Facile fabrication of superior nanofiltration membranes from interfacially polymerized CNT-polymer composites. *Journal of Membrane Science, 375*(1-2), 81-87.

Rundquist, E. M., Pink, C. J., & Livingston, A. G. (2012). Organic solvent nanofiltration: a potential alternative to distillation for solvent recovery from crystallisation mother liquors. *Green Chemistry, 14*(8).

Sairam, M., Loh, X., Bhole, Y., Sereewatthanawut, I., Li, K., Bismarck, A., Livingston, A. (2010). Spiral-wound polyaniline membrane modules for organic solvent nanofiltration (OSN). *Journal of Membrane Science, 349*(1-2), 123-129.

Sani, N. A. A., Lau, W. J., Nordin, N. A. H. M., & Ismail, A. F. (2016). Influence of organic solvents and operating conditions on the performance of polyphenylsulfone (PPSU)/copper-1,3,5-benzenetricarboxylate (Cu-BTC) solvent resistant nanofiltration (SRNF) membranes. *Chemical Engineering Research and Design, 115*, 66-76.

Sarango, L., Paseta, L., Navarro, M., Zornoza, B., & Coronas, J. (2018). Controlled deposition of MOFs by dip-coating in thin film nanocomposite membranes for organic solvent nanofiltration. *Journal of Industrial and Engineering Chemistry, 59*, 8-16.

Schapire, R. E. (2003). The boosting approach to machine learning: An overview. *Nonlinear estimation classification*, 149-171.

Schlenoff, J. B., Dubas, S. T., & Farhat, T. (2000). Sprayed polyelectrolyte multilayers. *Langmuir, 16*(26), 9968-9969.

Seah, M. Q., Lau, W. J., Goh, P. S., Tseng, H. H., Wahab, R. A., & Ismail, A. F. (2020). Progress of Interfacial Polymerization Techniques for Polyamide Thin Film (Nano)Composite Membrane Fabrication: A Comprehensive Review. *Polymers (Basel), 12*(12).

Selman A. Waksman, & Lechevalier, H. A. (1961).

Sforca, M., Yoshida, I., & Nunes, S. (1999). Organic–inorganic membranes prepared from polyether diamine and epoxy silane. *Journal of Membrane Science, 159*(1-2), 197-207.

Shao, L., Cheng, X., Wang, Z., Ma, J., & Guo, Z. (2014). Tuning the performance of polypyrrole-based solvent-resistant composite nanofiltration membranes by optimizing polymerization conditions and incorporating graphene oxide. *Journal of Membrane Science, 452*, 82-89.

Shawky, H. A., Chae, S.-R., Lin, S., & Wiesner, M. R. (2011). Synthesis and characterization of a carbon nanotube/polymer nanocomposite membrane for water treatment. *Desalination, 272*(1-3), 46-50.

Shinde, D. B., Cao, L., Wonanke, A. D. D., Li, X., Kumar, S., Liu, X., . . . Lai, Z. (2020). Pore engineering of ultrathin covalent organic framework membranes for organic solvent nanofiltration and molecular sieving. *Chemical Science, 11*(21), 5434-5440.

Shinde, D. B., Sheng, G., Li, X., Ostwal, M., Emwas, A. H., Huang, K. W., & Lai, Z. (2018). Crystalline 2D Covalent Organic Framework Membranes for High-Flux Organic Solvent Nanofiltration. *J Am Chem Soc, 140*(43), 14342-14349.

Shu, L., Xie, L.-H., Meng, Y., Liu, T., Zhao, C., & Li, J.-R. (2020). A thin and high loading two-dimensional MOF nanosheet based mixed-matrix membrane for high permeance nanofiltration. *Journal of Membrane Science*, 118049.

Siddique, H., Peeva, L. G., Stoikos, K., Pasparakis, G., Vamvakaki, M., & Livingston, A. G. (2012). Membranes for Organic Solvent Nanofiltration Based on

Preassembled Nanoparticles. *Industrial & Engineering Chemistry Research, 52*(3), 1109-1121.

Sinharay, S., Stern, H. S., & Russell, D. (2001). The use of multiple imputation for the analysis of missing data. *Psychological methods, 6*(4), 317.

Solomon, M. F. J., Bhole, Y., & Livingston, A. G. (2013). High flux hydrophobic membranes for organic solvent nanofiltration (OSN)—Interfacial polymerization, surface modification and solvent activation. *Journal of Membrane Science, 434*, 193-203.

Solomon, M. F. J., Bhole, Y., & Livingston, A. G. (2012). High flux membranes for organic solvent nanofiltration (OSN)—Interfacial polymerization with solvent activation. *Journal of Membrane Science, 423*, 371-382.

Soroko, I., & Livingston, A. (2009). Impact of TiO2 nanoparticles on morphology and performance of crosslinked polyimide organic solvent nanofiltration (OSN) membranes. *Journal of Membrane Science, 343*(1-2), 189-198.

Soroko, I., Lopes, M. P., & Livingston, A. (2011). The effect of membrane formation parameters on performance of polyimide membranes for organic solvent nanofiltration (OSN): Part A. Effect of polymer/solvent/non-solvent system choice. *Journal of Membrane Science, 381*(1-2), 152-162.

Soroko, I., Makowski, M., Spill, F., & Livingston, A. (2011). The effect of membrane formation parameters on performance of polyimide membranes for organic solvent nanofiltration (OSN). Part B: Analysis of evaporation step and the role of a co-solvent. *Journal of Membrane Science, 381*(1-2), 163-171.

Sorribas, S., Gorgojo, P., Tellez, C., Coronas, J., & Livingston, A. G. (2013). High flux thin film nanocomposite membranes based on metal-organic frameworks for organic solvent nanofiltration. *J Am Chem Soc, 135*(40), 15201-15208.

Sotto, A., Boromand, A., Balta, S., Kim, J., & Van der Bruggen, B. (2011). Doping of polyethersulfone nanofiltration membranes: antifouling effect observed at ultralow concentrations of TiO 2 nanoparticles. *Journal of Materials Chemistry, 21*(28), 10311-10320.

Sui, X., Yuan, Z., Yu, Y., Goh, K., & Chen, Y. (2020). 2D Material Based Advanced Membranes for Separations in Organic Solvents. *Small, 16*(50), e2003400.

Sun, P., Zhu, M., Wang, K., Zhong, M., Wei, J., Wu, D., . . . Zhu, H. (2013). Selective ion penetration of graphene oxide membranes. *ACS Nano, 7*(1), 428-437.

Sun, S. P., Chung, T. S., Lu, K. J., & Chan, S. Y. (2014). Enhancement of flux and solvent stability of Matrimid® thin-film composite membranes for organic solvent nanofiltration. *AIChE Journal, 60*(10), 3623-3633.

Suthaharan, S. (2016). Support vector machine. In *Machine learning models and algorithms for big data classification* (pp. 207-235): Springer.

Székely, G., Bandarra, J., Heggie, W., Sellergren, B., & Ferreira, F. C. (2011). Organic solvent nanofiltration: a platform for removal of genotoxins from active pharmaceutical ingredients. *Journal of Membrane Science, 381*(1-2), 21-33.

Szekely, G., Jimenez-Solomon, M. F., Marchetti, P., Kim, J. F., & Livingston, A. G. (2014). Sustainability assessment of organic solvent nanofiltration: from fabrication to application. *Green Chem., 16*(10), 4440-4473.

Tahir, M. N., Shahbazi, F., Rondeau-Gagne, S., & Trant, J. F. (2021). The biosynthesis of the cannabinoids. *J Cannabis Res, 3*(1), 7.

Tasis, D., Tagmatarchis, N., Bianco, A., & Prato, M. (2006). Chemistry of carbon nanotubes. *Chemical reviews, 106*(3), 1105-1136.

Teixeira, A. R. S., Santos, J. L. C., & Crespo, J. G. (2014). Solvent resistant diananofiltration for production of steryl esters enriched extracts. *Separation and Purification Technology, 135*, 243-251.

Tham, H. M., Japip, S., & Chung, T.-S. (2019). WS2 deposition on cross-linked polyacrylonitrile with synergistic transformation to yield organic solvent nanofiltration membranes. *Journal of Membrane Science, 588*.

Tham, H. M., Japip, S., & Chung, T.-S. (2019). WS2 deposition on cross-linked polyacrylonitrile with synergistic transformation to yield organic solvent nanofiltration membranes. *Journal of Membrane Science, 588*, 117219.

Thebo, K. H., Qian, X., Zhang, Q., Chen, L., Cheng, H.-M., & Ren, W. (2018). Highly stable graphene-oxide-based membranes with superior permeability. *Nature communication, 9*(1), 1-8.

Tian, M., Wang, R., Goh, K., Liao, Y., & Fane, A. G. (2015). Synthesis and characterization of high-performance novel thin film nanocomposite PRO membranes with tiered nanofiber support reinforced by functionalized carbon nanotubes. *Journal of Membrane Science, 486*, 151-160.

Tuteja, S. K., Chen, R., Kukkar, M., Song, C. K., Mutreja, R., Singh, S., Deep, A. (2016). A label-free electrochemical immunosensor for the detection of cardiac marker using graphene quantum dots (GQDs). *Biosensors and Bioelectronics, 86*, 548-556.

Valadez-Blanco, R., Ferreira, F. C., Jorge, R. F., & Livingston, A. G. (2008). A membrane bioreactor for biotransformations of hydrophobic molecules using organic solvent nanofiltration (OSN) membranes. *Journal of Membrane Science, 317*(1-2), 50-64.

Van Buuren, S. (2018). *Flexible imputation of missing data*: CRC press.

Vandezande, P., Gevers, L. E., & Vankelecom, I. F. (2008). Solvent resistant nanofiltration: separating on a molecular level. *Chem Soc Rev, 37*(2), 365-405.

Vanherck, K., Hermans, S., Verbiest, T., & Vankelecom, I. (2011). Using the photothermal effect to improve membrane separations via localized heating. *Journal of Materials Chemistry, 21*(16).

Vanherck, K., Vankelecom, I., & Verbiest, T. (2011). Improving fluxes of polyimide membranes containing gold nanoparticles by photothermal heating. *Journal of Membrane Science, 373*(1-2), 5-13.

Vanherck, K., Verbiest, T., & Vankelecom, I. (2011). Comparison of Two Synthesis Routes to Obtain Gold Nanoparticles in Polyimide. *The Journal of Physical Chemistry C, 116*(1), 115-125.

Vatanpour, V., Esmaeili, M., & Farahani, M. H. D. A. (2014). Fouling reduction and retention increment of polyethersulfone nanofiltration membranes embedded by amine-functionalized multi-walled carbon nanotubes. *Journal of Membrane Science, 466*, 70-81.

Venkatasubramanian, V. (2018). The promise of artificial intelligence in chemical engineering Is it here, finally? *AIChE Journal, 65*(2), 466-478.

Viet, N. D., & Jang, A. (2021). Development of artificial intelligence-based models for the prediction of filtration performance and membrane fouling in an osmotic membrane bioreactor. *Journal of Environmental Chemical Engineering, 9*(4).

Volkov, A., Tsarkov, S., Gokzhaev, M., Bondarenko, G., Legkov, S., Kukushkina, Y. A., & Volkov, V. (2012). Nanofiltration and sorption of organic solvents in poly (1-trimethylsilyl-1-propyne) samples of different microstructures. *Petroleum Chemistry, 52*(8), 598-608.

Volkov, A. V., Korneeva, G. A., & Tereshchenko, G. F. (2008). Organic solvent nanofiltration: prospects and application. *Russian Chemical Reviews, 77*(11), 983-993.

Volkov, A. V., Parashchuk, V. V., Stamatialis, D. F., Khotimsky, V. S., Volkov, V. V., & Wessling, M. (2009). High permeable PTMSP/PAN composite membranes for solvent nanofiltration. *Journal of Membrane Science, 333*(1-2), 88-93.

Wang, C., Park, M. J., Seo, D. H., Drioli, E., Matsuyama, H., & Shon, H. (2021). Recent advances in nanomaterial-incorporated nanocomposite membranes for organic solvent nanofiltration. *Separation and Purification Technology, 268*.

Wang, C., Park, M. J., Seo, D. H., Phuntsho, S., Gonzales, R. R., Matsuyama, H., Shon, H. K. (2022). Inkjet printed polyelectrolyte multilayer membrane using a polyketone support for organic solvent nanofiltration. *Journal of Membrane Science, 642*.

Wang, C., Park, M. J., Yu, H., Matsuyama, H., Drioli, E., & Shon, H. K. (2022). Recent advances of nanocomposite membranes using layer-by-layer assembly. *Journal of Membrane Science*, 120926.

Wang, J., Qin, L., Lin, J., Zhu, J., Zhang, Y., Liu, J., & Van der Bruggen, B. (2017). Enzymatic construction of antibacterial ultrathin membranes for dyes removal. *Chemical Engineering Journal, 323*, 56-63.

Wang, R., Xu, C., Sun, J., Gao, L., & Lin, C. (2013). Flexible free-standing hollow Fe3O4/graphene hybrid films for lithium-ion batteries. *Journal of Materials Chemistry A, 1*(5), 1794.

Wang, S., Mahalingam, D., Sutisna, B., & Nunes, S. P. (2019). 2D-dual-spacing channel membranes for high performance organic solvent nanofiltration. *Journal of Materials Chemistry A, 7*(19), 11673-11682.

Wang, Z., Si, Z., Cai, D., Li, G., Li, S., Qin, P., & Tan, T. (2019). Improving ZIF-8 stability in the preparation process of polyimide-based organic solvent nanofiltration membrane. *Separation and Purification Technology, 227*.

Wang, Z., Wang, Z., Lin, S., Jin, H., Gao, S., Zhu, Y., & Jin, J. (2018). Nanoparticle-templated nanofiltration membranes for ultrahigh performance desalination. *Nature communications, 9*(1), 1-9.

Wei, W., Gupta, K. M., Liu, J., & Jiang, J. (2018). Zeolitic Imidazolate Framework Membranes for Organic Solvent Nanofiltration: A Molecular Simulation Exploration. *ACS Appl Mater Interfaces, 10*(39), 33135-33143.

White, L. S. (2006). Development of large-scale applications in organic solvent nanofiltration and pervaporation for chemical and refining processes. *Journal of Membrane Science, 286*(1-2), 26-35.

White, L. S., & Wildemuth, C. R. (2006). Aromatics enrichment in refinery streams using hyperfiltration. *Ind. Eng. Chem. Res., 45*(26), 9136-9143.

Wood, K. C., Chuang, H. F., Batten, R. D., Lynn, D. M., & Hammond, P. T. (2006). Controlling interlayer diffusion to achieve sustained, multiagent delivery from layer-by-layer thin films. *Proceedings of the National Academy of Sciences, 103*(27), 10207-10212.

Wu, D., Huang, Y., Yu, S., Lawless, D., & Feng, X. (2014). Thin film composite nanofiltration membranes assembled layer-by-layer via interfacial polymerization from polyethylenimine and trimesoyl chloride. *Journal of Membrane Science, 472*, 141-153.

Wu, X., Zhou, G., Cui, X., Li, Y., Wang, J., Cao, X., & Zhang, P. (2019). Nanoparticle-Assembled Thin Film with Amphipathic Nanopores for Organic Solvent Nanofiltration. *ACS Appl Mater Interfaces, 11*(19), 17804-17813.

Xianfeng Li, Steven De Feyter, Dongju Chen, Steliana Aldea, & Vankelecom, I. F. J. (2008). Solvent-Resistant Nanofiltration Membranes Based on Multilayered Polyelectrolyte Complexes. *Chemistry of materials, 20*, 3876–3883.

Xing, D. Y., Chan, S. Y., & Chung, T.-S. (2014). The ionic liquid [EMIM] OAc as a solvent to fabricate stable polybenzimidazole membranes for organic solvent nanofiltration. *Green Chemistry, 16*(3), 1383-1392.

Xu, S. J., Shen, Q., Chen, G. E., & Xu, Z. L. (2018). Novel beta-CD@ZIF-8 Nanoparticles-Doped Poly(m-phenylene isophthalamide) (PMIA) Thin-Film Nanocomposite (TFN) Membrane for Organic Solvent Nanofiltration (OSN). *ACS Omega, 3*(9), 11770-11787.

Yang, H., Wang, N., Wang, L., Liu, H.-X., An, Q.-F., & Ji, S. (2018). Vacuum-assisted assembly of ZIF-8@GO composite membranes on ceramic tube with enhanced organic solvent nanofiltration performance. *Journal of Membrane Science, 545*, 158-166.

Yang, Z., Li, L., Jiang, C., Zhao, N., Zhang, S., Guo, Y., Niu, Q. J. (2021). Tailored thin film nanocomposite membrane incorporated with Noria for simultaneously overcoming the permeability-selectivity trade-off and the

membrane fouling in nanofiltration process. *Journal of Membrane Science, 640*, 119863.

Yang, Z., Zhou, Z.-w., Guo, H., Yao, Z., Ma, X.-h., Song, X., Tang, C. Y. (2018). Tannic acid/Fe3+ nanoscaffold for interfacial polymerization: toward enhanced nanofiltration performance. *Environ. Sci. Technol., 52*(16), 9341-9349.

Yeo, C. S. H., Xie, Q., Wang, X., & Zhang, S. (2020). Understanding and optimization of thin film nanocomposite membranes for reverse osmosis with machine learning. *Journal of Membrane Science, 606*.

Yuan, Q., Longo, M., Thornton, A. W., McKeown, N. B., Comesaña-Gándara, B., Jansen, J. C., & Jelfs, K. E. (2021). Imputation of missing gas permeability data for polymer membranes using machine learning. *Journal of Membrane Science, 627*.

Yuan, S., Zhu, J., Li, J., Volodine, A., Yang, J., Van Puyvelde, P., & Van der Bruggen, B. (2018). Nano/microstructure decorated thin film composite poly (arylene sulfide sulfone) membrane constructed by induced fouling in organic solvent ultrafiltration. *Chemical Engineering Journal, 348*, 180-190.

Yuan, Z., Wu, X., Jiang, Y., Li, Y., Huang, J., Hao, L., Wang, J. (2018). Carbon dots-incorporated composite membrane towards enhanced organic solvent nanofiltration performance. *Journal of Membrane Science, 549*, 1-11.

Zarrabi, H., Yekavalangi, M. E., Vatanpour, V., Shockravi, A., & Safarpour, M. (2016). Improvement in desalination performance of thin film nanocomposite nanofiltration membrane using amine-functionalized multiwalled carbon nanotube. *Desalination, 394*, 83-90.

Zhai, Z., Jiang, C., Zhao, N., Dong, W., Lan, H., Wang, M., & Niu, Q. J. (2018). Fabrication of advanced nanofiltration membranes with nanostrand hybrid morphology mediated by ultrafast Noria–polyethyleneimine codeposition. *Journal of Materials Chemistry A, 6*(42), 21207-21215.

Zhang, C., Wu, B.-H., Ma, M.-Q., Wang, Z., & Xu, Z.-K. (2019). Ultrathin metal/covalent–organic framework membranes towards ultimate separation. *Chemical Society Reviews, 48*(14), 3811-3841.

Zhang, H., Mao, H., Wang, J., Ding, R., Du, Z., Liu, J., & Cao, S. (2014). Mineralization-inspired preparation of composite membranes with polyethyleneimine–nanoparticle hybrid active layer for solvent resistant nanofiltration. *Journal of Membrane Science, 470*, 70-79.

Zhang, R., Yu, S., Shi, W., Zhu, J., & Van der Bruggen, B. (2019). Support membrane pore blockage (SMPB): An important phenomenon during the fabrication of thin film composite membrane via interfacial polymerization. *Separation and Purification Technology, 215*, 670-680.

Zhao, D. L., & Chung, T.-S. (2018). Applications of carbon quantum dots (CQDs) in membrane technologies: A review. *Water research, 147*, 43-49.

Zhao, D. L., Japip, S., Zhang, Y., Weber, M., Maletzko, C., & Chung, T. S. (2020). Emerging thin-film nanocomposite (TFN) membranes for reverse osmosis: A review. *Water Res, 173*, 115557.

Zhao, S., & Wang, Z. (2017). A loose nano-filtration membrane prepared by coating HPAN UF membrane with modified PEI for dye reuse and desalination. *Journal of Membrane Science, 524*, 214-224.

Zhao, Y., Tang, K., Liu, H., Van der Bruggen, B., Díaz, A. S., Shen, J., & Gao, C. (2016). An anion exchange membrane modified by alternate electro-deposition layers with enhanced monovalent selectivity. *Journal of Membrane Science, 520*, 262-271.

Zhu, L., Yu, H., Zhang, H., Shen, J., Xue, L., Gao, C., & van der Bruggen, B. (2015). Mixed matrix membranes containing MIL-53(Al) for potential application in organic solvent nanofiltration. *RSC Advances, 5*(89), 73068-73076.

Zinadini, S., Zinatizadeh, A. A., Rahimi, M., Vatanpour, V., & Zangeneh, H. (2014). Preparation of a novel antifouling mixed matrix PES membrane by embedding graphene oxide nanoplates. *Journal of Membrane Science, 453*, 292-301.